# MSc Thesis

## On the Design of a Micropropulsion Based Inflation System for Beyond Earth Orbit CubeSat Inflatable Reflectors

Sean Dunbar

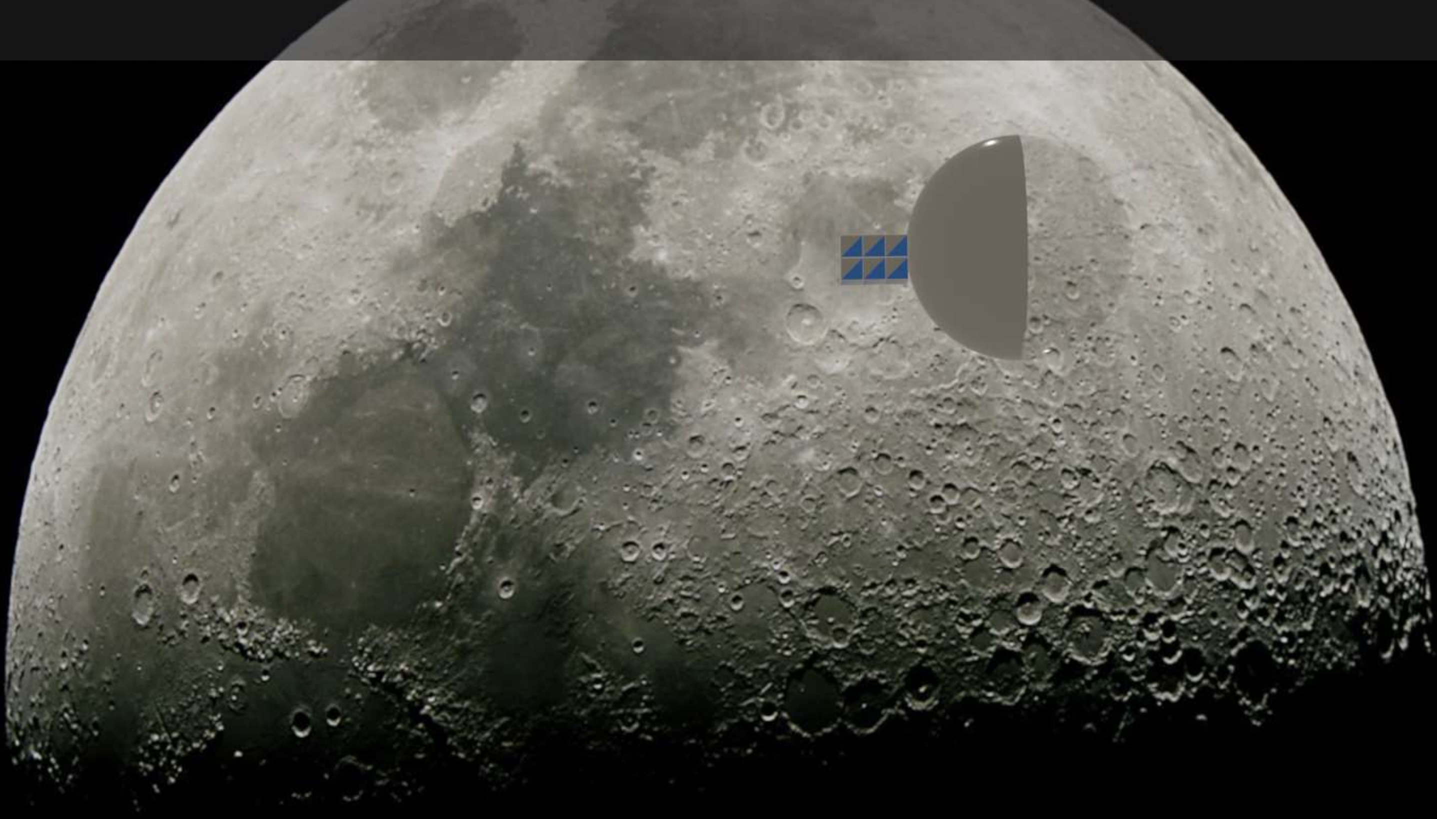

Delft University of Technology

# MASTERS THESIS PROJECT

## ON THE DESIGN OF A MICROPROPULSION BASED INFLATION SYSTEM FOR BEYOND EARTH ORBIT CUBESAT INFLATABLE REFLECTOR

by
**Sean DUNBAR**

in partial fulfilment of the requirements for the degree of
Master of Science in Aerospace Engineering
at the Delft University of Technology,
to be defended publicly on Tuesday, 11th October 2022 at 9:00

Student Number: 5164648
Project Duration: October, 2021 - August 2022
Examination Committee: Chair: Dr. Angelo Cervone
Supervisor: Dr. Chiara Bisagni
External Examiner: Ir. Ron Noomen

TU Delft Delft University of Technology

# Preface

This document contains my thesis project on the design of a micropropulsion based inflation system for beyond Earth orbit CubeSat inflatable reflectors. This project has been conducted in fulfillment of the MSc Aerospace Engineering programme at TU Delft. This has been an exciting and challenging process that I have thoroughly enjoyed exploring. I would like to express my sincere gratitude to my supervisors Dr. Chiara Bisagni and Dr. Angelo Cervone for their patience, guidance and valuable insights. Finally, having conducted a portion of this thesis project over the Covid-19 Pandemic, I would like to thank my family who have supported me while I worked from home as well as my friends who helped me to keep on track during the process.

# Contents

# List of Figures

# LIST OF TABLES

# Nomenclature

## Abbreviations

| *Abbreviation* | *Definition* |
|---|---|
| ADCS | Attitude Determination and Control System |
| AHP | Analytical Hierarchy Process |
| AO | Atomic Oxygen |
| Ar | Argon |
| AU | Astronomical Unit |
| BEO | Beyond Earth Orbit |
| BEOC | Beyond Earth Orbit CubeSat |
| CatSat | CubeSat Assessment and Test Satellite |
| CGG | Solid propellant Cool gas generators |
| COGEX | Cool Gas generator experiment |
| COTS | Commerical Off The Shelf |
| CO2 | Carbon Dioxide |
| CP | Colorless Polyimide |
| CR | Consistency Ratio |
| CSA | Cross Sectional Area |
| CTE | Coefficient of Thermal Expansion |
| DC | Duty Cycle |
| ESA | European Space Agency |
| ESEOD | Equivalent Square Edge Orifice Diameter |
| FUNC-IR | Inflatable Reflector FunctionInflation System Function |
| FUNC-IS | Inflation System Function |
| FVV | Fill/Vent Valve |
| GATR | Ground Antenna Transmit and Receive |
| GEO | Geostationary Earth Orbit |
| GH2 | Helium Gas |
| GN2 | Nitrogen Gas |
| HGA | High Gain Antenna |
| HIAD | Hypersonic Inflatable Aerodynamic Decelerator |
| HP | High Pressure |
| IAE | Inflatable Antenna Experiment |
| JPL | Jet Propulsion Laboratory |
| LEO | Low Earth Orbit |
| LP | Low Pressure |
| LTGG | Low temperature gas generators |
| LUMIO | Lunar Meteoroid Impact Observer |

| | |
|---|---|
| MarCo | Mars Cube One |
| MEMS | Micro-electromechanical system |
| MEPSI | MEMS PICOSAT Inspector |
| MEOP | Maximum Expected Operating Pressure |
| MGA | Medium Gain Antenna |
| MiPS | Micro Propulsion Systems |
| MIRIAM | Main Inflated Re-entry Into the Atmospher Mission test |
| MLI | Multi-Layer Insulation |
| MRO | Mars Reconnaissance Orbiter |
| NA | Not Applicable |
| NeaScout | Near-Earth Asteroid Scout |
| NIAC | NASA Innovative Advanced Concepts |
| OCSE | Optical Calibration Sphere Experiment |
| OD | Outer Diameter |
| OS4 | Outer Solar System SmallSat |
| PET | Polyethylene terephthalate |
| PF | Packaging Factor |
| PMD | Propellant Management Device |
| PR | Pressure Regulator Valve |
| PROP-G | Inflation Gas Property |
| PROP-M | Transparent Material Property |
| PROP-R | Reflective Coating Property |
| PW | Pulse Width |
| PWM | Pulse Width Modulation |
| PWPF | Pulse Width Pulse Frequency |
| RCS | Reaction Control System |
| REQ-BEOC | BEOC Mission Interface Requirement |
| REQ-IRI | Inflatable Reflector Interface Requirement |
| REQ-IRP | Inflatable Reflector Performance Requirement |
| REQ-ISI | Inflation System Interface Requirement |
| REQ-ISP | Inflation System Performance Requirement |
| RMS | Root Mean Square |
| RTG | Radioisotope Thermoelectric Generator |
| SA | Solar Absorptivity |
| SLPM | Standard Liter Per Minute |
| SSGG | Solid-State Gas Generator |
| SSIB | Solid State Inflation Balloon deorbiter |
| SPGG | Solid propellant gas generators |
| STP | Solar Thermal Propulsion |
| STK-A | Active Stakeholder |
| STK-P | Passive Stakeholder |
| TBD | To be determined |
| TOR | Trans- polyoctylene rubber |
| TRL | Technological Readiness Level |
| TST | TeraHertz Space Telescope |

| | |
|---|---|
| TuDelft | Delft University of Technology |
| UHF | Ultra High Frequency |
| UV | Ultraviolet |
| VDA | Vapour Deposited Aluminium |
| VHF | Very high frequency |
| VUV | Vacuum Ultraviolet |
| WGG | Warm gas generator |
| Xe | Xenon |

# SYMBOLS

| **Inflatable Structure** | | |
|---|---|---|
| *Symbols* | *Definition* | *Unit* |
| $a$ | Lunar Bond Albedo | - |
| $A$ | Area | $m^2$ |
| $c$ | Speed of light in a vacuum | $m/s$ |
| $D$ | Diameter | $m$ |
| $E$ | Youngs Modulus | $Pa$ |
| $F$ | Flux | $W/m^2$ |
| F($\beta$) | Lunar Visibility Factor | - |
| $G$ | Growth Rate | $1/s$ |
| $G_{dBi}$ | Antenna Gain | $dBi$ |
| h | altitude | $km$ |
| k | Altitude Factor | $\frac{R_M}{R_M+h}$ |
| m | Mass | $g$ |
| M | Mass | $Kg$ |
| $N$ | Micrometeroid Flux | $1/(cm^2 \cdot s)$ |
| P | Pressure | Pa |
| PE | Packaging Efficiency | % |
| $\dot{Q}$ | Radiation | $W$ |
| $R$ | Radius | $m$ |
| $R$ | Radius | $km$ |
| RPE | Reflector Packaging Efficiency | $m^2$/U |
| $T$ | Temperature | $K$ |
| T/D | Material Thickness to Micrometeroid Diameter | - |
| $t$ | Time | $s$ |
| $t$ | Thickness | $m$ |
| $U$ | Standard CubeSat Unit | - |
| $V$ | Volume | $m^3$ |
| $\alpha$ | Absorptivity | - |
| $\beta$ | Orbital Solar Angle | $^\circ$ |
| $\epsilon$ | Emissivity | - |
| $\lambda$ | Wavelength | $m$ |
| $\sigma$ | Stefan Boltzmann constant | $Wm^2/K^4$ |

| | | |
|---|---|---|
| $\sigma$ | Skin Stress | $MPa$ |

| *Subscripts* | *Definition* | - |
|---|---|---|
| c | Cold spot | |
| cr | Critical | |
| eq | Equilibrium | |
| h | Hot spot | |
| i | Internal | |
| M | Moon | |
| o | Outside/External | |
| p | Painted/Coated | |
| R | Reflected | |
| S | Sun/Solar | |
| s | Sunlit Conditions | |
| sh | Shadow Conditions | |
| T | Total | |
| u | Uncoated | |

| | **Inflation System** | |
|---|---|---|
| *Symbols* | *Definition* | *Unit* |
| $A$ | Area | $m^2$ |
| a | Speed of Sound | $m/s$ |
| $c^\star$ | Characteristic Velocity | $m/s$ |
| $C_d$ | Discharge Coefficient | - |
| $C_F$ | Thrust Coefficient | - |
| $C_{f,x}$ | Local Skin Coefficient | - |
| CV | Flow Coefficient | - |
| $D$ | Diameter | $m$ |
| e | Surface Roughness | $mm$ |
| F | Thrust | $N$ |
| f | Friction factor | - |
| $g_o$ | Standard Gravity | $m/s^2$ |
| $G$ | Growth rate | $1/s$ |
| $ISP$ | Specific Impulse | $s$ |
| $j_{bu}$ | Burst Safety Factor | 2.5 |
| $j_u$ | Ultimate Safety Factor | 1.25 |
| $L$ | Length | $mm$ |
| $m$ | Mass Flow Rate | $g/s$ |
| M | Mass | $g$ |
| M | Mach Number | - |
| $M_W$ | Molecular Weight | $Kg/mole$ |
| P | Pressure | $Pa$ |
| P | Pressure | $bar$ |
| Q | Volumetric Flow Rate | $SLPM$ |
| R | Radius | $mm$ |

| | | |
|---|---|---|
| Ra | Universal Gas Constant | $8.314 J/Kmol$ |
| $R_e$ | Reynolds Number | - |
| $T$ | Temperature | $K$ |
| $t$ | Time | $s$ |
| $V$ | Velocity | $m/s$ |
| $x_L$ | Divergent Length | $mm$ |
| $x_P$ | Throat Curvature Length | $mm$ |
| Z | Compressibility | - |
| $\alpha$ | Divergent Half Angle | $^\circ$ |
| $\beta$ | Convergent Half Angle | $^\circ$ |
| $\gamma$ | Gas Specific Heat Ratio | - |
| $\delta$ | Boundary Layer Thickness | $mm$ |
| $\delta^\star$ | Displacement Thickness | $mm$ |
| $\varepsilon$ | Expansion Ratio | - |
| $\theta$ | Momentum Thickness | $mm$ |
| $\lambda_n$ | Flow Divergence Factor | - |
| $\zeta$ | Resistance Coefficient | - |
| $\mu$ | Dynamic Viscosity | kg/m $\cdot s^{-1}$ |
| $\xi$ | Efficiency | - |
| $\rho$ | Density | kg/$m^3$ |
| $\sigma_u$ | Ultimate Stress | 1100 MPa |
| $\phi$ | Diameter | $m$ |
| $\varphi$ | Real Gas Correction Factor | - |
| $\Gamma$ | Vandenkerckhove constant | $\left(\sqrt{\gamma}\left(\frac{2}{\gamma+1}\right)^{\frac{\gamma+1}{2(\gamma-1)}}\right)$ |
| $\Delta$ | Loss | - |

| *Subscripts* | *Definition* |
|---|---|
| avg | Average |
| c | Nozzle Chamber |
| c | Contraction |
| cyl | Cylinder |
| capshp | Spherical Cap |
| e | Nozzle exit |
| e | Expansion |
| eff | effective |
| h | hydraulic |
| m | maintenance |
| t | Nozzle Throat |
| u | Longitudinal Radius |

# SUMMARY

In recent years an exciting new era of space exploration has begun with the advent of the beyond Earth orbit CubeSat (BEOC) missions. However, utilizing the CubeSat platform for such missions gives rise to a series of significant technological challenges. Fortunately, the field of inflatable space structures offers some tantalizing solutions to these challenges. Unfortunately, at present the development of these structures is hampered by a technological gap in the required inflation systems. In order to fill this gap, this thesis proposes the development of an inflation system optimized for such applications, based on the field of micropropulsion technology. This shall be done by first designing an appropriate inflatable structure and then designing the inflation system based on the requirements generated by the design of the structure.

Prior to this project, a literature study was conducted. In this study, the key design features of inflatable space structures were identified, with particular attention paid to those that specifically impacted the design of the inflation system. Following this, an investigation into the use of inflatable space structures for tackling the telecommunications, propulsion and power challenges facing BEOC missions was carried out. Inflatable reflectors were found as showing significant promise for such applications. Finally, the promising potential of micropropulsion technology for BEOC inflation systems is established and a range of promising design concepts identified. Based off of this literature study the framework for this thesis is developed and the requirements generated.

After a concept generation process, it is established that a spherical inflatable reflector provides the most promising structure for maximizing the relevance of the designed inflation system. As such the focus of the design of the reflector is on addressing the key design considerations that enable the requirements of the inflation system to be generated, while also highlighting the competitiveness of such structures relative to conventional reflectors. The designed structure has a 1.0 m diameter, that can be compactly stowed thanks to its 40% packaging efficiency. This packaging phase also requires the inflation system provide ascent venting to ensure a reliable deployment. Due to the use of the free deployment method, this need for a reliable deployment requires a high degree of inflation control. In addition, the limitations of current rigidization technology mean that pressure stabilization is required to maintain structural stability. This in turn necessitates the need for pressure maintenance, which is exacerbated by gas losses due to micrometeoroid punctures. In order to reduces these losses, a pressurization approach is selected that inflates the structure to 15% Yield strength to remove wrinkles before venting to 2% Yield strength. Meanwhile, simplified thermal analysis is carried out to gauge the inflation temperature and the mechanical properties of the structure are calculated, indicating its highly attractive mass and volume characteristics. The result of this design process is a preliminary design of an inflatable reflector that comfortably satisfies the desired reflector requirements while also enabling informed inflation system requirements to be generated.

Following the generation of the inflation system requirements, the design of the inflation system can begin. This starts by carrying out a trade off analysis of the micropropulsion based design candidates identified in the literature study. The result of this analysis is the selection of the cold gas candidate that utilizes regulated blowdown operation. Following this, nitrogen gas is selected as the most appropriate inflation gas due to its attractive blend of properties. With the system and gas types both selected, the next step is the design of the inflation scheme, which consists of four key stages; ascent venting, inflation, venting and pressure maintenance. Focusing on the inflation stage, a multi-phase inflation sequence is specified to ensure optimal control, with a pulsed mode of inflation identified as the best way to achieve this.

With the system type, inflation gas and inflation scheme all specified the required design adjustments to the cold gas system necessary to facilitate inflation were identified. While the majority of the system required minimal adjustments, it was found that a unique design approach was required for the cold gas micro nozzle. Driven by the desire to minimize the gas jet velocity and maximize its temperature, this approach required that the nozzle expansion ratio be minimized and its curvature be maximized. The result of this design approach is a system that can generate gas temperatures in excess of 190 K and velocities less than 460 m/s. In order to facilitate the required pulsed operation, this nozzle is mounted on an inflation control valve that is operated using a control logic based off that used for RCS thrusters. This enables it to generate a suitable inflation sequence, thereby demonstrating its potential for inflation control. Due to the similar operational requirements with an RCS thruster, a COTS cold gas thruster valve is suitable for this control valve. Indeed, apart from the nozzle the similarity of the inflation system to a conventional cold gas micropropulsion system enabled the widespread use of COTS components. This is even true for the additional components required in the feed system so as to facilitate venting. Having said that, the design approach taken for the design of the tank is slightly different to a conventional propulsion system so as to assess the impact of the gas losses due to micrometeriod punctures on the maintenance life of the structure. It was found that facilitating a long duration BEOC mission utilizing a pressure stabilized structure is infeasible, with the designed system capable of a maximum lifetime of around a month. However, this is the only requirement that cannot be met with the designed inflation system. Moreover, as the system functionality enables venting, its design shall remain relevant even with further advancements in rigidization technology. Coupled with the widespread use of COTS components, this is an exciting result for the inflatable space industry as it provides a clear indication that compact and highly controllable inflation systems can successfully be developed using conventional micropropulsion technology.

The end result of this thesis project is a feasible preliminary design for a compact cold gas micropropulsion-based inflation system that can provide a highly precise and controllable inflation process. Such a system can help fill the current technological gap associated with controllable CubeSat inflation systems, thereby enabling and enhancing the development of BEOC inflatable structures, the result of which could help usher in a new era of space exploration.

# 1

# INTRODUCTION

*This chapter provides an introduction to the thesis work detailed in this report.*

INFLATABLE space structures are a form of deployable structure that consist of a flexible chamber and an inflation system. Since the mid-20th century they have been identified as a structural form with enormous, if not revolutionary, potential. Their exciting promise stems from an attractive blend of distinguishing qualities including exceptionally high packaging efficiencies, ultra-low mass, minimal complexity and reduced development costs. This combination of highly attractive characteristics gives them a distinct advantage over many conventional space structures. This is particularly true when considering the development of beyond Earth orbit CubeSat (BEOC) missions, for which inflatable space structures have been identified as a key enabling technology.

This decade will usher in a new era of space exploration made possible by the development of the BEOC mission. Originally proposed by California Polytechnic State University in 1999, the CubeSat, a 10cm x 10cm x 10cm (1U) satellite, has become a hugely popular satellite platform. This popularity derives from their reduced cost, weight and power requirements coupled with their relatively rapid development cycles. These attractive characteristics have seen CubeSats identified as a tantalizing alternative to the current fleet of space exploration spacecraft which are large, complex and very expensive. Utilizing CubeSats for space exploration missions will enable humanity to explore the solar system in a cheaper, more flexible and more accessible way than ever before. However, the development of such BEOC missions have been inhibited by the three main challenges of telecommunications, power and propulsion, all of which stem from the enormous distances from both the Earth and Sun that these CubeSats will have to operate in and travel to. Inflatable space structures, with their unique mix of characteristics, offer some of the most promising solutions to these challenges. However, in order to ensure that inflatable space structures satisfy the demanding requirements of such applications, an optimal inflation system is essential.

Any inflatable space structure will, by definition, require an accompanying inflation system. This inflation system plays an integral role in ensuring that the shape transformation structures of the inflatable structure are successfully implemented. This is especially true for the deployment process, for which the inflation system plays a vital role. Given that the deployment process is the most important stage of an inflatable space structures life cycle, should the inflation system fail to ensure a successful deployment the resulting consequences could be catastrophic. This is particularly true for BEOC applications, whose need for high surface accuracies, among other considerations, shall require a precise and controlled deployment. However, despite the clear importance of inflation systems, they have received surprisingly little attention. Indeed, this lack of attention has yielded a relative dearth of information regarding the development of such systems. The reason for this is likely due to the current reliance on adapted conventional propulsion technology, which while bulky and non-optimal, has a high TRL relative to some of the other key design features of inflatable space structures. Given only a handful of inflatable space structures missions have been carried out, most of which have been demonstration missions, these systems have generally been considered sufficient. However, if inflatable space structures are to be considered a viable option for enabling BEOC missions, the development of new and optimized inflation systems suitable for CubeSat application is required.

Having explored different options in the literature study (Dunbar, 2021), the use of micropropulsion technology to develop a a suitable option was identified as having promising potential. Thus, in order to address this need for a controllable inflation system, suitable for enabling BEOC applications, this thesis project aims to explore the development of a micropropulsion based inflation system.

# 2
# Literature Review

*This chapter provides an overview of the literature study and its relevant findings. The overview is broken down into three sections; Inflatable space structures (section 2.2), Inflatable Structures and Beyond Earth Orbit CubeSat Missions (section 2.3) and finally Inflation Systems (section 2.4).*

## 2.1. INTRODUCTION

THIS chapter provides an overview of the relevant findings of the literature study, which was utilized as the starting point for this thesis. The first step of the literature study was to investigate the key design features that must be addressed in the successful implementation of an inflatable space structure as well as noting their impact on the design of the inflation system. A short recap of this investigation is provided in section 2.2. Next, an exploration of how inflatable space structure can be utilized to enhance and enable the development of beyond Earth orbit CubeSat (BEOC) missions is undertaken, a recap of which can be found in section 2.3. This exploration serves to highlight the revolutionary potential of these structures and by extension the key role that the development of optimized inflation systems plays in realizing this potential. Finally, with an understanding of the key design considerations of inflatable structures as well as their exciting potential for BEOC applications, the development of the inflation systems required to help make these structures a viable solution going forward is investigated. This investigation explores the extent to which micropropulsion technology can be utilized to assist in the development of inflation systems specifically tailored for BEOC applications. A short summary of this is presented in section 2.4.

## 2.2. INFLATABLE SPACE STRUCTURES

### 2.2.1. INTRODUCTION

INFLATABLE space structures can be defined as flexible-walled, expandable structures that distend through the use of internal gas pressure and are designed specifically for space applications. Research into their development has been carried out since the mid-20th century and they have been identified as a structural form with enormous potential, a potential recognised by the space industry as possibly revolutionary. This is succinctly put in a 1995 L'Garde Inc paper which states that, "In many ways they are the ideal deployable structure for use in space" (Cassapakis and Thomas, 1995). In order to understand why, this section shall provide an overview of what these structures are as well as a discussion regarding what their key design features are and how they impact the design of the inflation system.

### 2.2.2. CHARACTERISTICS

Inflatable space structures are seen as having enormous potential within the space industry due to their unique blend of attractive characteristics, giving them an advantage over current state of the art mechanical technologies. However, despite these exciting advantages, to date only a small handful of missions have utilized them and of these the majority have been experimental demonstration missions. This is due to some significant technological hurdles. In order to realise their potential, these hurdles must be overcome. A summary of the advantages of inflatable structures is provided in table 2.1 while a summary of the challenges they face in implementation is provided in table 2.2.

#### ADVANTAGES

| **Characteristic** | **Explanation** |
|---|---|
| Low Mass | Studies estimate that inflatable space structures can be between 50-80% lighter than their best mechanical counterparts (Cassapakis and Thomas, 1995; S. Veldman and Vermeeren, 2001). These mass savings are in large part due to the thin lightweight membrane materials used which enable areal densities significantly lower than a mechanical structure. |
| Low Volume | High packaging efficiencies are one of the clearest advantages that inflatable space structures have over their mechanical counterparts. They enable inflatable structures to be packaged into a stowage volume that is typically less than 25% of that for a mechanical structure (Cassapakis and Thomas, 1995). |
| Low Cost | Inflatables advantages in packaging efficiency and mass requirements have major ramifications for mission costs largely with respect to the potential for cheaper launch vehicle options. Coupled with other factors including the potential for cheaper fabrication processes, engineering of inflatables could be 50-90% cheaper than that of their mechanical counterparts (Cassapakis and Thomas, 1995; Chmielewski and Jenkins, 2005). |

| | |
|---|---|
| Low System Complexity | Inflatables enable the development of structures with relatively few components. This makes them far less mechanically complex and can thus lead to an increase in system reliability (M. S. Grahne and Cadogan, 1999). |
| Scalability | Inflatable structures provide engineers the opportunity to scale up their sizes with relatively few additional mechanical complexities (Chandra, 2015). This makes them an enabler technology for missions that require particularly large scale systems that would not be feasible given current launch capabilities. |

Table 2.1: Inflatable Space Structure Advantageous Characteristics

### CHALLENGES

| **Characteristic** | **Explanation** |
|---|---|
| Verification and Validation | Inflatable space structures lightweight and highly flexible nature makes ground testing on Earth exceedingly complex and problematic. Researchers must rely on complex simulation software in order to overcome this issue, the development of which is in itself extremely challenging. Thus, verification and validation has been one of the main obstacles to the widespread use and development of inflatable space structures to date. |
| Packaging | The challenge for packaging methods is that they are required to provide compact stowage as well as predictable and reliable deployment dynamics. Therefore, the chosen method must exhibit a high packaging efficiency, an ability to vent residual gas and low strain energy while in its stowed configuration (Schenk et al., 2014). |
| Deployment | The deployment process has historically been the highest source of failures in space systems and with inflatables the stakes are even higher. This is because the stiffness of the inflatable structure , and thus its load carrying capacity, is dependent on the degree of inflation which in turn is dependent on the state of deployment (Salama et al., 2000). Therefore ensuring that inflatables deploy reliably and predictably is of the utmost importance. |
| Stabilization | In order to ensure the long term viability of an inflatable structure it must be stabilized to overcome inevitable gas losses. The different stabilization methods available each have their own set of challenges that must carefully considered. |

| | |
|---|---|
| Fabrication | The flexible nature of the thin film membrane used makes fabricating inflatable space structures a challenging process. The most popular approach at present, the gore method, faces numerous challenges with fabrication that inhibit the uniformity and precision of the inflatable surface (Chandra et al., 2020). Other methods are in the early stages of development. |
| Precision | The precision of these structures, with respect to shape and surface accuracy, is largely dependent on overcoming the other challenges presented in this section. A detailed list of possible error sources that affect precision is given by Freeland et al., 1998. |

Table 2.2: Main Challenges Facing Inflatable Space Structure

### 2.2.3. CLASSIFICATION

Inflatable space structures can be organised and classified according to numerous different selection criteria including inflation requirements, stabilization methods, internal pressure loads, etc. Despite the numerous different ways that these structures can be categorised there are generally two major categories that are distinguished irrespective of the criteria. These categories are High Pressure (1-250 kPa) 'Heavy Duty' and Low Pressure (0.00001-1 kPa) 'Lightly Loaded' inflatable structures. Lightly loaded structures are unsurprisingly less robust than their heavy duty counterparts and thus tend to require a more controlled and precise inflation process.

#### HIGH PRESSURE 'HEAVY DUTY' INFLATABLE STRUCTURES

These structures are designed as load bearing structures and utilise high internal pressures in order to facilitate this. They can be further subdivided into two categories depending on whether they utilise these high pressures throughout their life time (pressurized structures) or just for deployment (rigidized structures). Examples of pressurized structures include the habitats and airlocks (Hinkle et al., 2008), designed to withstand internal loads, as well as re-entry systems (Olds et al., 2013), designed to withstand external loads. Examples of rigidized structures on the other hand generally take the form of small radius dual wall structures (S. L. Veldman, 2005) such as booms (Viquerat et al., 2014) or tori (M. S. Grahne and Cadogan, 1999) and are mostly used as support elements.

#### LOW PRESSURE 'LIGHTLY LOADED' INFLATABLE STRUCTURES

These structures are not designed to withstand large loads, rather they are purely designed to withstand small buckling loads (Defoort et al., 2005). They generally take the form of large low pressure membrane elements and can be thought of as having 'inflatable volumes' as opposed to 'inflatable walls' (Kröplin, 2005). Like their high pressure counterparts, low pressure lightly loaded structures can can be further subdivided into two categories. Pressurized structures (Freeland and Bilyeu, 1993) tend to be more common than rigidized structures (Babuscia et al., 2020) due to challenges associated with rigidizing such structures.

### 2.2.4. KEY DESIGN CONSIDERATIONS

WHEN designing an inflatable space structure, there are a number of important design considerations that must be examined. These key factors include the environment they will operate in, the materials they are made of, the fabrication methods used and most importantly their shape transformation functions. As deployable structures, inflatable space structures have to fulfil three underlying functions in addition to their primary design function; Packaging, Deployment and Stabilization. These underlying functions correspond specifically to the process of efficient shape transformation (Miura and Pellegrino, 2020) and thus are rarely chosen independently. Most relevant to this project, the selected combination of deployment and stabilization methods in particular has a major impact on the functional requirements of the inflation system.

#### ENVIRONMENT

In order to design any space structure knowledge of the environments that the structure will experience is crucial. This is particularly prevalent for inflatable space structures which have the most significant interaction with the space environment of any type of space structures (Freeland et al., 1998). This stems from the unique design requirements and applications of these structures such as the rigidization methods for rigidizable structures or the need to maintain inflation pressure in large lightly loaded structures. There are four major environments that must be considered in the design of an inflatable structure shall shall be briefly discussed.

- *Ground Environment:* The ground environment that an inflatable space structure experiences consists of the manufacturing environment and the storage and shipping environment. Both of these environments can have a detrimental impact on the structure if not carefully accounted for.

- *Launch and Pre-Deployment Environment:* The launch and pre-deployment environment defines two major environments during which the inflatable is in its packaged state. A major consideration during launch is the expansion is residual trapped gas, a by-product of the packaging process, which necessitates that the inflation system provide an ascent venting function. The stowage requirements of the packaged structure in the pre-deployment environment, also has a bearing on the inflation system design, e.g. storage life.

- *Deployment Environment:* The deployment environment, due to its dynamic nature, is the most challenging environment that an inflatable space structure must endure. The structure must be capable of withstanding the loads caused by the inflation process which should be carefully considered when designing an appropriate inflation system.

- *Operating Environment:* There are two main aspects of the space environment that inflatable space structures must withstand; physical damage from micrometeoroids and material property changes arising from environmental interactions such as extreme temperature and radiation. These interactions drive the stabilization requirements, which in turn impacts the inflation system functionality.

### PACKAGING

The choice of packaging scheme for an inflatable space structure is crucial for mission success as it effects packaging efficiency, deployment dynamics and the structural properties of the inflated structure. The ultimate goal of packaging is to maximise the packaging efficiency. There are a variety of different ways that packaging efficiency can be defined. Deployable reflectors typically use the ratio of the deployed diameter to the stowed volume ($m^2/U$), as seen in equation 2.1 (Chandra et al., 2020). In this thesis, this shall be referred to as the reflector packaging efficiency (RPE).

$$\text{Reflector Packaging Efficiency (RPE)} = \frac{\text{Deployed Reflector Cross Sectional Area}}{\text{Packaging Container Volume}} \tag{2.1}$$

While this definition is useful for the design of a deployable reflector, for inflatable space structures the most commonly used definition is given in equation 2.2 which can also be restated as the packaging factor as seen in equation 2.3 (M. Grahne and Cadogan, 2001).

$$\text{Packaging Efficiency (PE)} = \frac{\text{Inherent Material Volume}}{\text{Packaging Container Volume}} \times 100 \tag{2.2}$$

$$\text{Packaging Factor (PF)} = \frac{\text{Packaging Container Volume}}{\text{Inherent Material Volume}} \tag{2.3}$$

Inevitably for inflatable reflector structures a high PE value yields a high RPE value and it is therefore highly desirable to maximize PE. While trying to maximise PE, designers must also consider that the packaging scheme chosen can significantly impact spacecraft dynamics, most notably in the form of residual gas built up during packing. If not dealt with appropriately this will impart an initial velocity on the structure as it deploys leading to an unpredictable deployment. The typical PE values for an inflatable space structure consisting of little hardware, typically low pressure structures (e.g. balloons), are around 30-80% while more complex systems, such as those that utilize high pressure support structures along with other hardware are around 10-25% (M. Grahne and Cadogan, 2001). Unsurprisingly, packaging schemes can generally be divided into two separate categories; those for small radius high pressure structures and those for large volume low pressure structures. Both of these categories contain numerous different methods which are explored in detail in the literature study Dunbar, 2021. However, it should be noted that the majority of research has been done on inflatable booms and flat thin membrane structures, with the information regarding the packaging of large low pressure structures more sparse. The selection of an appropriate method is particularly important for the volume constraints of a BEOC mission.

### DEPLOYMENT

The deployment process is the most important stage of an inflatable space structures life cycle, largely due to the fact that the load carrying capacity of the inflatable structure is dependent on the state of deployment. Thus, the missions success is entirely dependent on a successful deployment. However, given the lightweight and highly flexible nature of inflatable structures this can be an extremely challenging task and has led to the development of a number of different deployment methods. They are as follows:

- *Free Deployment:* Free deployment allows the inflating structure to move about freely once released. The advantage of this method is that it requires less mass, volume, complexity and cost than the other methods. While largely unsuitable for small radius high pressure structures, this method is commonly used for simple low pressure structures such as the CubeSat inflatable antenna being developed by JPL (Babuscia et al., 2020). It must be noted that these inflatables still require an ejection mechanism to release the structure out into space.

- *Passively Controlled Deployment:* Passively controlled deployment means that no active system is utilised to influence the deployment of the structure. Instead a variety of mechanical resistive and energy control devices are used in order to restrict and thus control the deployment process (Salama et al., 2000). This means that the inflated segments of the structure are gradually released into space. It is the most popular method of deployment and is normally used for small radius high pressure structures.

- *Actively Controlled Deployment:* Active controlled deployment makes use of sensors and active actuators to provide maximal control over the deployment of the inflatable structure enabling highly accurate and reliable deployment. However, despite its potential advantages it has been the least popular deployment method to date, largely due to its undesirable complexity, mass and volume requirements although this is beginning to change with the advent of embedded intelligent materials Ruggiero and Inman, 2006.

Given the integral role of the inflation system in this process, it is apparent that delivering the inflation gas at a controlled rate is highly advantageous for maximizing the reliability of the deployment process and ensuring its success. This is particularly true for free deployment which unlike the other two methods does not utilize often bulky deployment mechanisms to control the deployment process.

#### STABILIZATION

Stabilization of inflatable space structures is integral for maintaining the long-term structural integrity of the structure after deployment. With threats like micrometeoroids and space debris, as well as imperfections in the inflatable wall, gas leakage due to the development of small holes is highly likely. There are two options that are available to counteract this.

- *Pressure Stabilization:* The first and simpler of the two is to bring make up gas in order to compensate for such leaks. Known as 'pressure stabilization' this option is attractive for its simplicity and has been widely proposed and utilized for low pressure inflatable applications. However, given the volume constraints of a BEOC mission, only a certain amount of make-up gas can be carried, inevitably limiting the duration for which the pressure in the structure can be maintained. Given the desire for long duration BEOC missions, it is apparent utilizing this method comes with its drawbacks. This is particularly true for high pressure structures which leak at higher rates than their low pressure counterparts.

- *Rigidization:* The second option is to utilize a rigidization process. By rigidizing the flexible walls of the inflatable structure and venting the gas, the structure no longer relies on internal gas pressure for structural stability making it impervious to gas leakage. Due to the range and complexity of spacecraft mission requirements, several different rigidization techniques, and thus materials, have been developed and investigated. These techniques draw from a wide range of external influences to instigate the rigidization process which can generally be grouped into three main categories (Defoort et al., 2005). They are:
  - *Mechanical Rigidization:* Rigidization occurs through pressure forces within the inflatable that induce stresses which are higher than the walls metallic layers yield stress. Primarily used with an aluminium-polymer laminate and so commonly known as "Aluminium rigidization" (Schenk et al., 2014).
  - *Physical Rigidization:* Rigidization occurs due a physically induced change in material properties. Methods include utilizing sub-glass transition temperature resins (Schenk et al., 2014). This is a reversible process.
  - *Chemical Rigidization* Rigidization occurs due a chemically induced change in material properties. Methods include utilizing UV light to cure thermoset resins (Defoort et al., 2005). This is an irreversible process.

These different stabilization methods invariably places different functional requirements on the design of the inflation system. Pressure stabilization requires that the inflation system have the capacity to provide pressure maintenance, mechanical rigidization requires it to over-pressurize the structure before venting it while physical and chemical rigidization typically require short term pressure maintenance while the the rigidization process occurs followed by venting.

### Materials

Materials are a vital enabling technology for inflatable space structures.The materials must be both thin and flexible while also being able to withstand the challenging environments inflatable space structures are exposed to. The materials used in inflatable space structures can be split into two categories according to their stabilization method. These categories are Film materials and Rigidizable materials.

- *Film Materials:* Film materials are generally single layer materials utilised in the development of pressurized structures. There are three types of polymer film materials that are most commonly used for this application, all of which have spaceflight heritage. They are polyesters, polyimides and perfluorinated polymers (Connell and Watson, 2001 ).
  - *Polyesters:* Polyethylene terephthalate (PET), commonly known under the tradename Mylar, has been the most commonly utilized film material to date. Its popularity stems from its attractive properties, it's low cost and it's commercial availability.
  - *Polyimides:* Known for their ability to maintain excellent mechanical properties pover a wide temperature range, polyimides such as Kapton HN have become an attractive alternative to Mylar in recent years.

- *Perfluorinated Polymers:* Commonly marketed under the tradename Teflon, these materials offer inherent resistance to atomic oxygen (AO) erosion, something the polyesters and polyimides are typically susceptible to. However, it has poor radiation resistance and relatively unattractive material properties.
- *Advanced Materials:* Advancements in inflatable technology has seen a number of new polymer materials emerge that show some promising properties. Examples include low cure polyimides, such as CP-1 (NEXOLVE REf), TOR and COR polymers as well as intelligent flexible materials such as such as PVDF and PolyMEMS (Pearson et al., 2010; Ruggiero and Inman, 2006)

- *Rigidizable Materials:* Rigidizable materials are materials that have two physical states. For storage they are flexible and foldable but in their deployed state they are hard and rigid. They typically consist of two multiple layered components; the MLI blanket and the support tube laminate. The support tube laminate consists of two main layers, the restraint/ bladder layer, typically a polymer film such as Mylar or Kapton, and the rigidizable layer. These laminates can generally be split into two main categories; metal laminate materials, for mechanical rigidization, and composite laminate materials, for physical and chemical rigidization (Chmielewski and Jenkins, 2005).

#### FABRICATION

While fabrication methods for small radius inflatable structures can vary dependent on the selected packaging and rigidization methods, in general the most common fabrication method for inflatable structures is through seaming together one or more thin flat sections, known as gores, to achieve the desired shape. Given the flexible nature of the thin films used, handling and cutting of these sections can be extremely challenging, particularly for curved low pressure inflatable structures such as reflectors or balloons. One way to overcome this is through the use of precision gore templates or precise automated cutting systems, both of which provide a high degree of dimensional accuracy and control (Freeland et al., 1998). However, the presence of non-smooth seams in the inflatable structures surface leads to a number of issues. Firstly, the faceted nature of using gores seamed together inhibits the uniformity and precision of the inflatable surface which can be a major issue for applications requiring high surface accuracies (Chandra et al., 2020). Additionally, it leads to areas of varying structural stiffness which can lead to undesirable thermal and mechanical properties. While other methods such as 3D forming (Smith et al., 2018) or thermal forming (Chandra et al., 2020), have been proposed in order to overcome these limitations, they are only in the early stages of development.

### 2.2.5. CONCLUSION

This investigation provides a clear description of what these structures are and why they are so attractive for deployable space applications. In addition, the key design considerations that must be addressed in order to successful provide the attractive characteristics of an inflatable space structure are identified and their impact on the required design features of the inflation system is highlighted. This influence derives largely from the interaction of the structure and the environmental conditions it must withstand.

The different environments play a significant role in determining the required functions of the inflation system. The launch and pre-deployment environmental conditions dictate the need for an ascent venting function, as well as the systems storage life, the deployment environment emphasises the need to provide appropriately controlled inflation loads, while the operating environment requires that the structure be sufficiently durable, by providing suitable pressure levels as well as pressure maintenance and/or venting. These three environments correspond directly to, and contribute to the choice of, the shape transformation functions; packaging, deployment and stabilization. In addition, they also impact the material choice and by extension the fabrication requirements.

## 2.3. INFLATABLE STRUCTURES AND BEYOND EARTH ORBIT CUBESAT MISSIONS

### 2.3.1. INTRODUCTION



HUMANITY is on the cusp of a new era of space exploration, ushered in by the advent of the CubeSat. Compared to conventional satellites, CubeSats cost less, weigh less, consume less power and have far shorter development cycles. Such characteristics also make CubeSats an alluring alternative to the conventional large, complex and expensive space exploration spacecraft. A quick comparison between the 2180 kg, $720 million Mars Reconnaissance Orbiter (MRO) (Graf et al., 2005) and the 13.5kg, $18.5 million Mars Cube One (MarCo) provides a clear example of why the space industry is so excited about BEOC missions. The overwhelming success of the MarCo mission, the first interplanetary Cubesat (Schoolcraft et al., 2017), has paved the way for a new fleet of interplanetary CubeSat missions, a few of which are mentioned in figure 5.8. These missions will enable a new age of exploration in our Solar system providing more accessible and affordable scientific information, as detailed in the Keck Institutes report titled *"Small Satellites: A Revolution in Space Science"* (Norton et al., 2014), as well as additional support for future manned missions. An excellent overview of BEOC missions is provided by Malphrus et al., 2021, outlining their unique advantages, requirements and challenges. An overview of how inflatable structures, and their inflation systems, can offer solutions to these unique challenges will be discussed in this section.

### 2.3.2. CHALLENGES

WHILE BEOCs can take advantage of the standardized CubeSat platform and the availability of a wide range of commercial components, designing them specifically to explore interplanetary space is an extremely challenging task. The main technological challenges facing the development of an interplanetary CubeSat include telecommunications, navigation, radiation hardening, power and propulsion. The literature study focused specifically on the challenges associated with deployable structures, namely telecommunications, power and propulsion. These challenges stem from the enormous distances from both the Earth and Sun that these spacecraft will have to travel to and operate in. Such requirements place a serious technological demand on these three subsystems that conventional LEO CubeSats do not have to consider and have, until recently, been the major stumbling block to BEOC missions.

- *Telecommunications:* The most significant hurdle to enabling BEOC missions is the telecommunications system. Typical CubeSat telecommunications systems operate on frequencies ranging from VHF to S-Band using low gain dipole, monopole or patch antennas (Babuscia et al., 2013). However, such systems are completely inadequate for interplanetary missions where high gain antennas (HGA) that operate at X-band and Ka-band frequencies are preferred due to the large distance and high data rates demanded (Cesarone et al., 2007). As gain is related to the antenna area, the volumetric constraints of the CubeSat necessitates the utilization of a deployable high gain antenna to meet these requirements.

- *Propulsion:* Propulsion systems that enable precise trajectory control and orbital maneuvering are essential to the success of stand alone interplanetary CubeSat missions. In order to meet these requirements, coupled with the difficulty in scaling down traditional propulsion systems, engineers have had to develop new alternative propulsion methods. Two of these systems were found to be of particular interest for inflatable structures are solar sails and solar thermal propulsion (STP).



- *Power:* BEOC's tend to have higher power requirements than their LEO counterparts due to the presence of both a propulsion system and more demanding telecommunication systems. Coupled with their increasing distance from the Sun, this puts significant strain on BEOC's electrical power systems. Given the issues with RTGs for small spacecraft and the limited efficiency of conventional photovoltaic solar arrays, alternative options may be required. One obvious option is to develop solar arrays with large collection areas, something for which inflatable structures may be well suited. Another option is to utilize solar concentrators to generate thermal or photovoltaic power.

### 2.3.3. Inflatable Structure Solutions

From examining the literature, it was established that inflatable structures have the potential to provide solutions to the different challenges facing BEOC missions. These solutions typically come in the form of two structural types; planar structures and curved structures.

#### Planar Structures

Planar structures are typically large, flat and thin structures that can be utilized for a variety of applications. They generally take the form of a thin membrane supported and tensioned by a high pressure inflatable support structure. They're simplicity and scalability are their most attractive features and make them suitable for applications requiring large areas. This large size enables them to maximize the quantity of radiation they receive/reflect making them ideal candidates for solar sails, solar arrays and antennas.

- *Telecommunications:* Planar antennas are composed of a thin flat or slightly curved reflecting surface and are the most common form of BEOC HGA to date (Chahat, Arya, et al., 2020; Chahat, Decrossas, et al., 2020; Hodges et al., 2015) . Their flat surface reflects an incident field directed via a feed from the spacecraft. While no inflatable planar antenna has yet been proposed for CubeSat applications, much research has been carried out into their development (Fang et al., 2002; Fang et al., 2008; Huang, 2001; Liu et al., 2017). Their ability to achieve larger areas and thus higher gain than other deployable reflectarrays (Arya et al., 2019) makes them very attractive. For example, a 10.5-m planar HGA would provide a 50 x increase in data volume transmission capability compared to current interplanetary spacecraft which typically fly a 1.5-m HGA (Cesarone et al., 2007).

- *Propulsion:* Planar structures can provide an alternative form of propulsion to conventional propulsion systems in the form of a solar sail. These must be large thin structures due to the low area density of the momentum provided by incident photons. Despite the gentle thrust provided by these photons, their persistent nature can eventually accelerate the solar sail to speeds approaching 10% the speed of light. This revolutionary technology is a simple but elegant BEOC propulsion solution as evidenced by their use on recent missions (Johnson et al., 2015). The use of inflatable booms as a support structure has seen much attention due to their attractive mass and volume characteristics (Kezerashvili et al., 2021; Lichodziejewski et al., 2003; Underwood et al., 2019).

- *Power:* Planar solar arrays are the most common form of power generation system on board CubeSats. However, conventional systems have a number of significant drawbacks including mass, volume and most significantly, limited efficiency. This necessitates that solar arrays be relatively large compared to the spacecraft in order to meet its power requirements. The relationship between solar array size and power generated is directly proportional to the solar flux, which decreases with increasing distance from the sun. The lightweight and scalable nature of inflatable solar arrays enables the development of large lightweight solar arrays that provide an attractive solution to the challenges associated with conventional systems (Cadogan and Lin, 1999; Johnson et al., 2014; Veal, 1991).

### CURVED STRUCTURES

Curved structures are typically large low pressure inflatable structures that come in either parabolic or spherical shapes. Their curved shape enables engineers to focus incoming radiation onto small areas thus enabling far more compact systems than their planar counterparts. This ability to focus incoming radiation is extremely beneficial for telecommunication application as well as for power and propulsion applications. Given this ability can be employed across all three applications, inflatable curved structures can also be utilized as hybrid structures that can provide the different functions in a single unique system.

- *Telecommunications:* Curved reflectors, particularly parabolic reflector, are the most common structural form for HGA's. This is largely due to their higher efficiency and higher gain levels relative to planar antennas. However, these advantages typically come at the expense of a larger stowage volume and increased complexity. Nevertheless, the appeal of curved reflector antennas, which most commonly take the form of deployable mesh reflectors, has led to the development of numerous CubeSat antennas in recent years. Unsurprisingly, inflatable structures have long been earmarked as promising solution to these volume and complexity issues, and are some of the only inflatable structures to have flight heritage, notable structures including the ECHO balloons (Clemmons, 1964) and IAE (Freeland and Bilyeu, 1993). This promise is currently being explored by three different inflatable CubeSat HGA proposals, the CubeSat inflatable antenna concept led by JPL (Babuscia et al., 2020), the BEOC inflatable gregorian reflector being developed at MIT (Fenn et al., 2021) and most notably the CatSat inflatable antenna (Chandra et al., 2021) designed by FreeFall Aerospace which is due to fly this year.

- *Propulsion:* Curved inflatable structures in the form of solar concentrators have drawn consideration attention for their ability to enable the unique STP system. STP utilizes thermal concentration to heat a propellant to very high temperatures and generate thrust. It could provide a unique propulsion system that provides higher specific impulse than chemical propulsion systems, reducing system mass, coupled with higher thrust levels than electric propulsion systems, enabling faster trasnfer times. Such a system would play an enormous role in increasing the scope and range of missions that BEOC's could undertake. Inflatable concentration systems are seen as a key enabling technology for such systems. This is evident from the system optimization analysis for the STP concept in development at TU Delft carried out by (Leverone, Cervone, et al., 2020). However, the literature to date on such systems is still quite limited, particularly for BEOC STP applications. At the time of writing, there are currently no systems in development that the author is aware of.

- *Power:* Solar concentrators offer an attractive alternative to the inefficient solar arrays. Typically taking the form of a parabolic reflector or of a fresnel lens, they can be utilized for two different types of power generation system, thermal concentration and photovoltaic concentration. Thermal concentration is utilized to generate power by using thermo-dynamic conversion devices such as a brayton, rankine or stirling cycle engine (Grossman and Williams, 1990; Leverone, Pini, et al., 2020). Photovoltaic systems, on the other hand, can be utilized to improve the efficiency of traditional solar power generation systems. While a promising solution for addressing BEOC power applications, to date, the use of inflatable solar concentrators for power generation is least explored of the three applications. This is partly due to the exciting potential of utilizing the solar concentration concept for propulsion systems.

- *Hybrid:* The main design characteristics for an inflatable curved reflector are relatively consistent across the three applications. This is not only true in terms of shape and function but also with respect to more detailed parameters such as materials. This gives rise to the multi-functional hybrid inflatable reflector. The potential of such a hybrid reflector is incredibly enticing and has already been explored for at least two large inflatable concepts (Lichodziejewski and Cassapakis, 1999; Redell et al., 2005) as well as for BEOC applications as part of a NASA Innovative Advanced Concepts (NIAC) task. Such a BEOC inflatable hybrid reflector could enable outer solar system missions that are 1/10th the cost and mass of conventional deep space missions (Staehle et al., 2020). However, while promising such systems are still only at the conceptual level.

### SUMMARY

It is evident that inflatable space structures can provide a range of solutions for the challenges of telecommunications, power and propulsion. Due to their use of high pressure support structures to support and tension the planar membrane, planar structures shall be categorized as high pressure structures, while their curved counterparts, despite sometimes also utilize high pressure support structures, can typically be categorized as low pressure structures. While planar inflatable structures hold promise, from the overview provided it can be established that curved inflatable structures offer greater potential for satisfying these challenges. This is perhaps best epitomized by the exciting hybrid reflector concept that could address all three challenges in one unique system.

### 2.3.4. CONCLUSION

In order to ensure that this thesis explored a suitable design for a BEOC inflatable space structure, and most importantly its inflation system, the design concepts, figure A.1, are proposed. They are accompanied by estimates of their TRL's. This overview serves to highlight the exciting potential inflatable space structures have for enhancing and enabling the development of revolutionary BEOC missions. In addition, as noted in section 2.4, the development of optimally suited inflation systems shall contribute to realising this potential.

## 2.4. INFLATION SYSTEMS

### 2.4.1. INTRODUCTION

THE inflation system is, unsurprisingly, a key component for enabling the success of an inflatable structure. Given that this inflation system plays an integral role in the successful deployment of the inflatable reflector, it is vital to ensure that it can provide a suitably controlled gas delivery. This is particularly true for BEOC inflatable reflectors, whose high surface accuracies require a precise and controlled deployment. Should the inflation system fail to ensure a successful deployment a reduced reflector performance and/or mission failure shall result. Given the essential role that they play in ensuring the inflatable structures successful operation, inflation systems have received surprisingly little attention relative to the other aspects of inflatable structures, with the majority of proposed systems relying on bulky adapted cold gas propulsion technology. While the reasons for this may be speculated on, it is likely that demand for simple, reliable and controllable inflation systems suitable for CubeSat inflatable applications will rise in the coming years as interest in such structures grows. This need for an optimized CubeSat inflation system is further emphasized by the role it shall play in enabling the development of BEOC missions.

In order to address this need, the literature study explored the potential suitability of utilizing micropropulsion technology in the development of an inflation system designed specifically for BEOC inflatable applications requiring a controlled and precise inflation process. In this pursuit, a variety of different systems inspired by both conventional inflation systems and current micropropulsion technology have been investigated. They shall be elaborated on hereafter.

### 2.4.2. INFLATION SYSTEM DESIGN CONSIDERATIONS

INFLATION as a means of deployment and structural support provides unique challenges for the development of inflatable space structures. As has been noted one of the main concerns is ensuring a precise and controlled inflation process, which is essential for BEOC inflatable reflector applications. In addition, challenges also arise from the desired stabilization method chosen, be it pressure maintenance for pressure stabilization or venting for rigidization. Addressing these challenges is exacerbated by the additional constraints imposed when considering BEOC missions. Given their limited size constraints as well as their large distances from Earth, these missions place extremely demanding requirements on the design of the inflation system, in terms of storage, reliability and size. A summary of these vital design considerations are as follows:

- Highly reliable and predictable deployment
- Limited mass requirements
- Limited volume requirements
- Suitable gas characteristics
- Long storage life
- Compatibility with stabilization method

### 2.4.3. TYPES OF INFLATION SYSTEMS

DESPITE the limited literature, a variety of different inflation system types have been utilized and proposed for inflatable space applications. This section shall provide an overview of these different systems types, highlighting those that may be suitably adapted with micropropulsion technology as well exploring potential systems that utilize, and are inspired by, micropropulsion technology.

#### INFLATION SYSTEM CATEGORIES

Inflation systems can be categorised into three different groups. These categories were identified by exploring both terrestrial and space operated systems.

- *Cold Gas Systems*
  - Cold gas systems have traditionally been the most popular category of inflation system for inflatable space structures. This is largely down to their attractive gas flow characteristics and extensive flight heritage as ADCS and pressurization systems, with the majority of proposed inflatable space structures to date relying on adapted cold gas systems
- *Chemical Gas Generation Systems*
  - Building on proven technology has also seen the exploration of chemical gas generation systems. These systems provide inflation via the chemical reaction of liquid and/or solid reactants which can be stored at low pressures, typically yielding mass and volume savings compared to cold gas systems. Such systems are commonly seen in terrestrial applications like automotive airbags and fire extinguishers as well as turbine drivers in large pump-fed launch vehicle propulsion systems.
- *Physical Phase Change Systems*
  - The finally category of design candidates are the physical phase change systems. These systems rely on changing the physical form, but not the chemical composition, of the propellant in order to generate inflation gas. This is the least developed category of inflation system

#### COLD GAS SYSTEMS

The most popular method for inflating inflatable space structures to date, these systems have largely consisted of either simple compressed gas cylinders, as used for ECHO I (Clemmons, 1964), or adapted conventional cold gas propulsion systems, as used for the IAE (Freeland and Bilyeu, 1993). Exploring both of these options as well as cold gas micropropulsion systems, which are the most mature form of micropropulsion system, two distinct types of cold gas inflation system were identified. These types are derived from the two different types of gas pressurization system, those that utilize blow down tanks and those that utilize regulated tanks. While both options are promising the use of pressurized tanks and the associated mass and volume requirements is seen as a drawback.

**Blow Down Systems**

The defining feature of a blow down system is that it consists of a single tank containing the pressurized inflatant. As the tank empties, the pressure on the inflatant decreases. The way this decrease in tank pressure is managed gives rise to two different forms of cold gas blow down system.

- *Straight Blow Down*
  - This is the simpler of the two forms, negating the use of pressure reduction/regulation. Thus, as the tank pressure decreases, the mass flow rate shall decrease leading to a drop in system performance. These systems have commonly utilized in the form of compressed gas cylinders for inflation purposes (Clemmons, 1964; Nakasuka et al., 2009; Nock et al., 2010).
  - In terms of micropropulsion technology, they are typically preferred for MEMS cold gas micropropulsion systems as they provide a simpler and less bulky option relative to regulated systems.
- *Regulated Blow Down*
  - The more typical form of a blow down tank system utilizes a pressure regulation system, enabling to provide a consistant performance despite the drop in tank pressure. These systems are the commonly utilized inflation system and are typically found among adapted cold gas propulsion systems (Freeland and Bilyeu, 1993; Lester et al., 2000; Thunnissen et al., 1995).
  - In terms of micropropulsion technology, these systems are a popular form of cold gas micropropulsion system and are one of the few micropropulsion systems identified whose promise as a CubeSat inflation system has already been demonstrated, with the AeroCube-3 inflatable balloon utilizing the MEMS PICOSAT Inspector (MEPSI). Indeed, Hinkley, 2008 clearly notes, “This same technology (micropropulsion regulated blow down system) can be used for holding gas or fluid for inflating structures in space.” This shall be further emphasized by the utilization of a regulated blow down system on the CatSat spherical inflatable CubeSat reflector that shall be launched this year (Chandra et al., 2021).

**Regulated Systems**

A regulated cold gas system consists of a inflatant tank that is pressurized by a separate high pressure pressurant tank. The flow of the pressurant is regulated so as to ensure a constant pressure in the inflatant tank resulting in a consistant performance throughout the operational lifespan of the system. These systems are significantly more complex than their blow down counterparts due to the requirement for a separate pressurant tank, explaining their relative unpopularity as both an inflation system and as a cold gas micropropulsion system. This is evidenced by the fact that only a single such inflation system could be found in the literature (Thunnissen et al., 1995).

### Chemical Gas Generation Systems

While less common than their cold gas counterparts, the potential mass and volume savings offered by chemical gas generation systems makes them a promising option for CubeSat inflation systems, especially when compared to the bulky cold gas systems. Three types of chemical gas generation system were identified which are derived from the method used to stow the inflation gas. They are solid, liquid and alternative.

**Solid Propellant Gas Generators**

Solid propellant gas generators (SPGG) are effectively small solid rocket motors. They operate by consuming a solid propellant grain, producing an inflation gas with a specified temperature, pressure and mass flow. SPGGs are the most commonly used form of gas generator and are popular for their simplicity, low cost and compact packaging. Storing the inflation gas as a solid grain is particularly beneficial for BEOC missions as it enables long term storage without the disadvantages associated with leakage or pressure. However, they tend to suffer from a rapid blow down operation. They are typically categorized into two groups according to the temperature of the gas stream generated, warm gas generators and cool gas generators.

- *Warm Gas Generators*
  - Warm gas generator (WGG), also referred to as a ‘pyrotechnic’ generator, ignite the solid propellant with the ensuing combustion process creating a hot gas at temperatures exceeding 700 K (Van Der List et al., 2004). While the operational temperature of these systems is typically limited to about 2000 K, the flame temperature of some WGG can exceed 3000 K.
  - A deviant on the conventional WGG, known as low temperature gas generators (LTGG), utilize coolant systems to reduce these high gas temperatures as well as remove particulates from the flow. Such a system was utilized for inflating the Mars Pathfinder landing airbags and produced gas temperatures between 550 K and 650 K (McGrath et al., 1998). Recent years has seen the development of systems with further temperature reductions, the most promising of which is is an LTGG spacecraft inflation system developed by Han et al., 2021.
  - Unsurprisingly, these warm gas generators are not a popular form of micropropulsion system although the system developed by Han et al., 2021 does show promise for CubeSat applications.
- *Cool Gas Generators*
  - Unlike their warm counterparts, solid propellant cool gas generators (CGG) produce a pure gas at ambient temperature. Coupled with their low mass and volume requirements, this makes them an attractive option for for CubeSat inflation systems. However, their rapid blow down nature is a distinct drawback. Two forms of the CGG system were identified, CGG straight and CGG refill.

- CGG straight systems deliver inflation gas produced by the CGG directly into the inflatable structure. These systems are highly compact and have already been demonstrated for CubeSat inflation applications having been utilized for InflateSail (Underwood et al., 2019) and DebrisSat-1 (Forshaw et al., 2020). However, due to the rapid blow down nature of CGG's, these system has very limited inflation control.
- The CGG refill systems yields a far more controllable inflation system and is based on a micropropulsion system utilized for the COGEX (Santandrea et al., 2013) and $T^3\mu PS$ (Migliaccio et al., 2010) systems. The system, which is also explored by Van Der List et al., 2004, consists of a number of CGG's connected to a plenum. When the system is initialized the first CGG is activated and releases gas filling the plenum. The gas then travels from this plenum to the nozzle. As the gas in the plenum is depleted, the pressure shall drop accordingly. When the pressure reaches a certain value, the next CGG is activated refilling the plenum to a certain pressure. This process shall enable a slower and more controlled inflation process. While it has no heritage as an inflation system, it has been proposed by Konstantinidis and Forstner, 2013 to inflate the Martian hypersonic inflatable drag balloon.

**Liquid Propellant Gas Generation System**

These systems were identified as a potential inflation system due to their potential mass and volume savings as well as their heritage as both conventional propulsion and micropropulsion systems. For the purposes of this investigation, two categories of liquid propellant gas generation system were distinguished, mono-propellant and bi-propellant systems.

- *Mono-propellant Systems*
  - Monopropellant systems operate by running a propellant over a catalyst where it decomposes exothermically, generating gas at high pressures and temperatures. Among the most popular chemical propulsion system, they have been used extensively across conventional spacecraft as attitude control thrusters as well as in the development of numerous micropropulsion systems. However, the hazardous characteristics of the propellants utilized in these systems is seen as a distinct disadvantage for inflation purposes, where avoiding damage to the membrane is of critical importance.
- *Bi-propellant Systems*
  - These same gas characteristics are also common among bi-propellant systems, whose additional complexity already marks them as an unattractive option. However, there is one interesting variation that may hold promise. The micropropulsion HYDROS thruster developed by Tethers Unlimited (James et al., 2017) could be utilized to develop an inflation system that stores liquid water until inflation at which point it can produce a controlled rate of hydrogen and/or oxygen inflation gas without the need for high temperatures or high pressure storage.

**Alternative Gas Generation System**
Given the relative lack of research into inflation systems for inflatable space structures it is not surprising that only a limited number of conventional gas generation systems have been explored. However, two additional systems have been identified that utilize relatively new gas generating technology.

- *Metal Hydrides*
  - Metal hydride alloys are capable of storing large amounts of hydrogen, approximately 1000 times the volume of the alloys themselves (Ino et al., 2015; Jain, 2009), the release of which can be carefully managed. They also the unique ability to be able to reabsorb the gas if desired. This could be beneficial for precision inflatable structures. However, due to their low TRL significant research and development would be required before they could be considered a viable option for BEOC inflatable structures.
- *Solid-state gas generator*
  - The Solid State Inflation Balloon deorbiter (SSIB) has been developed by the University of Arkansas and NASA (Roddy and Huang, 2019). The inflation system, which shall be utilized by the ArkSat CubeSats, utilises an MEMS device called the Solid-State Gas Generator (SSGG) which creates nitrogen gas on-demand by thermally decomposing sodium azide crystals. This advanced system could provide a potential option for BEOC inflation systems, although given its a relatively new development the available literature is still quite limited. One major drawback is that the quantity of gas that it can produce, at present, is quite limited.

### PHASE CHANGE SYSTEMS
The least common of the three categories of inflation system, physical phase change systems are most commonly found in the form of sublimation systems. However, liquid vaporization systems are also identified as a potential avenue for micropropulsion based inflation systems.

**Sublimation**
Solid sublimation systems are the least complex inflation system currently available. Two forms of the system have been distinguished. Conventional and controlled.

- *Conventional Sublimation*
  - These systems utilize passive sublimating powders stored inside the inflatable structure which upon exposure to the high vacuum of space change directly from solid to vapor thus inflating the structure. This relatively straight forward process negates the need for active inflation hardware and is thus simple and has minimal onboard mass and volume requirements. This makes it an attractive option for CubeSat inflation systems, as seen in the development of the inflatable CubeSat antenna project at JPL (Babuscia et al., 2020). However, the system is inherently uncontrollable which is a major drawback.

- *Controlled Sublimation*
  - In order to overcome the uncontrolled nature of the conventional sublimation system, Fenn et al., 2021 has proposed the use of a controllable sublimation system. This would involve storing the sublimating powders externally to the inflatable structure, enabling the release of gas to be controlled through small variations in the storage temperature/pressure. How the actuation of such a system would work requires extensive research and development

**Vaporization**
This type of inflation system, inspired by resistojet micropropulsion technology, would utilize a heating element to vaporize the inflatant which is stored as a liquid. While this system may offer attractive volume and mass characteristics relative to a comparable cold gas system, the increased temperature of the gas jet is likely drawback.

### BIMODAL INFLATION SYSTEM
All of the systems presented here were noted as solely inflation systems. However, it is also feasible to consider that a bimodal micropropulsion system could be developed. These systems could enable the development of 'propulsion-inflation' systems as is explored by Thunnissen et al., 1995 and by Griebel, 2011, who designs a propulsion-inflation system for a Mars inflatable drag balloon. Given both the high surface accuracy requirements and high precision pointing requirements of a BEOC inflatable reflector, a system that could provide both precise inflation and ADCS into one system could be highly advantageous. In addition, as pointed out by Thunnissen et al., 1995 and Griebel, 2011, incorporating the inflation system into an existing propulsion system can increase the volumetric efficiency of the system. Systems such as the VACCO hybrid MiPS, which combines green monopropellant and cold gas propulsion into one system, for the BEOC ArgoMoon (VACCO, 2012) mission serve as an example of the potential suitability of micropropulsion technology for the development a BEOC propulsion-inflation system.

### SUMMARY
This investigation identified a wide variety of potential micropropulsion based inflation systems. Cold gas systems, while having the largest mass and volume requirements, likely offer the most attractive solution thanks to their desirable gas characteristics and high degree of control. Of the the chemical gas generation systems, the solid propellant generators that provide low gas temperatures provide the most potential, with most of the other systems suffering from undesirable gas characteristics and/or limited heritage. The phase change systems while promising also suffer from limited heritage, while in the case of conventional sublimation the inherently uncontrolled nature of the system is unattractive. Finally, their is also the option of providing a bimodal system that combines the propulsion and inflation functions desired by a BEOC into a single system. This system could be highly advantageous.

### 2.4.4. CONCLUSION

In order to ensure that this thesis explores a suitable design for a BEOC inflation system the following design concepts, shown in figure B.1, are proposed. Each of these proposed candidates are deemed to have promising potential based on the design considerations previously outlined in section 2.4.2.

The variety of proposed concepts clearly shows that micropropulsion technology provides an extensive range of viable inflation system options that can be utilized the development of a BEOC inflation system. How each of these concepts meets the desired requirements for a controlled and precise BEOC inflation system shall be discussed in section 8.

## 2.5. CONCLUSION

The aim of this chapter is to provide a recap of the literature study and its findings. The key design considerations that must be accounted for in the successful design of the inflatable structure are identified and their potential impact on the inflation system is explored. Following this the exciting potential of inflatable space structures, most notably in the form of reflectors, for enabling the development of revolutionary BEOC missions is investigated. This investigation, which in conjunction to the importance of the inflation system already noted, emphasises the key contribution the design of an optimized system has to the advancement of not only inflatable space structures, but the space industry as a whole. Finally, the development of such an inflation system is explored, with the potential of micropropulsion technology for providing an optimized solution clearly demonstrated.

# 3

# THESIS FRAMEWORK

*This chapter provides a description of the framework that shall be utilized to carry out this thesis project. This entails first identifying the need for the research carried out in the thesis (section 3.1), followed by the generation of suitable research questions (section 3.2) and finally specifying the tasks and objectives required to answer these questions (section 3.3.)*

3

## 3.1. NEEDS AND OPPORTUNITIES

This section shall outline the needs and opportunities of the thesis as derived from the literature review.

**Need Statement**
*In order to enable the development of inflatable reflectors for beyond Earth orbit CubeSat missions, there is a need for suitable and controllable inflation systems.*

Following the logic of developing inflation systems adapted from propulsion technology, the literature study verified that micropropulsion technology could be successfully utilized in the development of new inflation systems suitable for BEOC inflatable reflector applications. Therefore, the mission statement for this thesis project can be given as follows:

**Mission Statement**
*The goal of this work is to design a micropropulsion based inflation system that provides a suitable and controllable inflation process for inflatable reflectors utilized in beyond Earth orbit CubeSat missions*

## 3.2. RESEARCH QUESTIONS

In order to guide the work done throughout the duration of the thesis a main research question shall be formulated followed by a series of sub-questions that will be used to define the necessary tasks to completed during the thesis.

### MAIN RESEARCH QUESTION

*What are the design adjustments required in order to adapt current micropropulsion technology so that it can be utilized in the development of a controllable inflation system for beyond Earth orbit CubeSat inflatable reflectors?*

In order to answer this research question the following sub-questions should be addressed.

### 1. WHAT ARE THE DESIGN CHARACTERISTICS OF THE BEOC INFLATABLE REFLECTOR?

Before designing an inflation system for a BEOC inflatable reflector it is first necessary to define the design characteristics of the inflatable reflector. As discussed in this literature review, the main design considerations that must be explored include:

- The function(s) of the inflatable reflector
- The geometry of the inflated structure
- The packaging method
- The deployment method

- The stabilization method
- The membrane material
- The fabrication method
- The thermal properties of the structure
- The mechanical properties of the structure



### 2. What are the design characteristics of the inflation system?

Once the design of the inflatable reflector has been completed the performance requirements for the inflation system can be generated. These requirements, coupled with the CubeSat constraints, will dictate the design of the inflation system. The main design considerations that must be explored include:

- The inflation system type
- The choice of inflation scheme
- The choice of inflatant
- The inflator nozzle
- The inflatant storage and pressurization system
- The inflatant feed system

### 3. What is the theoretical performance of the inflation system?

In order to determine if the design of the inflation system suitably meets the generated performance requirements, it is important to understand its performance characteristics. The key inflation performance characteristics that must be evaluated include:

- The mass flow rate of the inflating gases
- The velocity of the inflating gases
- The temperature of the inflating gases
- The rate of inflation
- The mass of the inflation system
- The volume of the inflation system

## 3.3. Research Objectives and Tasks

The research questions listed above can be utilized to define the research objectives and necessary tasks that need to be completed throughout the project. These tasks shall also be related to the structure and layout of the thesis work.

### OBJECTIVE 1 - DESIGN INFLATABLE REFLECTOR

In order to answer the first research question, it is necessary to design a BEOC inflatable reflector. This objective can be achieved by fulfilling the following tasks.

- Carry out trade off of BEOC inflatable reflector concepts presented in literature review
- Generate list of performance criteria based on chosen concept
- Convert criteria to list of requirements
- Develop design plan
- Utilize appropriate tools/methods to design the chosen concept
- Check if the design fulfils requirements

### OBJECTIVE 2 - DESIGN INFLATION SYSTEM

In order to answer the second research question, it is necessary to design the inflation system. This objective can be achieved by fulfilling the following tasks.

- Generate list of performance criteria based on the design of the inflatable reflector and the key design requirements for BEOC inflation systems developed in the literature review
- Convert criteria to list of requirements
- Carry out trade off of inflation systems presented in the literature review
- Identify and/or develop tools/methods appropriate to design chosen concept
- Develop design plan
- Utilize appropriate tools/methods to design the chosen concept

### OBJECTIVE 3 - EVALUATE INFLATION SYSTEM THEORETICAL PERFORMANCE

In order to answer the third research question, it is necessary to evaluate the theoretical performance of the designed inflation system. This objective can be achieved by fulfilling the following tasks.

- Utilizing the appropriate tools identified in objective 2, check if the theoretical performance of the designed inflation system fulfils the performance criteria.
- If the performance does not meet the desired requirements, return to objective 2 and modify the design. Else present results

# 4

# Requirements Generation

*This chapter provides a preliminary systems engineering analysis which resulted in the identification of the stakeholders (4.2), the desired system functions (4.3), the system requirements (4.4) and finally the system constraints (4.6). The systems engineering approach followed in this chapter is based on the guidelines presented in the book "Systems Engineering Fundamentals" (Lightsey, 2001).*

## 4.1. INTRODUCTION

A vital first step in the development of this thesis project is the requirement generation process. These requirements will guide the design of the inflatable system and will provide the backbone on which the success of the project shall be measured. In order to begin the requirement generation process, the project expectations must first be defined. They are derived from the need and mission statements (section 3) and stem from an operational deficiency in the field of inflation systems for inflatable space structures, more specifically those that can enable and enhance the development of BEOC missions. They can be neatly summarized in the following statements:

- Provide suitable and controllable inflation to a BEOC inflatable reflector
- Adapt current micro-propulsion technology in the pursuit of this goal.

These expectations shall lay the groundwork for the project and will be utilized to identify the relevant stakeholders, the desired functions the system must perform and the requirements that describe what the project is to achieve.

## 4.2. STAKEHOLDERS

In order to translate these project expectations into a more complete set of qualitative and quantitative expectations and requirements, the relevant stakeholders are identified. These stakeholders, both active and passive, are introduced in table 4.1 and are ranked in accordance with their relevance to and/or level of interaction with the project.

| **ID** | **Category** | **Stakeholder** | **Rationale** |
|---|---|---|---|
| STK-A-01 | Active | Researcher | The main stakeholder of the project. Responsible for the design and verification of the inflatable system. |
| STK-A-02 | Active | BEOC Reference Mission(s) | The reference mission(s) will affect the design parameters of the inflatable system. |
| STK-A-03 | Active | Support Companies | External companies can join the project to support and/or advise during its different phases. |
| STK-P-01 | Passive | TU Delft Space Engineering Supervisor | The Space Engineering supervisor plays a supportive and advisory role for the project. |
| STK-P-02 | Passive | TU Delft Aerospace Structures and Materials Supervisor | The Aerospace Structures and Materials supervisor plays a supportive and advisory role for the project. |

| | | | |
|---|---|---|---|
| STK-P-03 | Passive | Space Structures Industry | The space structures industry and particularly those companies/institutions focused on the development of inflatable space structures could benefit from the results of this project. |
| STK-P-04 | Passive | CubeSat Industry | The CubeSat Industry and particularly the beyond Earth orbit CubeSat and micropropulsion industries could benefit from the results of this project. |

Table 4.1: Project Stakeholders

The stakeholders have a significant impact on the project as they're expectations dictate what the functionality of the project shall look like. It is important to note, as is described in the research objectives (section 3.3), that in order meet the project and stakeholder expectations of designing a micropropulsion based inflation system for a BEOC inflatable reflector it is necessary to first design the inflatable reflector itself. This is because the performance requirements for the inflation system are dependent on the design parameters of this reflector. The coupled system will be referred to as the 'inflatable system' and its functionalities are described in the next section.

## 4.3. INFLATABLE SYSTEM FUNCTIONS

The basis for the derivation of an accurate requirement analysis starts with figuring out exactly what the inflatable system must do. The functions that the system must perform stem from the project and stakeholder expectations and describe the necessary functionality that the system must have in order for the project to be deemed successful. The top level function blocks that the system must perform are identified in figure 4.1.

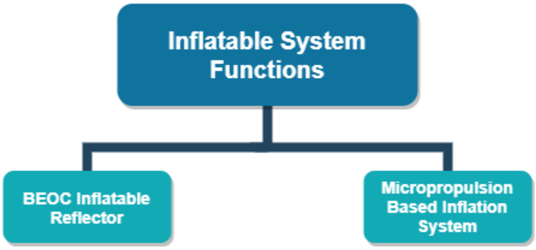


Figure 4.1: Top Level Function Blocks of the Inflatable System

As can be seen, the inflatable system must perform the functions of both a BEOC inflatable reflector and a micropropulsion based inflation system. In order to carry out a requirement analysis, it is necessary to expand on each of these functions so that there is a clear understanding of what the system must do. This can be seen in table 4.2, with FUNC-IR-# and FUNC-IS-# representing BEOC inflatable reflector and micropropulsion based inflation system respectively.

| ID | Stakeholder(s) | Function |
|---|---|---|
| FUNC-IR-01 | STK-A-01, STK-P-03 | Provide approximation of current inflatable reflector technology |
| FUNC-IR-02 | STK-A-02, STK-P-03, STK-P-04 | Provide reflector suitable for BEOC application |
| FUNC-IS-01 | STK-P-03 | Inflate the Inflatable Reflector |
| FUNC-IS-01-01 | STK-A-01, STK-P-03 | Provide regulated and controllable inflation flow rate |
| FUNC-IS-01-02 | STK-A-01, STK-P-03 | Provide inflation process compatible with selected stabilization method |

Table 4.2: Inflatable System Functions Expanded

## 4.4. REQUIREMENT ANALYSIS

Now that the top level functions of the system have been defined, the questions of how well, and in which environment, the functions must be performed can be put forward. These questions provide the basis for the development of the list of requirements generated for this project. They are known as the performance and interface requirements respectively. These requirements are generated for both function blocks along with some general interface requirements relating to the systems compatibility with the BEOC mission are generated.

### 4.4.1. BEOC MISSION INTERFACE REQUIREMENTS

| ID | Requirement | Rationale |
|---|---|---|
| REQ-BEOC-01 | The total (volume) footprint of the inflatable system shall be less than 25% of the total volume of a 12U CubeSat (3U) | One of the most attractive features of inflatable structures are their low volume requirements. In order to maximize this advantage relative to other conventional systems, notably the KaTENNa Antenna, it is important that the volume of the inflatable system be equal to or less such systems. See table C.2. This is particularly important for BEOC missions with their limited volume budgets. This requirement is also driven by the LUMIO payload volume (see section 5.4.2) |

| | | |
|---|---|---|
| REQ-BEOC-02 | The total mass of the inflatable system shall be less than 2.5 kg | One of the most attractive features of inflatable structures are their super lightweight nature. In order to maximize this advantage relative to other conventional systems it is important that the mass of the inflatable system be kept to a minimum. This is particularly important for BEOC missions with their limited mass budgets. This requirement is driven by the mass requirement for the state of the art KaTENna Parabolic mesh reflector, see table C.2 |
| REQ-BEOC-03 | The total power requirements of the inflatable system shall be less than 60 W | This value is derived from the power budget for the reference LUMIO mission. It is expected that during inflation most of the available spacecraft power, except that required for ADCS, can be utilized. This is based on the assumption that apart from ADCS the majority of the subsystems on board the CubeSat are not operational during deployment. |
| REQ-BEOC-04 | The inflatable system shall be suitable for a BEOC demonstration mission of 407 days | Given the extended lifespan of BEOC missions, it is desired that the inflatable system be capable of functioning for the duration of the demonstration missions lifespan. This requirement is derived from the LUMIO mission parameters (see section 5.4.2) |
| REQ-BEOC-04-01 | The inflatable system shall perform without hindrance after the 14 day transit time | Given the long transit times of BEOC missions, long duration stowage of the inflatable system will be necessary. It is imperative that the inflation system and inflatable structure operate as designed so as to ensure an accurate deployment. Failure to do so could lead to mission failure. This requirement is derived from the LUMIO mission parameters |
| REQ-BEOC-04-02 | The inflatable system shall withstand the space environment for the 393 days duration of its operational lifespan | The inflatable system must withstand the space environment in order to perform its required application for as long as required by the BEOC mission. This requirement is derived from the LUMIO mission parameters |

4

Table 4.3: BEOC Requirements

### 4.4.2. BEOC INFLATABLE REFLECTOR REQUIREMENTS

| ID | Requirement | Rationale |
|---|---|---|
| REQ-IRP-01 | The deployed area of the inflatable structure shall be 0.785 $m^2$ | The size of the deployed inflatable reflector has an important bearing on the performance of the reflector for all three BEOC applications. In order to compete with the high performing conventional structures, it is desired that the inflatable reflector provide a deployed area of at least comparable size. This requirement stems from the KaTENna parabolic mesh reflector, see table C.2. |
| REQ-IRP-02 | The inflatable structure shall have a rms error below TBD [mm] | The rms error refers to the shape error of the reflector with respect to the ideal geometry. For BEOC applications, high accuracy surface accuracies are required and thus the rms error should be kept to a minimum |
| REQ-IRI-01 | The structural shape of the inflatable structure shall be curved so as to maximize its potential for enabling and enhancing the development of BEOC missions | In the literature review it was established that curved inflatable reflectors offer more potential for overcoming the BEOC challenges of telecommunications, power and propulsion than their planar counterparts. This is true not only with respect to their performance characteristics, but also with respect to their role as a key enabling technology for exciting BEOC technologies such as STP and Hybrid reflectors (Dunbar, 2021) |

| | | |
|---|---|---|
| REQ-IRI-02 | The inflatable structures architecture shall utilize a single category of inflatable structure | The main aim of the inflatable reflector is to provide a suitable approximation of inflatable reflectors in order to enable the design and validation of micro propulsion based inflation system. It is therefore desirable that the complexity of the structure be kept to a minimum. This can be achieved by designing a reflector that utilizes a single category of inflatable structure as identified in the literature study (Dunbar, 2021). It will consist of either a high pressure 'heavy duty' inflatable structure or a low pressure 'lightly loaded' structure but not both. |
| REQ-IRI-03 | The structure shall consist of a transparent canopy and an interior reflector | As is clearly stated in the mission statement, the goal of this thesis is to design an inflation system for inflatable reflectors utilized in BEOC missions. Given requirements REQ-IRI-01 and REQ-IRI-02, a curved low pressure inflatable reflector shall be designed in this thesis (section 5). These structures consists of a transparent canopy to allow radiation to pass through and an inner reflective surface to act as the reflector. |
| REQ-IRI-04 | The reflector packaging efficiency (RPE) of the inflatable structure shall be at least $1.5m^2/U$ | This requirement derives from the minimum RPE (12 ft Sphere) of the spherical inflatable structures presented in table C.2. It can be seen from this table that the RPE (see equation 2.1) of inflatable structures is generally an order of magnitude higher than their mechanical counterparts. It is an important parameter for BEOC applications as a high RPE enables the stowage of high aperture inflatable reflectors within the limited volume constraints |

| | | |
|---|---|---|
| REQ-IRI-05 | The area density of the inflatable structure shall be less than $0.4 kg/m^2$ | This requirement derives from the maximum area density (12 ft Sphere) of the spherical inflatable structures presented in table C.2. It can be seen from this table that the area density of inflatable structures is generally an order of magnitude lower than their mechanical counterparts. It is an important parameter for BEOC applications as low area density enable the utilization of high aperture inflatable reflectors within the limited mass constraints |

4

Table 4.4: Inflatable Reflector Requirements

### 4.4.3. MICROPROPULSION BASED INFLATION SYSTEM REQUIREMENTS

| **ID** | **Requirement** | **Rationale** |
|---|---|---|
| REQ-ISP-01 | The inflation time shall take between 10 seconds and 100 seconds | The rate of inflation is the one of the most important performance parameters for the inflation system and can be derived from the desired inflation time. While the literature detailing inflation times is very limited, in general the inflation of inflatable space structures seems to take anywhere from a few seconds (small simple structures) to a few minutes (large complex structures). The reasoning for the selection of this inflation time frame range is discussed in section 7.5.1. |
| REQ-ISP-02 | The inflation system shall provide ascent venting | Ascent venting is an essential component for ensuring a reliable and controllable deployment. It allows residual gases trapped in the packaged structure to escape during the launch phase so as to not cause premature inflation and inhibit the deployment process. |

| | | |
|---|---|---|
| REQ-ISP-03 | The inflation system shall unfold the structure in a smooth controlled fashion | Moving the structure from its packaged state to its open/deployed state is the most important phase of the inflation process, particularly for freely deployed structures. If the initial inflation rate is too high, high stresses and accelerations could be induced in the unfolding structure leading to damage and an unpredictable deployment situation. |
| REQ-ISP-04 | The inflation system shall pressurize the inflatable structure to 15% of the inflatable membranes yield strength | The inflation system must be capable of producing the necessary pressure levels that remove wrinkles leftover from the packaging process and in turn inflate the reflector to its desired deployed state. |
| REQ-ISP-05 | The inflation system shall vent the structure to 2% of the inflatable membranes yield strength | The pressurization scheme chosen for the inflatable system entails venting the structure to a lower predetermined pressure post inflation. As discussed in section 6.7.3, this pressurization scheme is motivated by the desire to satisfy the mission statement as well for its similarity to the scheme used for rigidized structures. This shall enable the design of a system that shall be highly relevant to future missions. |
| REQ-ISP-06 | The inflation system shall provide pressure maintenance for the duration of the mission | As the structure is pressure stabilized, it shall leak gas due to micrometeroid punctures and membrane leakage. Make-up gas is required to counteract this. In addition, the system must be able to maintain the desired pressure as the structure undergoes thermal variations and the inflation gas expands and contracts. |

| | | |
|---|---|---|
| REQ-ISI-01 | The volume footprint of the inflation system shall be less than 1U. | As has been noted in REQ-BEOC-01, the total volume footprint of the inflatable system shall be less than 25% of the total volume of the 12U CubeSat, or 3U. However, determining an appropriate volume requirement for the inflation system is difficult due to the lack of detail regarding volume budgets for comparable structures found in the literature. Thus an estimate is made based off the analogous CatSat inflatable system where the inflation system is approximately 33% of the total inflatable deployment system (Chandra et al., 2021). |
| REQ-ISI-02 | The mass of the inflation system shall be less than 1 kg. | As has been noted in REQ-BEOC-02, the total mass of the inflatable system shall be less than 2.5 kg. An inflatable structure mass of 0.0677 kg (section 6), leaves 2.432kg for the ejection mechanism, inflation system and any additional equipment required. While, it is unlikely that the other major components shall have a mass greater than that of the inflation system, the uncertainty regarding these components, particularly in the case of those required for actual applications (e.g. antenna), means that a conservative mass requirement of 1kg for the inflation system shall be enforced. |
| REQ-ISI-03 | The power required for the inflation system shall be less than TBD | It is desired that the power requirements of the inflation system be kept to a minimum. Given the uncertainty regarding the power requirements for the ejection mechanism and any additional components this requirement is TBD. |
| REQ-ISI-04 | The inflation gas shall not impair the structural integrity of the inflatable membrane | This requirement is vital as not meeting it will more than likely result in mission failure. |

| | | |
|---|---|---|
| REQ-ISI-04-01 | The temperature of the inflation gas shall lie within the range of 160K to 430K | The temperature of the gas should be restricted in order to prevent damage to the inflatable membrane. The maximum acceptable temperature is dictated by the glass transition temperature of the polymer film used with an assumed safety margin of 25%. Given the lack of information regarding the interaction of low gas temperatures and the membrane, the minimum temperature shall be assumed based off the desire to maintain the inflation gas in its gaseous state. As such, the minimum acceptable temperature is dictated by the inflation gases critical temperature with an assumed safety margin of 25% (see 8.2.2). |
| REQ-ISI-04-02 | The inflation gas shall be non-hazardous | Hazardous inflation gases that are toxic, corrosive or chemically unstable should not be utilized as they will damage the inflatable membrane and possibly the inflation system. |
| REQ-ISI-04-03 | The inflation gas shall contain negligible particulates | Particulates in the gas flow are undesirable as they will cause degradation to the walls of the inflatable structure. |
| REQ-ISI-04-04 | The inflation gas jet velocity shall be less than Mach 1.5 | The gas jet velocity exiting the inflation nozzle shall not damage the material of the inflatable membrane. Given the gas exiting the throat is sonic (M=1), minimizing its increase as it expands through the nozzle is desirable. |

Table 4.5: Inflation System Requirements

## 4.5. KILLER AND KEY REQUIREMENTS

The next step in the requirement generation process is to identify the killer and key requirements. Identifying these requirements is an integral step in the concept generation process as they will be used in the identification of the design concepts most suitable for fulfilling the functional expectations during the trade off analysis.

### 4.5.1. KILLER REQUIREMENTS

Killer requirements are defined as requirements that are “uniquely tied to (the) success or failure” of the project (Gill, 2015). This success or failure is determined by the projects capacity to satisfy the need and mission statements as presented in section 4. Thus, these requirements are those that are most closely tied with the goal of designing a suitable and controllable inflation system for a BEOC inflatable reflector. With that in mind, the following requirements have been identified as the killer requirements for this project:



| ID | Requirement | Rationale |
|---|---|---|
| REQ-ISP-01 | The inflation time shall take between 10 seconds and 100 seconds | The deployment phase is the most important phase of an inflatable reflectors life. It must be carefully controlled in order to ensure the successful operation of the structure post deployment. Failure to do so will lead to reduced performance and/or mission failure. |
| REQ-ISI-04 | The inflation gas shall not impair the structural integrity of the inflatable membrane | The inflation gas characteristics must be carefully considered to avoid damaging the inflatable membrane. Failure to do so will lead to reduced performance and/or mission failure. |

Table 4.6: Killer Requirements

### 4.5.2. KEY REQUIREMENTS

Key requirements are those that drive the design process as they dictate the key desired characteristics of the inflatable system. The following requirements have been identified as the key requirements for this project:

| ID | Requirement | Rationale |
|---|---|---|

| | | |
|---|---|---|
| REQ-BEOC-01 | The total (volume) footprint of the inflatable system shall be less than 25% of the total volume of a 12U CubeSat (3U) | Due to the reduced performance efficiency of the inflatable reflector relative to conventional system, maximizing its minimal volume requirements is essential to ensuring it is a competitive and attractive alternative option. |
| REQ-BEOC-02 | The total mass of the inflatable system shall be less than 2.5 kg | Due to the reduced performance efficiency of the inflatable reflector relative to conventional systems (Dunbar, 2021), maximizing its minimal mass requirements is essential to ensuring it is a competitive and attractive alternative option. |
| REQ-BEOC-04 | The inflatable system shall be suitable for a BEOC demonstration mission of 407 days | To be suitable for long duration BEOC missions itis essential that the inflatable system be capable of long term operation |
| REQ-IRP-01 | The deployed area of the inflatable structure shall be greater than 0.785 $m^2$ | Due to the reduced performance efficiency of the inflatable reflector relative to conventional systems, maximizing its deployed area is essential to ensuring it is a competitive and attractive alternative option. |
| REQ-IRI-01 | The structural shape of the inflatable structure shall be curved so as to maximize its potential for enabling and enhancing the development of BEOC missions | Due to the challenges associated with BEOC reflector applications optimizing the performance of the inflatable reflector is essential. |
| REQ-IRI-02 | The inflatable structures architecture shall utilize a single category of inflatable structure | Due to the limited scope of this thesis project an inflatable reflector that consists of only one category of inflatable structure shall be designed |
| REQ-ISP-03 | The inflation system shall unfold the structure in a smooth controlled fashion | The unfolding phase is an integral aspect of the inflation process. Ensuring it is carefully controlled is essential for providing an optimal and successful deployment. |
| REQ-ISP-04 | The inflation system shall pressurize the inflatable structure to 15% of the inflatable membranes yield strength | Satisfying this requirement is essential for ensuring that wrinkling is removed from the reflector surface. Failure to do so shall lead to an uneven surface and reduced performance |

| | | |
|---|---|---|
| REQ-ISP-05 | The inflation system shall vent the structure to 2% of the inflatable membranes yield strength | Satisfying this requirement is essential to ensuring the relevance of the designed system for future inflatable reflectors that shall take advantage of advancements in rigidization techniques |
| REQ-ISP-06 | The inflation system shall provide pressure maintenance for the duration of the mission | Given that the structure is pressure stabilized, replenishing gas losses is essential for maintaining the structural integrity of the reflector |

Table 4.7: Key Requirements

4

## 4.6. CONSTRAINTS

In addition to the constraints imposed by the requirements generated in this section there are number of additional constraints that must also be considered. These constraints are derived from the design challenges associated with designing this inflatable system.

- Inflatable space structures lack of flight heritage.
  - Despite the revolutionary potential of inflatable space structures, up until this point, only a small number of missions have utilized them and of these the majority have been experimental demonstration missions. This low TRL shall invariably constrain this project given its limited scope.
- The lack of literature available on BEOC inflatable reflectors.
  - While inflatable reflectors offer exciting potential for addressing the telecommunications, power and propulsion challenges facing BEOC missions, the development of such structures is still in its infancy. In addition to this, the majority of inflatable space structure research to date has focused on high pressure load bearing inflatable structures with the literature on low pressure structures such as curved reflectors being relatively light in comparison.
- The lack of literature available on inflation systems for inflatable space structures.
  - Compared to other aspects of inflatable structures, inflation systems have received scant attention from the inflatable space structure industry (Dunbar, 2021). The limited research on these systems will inevitably act as a constraint for this project. This is particularly true for the use of micropropulsion technology in the development of CubeSat inflation systems.

Each of these constraints serve to highlight the difficulty in generating a well-performing and innovative inflatable system design. Coupled with the limited time and research constraints of a Masters Thesis, these constraints will inevitably limit the scope and completeness of the finalized design.

# Bibliography

Chandra, A., Pat, T., Tonazzi, J. C. L., & Walker, C. K. (2021). Development and flight qualification of a small satellite x-band spherical membrane antenna. *2021 IEEE Aerospace Conference (50100)*, 1–8.

Dunbar, S. (2021). Literature review study - inflatable space structures, beyond earth orbit cubesat missions and micropropulsion inflation systems.

Gill, E. (2015). Generating , evaluating and selecting concepts. In *Ae4s12 space systems engineering*.

Lightsey, B. (2001). *Systems engineering fundamentals* (tech. rep.). DEFENSE ACQUISITION UNIV FT BELVOIR VA.

# 5

# Inflatable Structure Concept Generation

*This chapter identifies the most suitable design candidate for the inflatable reflector. This process entails detailing a list of possible design candidates (section 5.2) followed by a comparative analysis (section 5.3). Once the selection process is complete a BEOC reference mission is selected to inform the BEOC requirements (section 5.4).*

## 5.1. Introduction

In order to maximize the relevance of the inflation system designed in this project, it is deemed prudent to tailor its design for a BEOC inflatable reflector whose continued development will play a key role in enabling and enhancing the development of both BEOC missions and inflatable space structures in general. As such,the concept generation process will entail a number of stages. Firstly, a range of suitable design candidates derived from those identified in the literature review shall be presented. Following this, a comparative analysis of these candidates shall be carried out so as to establish which is the most suitable candidate given the thesis requirements. Once this has been complete a reference BEOC mission shall be selected to as to provide realistic quantitative requirements that shall help guide the design of the structure.

## 5.2. Design Candidates

The first step in this process is to examine the wide range of possible design candidates identified during the literature review. It was established that inflatable space structures show enormous potential for providing attractive solutions to the main technological hurdles facing BEOC missions and by extension are seen as a prime candidate for enabling and enhancing the development of BEOC missions. These solutions come in the form of telecommunications, power, propulsion and hybrid subsystems. The potential candidates identified, which are typically planar or curved reflector structures, are grouped according to these different subsystems and are presented in figure A.1.

### 5.2.1. Refining The Set of Design Candidates

As noted in key requirement REQ-IRI-01, the literature review established that curved inflatable reflectors offer more potential for providing optimal solutions to BEOC reflector applications. Hence, the identification of the most suitable candidate can begin by removing any design candidates that do not have a curved structural shape. This means that the planar design candidates, which fall under the high pressure categorization, shall not be considered as viable design candidates for this thesis project. Furthermore, given the clear prevalence of spherical and parabolic reflectors, the Fresnel lens candidate shall also be discounted as exploring its design shall not provide a fair approximation of current inflatable technology (FUNC-IR-01). The refined set of design candidates can be seen in figure 5.1.

### 5.2.2. Accepted Design Candidates

It is clear from the design candidates presented in figure 5.1 that irrespective of application, inflatable curved reflectors can be split into two distinct configurations, parabolic and spherical. In order to establish the most promising candidate that shall be explored in this thesis, these configurations, as well as the different BEOC applications shall be compared.

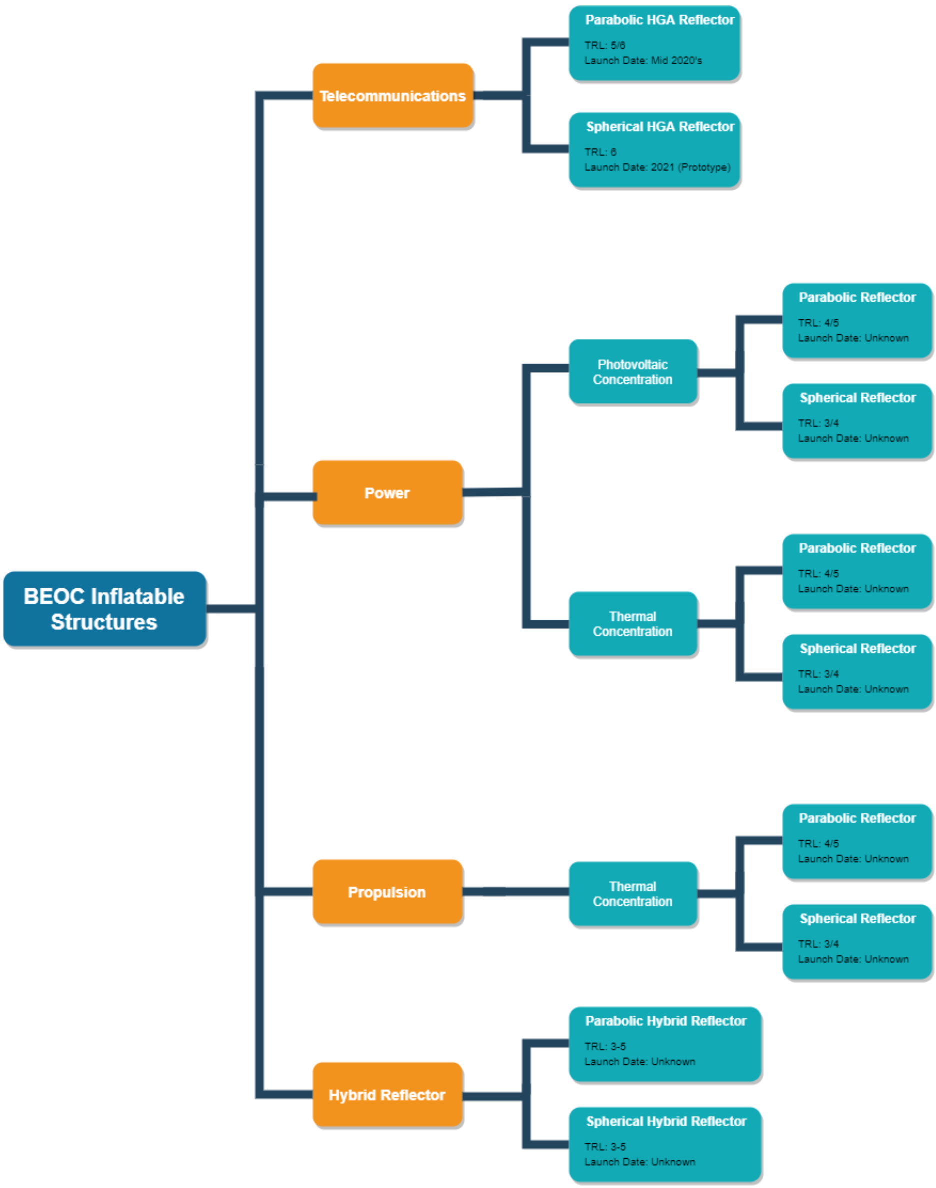


Figure 5.1: Refined design options for the application of an inflatable structure as solutions to the technological challenges facing BEOC missions

## 5.3. COMPARATIVE ANALYSIS

In order to establish the most suitable candidate for exploration in this thesis, the curved inflatable reflector design candidates identified shall be compared with respect to their structural configuration and application.

### 5.3.1. STRUCTURAL CONFIGURATION

As noted that curved inflatable reflector candidates can be split into two structural configurations parabolic and spherical. In order to be able to gauge the most suitable design candidate for this thesis it is important to qualify what these two configurations are and how they compare to each other.

#### PARABOLIC INFLATABLE REFLECTORS

The most popular form of inflatable curved reflector is the parabolic reflector. This is hardly surprising given that parabolic reflectors are the classic form for optical reflecting applications due to the innate geometric properties of the paraboloid shape. Any incoming radiation that enters the parabolic reflector parallel to its axis will be reflected to the focal point of the dish. Similarly energy radiating from the focus can be transmitted outward parallel to the axis. This can be clearly seen in figure 5.2.

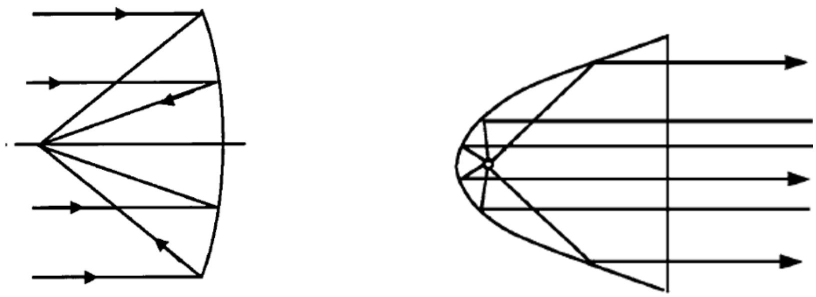

(a) Incoming Radiation (b) Outgoing Radiation

Figure 5.2: Parabolic Reflector (Fischer et al., 2008)

These reflectors can typically be split into two categories, focal led reflectors and dual reflectors. A focal led reflector reflects an incident field from and/or to a feed system/ receiver located at its focal point as can be seen in figure 5.3a. Dual reflectors use a sub-reflector to increase their effective focal length with the Cassegrain reflector using a hyperbolic sub-reflector and the Gregorian reflector using an elliptical sub-reflector.

Inflatable parabolic reflectors typically take the form of an inflatable volume enclosed by two parabolic membranes and are supported and tensioned by a torus structure. One of the membranes is referred to as the canopy and is optically clear to allow radiation to pass through while the other membrane is the reflector. The torus is required to both support and tension the reflecting surface as parabolic reflectors require high surface accuracies in order to ensure the required high performance characteristics, particularly for telecommunications applications, are met. This torus typically takes the

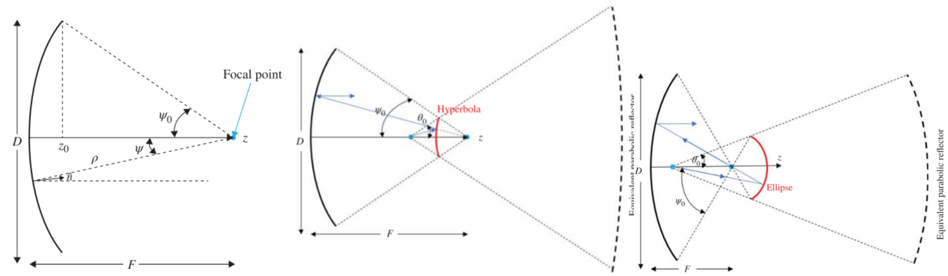


(a) Focal Led Reflector (b) Cassegrain Reflector (c) Gregorian Reflector

Figure 5.3: Parabolic Reflector Antennas (Chahat et al., 2021)

form of a high pressure inflatable tube as seen in figure 5.4. Without the torus, the inflation gas would distend the structure towards a spherical shape leading to issues with shape accuracy and performance Babuscia et al., 2020.



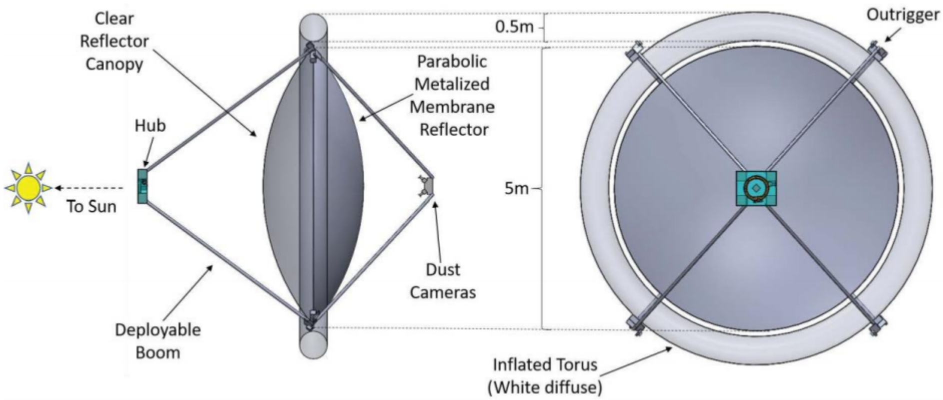


Figure 5.4: OS4 Hybrid Parabolic Reflector Concept (Staehle et al., 2020)

### SPHERICAL INFLATABLE REFLECTORS

The defining feature of spherical inflatable reflectors is that they make use of the simplest and lowest energy structure in nature; the sphere. Therefore, unlike their parabolic counterparts, these reflectors do not require a torus to maintain their desired structural shape. This is an extremely attractive property as it radically simplifies the inflatable system by removing the additional packaging, deployment and inflation complexities that an additional high pressure torus requires. But this simplification comes at a price.

A spherical surface has a constant surface slope rate of change across its surface. This means that unlike parabolic reflectors, spherical reflecting surfaces suffer from aberration, i.e. it does not have a precise focal point (figure 5.5a). This inevitably decreases their concentration efficiency and is detrimental to their performance as an antenna.

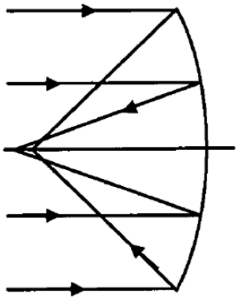

(a) Spherical Reflector Aberration (Fischer et al., 2008)


(b) Early Inflatable Spherical Reflector ECHO Balloon 1 (Freeland et al., 1998)

Figure 5.5: Inflatable Spherical Reflector



However, there are a number of corrective measures that can be utilized to compensate for the inaccuracies of the spherical reflector shape.

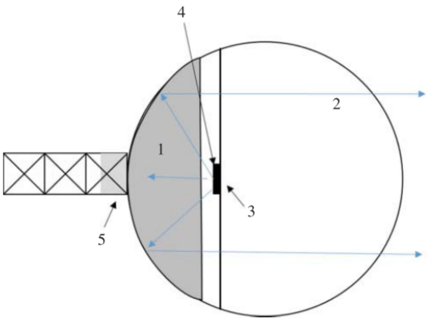


(a) Babuscia et al., 2020 Spherical Inflatable Antenna.
(1) Reflective region, (2) Transparant region,
(4) Patch Antenna on a support (3), (5) The stowed volume.

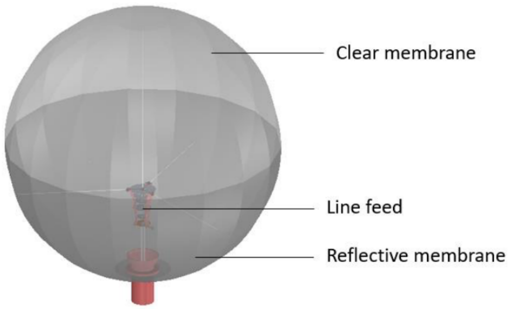


(b) CatSat Spherical Inflatable Reflector With Line Feed System (Chandra et al., 2021)

Figure 5.6: Inflatable Spherical Antenna Corrective Measures

The most straight forward method for correcting the spherical aberrations is to decrease the size of the reflective surface relative to the sphere. By doing this the spherical reflector becomes a better approximation of a parabolic reflector and thus leads to a reduction in aberration. However, this method comes with the drawback in reducing the overall reflective surface area of the reflector. While this may be more acceptable for concentration applications, particularly photovoltaic concentration, it will inevitably lead to a reduction in Gain for antenna applications, a vital performance characteristic for BEOC missions. Other methods include utilizing corrective optics and feed solutions as seen in figure 5.6. However, these solutions require additional components that must be deployed within the spherical inflatable structure. A more elegant solution may be found with the GATR inflatable antenna [1] (figure 5.7). This spherical inflatable reflector has

[1] https://www.cubic.com/solutions/c4isr/protected-communications/expeditionary-satcom

Figure 5.7: GATR Terrestrial Spherical Inflatable Antenna [1]

two pressure chambers separated by a parabolic membrane reflector which maintains its shape through the pressure differential between the two chambers. This reflector provides a solution that combines the attractive structural simplicity of a sphere with the high performance characteristics of a parabolic reflector.



### COMPARISON

Spherical and parabolic reflectors each have a range of advantages and disadvantages that must be weighed against each other in order to gauge which configuration is most suitable for this thesis project. As has been established, parabolic inflatable reflectors are the geometric configuration best suited to ensuring high telecommunications and concentration performances. However, in order to ensure that these reflectors conform to the strict surface accuracies required, a high pressure inflatable torus must be utilized to both support and tension the structure. Without this torus the reflector would naturally distend to a spherical shape. It is for this very reason that spherical antennas are attractive. Such structures are far less complex than their parabolic counterparts making them particularly well suited for CubeSat applications. This point is emphasized by the fact that of the three CubeSat inflatable reflectors currently in development, two of which are spherical (Babuscia et al., 2020; Chandra et al., 2021) and one parabolic (Fenn et al., 2021), the parabolic inflatable concept has a considerably more complex architecture, with three separate inflatable compartments at different pressure levels required. Despite the fact that spherical reflectors require additional infrastructure to compensate for their performance inaccuracies, their simple shape and single inflation compartment, which is desired by key requirement REQ-IRI-02, has made them the current front runner in the battle between these two configurations as evidenced by the CatSat spherical inflatable antenna which will become the first CubeSat inflatable reflector to be tested in space when launched sometime in 2022 (Chandra et al., 2021).

### 5.3.2. BEOC APPLICATION

The design candidates presented fall into four different application categories; telecommunications, propulsion, power and hybrid. These four different application categories are described in detail in the literature study (Dunbar, 2021), an overview of which is presented in the literature review (section 2.3). Thus no further description shall be given here and only the comparison shall be carried out.

#### COMPARISON

These categories are compared by ranking them according to their importance to the development of BEOC missions from 1 to 4, with 1 being the highest. The rationale for each ranking is also given.

1. Telecommunications:

    - From the literature review it is noted that the development of an appropriate telecommunications system is the most significant challenge facing the development of BEOC missions. This is further emphasised by the fact that there are three different CubeSat inflatable antenna projects currently under development (Babuscia et al., 2020; Chandra et al., 2021; Fenn et al., 2021), while inflatable CubeSat propulsion, power and hybrid systems have not moved beyond preliminary concept studies. This translates into a higher TRL for inflatable antenna systems than for other applications. This is important as it enables the design candidates to be assessed with respect to reference designs.

2. Propulsion:

    - Following telecommunications, propulsion is deemed as having significant BEOC potential due to the enabling role that inflatable concentration plays in the development of STP systems. An inflation system for such a system may play a key role in facilitating the development of a unique and highly exciting propulsion system.

3. Power:

    - Any developments in a thermal concentration system for STP will also be utilized for BEOC thermal applications. Indeed Leverone et al., 2020, has proposed a system that combines both applications in one system. This cross over relegates design candidates for photovoltaic systems to having the least BEOC potential of the three technological challenges presented.

4. Hybrid:

    - Although hybrid systems have enormous potential for facilitating the development of deep space BEOC missions, their reliance on developments in each of the other application categories means that for this project these design candidates are seen as providing the least relevance to BEOC development.

### 5.3.3. DISCUSSION

From this comparative analysis it is apparent that the most promising design candidate is the spherical high gain antenna reflector, stemming from the identification of the spherical structural configuration as the most desirable and the telecommunications application as having the most BEOC potential.

However, upon further reflection it is clear that advancements in the development of such a structure, particularly with respect to its inflation system, shall have an impact across across all application categories given the prevalence of the spherical reflector shape. Given this fact, it is deemed wiser to design a spherical reflector structure that is not tailored for one specific application but rather can be used as an approximate representation for all applications, either as an antenna, concentrator or hybrid structure. This approach is advantageous for a number of reasons. Firstly, it negates the need to account for the specific design considerations of different applications which, given the limited scope of the thesis, enables more time to focus on the primary objective of the thesis, the inflation system. Secondly, as the main design variations for the different applications stem from internal components and reflective characteristics, the spherical structural configuration of the reflector shall remain consistant. As a result it can be assumed that the key design features noted in the literature review (section 2.2), shall also remain consistant irrespective of application. This is particularly important when considering the shape transformation functions which, as has been noted, have a direct impact on the design requirements of the inflation system. As a consequence, an inflation system designed for a generic inflatable spherical reflector structure shall provide a suitable solution for all inflatable spherical reflector applications, although minor adjustments may be required.

It was thus decided that in order to maximize the relevance of the inflation system designed in this thesis, it would be prudent to explore the design a spherical inflatable reflector structure that is not adapted for any particular BEOC application but rather can be used as an approximation for all of those identified.

## 5.4. BEOC Mission Selection

In order to design an inflatable spherical reflector for a BEOC mission, some parameters regarding the structure and the mission must be established. In order to do this an examination of a number of reference systems is carried out.

### 5.4.1. Reference Deployable CubeSat Systems

In order to gauge the design parameters expected of the inflatable spherical reflector, a set of reference systems were examined. It must be noted that given the relatively recent developments in deployable CubeSat systems, particularly for inflatable structures, the number of reference systems is quite small. For this reason, early spherical structures developed by NASA in the 1960's are also referenced.

This small number of reference missions makes it difficult to make strong convincing inferences about the capabilities and parameters of these structure. In order to try and address this issue, a number of non-inflatable systems are included so that inferences can be easier spot by comparing the two categories. Table C.2 in the appendices, contains such a list of systems. This table contains educated estimates for values that were not clearly attainable from the literature (e.g. values with an $*$) . From the table the following inferences can made about the desired parameters of the inflatable structure and BEOC mission:

5

- 6 and 12U CubeSat platforms are the most popular for GEO and BEOC missions.
- The area density of the inflatable structures is at least an order of magnitude lower than their non-inflatable counterparts (<0.4 kg/$m^2$).
- The RPE of inflatable structures is generally an order of magnitude greater than non-inflatable systems. Unfortunately, due to the limited literature available on some of these structures their stowed volume could not be established and are thus marked as TBC. This makes is difficult to draw inferences about the desired RPE, although a minimum value of 1.5, derived from the 12 ft sphere, informs requirement REQ-IRI-04. However, as is discussed in section 6.3, packaging efficiency values according to the more common definition, referred to as PE in this thesis, of material volume over the packaging container volume for spherical inflatable structures range anywhere from 30-80%. Babuscia, for example has a PE, of 50%. Given that RPE also depends on the packaging container volume, equation 2.1, an RPE of 3.27 can be calculated for Babuscia. These values were likely achieved for the CatSat and NanoSat De-Orbit device structures and if we estimate that CatSat had a conservative PE of 30% this would yield an RPE of 6.56. The larger the material thickness of the structures the lower this value will be, as can be seen for the laminate structures.
- Non-inflatable parabolic reflector applications occupy approximately 25% of a BEOC volume. In order to maximize the low volume requirements of inflatable structures it is vital that an inflatable reflector have a system volume, including inflation system and deployment/ejection mechanism, at least equal to, but preferably less than that of a comparable non-inflatable reflector. This is particularly notable

when examining the data for the CatSat inflatable spherical reflector antenna and the KaPDA parabolic mesh reflector antenna. Both have the same deployed area and occupy the same volume of the CubeSat (1.5U) despite the CatSat inflatable structure likely having an RPE an order of magnitude greater. The reason for this lies with CatSats inflation system and ejection mechanism, both of which contribute the majority of the systems volume requirements. This is significant as the KaTENna antenna, as a mesh reflector, inevitably has higher performance characteristics than the inflatable CatSat. Therefore, when designing an optimized BEOC spherical inflatable reflector, minimizing the volume requirements of the inflation system (and the ejection mechanism) is vital in ensuring that it is an attractive alternative to its high performing non-inflatable counterparts.

### 5.4.2. Reference BEOC Missions


Figure 5.8: Sample of the exciting Beyond Earth Orbit CubeSat Missions due to launch in the next few decades (Dunbar, 2021)

To date only a single BEOC mission has been completed, the MarCo mission (Schoolcraft et al., 2017). Ideally the mission would have used a parabolic antenna for its telecommunication system, however the strict volume requirements and short development timescale meant the team developed a planar reflectarray that was stowed on the side of the CubeSat structure. This system was quite successful and is now due to be utilized onboard the M-ARGO BEOC mission (Walker et al., 2017). Unfortunately, the budgetary data on both MarCo and M-ARGO, as well as the inflatable CubeSat antenna concepts already discussed, could not be found in the literature. Therefore, as no reference BEOC curved reflector mission, inflatable or otherwise, could be utilized to provide preliminary parameters for the design of the inflatable system, it was decided that this thesis would design an inflatable system for a lunar spherical inflatable reflector demonstration mission. This decision was based on the relevance of such a mission, with a significant number of Lunar CubeSat missions planned for the next few years (figure 5.8), as well as the fact that the TU Delft space engineering department is involved in the development of the LUMIO BEOC mission (Cervone et al., 2021). The LUMIO CubeSat will provide the base concept for the CubeSat with the only major difference being the payload, which shall be the inflatable system for this a demonstration mission. As such the payload parameters of LUMIO shall be used as a guide for the design requirements of the inflatable system. These parameters are listed in table 5.1 and are used to further refine the requirements listed in section 4.4.

Table 5.1: LUMIO CubeSat Mission Parameters (Cervone et al., 2021; Menicucci et al., 2021)



| **Size** | **Dry Mass** | **Total Mass** | **Payload Volume** | **Payload Mass** | **Payload Power** | **Transit Time** | **Operational Lifespan** |
|---|---|---|---|---|---|---|---|
| 12U | 21.1 kg | 28.7 kg | ≈ 3U | ≈ 3 kg | TBD | 14 days | 393 days |

# Bibliography


Babuscia, A., Sauder, J., Aman, C., & Thangavelautham, J. (2020). Inflatable antenna for cubesat. *CubeSat Antenna Design*, 197–230.

Cervone, A., Topputo, F., Speretta, S., Menicucci, A., Di Lizia, P., Massari, M., Franzese, V., Giordano, C., Merisio, G., Labate, D., et al. (2021). Design challenges and opportunities offered by the lumio spacecraft: A cubesat for observing and characterizing micro-meteoroid impacts on the lunar far side. *72nd International Astronautical Congress (IAC 2021)*, 1–11.

Chahat, N., Sauder, J., Babuscia, A., & Thomson, M. (2021). Chapter 3 - radar in a cubesat: Raincube. In *Cubesat antenna design* (pp. 91–136). John Wiley & Sons.

Chandra, A., Pat, T., Tonazzi, J. C. L., & Walker, C. K. (2021). Development and flight qualification of a small satellite x-band spherical membrane antenna. *2021 IEEE Aerospace Conference (50100)*, 1–8.

Dunbar, S. (2021). Literature review study - inflatable space structures, beyond earth orbit cubesat missions and micropropulsion inflation systems.

Fenn, A. J., Mills, J., Robey, F., Finnell, J. W., Hassan, B., Crowley, S., et al. (2021). Inflatable reflector antenna and related methods [US Patent 10,916,859].

Fischer, R., Tadic-Galeb, B., & Yoder, P. (2008). *Optical system design*. McGraw-Hill Education.

Freeland, R., Bilyeu, G., Veal, G., & Mikulas, M. (1998). Inflatable deployable space structures technology summary.

Leverone, F., Cervone, A., Pini, M., & Gill, E. (2020). Design of a solar thermal propulsion and power system for mini-satellite lunar orbit insertion. *2020 IEEE Aerospace Conference*, 1–17.

Menicucci, A., Cervone, A., Speretta, S., Bertels, E., Topputo, F., et al. (2021). The radiation environment and effects analysis of the lumio mission. *72nd International Astronautical Congress (IAC 2021)*, 1–7.

Schoolcraft, J., Klesh, A., & Werne, T. (2017). Marco: Interplanetary mission development on a cubesat scale. In *Space operations: Contributions from the global community* (pp. 221–231). Springer.

Staehle, R. L., Babuscia, A., Beregovski, Y., Chahat, N., Chien, S., Cochrane, C., Duncan, C., Garrett, H., Landau, D., Liewer, P., Mouroulis, P., Murphy, N., Tang, A., Puig-Suari, J., Bellardo, J., Gillespie, C., Bonafede, N., Fernandez, M., Gordon, M., . . . Austin, A. (2020). *Low-Cost SmallSats to Explore the Outer Solar System Final Report on NIAC task to define an architecture for Outer Solar System SmallSats (OS4) 2020 September 15* (tech. rep.).

Walker, R., Koschny, D., Bramanti, C., Carnelli, I., Team, E., et al. (2017). Miniaturised asteroid remote geophysical observer (m-argo): A stand-alone deep space cubesat system for low-cost science and exploration missions. *6th Interplanetary CubeSat Workshop, Cambridge, UK*, *30*(05).

# 6

# INFLATABLE STRUCTURE DESIGN

*The BEOC inflatable reflector is designed in this section. The first step consists of considering the structures key design features. This involves exploring its geometry (section 6.2), its shape transformation functions (section 6.3), suitable materials (section 6.4) its fabrication methods (section 6.5) and the environmental orbital conditions it shall operate in (section 6.6). Once these have been established the mechanical properties of the structure are calculated (section 6.7). The output of this process is a preliminary design of a spherical inflatable reflector that can be utilized to generate the inflation system requirements.*

## 6.1. INTRODUCTION

Following the concept generation process and selection of the inflatable spherical structure for a Lunar CubeSat demonstration mission, the design of the structure can begin. The focus of this design process shall be on addressing the main design considerations, as discussed in section 2.2, to an acceptable degree so that the requirements set out in section 4.4 are met and informed requirements for the inflation system can be generated. As such the reflective performance of the reflector shall not be assessed and any additional reflector components, such as internal corrective components required for spherical reflector applications, shall not be explored. Instead, as is desired by requirement REQ-IRI-03, the designed spherical inflatable structure shall consist of a transparent canopy and an interior reflector. This section shall explore the geometry, shape transformation functions, materials, environmental conditions and mechanical properties of such a structure within the constrained scope of the requirements. These key design considerations shall inform the design requirements of the inflation system.

## 6.2. GEOMETRY OF STRUCTURE



As this spherical structure shall be utilized for demonstrating the development of a micropropulsion based inflation system, the sizing of the structure shall not be tailored to either telecommunication, power or propulsion applications. However, in order to demonstrate the potential of these structures, key requirement REQ-IRP-01 desires that the deployed area of the inflatable structure be at least comparable with the KaTENna parabolic mesh reflector, the latest high performing 12U CubeSat reflector. As given in table C.2, this equates to a deployed cross sectional area of 0.785 $m^2$. This antenna can be seen in figure 6.1a.

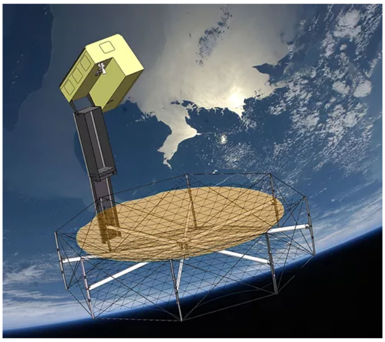

(a) KaTENna Antenna Parabolic Mesh Reflector [a]

[a]https://www.tendeg.com/products

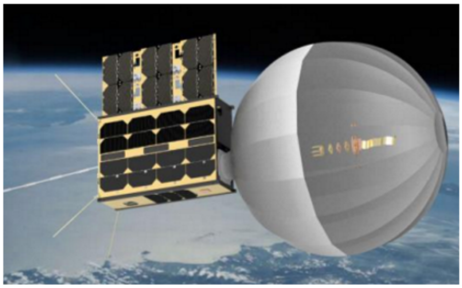

(b) CatSat Spherical Inflatable Antenna (Chandra et al., 2021)

Figure 6.1: Comparable Reflector structures

Such a cross sectional area is 4 times the size of the CatSat inflatable reflector, given in figure 6.1b, due to launch sometime in 2022. Given that CatSat is being developed for LEO applications, such an increase in size shall be necessary in order to compensate for the operational distances from the Earth/Sun required by BEOC reflector applications. Taking telecommunications as an example, in section 2.3 it is noted that high gain antennas are desired for BEOC missions. As gain is proportional to antenna cross sectional area, these higher gain levels require higher larger cross sectional areas. While the specifics of these reflective applications shall not be explored, designing an inflation system for a structure of this size shall enable the demonstration of both the potential of micropropulsion based inflation systems for BEOC missions as well as the volume and mass advantages an inflatable reflector possesses over the comparably sized state of the art KaTENna Antenna parabolic mesh reflector. As such, the required diameter of the inflatable spherical structure shall be 1.0 m.

## 6.3. Shape Transformation Functions

The shape transformation functions correspond to the packaging, deployment and stabilization functions of the inflatable structure. As noted in the literature review (section 2.2), the selected combination of these functions has a major impact on the functional requirements of the inflation system. However, due to the limited scope of this thesis project they shall only be explored in limited detail, with an optimal design for each function likely requiring a full thesis on their own.

### 6.3.1. Packaging

The packaging scheme for the inflatable structure plays a crucial role in the mission success as it impacts the packaging efficiency, deployment dynamics and structural properties of the inflated structure. For this thesis, the packaging efficiency and its impact on the stowed properties of the structure shall be assessed, with its impact on both the deployment dynamics and structural properties neglected. Both of these considerations require testing and complex simulations to accurately assess and so shall be left for future work. In the case of of its impact on the deployment dynamics, which arises primarily due to the build up of residual gas, this issue is typically dealt with through the use of ascent venting. As such, this shall be taken into consideration for the design of the inflation system, as noted in requirement REQ-ISP-02.

As observed in the literature review, high packaging efficiencies are one of the most attractive advantages that inflatable space structures possess over their mechanical counterparts. As such REQ-IRI-04 specifies that the packaging scheme enable an RPE of at least 1.5m$^2$/U. As noted in the literature study (section 2.2), this definition of packaging efficiency (deployed area/stowed volume) is commonly utilized for deployable antennas and concentrators and is given in equation 2.1. Given that the structure being designed is an inflatable reflector this seems appropriate. However, the more commonly used definition of packaging efficiency for inflatable structures is referred to as PE, and is given in equations 2.2 and 2.3. As such, given both RPE and PE depend on the packaging container volume, PE shall be utilized to calculate RPE. First though, a suitable packaging scheme must be established.

#### The Packaging Scheme

Grahne and Cadogan, 2001 claim that spherical inflatable structures "consisting of little hardware. . . could expect a packaging efficiency (PE) of 50 to 80% [Packaging Factor (PF) of 2 to 1.25] depending on material density and modulus and packaging method (by

6

hand or hydraulically) used". However, unlike inflatable booms and flat thin membrane structures (Dunbar, 2021), the literature on packaging methods (schemes) for these structures is quite limited. This makes the validity of Grahne and Cadogan, 2001's claim difficult to gauge.

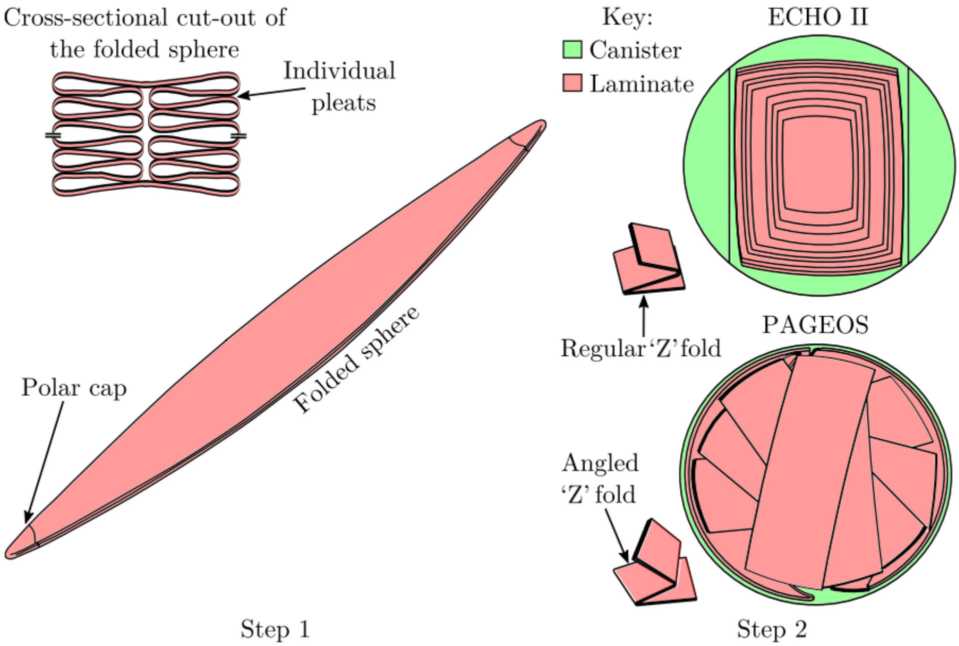


Figure 6.2: Inflatable Spherical Structure Packaging Techniques (Secheli, 2018)

Recently Babuscia et al., 2014 explored a number of packaging schemes for an inflatable CubeSat antenna based around the popular Z-folding method while Nakasuka et al., 2009 utilized a tangential wrapping packaging configuration for the spherical NanoSat de-orbit device. However, the detail surrounding these configurations is again quite limited and no quantitative values for the PE values are given. Fortunately, more detail on packaging schemes for spherical structures can be found in the literature detailing the design and fabrication of NASA's early inflatable balloon projects. The techniques involved utilizing initial pleat folding of the individual gores in the structure followed by one of a number of z folding patterns (figure 6.2) similar to those explored by Babuscia et al., 2014.

A detailed evaluation and examination of these packaging methods is deemed beyond the scope of this thesis project and so further elaboration on these methods will not be presented. However, a detailed description of the methods is given by Talentino, 1966, while a more accessible summary is available in Secheli, 2018. These spherical structures achieved a PF of 3 (PE of 33%), with attempts at a PF of 2.5 (PE of 40%) failing. These PE values are substantially lower than the possible 80% claimed by Grahne and Cadogan, 2001 although it must be kept in mind that these structures contained sublimating powders which inevitably decreased their efficiency. Given that the structure being designed for this project shall not contain sublimate powders, coupled with modern advancement in packaging, it seems prudent to assume a PE of at least 50% is feasible. Despite this, it must be acknowledged that this structure is being designed for a demonstration mission and that while it shall not contain internal spherical aberration corrective components, realistic BEOC spherical structures shall. Therefore, a more conservative PE value of 40% shall be assumed for this project. This PE value shall inform the fufilment of REQ-IRI-04.

### 6.3.2. DEPLOYMENT

The deployment process is the most important stage of an inflatable space structures life cycle. Of the three deployment methods discussed in the literature study, section 2.2.4, the free deployment method shall be employed for this spherical inflatable reflector. This decision is based off the fact that of the three methods, it is the only one utilized to date for similar low pressure inflatable spherical structures including the OCSE (Guidanean and Veal, 2003), MIRIAM and ARCHIMEDES (Griebel, 2011), as well as the Inflatable CubeSat Antenna (Babuscia et al., 2017) and CatSat (Chandra et al., 2020), see figure 6.3.

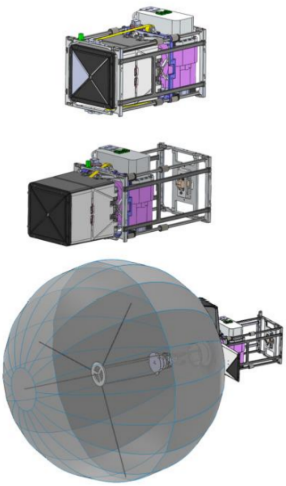

(a) CatSat deployment system (Chandra et al., 2022)

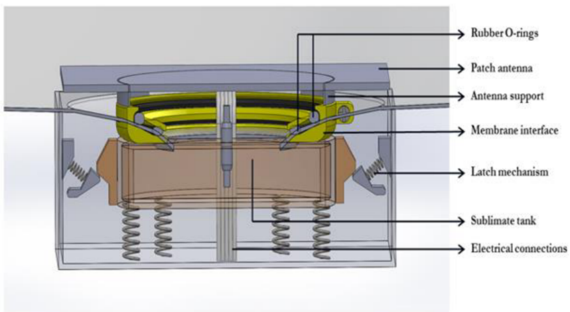


(b) Ejection Mechanism for spherical inflatable structure (Babuscia et al., 2017)

Figure 6.3: Free Deployment

Free deployment involves ejecting the packaged structure out into space and is thus generally not constrained or controlled in any significant fashion during the inflation process. It entails a number of components including the packaging container, an ejection plate/mechanism and of course the inflation system. Two examples of mechanisms used for free deployment are seen in figure 6.3. The ejection mechanism used seen in figure 6.3b, is evidently simpler likely arising from its use of sublimation powder. Unfortunately, the literature surrounding the design of both of these mechanisms is quite limited and to design a custom mechanism would likely require an entire thesis by itself. As such, its design shall not be explored with the primary focus of the deployment system being the inflation system.

As has been noted, unlike controlled deployment methods which utilize passive or active means to control the deployment of the structure during inflation, the free deployment method provides limited-to-no control. Thus in order to ensure that the structure unfolds and deploys successfully successful, the inflation process must be solely relied upon. Thus, in order to satisfy requirements REQ-ISP-01 to REQ-ISP-05, this inflation process must be carefully managed and a suitable inflation scheme must be designed. This is explored in greater detail in the design of the inflation system, sections 7.5 and 8.3.3.

### 6.3.3. Stabilization

As is explored in the literature study (Dunbar, 2021) and briefly discussed in section 2.2.4, there are a variety of different ways to stabilize the inflatable structure so as to ensure its structural integrity. Unlike for deployment where free deployment is the primary method used for low pressure spherical structures, in the case of stabilization there are three main methods that are typically utilized. They are pressure stabilization, aluminium rigidization and UV rigidization. In order to select a suitable stabilization method for this project, these three methods must be discussed.

6

#### Pressure Stabilization

Pressure stabilization relies solely on the internal pressure provided by the inflation gas to maintain the structural integrity of the membrane walls, as is the case for typical balloon structures utilized in terrestrial applications. Of the three methods discussed here, pressure stabilized structures provide the most extensive heritage for inflatable reflector applications having been utilized for structures such as IAE (Freeland et al., 1997) and PAGEOS (Teichman, 1968) as well as being proposed for the OASIS (Walker et al., 2019) and TST inflatable telescopes (Walket et al., 2017). Most notably it has also been proposed for the CatSat spherical inflatable antenna (Chandra et al., 2021), which shall become the first inflatable CubeSat antenna tested in space.

It's popularity largely stems from its excellent optical properties which is ensured by its use of a thin membrane that also maximizes the mass and volume benefits of inflatable structures. However, this thin membrane is highly susceptible to threats such as micrometeoroids and space debris which lead to the development of small holes in the structure. In order to compensate for the gas leaks instigated by these holes additional make-up gas is required. This leads to a dilemma relating to the system mass and the structures lifetime, with the lifetime limited by the quantity of gas that can be carried within the mass and volume constraints of the CubeSat.

#### Aluminium Rigidization

Aluminium rigidization entails pressurizing an aluminium laminate membrane to just past the yield stress of the aluminium layer, after which point the structure is vented. This enables the structure to be stabilized without the need for inflation gas giving it a significant advantage over pressure stabilization as no make-up gas is required. While the laminate yields a slightly lower RPE, due to its lower PE, and areal density relative to the thin membrane utilized for the pressure stabilized structure, the increased environmental durability and negation of make-up gas has seen it become a highly successful rigidization method, having been utilized for numerous inflatable spherical reflector satellites including ECHO II (Staugaitis and Kobren, 1966), Explorer IX (Coffee et al., 1962) and OCSE (Guidanean and Veal, 2003). It has also most recently been used in the InflateSail and Debris-Sat CubeSat boom-based Inflatable Structures (Underwood et al., 2019). However, as the structure is composed of an aluminium laminate it can only act as a reflective surface. This makes it unfeasible for the desired inflatable reflector structure which shall consist of a transparent canopy and an inner reflective surface.

### UV Rigidization

UV rigidization entails utilizing UV light to cure a thermoset matrix resin thus rigidizing the structure and removing the reliance on gas pressure for structure integrity. It holds the most promise for long duration BEOC inflatable reflector applications of the three methods as it is the only method that can provide both viable optical properties and long term environmental durability.

The method is currently being investigated by Babuscia et al., 2020 and Staehle et al., 2020 who propose the use of UV-resin filled ribs that are built into the gores of the structure in a 'venous web' as seen in figure 6.4. However, the TRL of this method is still quite low with the current technology incapable of fully maintaining the desired inflated shape of the reflector. This is due to the fact that applying the UV resin uniformly to the reflector surface leads to excessive mass and volume increases, as seen in a preliminary investigation by Babuscia et al., 2020. Indeed Staehle et al., 2020 estimates that 4.9 kg of UV resin would be required for the OS4 inflatable reflector, thus raising the areal density of the OS4, as noted in table C.2, from 0.368 to 0.6173 kg/m$^2$, exceeding requirement REQ IRI-05 Given that the shape cannot be fully maintained this in turn leads to issues with the reflector shape and its ability to operate successfully.

Figure 6.4: UV Rigidization Webbing (Chandra, 2015)

While this stabilization method shows promise, it's low TRL at present means that it is unsuitable for the desired application. Further research and testing is required before it can considered a feasible option for inflatable reflector applications.

#### DISCUSSION

It is apparent that of the three stabilization methods only the pressure stabilization method can provide a suitable option at this moment in time. The inability of aluminium rigidization to provide a canopy reflector and the issues associated with the low TRL of UV rigidization mean that despite the need for make-up gas, the pressure stabilization method is currently the only method capable of meeting the desired requirements of a BEOC CubeSat inflatable reflector. Indeed this need for makeup gas informs the functional requirements of the inflation system necessitating key requirement REQ-ISP-06. However, this comes at the price of the mission duration, which is inevitably limited by the need to constantly replenish the gas losses. The effect this has on the feasible mission duration shall be explored in greater detail in section 8.4. As noted by Chandra et al., 2022, further research on suitable rigidization methods is required for these inflatable reflectors.

### 6.3.4. SHAPE TRANSFORMATION SUMMARY

This investigation regarding the required shape transformation functions of the spherical inflatable structure satisfies the requirements of the inflatable structure and informs those of the inflation system in a variety of ways. Firstly, the packaging efficiency selected shall enable the fulfilment of REQ-IRI-04, thereby ensuring that the designed structure provides a competitive alternative to conventional reflectors. Secondly, the use of the free deployment method, requires that the inflation process be carefully managed so that the structure unfolds and pressurizes in a suitably controlled manner. This in turn informs requirements REQ-ISP-01 to REQ-ISP-03 and necessitates the need for an inflation scheme. This is explored in greater detail in section 7.5. Finally, as pressure stabilization is the only suitable option given current rigidization technology, the inflation system must be capable of providing pressure maintenance. This in turn informs the functional requirements of the inflation system, as dictated by REQ-ISP-06.



## 6.4. MATERIAL

As alluded to in section 2.2.4, materials play a key role in enabling the development of inflatable space structures. The material selected for this pressure-stabilized structure must be both thin and flexible while also being able to withstand the challenging lunar environment. In addition, as the reflector structure shall consist of two separate sections, a clear transparent canopy and an interior reflecting surface (courtesy of a reflective coating) as desired by requirement REQ-IRI-03, the material must also provide high optical transparency and be suitable for coating/ metallization. Before exploring the potential materials for this application the material requirements must first be specified.

### 6.4.1. MATERIAL PROPERTIES

While a detailed exploration of the optical properties of the material shall not be carried out in this thesis, a list of desirable material properties stemming from the requirements outlined in section 4.4 can be generated. The motivation for the selection of certain desirable material properties is informed by Connell and Watson, 2001; Friese et al., 1983 and Liu et al., 2017. They are presented in table 6.1.

| ID | Property | Rationale |
|---|---|---|
| PROP-M-01 | Density | This defines the mass per unit volume of the material. It is desirable to be keep the density of the material to a minimum, thereby minimizing mass requirements. |
| PROP-M-02 | Young's Modulus | This is a measure of the stiffness of a material. A low Youngs Modulus, which yields an elastic and flexible material, is clearly desirable for inflatable space structure and is a particularly important parameter for the PE of the structure. However, if it is too low undesirable pliant behaviour, such as that experienced by rubber inflatable balloons which undergo significant stretching during inflation, would result. To negate this, inflatable space structures generally utilize materials with a Youngs modulus an order of magnitude higher than their rubber counterparts. Based off relevant literature, this equates to a minimum Youngs Modulus of 1 GPa. |
| PROP-M-03 | Yield Strength | The yield strength is the stress at which a material suffers permanent (plastic) deformation. In order to remove wrinkles from the inflatable structure it is must be initially inflated to about 15 % of the yield strength (section 6.7.3). Thus, in order to minimize inflation gas requirements, it is desirable that the yield strength be minimized. As this value is derived from the Young's modulus, this further emphasis the desire to minimize the Youngs Modulus. |
| PROP-M-04 | Radiation Resistance | Radiation in the lunar orbital environment can cause degradation to inflatable space structures. High radiation doses associated with solar flares and galactic cosmic rays (Menicucci et al., 2021 as well as high energy solar radiation, particularly that in the VUV and X-ray range, have sufficient energy to dramatically alter the structures material properties. It is therefore imperative that the selected material for this structure have sufficient radiation resistance to withstand the lunar radiation environment. |
| PROP-M-05 | Coefficient of Thermal Expansion | This a measure of the expansion of the material with temperature. The extreme temperature environment that can be experienced in lunar orbit necessitates a low coefficient in order to ensure consistent material properties over wide temperature ranges. |

| | | |
|---|---|---|
| PROP-M-06 | Transmittance | This is a measure of the fraction of incident radiation on a surface that passes through the surface. High optical transparency is a key performance parameter for inflatable reflector canopies. |
| PROP-M-07 | Emissivity | This is a measure of the amount of thermal radiation a body emits to its environment. It is desired that it be as high as practical in order to achieve reasonably even temperatures across the surface for the canopy. |
| PROP-M-08 | Solar Absorptivity | This is a measure of the amount of solar radiation absorbed by the material. It should be kept to a minimum in order to minimize temperature differentials across the surface. |
| PROP-M-09 | Metallizability | The material should have the ability to be metallized or coated for the reflective surface. |

Table 6.1: Desirable Material Properties

As is noted by Connell and Watson, 2001, tensile strength is not included in the material requirements. This is due to the fact that the materials being considered are ductile and for inflatable applications are generally lightly loaded. As noted for PROP-M-03, the maximum inflation pressure yields a skin stress of a maximum 15% of the yield strength, well below the tensile strength.

6

### 6.4.2. CANDIDATE MATERIALS

The most popular materials for the pressure stabilized reflector applications are polymer film materials. These materials are utilized in a wide range of space applications and their low weight and foldability make them particularly well suited to inflatable applications. The three most popular polymer film types utilized for inflatable space structures are polyesters, polyimides and Perfluorinated polymers. In the literature study (Dunbar, 2021) it was established that Perfluorinated polymers have less desirable properties relative to polyesters and polyimides and so they shall not be discussed in this thesis. Instead, the material selection is based around the most popular polyester and polyimide films that have been utilized in inflatable reflector applications. They are as follows:

- *Mylar:* Mylar, a polyester film, has been by far the most commonly utilized film material in pressure stabilized inflatable reflectors to date and has been used on structures including ECHO 1 (Clemmons, 1964), PAGEOS (Teichman, 1968), IAE (Freeland et al., 1997) and most recently CatSat (Chandra et al., 2021). It's popularity stems from its attractive combination of properties and more importantly it's low cost and commercial availability. Its material properties can be found using MatWeb[1] and DuPont Teijin Films website[2], as well as this DuPont Teijin Films optical properties PDF [3].

[1] http://www.matweb.com/index.aspx
[2] https://europe.dupontteijinfilms.com/
[3] https://usa.dupontteijinfilms.com/wp-content/uploads/2017/01/Mylar_Optical_Properties.pdf

- *Kapton HN:* Kapton HN has extensive space heritage and is the standard polyimide film utilized in space applications. Its ability to maintain excellent material properties over a wide range of temperatures as well as its greater radiation resistance have seen it become an attractive alternative to Mylar. Its material properties can be found using MatWeb[1] and on DuPont Teijin Films website[17].
- *Upilex S:* Like Kapton HN, Upilex-S is a popular high performing polyimide film for inflatable space applications. Its outstanding thermal properties, the best of any polymer film according to its manufacturers UBE industries[4], as well as its exceptional mechanical properties make it an attractive option for inflatable applications in harsh BEO space environments. Its material properties can be found using MatWeb[1] and on UBE industries website[4].
- *CP-1:* CP-1 is a colorless polyimide that offers superior optical properties relative to the other polyimides presented here although its mechanical properties are slightly inferior. It is particularly well suited for inflatable reflector applications and has been utilized in the development of both high precision inflatable reflector antennas and concentrators (Chodimella et al., 2006; Fay et al., 1999; Pearson et al., 2010). In addition, its greater radiation resistance relative to mylar makes it particularly well suited for reflector applications in harsh BEO space environment. This is emphasised by its selection for two CubeSat solar sail missions that will both operate in the lunar vicinity, Lunar Flashlight and NeaScout (Johnson et al., 2015). Its material properties can be found using MatWeb[1] and on NeXolve's website[5].

The key material properties for each material are listed in table 6.2.

6

[4]https://www.ube.com/upilex/en/index.html
[5]https://nexolve.com/wp-content/uploads/2021/10/TDS_CP1_Clear.pdf

| Property | Mylar | Kapton HN | Upilex-S | CP1 |
|---|---|---|---|---|
| Density (kg/$m^3$) | 1380 | 1420 | 1470 | 1540 |
| Min Thickness ($\mu$m) | 6 | 13 | 23 | 2.5 |
| Tensile Strength (MPa) | 172 | 231 | 520 | 87 |
| Young Modulus (GPa) | 3.5 | 2.76 | 9.121 | 2 |
| Yield Strength (MPa) | 103 | 69 | 255 | $54.5^*$ |
| Poisson's Ratio | 0.5 | 0.34 | $0.34^\star$ | $0.34^\star$ |
| CTE ($\mu$m/m°C) | 17 | 20 | 12 | 51 |
| Transmissivity | 0.85 | 0.7 | TBC | 0.83 |
| Emissivity | 0.5 | TBC | TBC | 0.45 |
| Absorptivity (SA) | 0.08 | >> CP1$^\dagger$ | >> CP1$^\dagger$ | 0.08 |
| Radiation Resistance | Low | High | High | High |

$^*$ = 0.0274× Youngs Modulus - Average of Kapton HN and Upilex-S Values
$^\star$ = Assumed Poisson Ratio of a Polyimide (MatWeb)
TBC = To be confirmed (i.e. Value couldn't be found)
SA = Solar absorptivity
$^\dagger$ = Known for being high although value couldn't be found

Table 6.2: Material Properties

6

### 6.4.3. MATERIAL SELECTION

In order to assess the properties of each material with respect to the material requirements a graphical trade off table shall be utilized. In addition, while a graphical trade-off is qualitative by nature, this trade off analysis is informed by the quantitative data provided by table 6.2. The trade off is presented in tables 6.3 and 6.4. For more information on the color scheme see appendix D.

| Gas | PROP-M-01 | PROP-M-02 | PROP-M-03 | PROP-M-04 |
|---|---|---|---|---|
| Mylar | 1380 kg/$m^3$ | 3.5 GPa | 103 MPa | Unsuitable for BEOC |
| Kapton HN | 1420 kg/$m^3$ | 2.76 GPa | 231 MPa | 10 year rated GEO |
| Upilex-S | 1470 kg/$m^3$ | 9.121 GPa | 520 MPa | 10 year rated GEO |
| CP-1 | 1540 kg/$m^3$ | 2 GPa | 87 MPa | 10 year rated GEO |

Table 6.3: Material Graphical Trade Off

| Gas | PROP-M-05 | PROP-M-06 | PROP-M-07 | PROP-M-08 | PROP-M-09 |
|---|---|---|---|---|---|
| Mylar | 17 $\mu$m/m°C | 0.85 | 0.5 | 0.08 | Yes |
| Kapton HN | 20 $\mu$m/m°C | Amber colour due to high SA | TBC | >> CP1 | Yes |

| | | | | | |
|---|---|---|---|---|---|
| Upilex-S | 12 $\mu$m/m°C | Amber colour due to high SA | TBC | >> CP1 | Yes |
| CP-1 | 51 $\mu$m/m°C | 0.83 | 0.45 | 0.08 | Yes |

Table 6.4: Material Graphical Trade Off

### EVALUATING THE MATERIALS

- *Mylar:* As can be seen, Mylar provides highly desirable properties across the range of criteria. It has excellent optical properties and provides the lowest density levels of any material. However, it has a number of drawbacks. Its Youngs modulus and yield strength values are higher than the best performing material CP1 and more importantly its poor radiation resistance makes it unsuitable for BEOC applications. Mylar is particularly susceptible to degradation from radiation exposure even with VDA coating (Connell and Watson, 2001). For this reason it is most commonly utilized for demonstration inflatable reflector missions in Earth orbit where long term environmental durability is not a concern. While this thesis is focused on the development of a demonstration mission, the desire to design a suitable approximation of a BEOC reflector necessitates the need for environmental durability.

- *Kapton HN:* Kapton HN on average provides the best mechanical properties of any of the materials. It has the second lowest density value, young's modulus value, yield strength and CTE. In addition, it provides excellent radiation resistance for extended periods in GEO and at the L2 Lagrangian point (Russell et al., 2000; Wooldridge et al., 2001). However, its optical properties leave a lot to be desired. Kapton HN, like Upilex-S, is known for its high solar absorptivity. This leads to a yellow/amber coloring which in turn reduces the optical performance of the material (Connell and Watson, 2001). This reduces its desirability for reflector applications requiring a transparent canopy. This is clearly reflected in the literature where no example of a Kapton HN transparent canopy could be found.

- *Upilex S:* Upilex-S provides the lowest CTE of any material, highlighting its stability over large temperature ranges. However, other than that and its radiation resistance, its properties are less desirable than those of all the other materials. Its yield strength and Youngs modulus are excessively high and would lead to undesirable inflation requirements and a reduced PE respectively. Furthermore, it has undesiable optical properties which, like Kapton HN, has led to no examples of Upilex-S canopies for reflector applications in the literature.

- *CP-1:* CP-1 provides the most desirable mix of properties of any of the materials presented. It has the lowest Youngs modulus and Yield strength (which negate its high density), excellent radiation resistance (although less than Kapton HN and Upilex-S (Russell et al., 2000; Wooldridge et al., 2001)) and excellent optical properties. This makes it a more attractive option than the radiation susceptible Mylar as well as more suitable for reflector applications than Kapton HN and Upilex-S. The only major drawback for the material is its CTE value. This will undoubtedly cause issues for thermal control of the structure and coupled with the low Young's modulus may lead to concerns if the structure undergoes large thermal cycles (Smith et al., 2018). However, its application for high precision inflatable reflector applications would suggest this is not a major issue and can be managed. As such, CP-1 is clearly the most suitable material based on the material requirements laid out in this thesis.

### THE COATING

In order to satisfy requirement REQ-IRI-03, a reflective coating must be selected to act as the interior reflective surface. As is the case for the structural material, a detailed analysis of the reflective optical properties shall not be carried out. However, from the same sources used to inform the material properties of the structure, the following two material properties, see table 6.5, of the reflective coating are given to be particularly desirable.

| ID | Property | Rationale |
|---|---|---|
| PROP-R-01 | Reflectivity | This is a measure of the fraction of incident radiation on a surface that is reflected. It is desired that the coating possess high reflectivity so as to ensure that the desired wavelengths of light are reflected. |
| PROP-R-02 | Emissivity | It is desired that the coating possess a low emissivity to reduce heat generated within the structure. |

Table 6.5: Desirable Reflective Coating Properties

The most obvious option is to utilise a VDA coating as CP1 coated in VDA is commercially available [7]. Indeed, it has been utilized for the Lunar Flashlight and NeaScout solar sails, with NeaScout utilizing a 10nm coating of aluminium (Heaton et al., 2017). In order to gauge both the properties of uncoated CP-1 as a transparent material and VDA coated CP-1 as a reflective material, tests were conducted onboard the ISS in in the early 2000's (Finckenor et al., 2015). The results indicated that CP-1, both uncoated and VDA coated, has high performing optical qualities with the reflectivity of the VDA coated material above 90%. In addition, the low emissivity of the coating can be seen in table 6.6 further solidifying its suitability for this application. These properties are taken from SMAD (Larson and Wertz, 1992) and Matweb[1].

| Property | Value |
|---|---|
| Density (kg/$m^3$) | 2700 |
| Thickness (nm) | 30 |
| CTE ($\mu$m/m°C) | 24 |
| Emissivity | 0.04 |
| Absorptivity | 0.08 |

Table 6.6: Properties of VDA

The thickness of the coating is typically 400-800 Å (40-80 nm) (Connell and Watson, 2001) although the the solar sails are utilizing 10nm thick VDA. For this structure a VDA thickness of 30nm, as will be utilized by the Gregorian inflatable reflector (Fenn et al., 2019), will be assumed. It should be noted, that a coating on the external side of the membrane surface is also likely necessary, although, once again, this shall not be investigated.

## 6.5. FABRICATION

For the preliminary design of this structure, it shall be assumed that the structure is an ideal spherical shell constructed from a homogeneous material. This shall be done as assessing the impact of the fabrication method was deemed beyond the scope of this thesis. Despite this, a brief overview of the potential fabrication methods for a spherical inflatable structure shall be presented due to fabrication being a key design consideration for future iterations of the inflatable structures design process.

### 6.5.1. SPHERICAL INFLATABLE FABRICATION

The baseline ideal design for the structure is a that of a spherical shell. However, as noted in the literature study, manufacturing a large monolithic and seamless spherical structure from thin polymer films is extremely challenging. It is therefore no surprise that one of the most significant challenges in realizing this ideal shape is the fabrication process (Lesser et al., 2015). A recent paper by Smith et al., 2018 from the University of Arizona and Freefall Aerospace (the developers of the CatSat inflatable spherical structure) investigated several different fabrication methods with which to construct spherical inflatable structure as part of NASA Advanced Innovative Concept (NIAC) research program. They identified three different methods; The gore approach, the 'soccer ball' approach and the 3D casting approach. A brief exploration of the papers findings for each of these methods shall be provided here.

#### THE GORE APPROACH

As noted in the literature study, this is the classical approach that has been utilized for decades in the fabrication of inflatable reflectors structures as well as large high-altitude scientific balloons. To the best of the authors knowledge it is the only tried and flight tested method of fabricating such structures. The method involves fabricating the structure from flat film gores that are then assembled into a near perfect spherical structure by seaming the gores together as seen in figure 6.5 although as noted handling and cutting precise gores is very challenging.

The non-smooth faceted surface that results from utilizing this method is a major drawback for precision reflector applications. This is particularly true for a sphere fabricated from a small number of gores which in turn requires higher pressures so as to deform the material into a more desirable spherical shape. However, high pressures can lead to undesirable structural consequences as well as increasing the demands on the inflation system. A solution to this issue is to utilize a higher number of gores. However, this also has drawbacks as the large number of converging seams at the apex and nadir lead to an undesirable stiffening at the poles of the sphere. Not only does this lead to variable structural stiffness along the length of the structure but is also requires polar

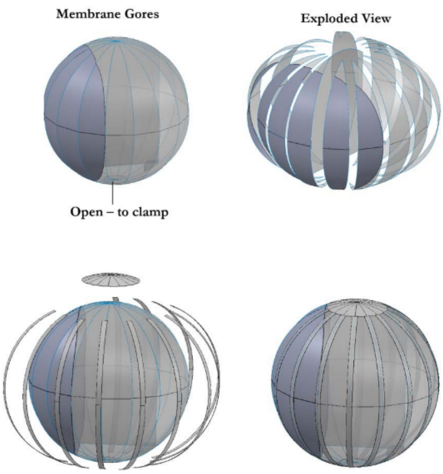


Figure 6.5: The Gore Approach (Chandra et al., 2020)



caps, as seen in figure 6.5, which in turn increase the mass and volume requirements of the structure.

After developing a range of spheres of various sizes, Smith et al., 2018 state that while the gore approach is suitable for spheres with a diameter of 5 metres or greater, its use is undesirable for spheres smaller than this. Thus despite the CatSat spherical inflatable structure utilizing this approach, Smith et al., 2018 state that an alternative method for CubeSat spherical reflectors is desirable.

### THE SOCCER BALL APPROACH

This approach was identified by Smith et al., 2018 as showing promise for CubeSat spherical inflatable reflectors. The method is like that utilized for soccer balls where flat hexagonal and pentagonal sections are cut and then seamed together into a structure called a Goldberg polyhedron, figure 6.6a. The researchers also investigated using triangular elements, as seen in figure 6.6b. While the soccer ball method would provide a more uniform structural thickness distribution relative to the gore approach, the approach leads to an increased number of complex seams which increases the risk of fabrication errors. In addition, a significant degree of wrinkling was created.

### THE 3D FORMING APPROACH

This approach involves forming elements of the structure using a 3D mandrel. It is seen as holding the most promise of the three approaches identified by Smith et al., 2018 who constructs a sphere using the triangular soccer ball approach with the 3D triangular elements fabricated using this method. This allowed them to address the wrinkling issue present in the soccer ball approach and produce a sphere with what appears to be a high degree of surface smoothness, as seen in figure 6.7. It is evident that this method shows promise, particularly for CubeSat spherical structures although as Smith et al., 2018 state, it requires further research.

(a) Pentagonal Elements (b) Triangular Elements

Figure 6.6: The Soccer Ball Approach

Figure 6.7: 1 metre sphere fabricated using the 3D forming approach

### Summary

It is apparent that the fabrication of precision spherical inflatable reflectors is still in its early days. While the 3D Forming Approach in particular shows promise, further research must be carried out to assess its suitability for space applications and also to assess its impact on the shape transformations of the structure. As noted, this is left for future work with the fabrication method and its impact on the structure not considered in this thesis.

## 6.6. Environmental Orbital Conditions

As discussed in the literature review (section 2.2.4), the environmental conditions that the structure must withstand play a substantial role in the required functionality of the inflation system. The discussion on packaging (see section 6.3) notes that ascent venting is required to vent the residual gases during the launch and pre-deployment environment, while the discussion on deployment (see section 6.3) points out that the inflation loads be appropriately controlled during the dynamic deployment environment. However, for this discussion, the focus shall be on the operating environment, i.e. the space environment.

As dictated by key requirement REQ-BEOC-04-02, this structure, which will operate in Lunar Orbit, must be capable of withstanding the lunar environment. As is alluded to in the literature review, this lunar environment is composed of two main aspects that the inflatable structure must be able to withstand; physical damage from micrometeoroids and material property changes arising from environmental interactions, most notably temperature extremes and radiation. As the radiation resistance of CP1 has already been established in section 6.4, only micrometeoroids and the thermal environment shall be discussed here. In addition, as a detailed analysis of the orbit is not carried out in this thesis, it is assumed that the structure shall operate in a 500 km-altitude circular orbit about the moon. This orbit is based off one of the options discussed by Cipriano et al., 2018, who discusses the LUMIO missions lunar orbital design.

### 6.6.1. MICROMETEOROIDS

6

As is described in the literature study, high velocity impacts from micrometeoroids can damage the inflatable structure. In order to gauge the threat posed by micrometeoroids to the pressure stabilized structure, the micrometeoroid flux in the lunar environment must be quantified. By doing this, the rate of hole growth due to micrometeoroid punctures can be estimated and the mass of make-up gas required by the inflation system gauged.

Due to the limited nature of the literature surrounding the calculation of these parameters only a handful of papers detailing this process could be found. Of these, both Grossman and Williams, 1990 and Chodimella et al., 2006 used a Near Earth-Lunar model (Cour-Palais, 1969) for estimating the hole growth in inflatable concentrator and antenna structures respectively. However, neither provided a detailed exploration of the analysis nor the calculated results. In addition, while a variety of different models are available for calculating the lunar flux, such as those presented by Badyukov, 2020, few, if any, have been utilized for such calculations. As a consequence it was decided that the approach presented by Thomas and Friese, 1980 would be followed due to the fact that the method could be validated using results presented in the paper.

#### APPROACH

Using the micrometeoroid flux model developed by Whipple, 1967, the accumulated number of micrometeoroid impacts on the structure per $cm^2$ per second, i.e. the flux, can be calculated using the following equations 6.1 and 6.3 over a micrometeoroid mass range of $10^{-12}$ to $10^2$ grams. Equations 6.2 and 6.4 give the derivatives of these equations with respect to mass and allow the number of impacts with mass between m and m + dm to be found.

- For m < $10^{-5.2}$ grams:

$$N = 1.41 \times 10^{-14} \cdot m^{-0.51} \tag{6.1}$$

$$dN = -7.19 \times 10^{-15} \cdot m^{-1.51} dm \tag{6.2}$$

- For m > $10^{-5.2}$ grams:

$$N = 3.31 \times 10^{-19} \cdot m^{-1.4} \tag{6.3}$$

$$dN = -4.63 \times 10^{-19} \cdot m^{-2.4} dm \tag{6.4}$$

where:

- N = Micrometeoroid Flux ($\frac{1}{cm^2 \cdot s}$)
- dN = Flux between m and m + dm ($\frac{1}{cm^2 \cdot s}$)
- m = mass (grams)
- dm = mass step size (m$\times 10^{0.1}$)

In order to find the change in hole area due to micrometeoroid damage, i.e. the rate of hole growth, the hole generated by a micrometeoroid of a certain mass is multiplied by the flux at that mass and then integrating this across the entire micrometeoroid mass range. This is expressed in equation 6.5.

$$G = \int_m A_o(m) dN(m) \tag{6.5}$$

where:

- $A_o(m)$ = Area of hole generated by micrometeoroid of mass $m$

6

Assuming that all micrometeoroids are spherical in shape, $A_o(m)$ can be calculated by finding the diameter of the micrometeoroid of mass $m$. This can be done by finding the volume of the micrometeoroid using the appropriate density value. Instead of using a uniform density across the entire mass range as is done by Thomas and Friese, 1980, it was decided to use the more realistic mass-density relations from Grossman and Williams, 1990. These are given in equation 6.6.

$$\begin{aligned} m < 10^{-6} g &= 2.0 gcm^3 \\ 10^{-6} g < m < 0.01 g &= 1.0 gcm^3 \\ m > 0.01 g &= 0.05 gcm^3 \end{aligned} \tag{6.6}$$

In addition, Grossman and Williams, 1990 determined that the size of the hole generated by the micrometeoroid shall depend on the material thickness-to-micrometeoroid diameter ratio (T/D). This T/D ratio can yield three different damage scenarios as seen in figure 6.8. A quantitative indication of “Small”, “Intermediate” or ”Large” (figure 6.8) and the damage hole size $D_h$ they yield is given by the following expressions (Chodimella et al., 2006). These expressions are as follows:

1. If the T/D ratio is less than 0.33, i.e the particles diameter is significantly larger than the material thickness, the particle will pierce through both sides of the structure. Due to some uncertainty regarding the expression given by Chodimella et al., 2006, it shall be assumed that a hole slightly larger (1.1 times) than the meteoroid diameter is created in both sides (Grossman and Williams, 1990).

$$T/D < 0.33 \Rightarrow D_{hole} = 1.1 \times D \tag{6.7}$$

2. If the T/D ratio is between 0.33 and 3, the particle will break up on impact and create a hole significantly larger than the meteoroid diameter.

$$0.33 < T/D < 3 \Rightarrow D_{hole} = 3.44 \times D \tag{6.8}$$

3. If the T/D ratio is greater than 3, no hole is created although a crater is formed in the material. The effects of this cratering on the local material properties of the structure are not considered in this thesis.

$$T/D > 3 \Rightarrow \text{No penetration} \tag{6.9}$$

A graphical indication of these relations is presented in figure 6.8.

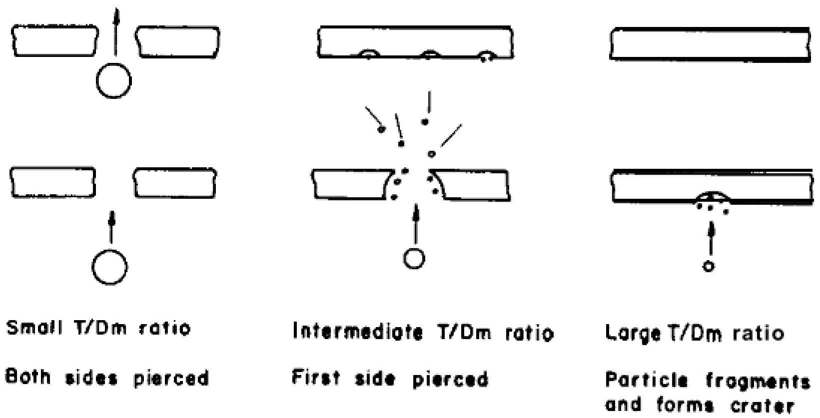


Figure 6.8: Effect of micrometeroid particle size on damage caused to inflatable. (Grossman and Williams, 1990)

From this exploration it can be said that the area of hole generated by micrometeoroid of mass m $A_o(m)$ can be found using equation 6.10, which for T/D<0.33 is multiplied by 2 to account for holes generated in both sides of the structure.

$$A_o(m) = \pi \cdot \left(\frac{D_{hole}}{2}\right)^2 \tag{6.10}$$

Integrating equation 6.5 across the micrometeoroid mass range yields the rate of hole growth. However, as the micrometeoroid flux model is originally derived for calculating the micrometeoroid flux in Earth orbit (Whipple, 1967) a correction factor is introduced to express this hole growth rate as a function of the flux in lunar orbit. This is correction factor is taken to have a value of 0.7 (Badyukov, 2020).

$$G_M = G_E \times F_M \tag{6.11}$$

where:

- $G_M$ = Growth rate in Lunar orbit

- $G_E$ = Growth rate in Earth orbit
- $F_M$ = Micrometeoriod correction factor (0.7)

#### RESULTS

Calculating $G_M$ for a range of different membrane thicknesses yields the following results. Comparing these growth rates to that calculated by Thomas and Friese, 1980 (6.23E-14 1/s) or Thunnissen et al., 1995 (1.0869E-15 1/s) for inflatable reflector structures in Earth Orbit, it can be seen that the approach utilized generates realistic values.

| **Thickness ($\mu$m)** | **Growth rate (1/s)** |
|---|---|
| 2.5 | 2.61986E-14 |
| 5 | 3.21421E-14 |
| 12.7 | 4.13974E-14 |
| 25.4 | 5.20799E-14 |
| 50 | 6.19771E-14 |

Table 6.7: Growth rate, G, in membrane wall due to Micrometeroids

However, as can be seen from table 6.7 the growth rate results reveal an unexpected phenomenon. Smaller wall thickness actually yield a lower rate of hole growth in the inflatable membrane relative to larger thicknesses. It is presumed that this is primarily due to the relationship between hole size and the T/D ratio, with larger holes being generated at higher thicknesses despite the lower flux levels. Unfortunately due to the relatively scant information regarding the development of holes in inflatable space structures, further elaboration on this phenomena could not be found with the limited detail provide by Grossman and Williams, 1990 and Chodimella et al., 2006 being of little use. As such, this phenomena would be worth exploring in future work. Moreover, future work should also utilize more accurate lunar flux models to more precisely gauge the rate of hole growth for an inflatable structure in lunar orbit.

#### SUMMARY

Using the method described in this section, the growth rate of holes on the structures surface due to micrometeroid damage can be estimated. This growth rate, which varies with material thickness as seen in table 6.7, shall inform the selection of an appropriate material thickness for the structure, impacting its mass, volume and pressure requirements. With the selection of the material thickness, the associated growth rate can be used to calculate the mass of makeup gas required to compensate for the loss of gas due to the development of these holes, and thus maintain the structures structural integrity. This is discussed further in the design of the inflation system, sections 7.4 and 8.4. It should be noted that the affect of the VDA coating is assumed to be negligible in these calculations.

### 6.6.2. THERMAL ENVIRONMENT

In this section, a preliminary investigation into the expected on-orbit temperatures shall be carried out. However, while these on-orbit temperatures are a key consideration in the design of an inflatable space structure, accounting for the thermal cycling the reflector undergoes as it orbits the moon, and the resultant variations in gas pressure and skin stress, requires a detailed Finite Element thermal Analysis (FEA). This is further emphasized by the need to model the complex thermal behaviour of a structure composed of a transparent canopy and internal reflective surface, with the internal radiation requiring numerical solutions coupled with ray tracing models to be developed (Thomas and Friese, 1980). As such an analysis was deemed beyond the scope of this thesis, a simplified approach is necessary to at least gauge a preliminary estimate of the expected on-orbit temperatures.

It was decided that the relatively simple, and verifiable, analytical method previously utilized for NASA spherical inflatable structures (Clemmons, 1964; Coffee et al., 1962; Teichman, 1968; Wood and Carter, 1959) shall be suitable for achieving this goal. While this approach shall allow a simplified thermal analysis to be carried out, one of its main downsides is that the structure must be considered both homogeneous and opaque, thus neglecting the fact that the structure is composed of a transparent canopy and interior reflector (REQ-IRI-03). This assumption, while not accounting for the real thermal behaviour of the structure, shall help to give a preliminary indication of the expected on-orbit temperatures. However as the structure shall be considered opaque, i.e. coated in a particular thermal coating, before further exploring this method, it was deemed prudent to first establish suitable thermal requirements for the analysis.



### Thermal Requirements

Utilizing this method requires the simplified assumption that this structure is a uniform opaque spherical structure. Thus, as CP-1 is a transparent material, it shall be assumed for this analysis that the structure is uniformly coated with a non-transparent coating. In order establish a reasonable initial estimate of the anticipated on-orbit structural temperatures, a suitable coating must be selected. This shall be done by evaluating the thermal performance of different coatings with respect to two distinct thermal requirements; the temperature differential across the structure and the equilibrium 'operational' temperature of the structure.

As no inflatable reflectors have been designed for lunar orbit an accurate gauge of suitable on-orbit thermal requirements could not be found in the literature. Therefore, it was decided to turn to pressure-stabilized inflatable reflectors in Earth Orbit in order to gain insight into the desirable thermal requirements for such a structure in Lunar Orbit. While this comparison isn't perfect, it will be helpful for gauging appropriate structural temperatures. In addition, while opaque structures that consist of a fully coated exterior shall be referenced, the temperatures of structures with a transparent canopy and internal reflector shall take priority when determining the suitable thermal requirements. A summary of these thermal requirements is given in table 6.8.

- *Temperature Differential:*
  - Uneven heating of the structure during its orbit shall result in hot and cold regions, leading to a temperature differential ($\Delta_T$) across the structure. This differential can cause significant problems for maintaining shape accuracy of the structure. It is therefore desirable that this temperature differential be kept to a minimum (Friese et al., 1983).

- ECHO 1 and PAGEOS (Clemmons, 1964; Teichman, 1968), from which the simplified thermal model stems, had temperature differentials of 20 K and 25 K respectively, both having a fully reflective aluminium coating on their exterior. Examining structures with interior reflective components, a recent study by Smith et al., 2018 performed a thermal analysis on a large pressure-stabilized inflatable sphere in an LEO sun synchronous orbit. They found a similar temperature differential of about 30 K across the structure. Other structures with internal reflective components also yield differentials of 20-30 K (Freeland and Bilyeu, 1993; Friese et al., 1983; Pino, 2016). Therefore, based off this research it is assumed that a temperature differential between the hot and cold spots on the structure of between 20-30 K is acceptable.

| **Thermal Requirement** | **Value (K)** |
|---|---|
| Temperature Differential ($\Delta_T$) | 20-30 |
| Sunlit Temperature ($T_{eq_s}$) | 300 +/- 50 |
| Shadow Temperature ($T_{eq_{sh}}$) | 200 +/- 50 |

Table 6.8: Thermal Requirements

- *Operational Temperature:*
  - Deciding on an appropriate operational temperature is a slightly more tricky process. Factors that must be considered include the reflective application, the characteristic of the inflation gas and of course the relevant thermal environment. However, as has been stated, given no relevant lunar inflatable structures could be found in the literature, operational temperatures are derived from Earth orbiting structures.
  - The operational sunlit temperatures ($T_{eq_s}$) of the fully externally coated ECHO 1 and PAGEOS structures are approximately 380 K-410 K, while the operational shadow temperatures ($T_{eq_{sh}}$) are significantly lower, getting as cold as 123K. Thomas and Friese, 1980 evaluate the theoretical temperature profiles of a variety of semi-transparent spherical black balloons in Earth orbit giving temperatures varying from about 220K to 350K with varying solar angle. Examining, structures with interior reflective components unsurprisingly yields lower sunlit operational temperatures. The CATSAT inflatable spherical reflector (Chandra et al., 2020; Chandra et al., 2021) in a sun synchronous orbit has an average operational temperature of about 300 K, while IAE's temperature as the sun is entering the shadow is about 315K and then plummets to 205 K in shadow (Freeland et al., 1997). Meanwhile, Friese et al., 1983 calculates values varying from approximately 210 K to 400 K for an inflatable reflector depending on sun angle. Finally, a parabolic reflector designed by Thunnissen et al., 1995 for the purpose of designing low mass inflation systems assumes an operational temperature of about 293 K.
  - Based off this research it is assumed that an inflatable space structure can typically survive and likely operate in temperatures ranging from 100K to

6

400K. As such, it shall be assumed that nominal sunlit operational temperatures of around 300 K +/- 50 K (-23°C to 77 °C) are desirable, while shadow temperatures of around 200 K are +/- 50 K are deemed acceptable. As extreme thermal variations between the sunlit and shadow temperatures exacerbate the thermal distortions of the structure, it is highly desirable to minimize the time the structure spends in shadow. As a detailed analysis of an appropriate orbit for the structure is not carried out, this shall be left for future work.

### THE LUNAR THERMAL ENVIRONMENT

The thermal analysis of a homogeneous opaque spherical inflatable structure in lunar orbit shall be now be carried out using the analytical method referred to previously. The first step in this analysis is to evaluate the thermal environment. As the structure is in orbit around the moon, it can only interact with the lunar thermal environment by radiation. The different sources of radiation are:

1. Direct Solar Radiation
2. Lunar Albedo
3. Thermal Energy from the Moon
4. Reflected solar radiation from the CubeSat

6

The spherical structure will experience thermal equilibrium if the sum of the these radiation sources, along with any thermal energy generated internally by the reflector as well as that conducted from the CubeSat, is equal to the energy that the structure radiates out into space. This thermal balance will enable the calculation of the temperature of the inflatable structure (Fortescue et al., 2011). However, before this can be done it is first necessary to quantify the radiation sources present in the lunar thermal environment. It is important to note that for this thermal analysis that thermal energy from the CubeSat, whether by reflected solar radiation or conduction, is neglected.

**Direct Solar Radiation**

As the angle subtended by the Sun at Earth is around 0.5°, the solar radiation incident on the structure can be approximated as a parallel beam (Fortescue et al., 2011). The intensity of this solar radiation is given by the solar flux, $F_s$, and at the Moon is about the same as at Earth, 1361 W/m$^2$ [6]. The amount of energy absorbed by the spherical structure can be written using equation 6.12.

$$\dot{Q}_S = \pi R^2 \cdot F_S \cdot \alpha_S \tag{6.12}$$

where:

- $\dot{Q}_S$ = Solar radiation absorbed by structure (W)
- $\pi R^2$ = Area of structure receiving solar radiation ($m^2$)
- $F_s$ = Solar flux (1361 W/m$^2$)
- $\alpha_s$ = Absorptance of structure to solar radiation

[6] https://nssdc.gsfc.nasa.gov/planetary/factsheet/moonfact.html

**Lunar Albedo**

The lunar albedo represents the fraction of the solar radiation that is reflected off the surface of the moon. While the Albedo, a, across the surface of the moon will inevitably vary, a value of 0.11 (the bond albedo) [6] can be utilized as an average approximate value. Utilizing averaged properties for thermal analysis is customary. The intensity of the solar radiation that is reflected off the lunar surface tends to be a function of the orbital solar angle $\beta$. It can be represented by a visibility factor $F$. An approximate representation of this visibility factor can be made as a function of $\beta$. F=1 when the structure lies on the moon-sun line, i.e. the sun's rays are in the orbital plane, ($\beta = 0$) and F = 0 when the structure is about to enter the moons shadow, i.e the orbital plane is perpendicular to the sun's rays (assumed $\beta = 90°$) (Teichman, 1968).This approximation contributes to the calculation of the structures maximum and minimum temperature values while in sunlight. In addition, considering an altitude of 500 km (Cipriano et al., 2018), the altitude factor k also affects the amount of radiation absorbed. The amount of energy absorbed by the spherical structure can be written using equation 6.13.

$$\dot{Q}_R = \pi R^2 \cdot F_S \cdot \alpha_S \cdot a \cdot F(\beta) \cdot \left[1 - \sqrt{(1-k^2)}\right] \tag{6.13}$$

where:

- $\dot{Q}_R$ = Reflected solar radiation absorbed by structure (W)
- a = Lunar bond albedo
- $F(\beta)$ = Lunar visibility factor
- k = Altitude factor ($\frac{R_m}{R_m+h}$)
  - h = Altitude (500km)
  - $R_m$ = Radius of moon (1,737.4 km)

**Lunar Thermal Radiation**

Like all planetary bodies, the moon has a non-zero temperature (270.4 K [6]) and thus radiates heat. Given that practically all of the heat received by the moon is either reflected or radiated, the amount of energy absorbed by the spherical structure can be approximated using equation 6.14.

$$\dot{Q}_M = \pi R^2 \cdot F_S \cdot \alpha_M \cdot \frac{1-a}{2} \cdot \left[1 - \sqrt{(1-k^2)}\right] \tag{6.14}$$

where:

- $\dot{Q}_M$ = Lunar thermal radiation absorbed by structure (W)
- $\alpha_M$ = Absorptance of structure to lunar thermal radiation. According to Kirchoff's law this is equal to the structures infrared emittance $\epsilon_o$ (Fortescue et al., 2011)

6

### THERMAL BALANCE

As has previously stated, the temperature of the structure is dependent on the thermal balance between the heat received by the structure and the heat it radiates into the thermal vacuum of space. The general equation for a single node thermal analysis is given in equation 6.15.

$$\dot{Q}_{in} = \dot{Q}_{out} = \dot{Q}_{absorbed} + \dot{Q}_{internal} = \dot{Q}_{emitted} \tag{6.15}$$

For this analysis, internal heat generation, $\dot{Q}_{internal}$, is neglected. This means that, as has been already stated, the impact of the internal radiation on the temperature of the structure is not considered. In addition, it is assumed that the spherical shell structure is isothermal and remains in thermal equilibrium its environment (Clemmons, 1964). This yields the following equation.

$$\dot{Q}_{emitted} = 4\pi R^2 \cdot \epsilon_o \cdot \sigma \cdot T_{eq}^4 = \dot{Q}_S + \dot{Q}_R + \dot{Q}_M \tag{6.16}$$

where:

- $\dot{Q}_{emitted}$ = Thermal radiation emitted by the structure (W)
- $\epsilon_o$ = External surface emissivity
- $\sigma$ = Stefan-Boltzmann constant $\left(5.67 \times 10^{-8} W/(m^2 \cdot K^4)\right)$
- $T_{eq}$ = Structure equilibrium temperature (K)

For this thesis, the average equilibrium temperature of the structure is of interest as a means of determining the median temperature of the structure. This value can then be utilized for calculations relating to the inflation system. It shall be calculated for both sunlight and shadow conditions in order to gauge the temperature differentials.

**Sunlit Conditions**

While the structure is in sunlight, equation 6.16 can be written so as to yield an equilibrium temperature, $T_{eq_s}$, of the structure in this environment as seen in equation 6.17. The variation of this temperature with orbital angle $\beta$ can be calculated by using the visibility factor F. For this study, only the maximum and minimum equilibrium temperatures are of interest and can be obtained by setting F=0 and F=1. These worst case conditions must be defined in order to ensure the structure stays within acceptable limits.

$$T_{eq_s}^4 = \frac{F_S \cdot \alpha_S}{4 \cdot \epsilon_o \cdot \sigma} \cdot \left(1 + 2\left[a \cdot F(\beta) + \frac{1-a}{4} \cdot \frac{\alpha_M}{\alpha_S}\right] \cdot \left[1 - \sqrt{(1-k^2)}\right]\right) \tag{6.17}$$

Meanwhile the hottest and coldest spots on the surface of the structure can be calculated using the following equations. These local hot and cold spots arise due to uneven heating of the structure and exacerbate the challenge with shape accuracy. It is thus important to calculate these values as it allows the temperature differential across the structure to evaluated. See reference sources for derivations.

$$T_{h_s}^4 = \frac{F_s \cdot \alpha_s + \frac{1}{4} \cdot \frac{\epsilon_i}{\epsilon_o} \cdot F_s \cdot \alpha_S \cdot \left(1 + 2\left[a \cdot F(\beta) + \frac{1-a}{4} \cdot \frac{\alpha_M}{\alpha_S}\right] \cdot \left[1 - \sqrt{(1-k^2)}\right]\right)}{\sigma \cdot (\epsilon_i + \epsilon_o)} \tag{6.18}$$

$$T_{c_s}^4 = \frac{\frac{1}{4} \cdot \frac{\epsilon_i}{\epsilon_o} \cdot F_S \cdot \alpha_S \cdot \left(1 + 2\left[a \cdot F(\beta) + \frac{1-a}{4} \cdot \frac{\alpha_M}{\alpha_S}\right] \cdot \left[1 - \sqrt{(1-k^2)}\right]\right)}{\sigma \cdot (\epsilon_i + \epsilon_o)} \tag{6.19}$$

where:

- $T_{eq_s}$ = Equilibrium temperature in sunlit conditions (K)
- $T_{h_s}$ = Hotspot temperature in sunlit conditions (K)
- $T_{c_s}$ = Coldspot temperature in sunlit conditions (K)
- $\epsilon_i$ = Internal surface emissivity

**Shadow Conditions**

While the structure is in the shadow of the moon, not accounting for shadows cast by the Earth on the moon due to their rarity, equation 6.16 can be written so as to yield an equilibrium temperature, $T_{eq_sh}$, of the structure in this environment as seen in equation 6.20.

$$T_{eq_{sh}}^4 = \frac{F_S \cdot \alpha_S}{4 \cdot \epsilon_o \cdot \sigma} \cdot \left(\frac{1-a}{2}\right) \cdot \frac{\alpha_M}{\alpha_S} \cdot \left[1 - \sqrt{(1-k^2)}\right] \tag{6.20}$$

Once again the hottest and coldest spots on the surface of the structure can be calculated using the following equations. See reference sources for derivations.

$$T_{h_{sh}}^4 = \frac{F_s \cdot \alpha_s \cdot \left(\frac{1-a}{4}\right) \cdot \left(\frac{1}{2} \cdot \frac{\epsilon_i}{\epsilon_o} \cdot \left[1 - \sqrt{(1-k^2)}\right] + k^2\right)}{\sigma \cdot (\epsilon_i + \epsilon_o)} \tag{6.21}$$

$$T_{c_{sh}}^4 = \frac{\frac{1}{4} \cdot \frac{\epsilon_i}{\epsilon_o} \cdot F_s \cdot \alpha_s \cdot \left(\frac{1-a}{2}\right) \cdot \left[1 - \sqrt{(1-k^2)}\right]}{\sigma \cdot (\epsilon_i + \epsilon_o)} \tag{6.22}$$

where:

- $T_{eq_{sh}}$ = Equilibrium temperature in shadow conditions (K)
- $T_{h_s}$ = Hotspot temperature in shadow conditions (K)
- $T_{c_s}$ = Coldspot temperature in shadow conditions (K)

6

**Results**

For this thermal analysis, a variety of different thermal coatings commonly utilized in thermal control shall be evaluated with respect to the desired thermal requirements. Generally, these coatings are applied to a percentage of the structures external surface area to adjust the effective absorptivity and emissivity of the structure. The effective values can be calculated using the following equations (Coffee et al., 1962):

$$\alpha_S = \left(\alpha_{S_p} - \alpha_{S_u}\right)\frac{A_c}{A_T} + \alpha_{s_u} \tag{6.23}$$

$$\epsilon_o = \left(\epsilon_{o_p} - \epsilon_{o_u}\right)\frac{A_c}{A_T} + \epsilon_{o_u} \tag{6.24}$$

where:

- p = coated
- u = uncoated
- $A_c$ = Area Coated
- $A_T$ = Total Area

6

As the structure shall be uniformly coated these equations can be reduced to:

$$\alpha_S = \alpha_{S_p} \tag{6.25}$$

$$\epsilon_o = \epsilon_{o_p} \tag{6.26}$$

Table 6.9 details the thermal characteristics of a variety of different coatings on the spherical structure in both sunlight and shadow. All these calculations are carried at F=1.

| **Coating** | $\alpha_{s_p}$ | $\epsilon_{o_p}$ | $T_{eq_s}$ °$C$ | $T_{h_s}$ °$C$ | $T_{c_s}$ °$C$ | $T_{eq_{sh}}$ °$C$ | $T_{h_{sh}}$ °$C$ | $T_{c_{sh}}$ °$C$ |
|---|---|---|---|---|---|---|---|---|
| VDA | 0.08 | 0.04 | 70.6 | 86.58 | 63.38 | -95.86 | -88.19 | -99.59 |
| Bare Aluminium | 0.17 | 0.1 | 57.96 | 89.27 | 41.76 | -95.86 | -79.92 | -104.53 |
| VDG | 0.3 | 0.03 | 233.48 | 253.22 | 225.37 | -95.86 | -89.90 | -98.69 |
| Gold | 0.25 | 0.04 | 178.32 | 200.67 | 168.81 | -95.86 | -88.19 | -99.59 |
| Polished Beryllium | 0.44 | 0.01 | 458.47 | 468.93 | 454.47 | -95.68 | -93.718 | -96.83 |
| Polished Titanium | 0.6 | 0.6 | 20.91 | 87.2 | -35.22 | -95.68 | -55.018 | -129.701 |
| 3M Black Velvet | 0.97 | 0.84 | 30.32 | 107.56 | -39.92 | -95.68 | -50.85 | -137.16 |
| White Paint | 0.2 | 0.85 | -49.21 | -13.24 | -101.38 | -95.68 | -50.71 | -137.16 |
| Silver Paint | 0.37 | 0.44 | 10.19 | 66.05 | -34.23 | -95.68 | -59.29 | -123.65 |

Table 6.9: Effects of various coatings (Fortescue et al., 2011; Larson and Wertz, 1992)

It can be clearly seen from table 6.9 that both VDA and bare aluminium are the most appropriate coatings for the inflatable structure given the thermal requirements presented in table 6.8. The sunlit equilibrium temperature of both coatings meet the desired operational temperature requirement. These temperatures vary by only about 5 $^\circ C$as F tends towards 0 due to the uniformity of the coatings. However, while the thermal differential of VDA (23.2K) meets the desired thermal differential requirements, the value for bare aluminium (47.51K) does not. Hence, VDA can be considered the most suitable thermal coating for this thermal analysis. This suitability is further emphasized by the fact that VDA coated CP-1 is manufactured by NeXolve [7].

| **Property** | **Value (K)** |
|---|---|
| Sunlit Temperature Differential ($\Delta_{T_s}$) | 23.2 |
| Sunlit Temperature ($T_{eq_s}$) | 343.75 |
| Shadow Temperature ($T_{eq_{sh}}$) | 177.29 |

Table 6.10: Structures Thermal Properties

The sunlit results for VDA presented in table 6.9 are calculated for when the structure lies on the moon-sun line, F = 1, and represent the maximum structural equilibrium temperature. As noted, this temperature shall drop by about 5 $^\circ C$ as F tends towards 0. In a more detailed thermal analysis it may be worth examining this variation as the structure orbits the moon, including the rapid change in thermal properties as the structure enters the shadow region, in order to gain a more detailed understanding of the structures thermal cycling. However, this shall be left for future work. The results presented in table 6.10 are deemed sufficient for a preliminary thermal analysis with $T_{eq_s}$ being taken as the structures equilibrium temperature during all inflation stages.

### CONCLUSION

Ideally a comprehensive thermal analysis utilizing FEA and ray tracing models would be carried out to evaluate the thermal properties of this lunar spherical inflatable reflector. However, due to the limited scope of this thesis project a simplified thermal analysis of the structure was carried out by approximating it as a uniform opaque spherical reflector coated in VDA, similar to the ECHO and PAGEOS satellite reflectors. This enabled a simple yet verifiable thermal analysis to be carried out. While not fully reflective of the real thermal properties of an inflatable reflector with a transparent canopy and interior reflective surface, the analysis yielded a preliminary estimate of the on-orbit conditions that satisfies the thermal requirements informed by comparative structures that consist of such a canopy and reflector.

[7] https://nexolve.com/

## 6.7. MECHANICAL PROPERTIES

The final stage in the design of this inflatable spherical structure is to determine its mechanical properties. The determination of these properties is constrained to those that are required to ensure that the designed structure complies with the mission requirements as well as the reflector requirements that follow. Once this compliance has been established, the inflation system requirements can be finalized, thereby enabling the design process for the inflation system to begin.

The key mechanical properties that shall be established in this section include the primary parameters of stowed volume and mass followed by the structural loads that the struture must withstand. These parameters shall enable the selection of the most suitable membrane thickness based on the desired structural requirements. For all of these calculations, the structure is assumed to be a uniform thin shell structure.

### 6.7.1. STOWED VOLUME

As the structure is assumed to be a uniform thin shell structure, the material volume of the CP1 structure can be calculated using equation 6.27. This method, although an approximation which does not consider the individual gores nor the adhesive, provides an accurate approach for calculating the mass and volume of the structure and has been verified for both ECHO 1 and PAGEOS structures, yielding a difference of <5 % from the recorded value.

6

$$V_{CP1} = \frac{4}{3}\pi\left(R^3 - (R-t)^3\right) \tag{6.27}$$

where:

- $V$ = Volume ($m^3$)
- $R$ = Deployed radius (0.5 m)
- $t$ = Material thickness (m)

In addition, to the material volume of the CP1 inflatable structure, the material volume of the VDA coating must be calculated. This can also be done using a value of 30 nm (VDA coating thickness) for t in equation 6.27 and diving the result by 2, given that the coating is on only one half of the structure. This yields a material volume for VDA of $V_{VDA} = 4.71\times 10^{-8} m^3$. Adding this to $V_{CP1}$ yields the total material volume of the structure. Considering an additional margin of 10 % to account for other contributions not considered in this calculation such as residual gas, adhesives, etc, the total material volume of the structure can be calculated using equation 6.28.

$$V_{material} = (V_{CP1} + V_{VDA}) \times 1.10 \tag{6.28}$$

From the discussion on the packaging of a spherical inflatable structure (section 6.3), a PE of 40% is assumed. Thus, using equation 2.2, the packaging container volume (i.e. the stowed volume) of the structure can be calculated. Once this has been done, the RPE of the structure can be calculated using equation 2.1. REQ-IRI-04 desires a minimum RPE value of $1.5 m^2$/U.

### 6.7.2. MASS

The mass of the structure can be calculated using equation 6.29. As is the case for volume an additional margin of 10 % is considered.

$$M_{material} = \left(V_{CP1} \cdot \rho_{CP1} + V_{VDA} \cdot \rho_{VDA}\right) \times 1.10 \tag{6.29}$$

Where:

- $M$ = Mass (Kg)
- $\rho$ = Density (Kg/$m^3$)

Dividing this value by the deployed cross sectional area of the structure, its areal density can be found. As noted in requirement REQ-IRI-05, it is desired that this value be less than 0.4 kg/$m^2$.

### 6.7.3. STRUCTURAL LOADS

In order to assess whether the structure can maintain its structural integrity while in lunar orbit, a preliminary structural analysis must be carried out. For this analysis the on-orbit loads that the structure shall experience must be determined. This shall be done in this section. The main loads an inflatable spherical structure shall experience on-orbit, according to the following sources (Clemmons, 1964; Guidanean and Veal, 2003; Smith et al., 2018) are as follows. It should be noted that given the limited nature of the thermal analysis carried out, an exploration of thermal loading is left for future work.

- Internal Pressure Loading
- Thermal Loading
- Deforming Loads
  - Solar radiation/ Photonic pressure
  - Atmospheric drag pressure
  - Micrometeroid pressure
  - Gravity gradient loading
  - Spacecraft induced Loads

#### PRESSURE

Unsurprisingly, the most dominant loading for the spherical structure is the pressure difference between the structures internal pressure and the vacuum of space. This internal pressure provides the pressure-stabilized structure both with its initial desired shape post inflation as well as its structural stability for the duration of the mission. The required internal pressure for the fully inflated state of the spherical structure is determined from the desired stress level in the skin and can be calculated using the equation for a thin wall sphere (Clemmons, 1964).

$$P_i = \frac{2t\sigma}{R} + P_o \tag{6.30}$$

Where:

- $P_i$ = Internal pressure (Pa)
- $P_o$ = External pressure (Pa)
  - Assumed to be negligible due to vacuum of space.
- $\sigma$ = Skin stress (Pa)

The desired skin stress level $\sigma$ is dependent on a couple of factors. A low skin stress is desirable as it reduces the pressure differential with the space vacuum environment and be extension reduces the required make-up gas. However, the skin stress must also be chosen so as to minimize and remove the wrinkles leftover from the packaging process as well as maximize the performance of the reflector (Mills et al., 2019). From the literature there appears to be two approaches to how an inflatable pressure-stabilized reflector should be pressurized to satisfy this process shall be addressed here.

**Approach 1**

The most popular approach found in literature is to pressurize the structure to the minimum stress level at which the wrinkles can be removed and maintain this pressure level with no additional venting. From the literature it appears that this approach has been followed by the vast majority pressure-stabilized reflectors to date with notable examples including the IAE lenticular reflector. The IAE was pressurized to a skin stress of 6.89 MPa which had been shown to be the minimum stress level at which packaging wrinkles could be removed (Freeland and Bilyeu, 1993). In order to determine this minimum stress level prototyping and characterization is typically required. However, Mills et al., 2019 notes that in general an operating skin stress of at least 15% of the yield stress is desirable.

| Mission | Skin Stress (MPa) | % Yield Strength |
|---|---|---|
| ECHO I | 3.5 | 4 |
| IAE | 6.89 | 7* |
| CatSat | 15 | 14.6* |
| Gregorian | 18.3 | 15 |
| Babuscia | 6.59 - 13.6 | 6.4 - 13* |

* = Assumed yield Strength of 103 MPa

Table 6.11: Skin Stress levels in Inflatable Reflectors: Approach 1

Examining table 6.11, it can be seen that while older inflatable structures such as ECHO I (Clemmons, 1964) and IAE (Freeland and Bilyeu, 1993) utilize skin stress values at a lower % than this, the more recent CubeSat reflector developments (Babuscia et al., 2020; Chandra et al., 2021; Fenn et al., 2021) all utilize skin stress values in and around this 15% mark.

**Approach 2**

The second approach entails a two step pressurization method and was specifically designed for pressure-stabilized applications. Originally proposed by Friese et al., 1983, the structure should first be pressurized to approximately its yield stress to eliminate packaging wrinkles. Following this, the structure should then be vented down to a predetermined maintenance pressure so as to reduce make-up gas requirements. While this process seems logical, it only appears in one other publication by Thunnissen et al., 1995, which details the design of pressure-stabilized parabolic reflector for the purpose of designing low mass inflation systems. Unfortunately, no further discussion of the approach could be found. This may be due to the lack of literature surrounding the development of inflation systems for such structures, with these two publications being two of the only papers to discuss inflation system sequencing (see section 7.5). Table 6.12 provides a breakdown of the skin stress values required by this two step approach for the inflatable reflector designed by Thunnissen et al., 1995. As the values from Friese et al., 1983 are unclear, these skin stress values shall be used as a guide for this approach.

| Stage | Skin Stress (MPa) | % Yield Strength |
|---|---|---|
| 1. Yield Stress | 77.5 | 100 |
| 2. Maintenance Stress | 0.3447 | 0.5 |

Table 6.12: Skin Stress levels in Inflatable Reflectors: Approach 2



**Discussion**

Evidently pressurizing the structure to a minimum skin stress level of around 15% yield strength, as done in approach 1, yields reduced pressurization gas mass requirements. In addition, it may be a safer approach than pressurizing to approximately the yield strength, which could potentially lead to deformation of the inflatable membrane if not carefully managed. However, maintaining the pressure within the structure at this higher level and not reducing to a small maintenance pressure, as is done in approach 2, leads to increased make-up gas requirements. This leads to a reduction in the mission lifetime, as the amount of make-up gas that can be carried is constrained by the CubeSats mass and volume constraints. Why exactly approach 1 is more popular is not entirely clear from the literature but it may be the case that the higher operational skin stresses enable a higher surface accuracy and thus better optical properties. However, this is TBC and as such is left for future work. In addition, it may also be because most of the structures that have been developed to date have either been short term demonstration missions, such as IAE and CatSat, or are intended to be rigidized after a certain time period, such as for the Babusica Inflatable CubeSat Antenna and the Gregorian inflatable reflector. Both scenarios do not require long operational lifespans.

Regardless of the reason for its popularity, the higher operational pressure levels of approach 1 (15% vs 0.5%) lead to a reduction in the mission lifetime. While a reduced mission lifetime is inevitable with pressure stabilized structures, until there are further advancements in rigidization technology, maximizing the operational lifespan of the structure is desirable. In this regard approach 2 offers a more attractive option. Not only do the reduced operational pressures enable a longer lifespan, the venting operation post initial inflation replicates the venting process required for a rigidizable inflatable structure. This is advantageous as it shall enable the design of an inflation system that shall be highly relevant to future missions that utilize advancements in rigidization technology, while also enabling the design of a BEOC reflector based on current technology. However, the need to initially pressurize the structure to the yield stress is a significant drawback of approach 2, while the reduced maintenance skin stress levels may lead to a reduction in surface accuracy, thereby inhibiting reflector performance. This pressurization scheme enables the generation of the inflation system requirements REQ-ISP-04 and REQ-IPS-05.

**Result**
It was decided that a hybrid approach is the most suitable for the design of this structure, thereby maximizing the benefits of each approach and minimizing the drawbacks. As such, the inflatable structure shall be pressurized to at least 15% of its Yield Strength, based on approach 1, and after a period of time, shall then be vented to a reduced % of its Yield strength, based off approach 2. While it remains to be confirmed whether the reduced skin stress levels at 0.5% dramatically inhibit the surface accuracy/reflector performance, it shall be assumed that a higher stress level of 2% is more appropriate. The validation of this assumption should be explored in future work. These two values shall be used to calculate the inflation pressure and stabilization pressure respectively.

6

However, these skin stress values are not constant and shall vary with temperature, with the membrane Yield strength inversely proportional and the gas pressure proportional to temperature. Considering this variation requires complex thermal analysis to account for the thermal interactions between the gas jet, the already present inflation gas and the structural membrane as they interact with each other and the thermal space environment. As was discussed for the thermal analysis, such modelling is beyond the scope of this thesis. Thus, assuming inflation occurs during the sunlit phase of the orbit, the skin stress shall be calculated for the sunlit thermal equilibrium temperature of 343 K. Unfortunately, due to a lack of information regarding the variation in CP1's mechanical properties with thermal variations, the yield strength of the material is only known at 300K. Thus, given that the Yield strength of CP1 shall be lower at 343 K, and the pressure exerted by the gas higher, it shall be assumed that the pressurization skin stress can be calculated as 10% Yield strength and the stabilization skin stress can be calculated at 4/3% Yield strength, both at 300 K.

### DEFORMING LOADS
Inflatable reflectors are by nature lightly loaded. Thus they are not designed to withstand large loads, but rather they are purely designed to withstand small buckling loads (Defoort et al., 2005). In order to assess whether the structure can withstand these buckling loads while in lunar orbit, the loads must be assessed. The first step in this process is to calculate the critical buckling pressure of the structure. This can be done by once again assuming it is a smooth, thin-walled sphere using equation 6.31 ( Teichman, 1968).

$$P_{cr} = \frac{2E \cdot t^2}{R^2 \left[3(1-\nu^2\right]^{1/2}} \tag{6.31}$$

Where:

- $E$ = Youngs Modulus (Pa)
- $\nu$ = Poissons ratio (0.34 from table 6.2)

As has been noted there are a number of external 'environmental' loads that impinge on the structure that should be considered. The most notable of these loads include; solar radiation pressure, atmospheric drag pressure, micrometeoroid pressure and gravity gradient loading. Clearly atmospheric drag is an insignificant consideration in Lunar orbit. As noted during the design of ECHO I and PAGEOS, when the effects of atmospheric pressure are negligible, the maximum environmental deforming load is the solar radiation pressure. Thus, it is assumed that if the structure can withstand this pressure it can withstand the remaining environmental deforming loads. The solar radiation pressure is proportional to the solar flux and can be expressed using the following equation (Teichman, 1968):

$$P_s = \frac{2F_s}{c} \tag{6.32}$$

Where:

- $c$ = Speed of light in a vacuum (299,792,458 m/s)

In lunar orbit, this results in a value $9.08\times10^{-6}$ Pa yielding a large deformation safety factor $P_s/P_{cr}$, as seen in table 6.13. This indicates that the structure can comfortably survive the on orbit deforming loads. However, it must be noted that the structure shall also be subject to dynamic loads, such as spacecraft induced loads, from inputs including propulsive dynamics. It may be prudent to assume that once the structure has been deployed and the CubeSat is in orbit such firings wont happen. Thus induced loads and vibrations could be assumed minimal. However, further exploration of this topic and other dynamic loads on the structure is left for future work due to the limited time constraints of this thesis project.

### 6.7.4. MATERIAL THICKNESS

Before compiling a finalized list of the mechanical properties of the inflatable structure determined in this investigation, an appropriate material thickness must first be specified.

Table E.1 possesses a list of suitable reference structures and the membrane thickness values used in their development. From these reference structures a range of thickness values were determined. The variation in growth rate and mechanical properties of the structure with these different growth rates is presented in table 6.13. From this table it can be seen that requirements REQ-IRI-04, desiring an RPE of at least 1.5 $m^2/U$, and REQ-IRI-05, desiring an area density of at least 0.4 $m^2/kg$, are satisfied. In many respects this is unsurprising seeing as these minimum and maximum values were derived

| **Property** | **2.5** $\mu m$ | **5** $\mu m$ | **12.7** $\mu m$ | **25.4** $\mu m$ | **50** $\mu m$ |
|---|---|---|---|---|---|
| Structure Type | Solar Sail | Solar Sail | Reflector | Reflector | Reflector |
| Growth Rate (1/s) | 2.619E-14 | 3.214E-14 | 4.140E-14 | 5.208E-14 | 6.198E-14 |
| Stowed Volume (U) | 0.022 | 0.04 | 0.11 | 0.22 | 0.43 |
| RPE ($m^2/U$) | 36.14 | 18.18 | 7.15 | 3.58 | 1.82 |
| Mass (Kg) | 0.013 | 0.026 | 0.0677 | 0.135 | 0.266 |
| Area Density ($m^2/kg$) | 0.017 | 0.034 | 0.086 | 0.172 | 0.338 |
| Inflation Pressure (Pa) | 54.5 | 109 | 276.86 | 553.72 | 1090.0 |
| Maintenance Pressure (Pa) | 7.26 | 14.53 | 36.91 | 73.83 | 145.33 |
| Deformation Safety Factor | 6.76E3 | 27.04E3 | 174.48E3 | 697.94E3 | 2704.5E3 |

Table 6.13: The impact of membrane thickness on the mechanical properties

6

from the 12 ft Sphere (see table C.2) which utilizes a laminate material, thereby yielding a higher mass and lower packaging efficiency than a single polymer film structure. However, the degree to which these requirements are met does vary with thickness. For example, at 50 $\mu m$ the resulting structure just satisfies the requirements, yielding an RPE of 1.82 $m^2/U$ and area density of 0.338 $m^2/kg$. However, at 12.7 $\mu m$ the requirements are comfortably met, yielding values of 7.15 $m^2/U$ and 0.086 $m^2/kg$ respectively. Evidently, as seen in table 6.13, lower thickness values yield more attractive mechanical properties, not only in terms of stowed volume and mass, hence their more attractive RPE and area density characteristics, but also in terms of the required inflation and maintenance pressure values. This is highly attractive as it reduces the mass of gas needed, thereby reducing the size of the inflatant tank and/or extending the mission lifetime. This advantage is also reinforced by the decrease in hole growth rate with thickness. It should be noted that while the critical buckling pressure, and thus deformation safety factor, does decrease with decreasing thickness it is evident from the large deformation safety factors that at these thickness values this not a defining issue.

While lower thickness values are clearly more attractive, the values of 2.5 $\mu m$ and 5 $\mu m$ have only been found in solar sail applications with 12.7 $\mu m$ being the minimum thickness found for pressure stabilized reflector applications. The reasons for this are likely due to the increased complexity of fabricating inflatable reflector structures using these lower thicknesses, although it may also be due to the effects of thermal or dynamic loading on the structure. Further exploration of this shall be left for future work. As such, according to the mechanical properties evaluated in this section, as well as the growth rate of holes due to micrometeoroid punctures, it was decided that a thickness of 12.7 $\mu m$ is the most appropriate value.

### 6.7.5. SUMMARY OF REFLECTOR PROPERTIES

A summary of the preliminary design for a spherical inflatable reflector for lunar applications is given in figure 6.9.

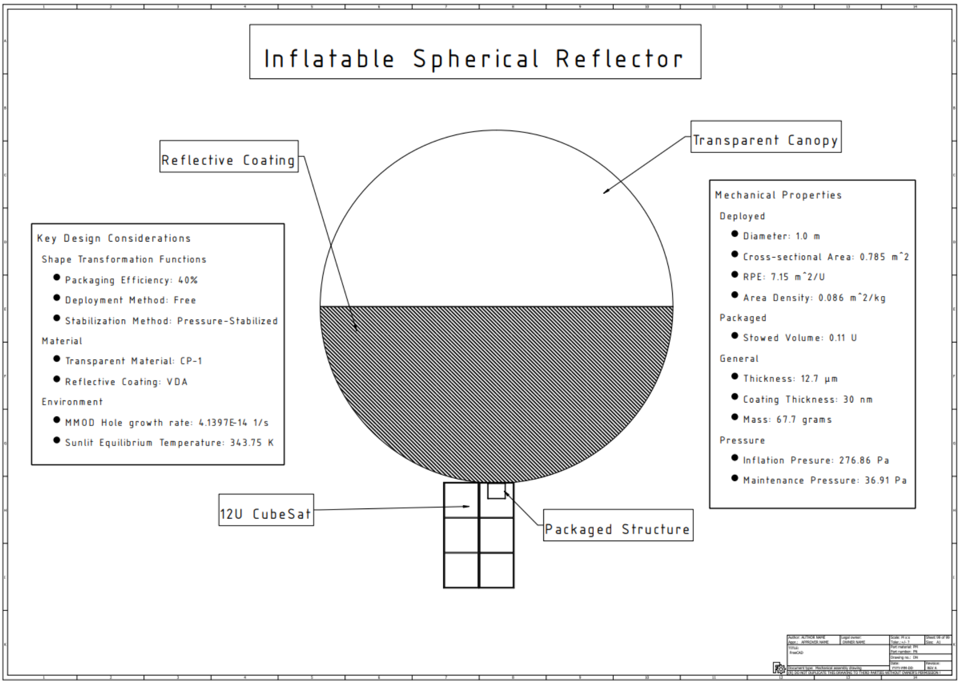


Figure 6.9: Graphic Summary of the Inflatable Spherical Reflector

## 6.8. CONCLUSION

At the start of this chapter, the focus for the design of the inflatable reflector was specified as aiming to address the main design considerations of the inflatable structure so as to both satisfy the inflatable reflector requirements and inform the generation of the inflation systems requirements. As elaborated in section 9.2 with regards to the inflatable reflector requirements this aim was fulfilled with the exception of REQ-IRP-02 due to the lack of emphasis placed on analyzing the structures performance as a reflector. Despite this, and the simplified analytical approach utilized in the thermal and structural analysis, the preliminary design of the structure presented successfully addresses the main design characteristics of the BEOC inflatable reflector, enabling informed requirements for the inflation system to be generated. These requirements are presented in table 6.14, while the key assumptions made in the design of the structure are presented in the appendices section E.

| ID | Inflation System Requirement | Design Consideration |
|---|---|---|
| REQ-ISP-01 | The inflation time shall take between 10 seconds and 100 seconds | Deployment Method, Geometry of Structure |
| REQ-ISP-02 | The inflation system shall provide ascent venting | Packaging Method, Deployment Method |
| REQ-ISP-03 | The inflation system shall unfold the structure in a smooth controlled fashion | Deployment Method |
| REQ-ISP-04 | The inflation system shall pressurize the inflatable structure to 15% of the inflatable membranes yield strength | Internal Pressure Loading, Geometry of Structure, Thermal Environment |
| REQ-ISP-05 | The inflation system shall vent the structure to 2% of the inflatable membranes yield strength | Internal Pressure Loading, Geometry of Structure, Thermal Environment |
| REQ-ISP-06 | The inflation system shall provide pressure maintenance for the duration of the mission | Stabilization Method, Micrometeroids |

Table 6.14: Inflation System Performance Requirements Generated By Key Inflatable Structure Design Decisions

# Bibliography


Babuscia, A., Sauder, J., Aman, C., & Thangavelautham, J. (2020). Inflatable antenna for cubesat. *CubeSat Antenna Design*, 197–230.

Babuscia, A., Sauder, J., Chandra, A., Thangavelautham, J., Feruglio, L., & Bienert, N. (2017). Inflatable antenna for cubesat: A new spherical design for increased x-band gain. *2017 IEEE Aerospace Conference*, 1–10.

Babuscia, A., Wei, Q. J., Pan, S., Mohan, S., & Seager, S. (2014). *Inflatable Antenna for CubeSat: Fabrication, Deployment and Results of Experimental Tests*.

Badyukov, D. (2020). Micrometeoroids: The flux on the moon and a source of volatiles. *Solar System Research*, *54*(4), 263–274.

Chandra, A., Lopez Tonazzi, J. C., Stetson, D., Pat, T., & Walker, C. K. (2020). Inflatable membrane antennas for small satellites. *2020 IEEE Aerospace Conference*, 1–8. https://doi.org/10.1109/AERO47225.2020.9172737

Chandra, A. (2015). Inflatable Parabolic Reflectors for Small Satellite Communication. *Development*, (November), 33–34.

Chandra, A., Pat, T., Tonazzi, J. C. L., & Walker, C. K. (2021). Development and flight qualification of a small satellite x-band spherical membrane antenna. *2021 IEEE Aerospace Conference (50100)*, 1–8.

Chandra, A., Pat, T., & Walker, C. (2022). Catsat: A 6u inflatable antenna technology demonstration mission.

Chodimella, S., Moore, J., Otto, J., & Fang, H. (2006). Design evaluation of a large aperture deployable antenna. *47th AIAA/ASME/ASCE/AHS/ASC Structures, Structural Dynamics, and Materials Conference 14th AIAA/ASME/AHS Adaptive Structures Conference 7th*, 1603.

Cipriano, A. M., Dei Tos, D. A., & Topputo, F. (2018). Orbit design for lumio: The lunar meteoroid impacts observer. *Frontiers in Astronomy and Space Sciences*, *5*, 29.

Clemmons, D. L. (1964). *The echo i inflation system*. National Aeronautics; Space Administration.

Coffee, C. W., Bressette, W. E., & Keating, G. M. (1962). *Design of the nasa lightweight inflatable satellites for the determination of atmospheric density at extreme altitudes*. National Aeronautics; Space Administration.

Connell, J. W., & Watson, K. A. (2001). Materials for inflatables in space. In *Gossamer spacecraft: Membrane and inflatable structures technology for space applications* (pp. 203–256). American Institute of Aeronautics; Astronautics.

Cour-Palais, B. (1969). *Nasa space vehicle design criteria-environment. meteorid environment model-1969/near earth to lunar surface* (tech. rep.).

Defoort, B., Peypoudat, V., Bernasconi, M., Chuda, K., & Coqueret, X. (2005). Recent advances in the rigidization of gossamer structures. *Textile Composites and Inflatable Structures*, 259–283.

Dunbar, S. (2021). Literature review study - inflatable space structures, beyond earth orbit cubesat missions and micropropulsion inflation systems.

Fay, C. C., Stoakley, D. M., & Clair, A. K. S. (1999). Molecularly oriented films for space applications. *High Performance Polymers*, *11*(1), 145–156.

Fenn, A. J., Mills, J., Robey, F., Finnell, J. W., Hassan, B., Crowley, S., et al. (2021). Inflatable reflector antenna and related methods [US Patent 10,916,859].

Fenn, A. J., Mills, J. H., Robey, F. C., Dufilie, P., & Hecht, M. H. (2019). Axisymmetric gregorian reflector system for a space-deployed inflatable antenna: Simulations and measurements. *2019 IEEE International Symposium on Phased Array System & Technology (PAST)*, 1–4.

Finckenor, M., Rodman, L., & Farmer, B. (2015). *Analysis of fluorinated polyimides flown on the materials international space station experiment*. National Aeronautics; Space Administration, Marshall Space Flight Center.

Fortescue, P., Swinerd, G., & Stark, J. (2011). *Spacecraft systems engineering*. John Wiley & Sons.

Freeland, R., & Bilyeu, G. (1993). In-step inflatable antenna experiment. *Acta Astronautica*, *30*, 29–40.

Freeland, R., Bilyeu, G., Veal, G., Steiner, M., & Carson, D. (1997). Large inflatable deployable antenna flight experiment results [Developing Business]. *Acta Astronautica*, *41*(4), 267–277. https://doi.org/https://doi.org/10.1016/S0094-5765(98)00057-5

Friese, G., Bilyeu, G., & Thomas, M. (1983). Initial'80s development of inflated antennas.

Grahne, M., & Cadogan, D. (2001). Deployment control mechanisms and packaging methodologies for inflatable and membrane space structures. In *Gossamer spacecraft: Membrane and inflatable structures technology for space applications* (pp. 417–431). American Institute of Aeronautics; Astronautics.

Griebel, H. S. (2011). *Reaching high altitudes on mars with an inflatable hypersonic drag balloon*. Springer Science & Business Media.

Grossman, G., & Williams, G. (1990). Inflatable concentrators for solar propulsion and dynamic space power.

Guidanean, K., & Veal, G. (2003). An inflatable rigidizable calibration optical sphere. *44 th AIAA/ASME/ASCE/AHS/ASC Structures, Structural Dynamics, and Materials Conference*.

Heaton, A., Ahmad, N., & Miller, K. (2017). Near earth asteroid scout thrust and torque model.

Johnson, L., Sobey, A. R., & Sykes, K. (2015). Solar sail propulsion for interplanetary cubesats. *51st AIAA/SAE/ASEE Joint Propulsion Conference*, 3895.

Larson, W. J., & Wertz, J. R. (1992). *Space mission analysis and design* (tech. rep.). Torrance, CA (United States); Microcosm, Inc.

Lesser, D., Walker, C. K., Smith, I. S., Goldsmith, P. F., Cortes, G., Dougherty, S., Swift, B., Kloosterman, J., Honniball, C., Young, A., et al. (2015). 10 meter sub-orbital large balloon reflector (lbr). *2015 40th International Conference on Infrared, Millimeter, and Terahertz waves (IRMMW-THz)*, 1–2.

Liu, Z.-Q., Qiu, H., Li, X., & Yang, S.-L. (2017). Review of large spacecraft deployable membrane antenna structures. *Chinese Journal of Mechanical Engineering*, *30*(6), 1447–1459.

Menicucci, A., Cervone, A., Speretta, S., Bertels, E., Topputo, F., et al. (2021). The radiation environment and effects analysis of the lumio mission. *72nd International Astronautical Congress (IAC 2021)*, 1–7.

Mills, J. H., Fenn, A. J., Crowley, S., Hassan, B., Robey, F. C., Dufilie, P., & Hecht, M. H. (2019). Space-deployed inflatable dual-reflector antenna: Design and prototype measurements.

Nakasuka, S., Senda, K., Watanabe, A., Yajima, T., & Sahara, H. (2009). Simple and small de-orbiting package for nano-satellites using an inflatable balloon. *Transactions of the Japan Society for Aeronautical and Space Sciences, Space Technology Japan*, *7*(ists26), Tf_31–Tf_36.

Pearson, J., Moore, J., & Fang, H. (2010). Large and high precision inflatable membrane reflector. *51st AIAA/ASME/ASCE/AHS/ASC Structures, Structural Dynamics, and Materials Conference 18th AIAA/ASME/AHS Adaptive Structures Conference 12th*, 2500.

Pino, D. (2016). Solar concentrator demonstrator for pocketqubes.

Russell, D. A., Fogdall, L. B., & Bohnhoff-Hlavacek, G. (2000). *Simulated space environmental testing on thin films*. National Aeronautics; Space Administration, Langley Research Center.

Secheli, G. A. (2018). *Modelling of packaging folds in metal-polymer laminates*. University of Surrey (United Kingdom).

Smith, I. S., Chaffee, E. A., & Walker, C. (2018). Recent developments in a large inflatable antenna. *2018 IEEE Aerospace Conference*, 1–8.

Staehle, R. L., Babuscia, A., Beregovski, Y., Chahat, N., Chien, S., Cochrane, C., Duncan, C., Garrett, H., Landau, D., Liewer, P., Mouroulis, P., Murphy, N., Tang, A., Puig-Suari, J., Bellardo, J., Gillespie, C., Bonafede, N., Fernandez, M., Gordon, M., … Austin, A. (2020). *Low-Cost SmallSats to Explore the Outer Solar System Final Report on NIAC task to define an architecture for Outer Solar System SmallSats (OS4) 2020 September 15* (tech. rep.).

Staugaitis, C. L., & Kobren, L. (1966). *Mechanical and physical properties of the echo ii metal-polymer laminate.* (tech. rep.). NATIONAL AERONAUTICS and SPACE ADMINISTRATION GREENBELT MD GODDARD SPACE …

Talentino, J. (1966). Development of the fabrication and packaging techniques for the echo ii satellite.

Teichman, L. A. (1968). *The fabrication and testing of pageos i* (Vol. 4596). National Aeronautics; Space Administration.

Thomas, M., & Friese, G. (1980). Pressurized antennas for space radars. *Sensor Systems for the 80's Conference*, 1928.

Thunnissen, D. P., Webster, M. S., & Engelbrecht, C. S. (1995). Low-mass inflation systems for inflatable structures. *In Jet Propulsion Lab, California Inst. of Tech, Proceedings of the International Conference on Integrated Micro/Nanotechnology for Space Applications p(SEE N 96-36329 12-12), 1995.*

6

Underwood, C., Viquerat, A., Schenk, M., Taylor, B., Massimiani, C., Duke, R., Stewart, B., Fellowes, S., Bridges, C., Aglietti, G., et al. (2019). Inflatesail de-orbit flight demonstration results and follow-on drag-sail applications. *Acta Astronautica*, *162*, 344–358.

Walker, C., Kulesa, C., Smith, I. S., Perry, W., Kim, D., Palisoc, A., Cassapakis, C., Crowe, D., & Pierce, D. (2019). Orbiting astronomical satellite for investigating stellar systems (oasis).

Walket, C. K., Smith, I. S., Goldsmith, P. F., O'Dougherty, S., Takashima, Y., & Kim, D. (2017). Spherical reflectors for space based telescopes. *2017 IEEE MTT-S International Microwave Symposium (IMS)*, 1884–1887.

Whipple, F. (1967). On maintaining the meteoritic complex. *Studies in interplanetary particles: Smithson. Astrophys. Observ. Spec. Rep*, (239), 3–45.

Wood, G. P., & Carter, A. F. (1959). *Predicted characteristics of an inflatable aluminized-plastic spherical earth satellite with regard to temperature, visibility, reflection of radar waves, and protection from ultraviolet radiation* (Vol. 115). National Aeronautics; Space Administration.

Wooldridge, E., Powers, C., Townsend, J., Peters, W., Cadogan, D., & Lin, J. (2001). Effects of manufacturing and deployment on thin films for the ngst sunshade. *19th AIAA Applied Aerodynamics Conference*, 1349.

# 7

# Inflation System Concept Generation

*This chapter provides a systems engineering analysis which resulted in the identification of the design concept for the inflation system as well as the choice of inflatant gas and inflation scheme. The concept generation process starts with the identification of acceptable design candidates (section 7.2), followed by a detailed concept selection trade off (section 7.3). Once the most suitable candidate is selected, a trade of of potential inflation gases is carried out (section 7.4). Finally, the inflation scheme is discussed (section 7.5).*

## 7.1. INTRODUCTION

In order to ensure that this thesis explores a suitable design for a micropropulsion based inflation system a number of key design parameters must first be determined. This begins with establishing a suitable inflation design candidate, based off those identified in the literature review, via a comprehensive trade off analysis. Following this, the most suitable inflation gas shall be determined followed by a discussion regarding an inflation scheme. This is necessary in order to facilitate the controlled inflation required by an inflatable system using the free deployment method. As a result this chapter shall determine, based on the requirement analysis presented in section 4.4, the most suitable micropropulsion based inflation system design candidate, inflation gas and inflation scheme.

## 7.2. INFLATION SYSTEM DESIGN CANDIDATES

As is the case for the inflatable structure concept generation, section 5, the first step in this process is to present a wide range of possible design candidate. These candidates were identified in the literature review, section 2.4, and can be seen in the design option tree presented in figure B.1. Following the identification of these candidates, the list of satiable candidates shall be reduced by removing clearly unacceptable options. Finally, with the remaining candidates a trade off analysis shall be carried out in order to determine the most suitable concept for this project.

As can be seen from figure B.1, the inflation system design candidates identified in the literature review can be grouped according to three broad categories; cold gas systems, chemical gas generation systems and physical phase change systems. It should also be noted that it is assumed that the candidates presented can be also be utilized in the multimode propulsion-inflation system.



### ELIMINATE THE OBVIOUS LOSERS

The first step in reducing this number is to identify those candidates that produce gas with characteristics which violate killer requirement REQ-ISI-04. This includes any candidates that generate gases at temperatures exceeding those dictated in REQ-ISI-04-01 and/or are hazardous as dictated by REQ-ISI-04-02. In addition, any candidates that cannot meet the desired pressure levels as dictated by key requirement REQ-ISP-04 or are inherently uncontrollable are also removed. This leads to the following candidates being rejected:

- Violates REQ-ISI-04
  - Conventional WGG System
  - Monopropellant System
  - Conventional Bipropellant System
  - Resistojet Based System
- Cannot meet REQ-ISP-04
  - Solid State Gas Generation (SSGG)

- Inherently uncontrollable
  - Conventional Sublimation System

### ELIMINATE CONCEPTS BEYOND SCOPE OF PROJECT

The next step in reducing the number of design candidates is to identify and eliminate the concepts, that might be workable, but are not worth pursuing now. These concepts may rely on a new technology that requires time and resources that are not available to a masters thesis project or they may be too difficult to analyze within the given project time frame. This leads to the following candidates being rejected:

- Multimode Propulsion-Inflation System
- Bipropellant Electrolysis System
- Metal Hydride System
- Controlled Sublimation System

While these concepts are rejected for this thesis they provide an interesting list of possible CubeSat inflation systems that may be worth investigating in future work.

## 7.2.1. ACCEPTED DESIGN CANDIDATES

A refined design option tree containing the accepted design candidates is presented in figure 7.1. For descriptions of each of the design candidates, the reader is referred to section 2.4 of the literature study overview.



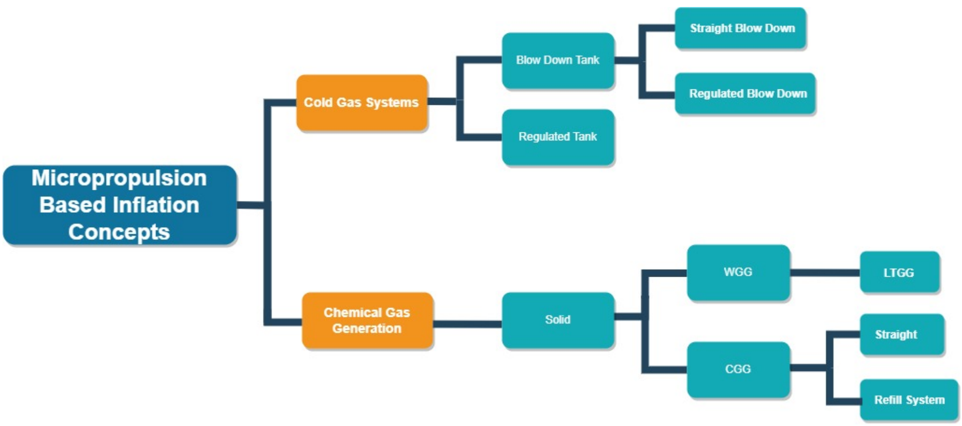


Figure 7.1: Refined Design Option Tree of Potential Design Candidates

# 7.3. CONCEPT SELECTION

In order to choose the most suitable design candidate for this thesis from those presented, the candidates must be evaluated under certain criteria. The candidate that meets these criteria the best shall be chosen as the most suitable for this project. These selection criteria are dictated by the requirements laid out in section 4.4 and are weighted according to their perceived importance to the project.

### 7.3.1. SELECTION CRITERIA

#### CONCEPT MATURITY

This criterion is of vital importance to the selection of the most suitable candidate. The maturity of a concept is closely related to TRL and is dependent on the flight heritage and available background literature for a design candidate. For this thesis project the maturity of a design candidate must be evaluated with respect to its maturity as an inflation system and as a micropropulsion system. Maturity as an inflation system will enable the design of a more predictable system while maturity as a micropropulsion system is essential to fulfilling the project mission statement which explicitly desires the design of an inflation system based on micropropulsion technology. Therefore, a design candidate that has a high maturity as both an inflation system and a micropropulsion system is imperative to the success of this thesis.

#### INFLATION CONTROL

As is clearly stated in the need statement for this project, the development of a controllable inflation process shall play a key role in enabling the development of inflatable reflectors for beyond Earth orbit CubeSat missions. This need is clarified in the mission statement for this project which dictates that “the goal of this work is to design a micropropulsion based inflation system that provides a suitable and controllable inflation process for (BEOC) inflatable reflectors”. This is emphasized by the use of the free deployment method, as discussed in section 6.3, which provides limited-to-no control over the deployment process during inflation. It is therefore imperative that the selected design candidate be capable of providing the desired degree of controllability for the inflation process. This is qualified in killer requirements REQ-ISP-01, which desires a suitable inflation time, and key requirement REQ-ISP-03 which dictates that the inflation system shall be capable of unfolding the structure in a smooth controlled fashion. In addition, as the structure is pressure stabilized it is highly desirable for the inflation system to be capable of providing precise pressure maintenance as noted in key REQ-ISP-06. As is discussed in section 8.3, these requirements are best met by a pulsed mode of inflation. Thus this capability is essential.

#### VOLUME FOOTPRINT

As specified in requirement in REQ-ISI-01, the volume footprint of the inflation system shall be less than 1U. This requirement derives from key requirement REQ-BEOC-01 and is essential in ensuring the designed inflatable system is competitive relative to more conventional technologies. Minimizing the volume of the inflation system is key to fulfilling this requirement. As there is no analysis done on the concepts, the absolute volumes are not evaluated. Instead, given that the volume of the inflation system is dependent on the hardware and propellant storage requirements, these parameters shall be used to distinguish the different design candidates.

### Mass

Due to uncertainty regarding the mass required for the ejection mechanism and any additional equipment, such as that needed for the reflectors application (e.g. antenna), REQ-ISI-02 specifies that the mass of the inflation system shall be less than 1kg. This conservative requirement derives from key requirement REQ-BEOC-02 and while key to ensuring the designed inflatable system is competitive relative to more conventional technologies is seen as being more flexible than the volume footprint. As is the case for the volume footprint, no absolute values are available regarding the mass of each system and so estimates are made based on the candidates hardware and the mass of similar systems.

### Complexity

It is desirable to keep the complexity of the system to a minimum. The complexity of the system is generally associated with the number of system components and the number of interactions between different elements within the system. This in turn gives a good representation of the reliability of the system with simpler systems tending to be more reliable than complex ones. In addition, this criteria also has a bearing on the mass and volume requirements of the system as has been already noted. However, simplicity may also come at the cost of controllability. This must be balanced accordingly.

## 7.3.2. Criteria Weighting

In order to establish the weighting of these selection criteria a common systems engineering approach known as the analytical hierarchy process (AHP) shall be utilized. Using this method, the criteria are compared against each other enabling the weightings to be found by establishing the relative importance of each criteria. A description of the AHP method used can be found in the following sources (Gill, 2015; Nadja and Karlheinz, 2004) with the calculations being carried out using an Excel spreadsheet. This process yields the criteria weightings as seen in table 7.1. In order to ensure that consistent weights have been determined and the approach is numerically valid the consistency ratio (CR) should be less than 10%. For this analysis, the CR was calculated to be 1.1%, well below the desired threshold.

| **Selection Criteria** | **Weighting** |
|---|---|
| Concept Maturity | 0.2768 |
| Inflation Control | 0.3636 |
| Volume Footprint | 0.1678 |
| Mass | 0.1205 |
| Complexity | 0.0712 |

Table 7.1: Selection Criteria Weightings

### Reflection on the criteria weighting

As has been alluded to the criteria weightings stem from a pairwise comparison of each criteria. This comparison matrix is shown in table 7.2, with the importance of each criteria relative to the others indicated by a number according to the AHP grading scale. This matrix shall be utilized to reflect on the criteria weightings and discuss why the author selected the chosen grades.

| Criteria | Concept Maturity | Inflation Control | Volume Footprint | Mass | Complexity |
|---|---|---|---|---|---|
| **Concept Maturity** | 1.0 | 0.67 | 2.0 | 2.50 | 3.50 |
| **Inflation Control** | 1.50 | 1.0 | 2.50 | 3.0 | 4.0 |
| **Volume Footprint** | 0.50 | 0.40 | 1.0 | 1.50 | 3.0 |
| **Mass** | 0.40 | 0.33 | 0.67 | 1.0 | 2.0 |
| **Complexity** | 0.29 | 0.25 | 0.33 | 0.50 | 1.0 |

Table 7.2: Selection Criteria Comparison Matrix

- Concept Maturity
  - Concept maturity criteria has the second highest weighting, deriving from its importance in predicting the inflation systems performance and in successfully fulfilling the project mission statement. As such it is deemed moderately more important than volume footprint, mass and complexity although marginally less important than inflation control.
- Inflation Control
  - Inflation control is the most important selection criteria. This importance stems from its critical role in addressing the project mission statement for this project and in accounting for the use of the free deployment method. As a consequence, it is graded as moderately more important than volume footprint, mass and complexity and marginally more important than concept maturity.
- Volume Footprint
  - The volume footprint criteria has the third highest weighting. It derives from a desire to ensure that the inflatable system is competitive with more conventional CubeSat reflector systems. It is seen as marginally and moderately more important than the mass and complexity criteria respectively but it is deemed less important than inflation control and concept maturity as it is not essential to satisfying the project mission statement.
- Mass
  - The mass criteria also stems from a desire to ensure that the inflatable system is competitive with more conventional CubeSat reflector systems. However, the mass requirement for the system is seen as more flexible than the volume

requirement and thus this criteria is weighted marginally lower. However, it is deemed more important than complexity.

- Complexity
  - Complexity is the lowest weighted criteria. This is because minimizing complexity is not critical for satisfying the project mission statement and while desirable, it is not necessary for ensuring the competitiveness of the system with conventional CubeSat reflector systems.

### 7.3.3. THE TRADE OFF

Following on from the establishment of the criteria weighting, the AHP method shall be utilized to determine the relative merit of each design candidate with respect to each selection criteria. Once this has been done for each criteria, the grades are then multiplied by the associated weights and are then summed up for each design candidate. The design candidate with the highest overall score is deemed to be the most suitable candidate. Once again, a Microsoft Excel spreadsheet was utilized to carry out the necessary matrix multiplication. In addition, as before the consistency ratios are calculated for each criteria in order to ensure that consistent weights have been determined and the approach is numerically valid. These ratios are shown in table 7.3 and all are well below the 10% threshold.

| Selection Criteria | Consistency Ratio |
|---|---|
| Concept Maturity | 2.14% |
| Inflation Control | 0.93% |
| Volume Footprint | 0.74% |
| Mass | 0.71% |
| Complexity | 2.48% |

Table 7.3: Selection Criteria Consistency Ratios

The final AHP trade-off matrix can be seen in table 7.4. As can be seen the cold gas regulated blow down candidate provides the most attractive candidate by a considerable margin. This is despite the fact that it is the worst performing candidate with respect to volume footprint and mass with its attractiveness instead stemming from its extensive concept maturity and excellent inflation control. It is followed in second by the CGG refill candidate which incorporates the attractive mass, volume and complexity characteristics of CGG technology with the increased inflation control offered by the use of a refillable plenum. It is evident from table 7.4 that it provides the best combination of characteristics only falling behind the cold gas regulated blow down candidate in concept maturity and inflation control, both of which could be improved. In third comes the cold gas regulated candidate who's increased inflation control sees it outperform the cold gas straight blow down candidate despite performing relatively poorly on the remaining criteria. Finally, the CGG Straight and LTGG candidates even with the most attractive mass, volume and complexity characteristics bring up the rear, suffering heavily from their poor inflation control capabilities and low concept maturity.

As can be seen the grades of each candidate relative to each selection criteria clearly indicated. The justification for the grades attributed to each candidate shall now be discussed in order to ensure that a clear understanding of the authors subjective input into the objective AHP process is presented. The selection of these grades is crucial to the AHP trade off process and hence a transparent explanation of the rationale behind their selection is important particularly given that no prior analysis has been done on the design candidates.

| **Criteria/Candidate** | *Weight* | **CGB Straight** | **CGB Regulated** | **CG Regulated** | **LTGG** | **CGG Straight** | **CGG Refill** |
|---|---|---|---|---|---|---|---|
| **Concept Maturity** | *0.2768* | 0.2738 | 0.3457 | 0.1068 | 0.430 | 0.0711 | 0.1595 |
| **InflationControl** | *0.3631* | 0.1171 | 0.3084 | 0.3084 | 0.0483 | 0.0370 | 0.1808 |
| **Volume Footprint** | *0.1678* | 0.09014 | 0.0669 | 0.0669 | 0.2791 | 0.3200 | 0.1756 |
| **Mass** | *0.1205* | 0.1137 | 0.0668 | 0.0668 | 0.2766 | 0.3169 | 0.1591 |
| **Complexity** | *0.0712* | 0.1201 | 0.0852 | 0.0507 | 0.2509 | 0.3236 | 0.1696 |
| | **Result** | 0.1560 | 0.2332 | 0.1646 | 0.1276 | 0.1481 | 0.1706 |
| | **Weighted Result** | 0.67 | 1.00 | 0.71 | 0.55 | 0.63 | 0.73 |

CGB = Cold Gas Blowdown
LTGG = Low Temperature Gas Generator
CGG = Cool Gas Generator
CG = Cold Gas

Table 7.4: AHP Trade Off Table

### REFLECTION ON WEIGHTING

As noted the AHP method, through pairwise comparison, is used to determine the weighting of each candidate with respect to each of the selection criteria, thus enabling the selection of the most suitable design candidate. In order to provide greater clarity on how these weightings were determined, a brief discussion on the comparison matrix of each selection criteria shall be presented. These comparison matrices can be found in appendix F.

- Concept Maturity
  - As can be seen from table 7.4, the two cold gas blow down candidates score significantly better than the remaining candidates with respect to concept maturity. This is demonstrated in table F.1 where the two candidates are graded as having moderately better maturity than the cold gas regulated and CGG refill candidates and a moderate to strong degree of maturity relative to CGG straight and LTGG candidates. This strong performance stems from the extensive heritage of both candidates for micropropulsion and inflation applications, with the regulated blow down candidate scoring marginally higher due to its increased heritage as an inflation system.
  - They are followed by the CGG refill candidate which, despite not yet having flight heritage as an inflation system, scores strongly due to its maturity for micropropulsion applications. As such it is graded as having moderately better maturity than the CGG straight and LTGG candidates, neither of which have such heritage. It also scores marginally better than the cold gas regulated candidate, which despite having heritage as a conventional propulsion system, is unpopular for micropropulsion applications.
  - The three candidates that score the lowest for concept maturity are the cold gas regulated, CGG Straight and LTGG candidates. Despite having flight heritage as a CubeSat inflation system, the CGG straight candidate has only been utilized for high pressure structures, being ill suited for low pressure applications. Like the LTGG candidate, which also has very limited heritage as an inflation system, the utilization of the CGG straight candidate as a propulsion system is non-existent. As such the two candidates are deemed to score marginally to moderately worse than the cold gas regulated candidate which is deemed to have greater maturity due to its heritage as a conventional propulsion system as well as its proposed, but as yet unexplored, use for the controlled inflation of inflatable reflectors.
- Inflation Control
  - The two cold gas regulated candidates score the highest with respect to inflation control thanks to their use of a regulation system as well and their capacity for pulsed operation. It is assumed that both candidates offer the same degree of controllability. This can be seen in table F.2 where they are both graded as having moderately greater control than the CGG refill and cold gas straight blow down candidates and strongly greater control than the CGG Straight and LTGG candidates.

7

  - The CGG refill and cold gas straight blow down candidates perform moderately worse than their regulated counterparts due to their degradation in performance over time. However, due to the CGG refill candidates ability to recharge its plenum, this system scores marginally better than the cold gas straight blow down candidate. Despite this both candidates yield moderately to strongly better control than the CGG Straight and LTGG candidates both of whom lack the capacity for pulsed operation.
  - Due to their rapid blow down nature and unsuitability for rapid on/off actuation required by the pulsed mode of operation, it is hardly surprising that the CGG Straight and LTGG candidates perform the poorest with respect to inflation control. However, the LTGG candidate, does score marginally better than the CGG straight candidate, being capable of producing an inflation rate 3-5 times slower.

- Volume Footprint
  - The CGG straight and LTGG candidates, both of which are assumed to be based on current systems (Underwood et al., 2019 and Han et al., 2021 respectively) that are appropriately sized, are deemed to yield the lowest volume requirements. This is because they shall provide inflation gas, initially stored as a solid propellant, directly into the inflatable structure with minimal need for a feed system. As such they are deemed to provide moderately lower volume requirements than the bulkier tanked cold gas systems and marginally lower than the CGG refill candidate. This can be seen in table F.3 where it can also be noted that the CGG straight candidate marginally outperforms than the LTGG candidate as it does not require a coolant system to provide suitable gas characteristics.
  - The CGG refil candidate provides the third most attractive volume characteristics, primarily thanks to its use of a number of smaller solid propellant canisters although the need for a feed system and plenum is a drawback relative to the other solid propellant candidates. Despite this, it does provide moderately better volume requirements than the cold gas candidates.
  - The three cold gas candidates all score poorly due to their need for bulky inflatant tanks and feed systems. The two regulated candidates are assumed to have similar volume requirements with the cold gas regulated blow down candidate having higher tank requirements but lower additional component requirements than the cold gas regulated candidate. In addition, both candidates are graded marginally worse than the cold gas straight blow down candidate due to their use of a pressure regulator.

- Mass
  - The motivation for the candidate weighting with respect to the mass criteria, as shown in table F.4, is effectively the same as volume footprint and so no further reflection was deemed necessary.

- Complexity

– As is the case for mass, the motivation for the candidate weighting with respect to complexity, as shown in table F.5, is largely the same as that provided for the volume footprint. However, there is one major point of difference, that being the additional complexity of the regulated cold gas candidate relative to the cold gas regulated blow down candidate. This is due to its need for an additional pressurant tank and associated components. It is this additional complexity that is likely the main reason for the difference in concept maturity of the two candidates.

### 7.3.4. CONCLUSION

This section presents a trade off analysis of the inflation system design candidates considered promising for the development of a micropropulsion based inflation system for this project. This trade off analysis utilized the AHP method, which is very useful for providing a quantitative indication of the performance of each of the candidates according to the criteria despite the lack of prior analysis. However, it must noted that it is still subject to the assumptions made by the author. Therefore, given the importance that this trade off decision plays in the successful development of an appropriate concept, a comprehensive and transparent overview of the decision making process behind both the criteria weightings and selection of design candidate relative grades is presented. In addition, as has been previously noted the consistency ratios for both the criteria weighting matrix and the relative grade matrices all lie comfortably within the acceptable threshold, indicating the numerical validity of the trade off and by extension its reliability. Therefore, the resulting selection of the cold gas regulated blow down design candidate presented in this trade off analysis is justified to the best extent possible and shall provide the basis for the design of a micropropulsion based inflation system. With respect to the other candidates explored here, it is apparent that the CGG refill candidate with its attractive combination of CGG technology and conventional cold gas propulsion system design is a highly promising solution. While providing lower inflation control relative to the regulated blow down design candidate, its mass and volume properties make it an exciting concept worthy of exploration for BEOC inflation systems.



## 7.4. INFLATION GAS

The next stage in the concept generation process is the selection of a suitable inflation gas. This process is not immediately straight forward and depends on a number of important factors. In order to select a suitable inflation gas for this thesis project, a range of potential of gases shall be explored with their characteristics being examined relative to a range of important factors.

### 7.4.1. GAS OPTIONS

As has been alluded to in the previous section, cold gas inflation systems are the most mature type of inflation system. During the literature review process, a number of gases were identified as the most typically utilized for such systems. As such this seemed like the most obvious place to start in the gas selection process. The identified gases are presented in table 7.5.

| Gas | Molecular Weight (Kg/mol) | Gas specific heat ratio |
|---|---|---|
| Hydrogen | 0.002 | 1.404 |
| Helium | 0.004 | 1.67 |
| 70/30 Nitrogen-Helium | 0.01121 | 1.308 |
| Nitrogen | 0.02802 | 1.4 |
| 95/5 Argon-Helium | 0.03815 | 1.482 |
| Argon | 0.0399 | 1.67 |
| Carbon Dioxide | 0.044 | 1.28 |
| Xenon | 0.1313 | 1.67 |

Table 7.5: Potential inflation gas

Nitrogen is by far the most popular inflation gas and has been utilized across a vast array of inflatable structures, including numerous spherical structures (Coffee et al., 1962; Guidanean and Veal, 2003; Nakasuka et al., 2009). Helium and Hydrogen possess the most attractive mass properties of any gas thanks to their low molecular weight and are commonly found in terrestrial inflatable applications as well as inflatables proposed for other planets (Griebel et al., 2004; Griebel, 2011). Xenon, on the other hand, is the heaviest of the proposed gases and as such is less commonly used for inflation purposes although it was utilized for the AeroCube-3 inflatable de-orbit balloon (Hinkley, 2008). Carbon dioxide and Argon, while often utilized in cold gas automotive airbag inflation systems (Shi et al., 2009) are relatively uncommon among inflatable space applications. However in the case of Argon, the CatSat inflatable spherical antenna does propose the use of a 95/5 Argon-Helium mixture (Chandra et al., 2021). The use of optimized gas mixtures is likely the best way to provide an optimal inflation gas for a given application. This is noted by Roe, 2001, who discusses the use of a 30/70 Nitrogen-Helium mixture for the ARISE inflatable antenna. Such a mixture was chosen so as to provide the optimal gas molecular weight that minimizes the wet mass of the antenna. As the development of an optimized gas mixture for this specific structure is beyond the scope of this thesis, these two gas mixtures shall also be evaluated.

### 7.4.2. DESIRABLE GAS CHARACTERISTICS

There are a number of important properties that must be considered when selecting an inflation gas for this project.

| ID | Property | Rationale |
|---|---|---|
| PROP-G-01 | Minimal volume requirements | Derived from REQ-ISI-01, this plays an essential role in minimizing the volume requirements and satisfying key requirement REQ-BEOC-01. |
| PROP-G-02 | Minimal mass requirements | Derived from REQ-ISI-02, this plays an essential role in minimizing the mass requirements and satisfying key requirement REQ-BEOC-02. |

| | | |
|---|---|---|
| PROP-G-03 | Stability at expected temperature and pressure ranges | Derived from REQ-ISI-04-01, this is vital in ensuring that the gas does not cause degradation to the inflatable membrane, with condensation or deposition of the gas within the inflation system or the inflatable structure highly undesirable. |
| PROP-G-04 | Non-hazardous | Derived from REQ-ISI-04-02, this is vital in ensuring that the gas does not cause degradation to the inflatable membrane or indeed the inflation system/ CubeSat |
| PROP-G-05 | Minimal gas speed of sound | Derived from REQ-ISI-04-04, minimizing the gas speed of sound is desirable as it plays a key role in ensuring that the gas jet doesn't damage the inflatable membrane. |
| PROP-G-06 | Heritage | Available experience being used for inflation purposes, particularly inflatable space structures is desired. |

Table 7.6: Desirable Inflation Gas Properties

### 7.4.3. INFLATION GAS SELECTION

As can be seen from these desired gas properties, the molecular weight plays a leading role in the selection of the most suitable inflation gas, playing a key role in satisfying the mass, volume and velocity requirements of the system. As such, the first step taken in the gas selection shall be establishing the impact of molecular weight on these requirements.

7

#### MOLECULAR WEIGHT

Firstly, the mass requirements for the inflation process can be split into two categories; mass of gas for initial inflation, i.e. pressurization, and mass of gas for pressure maintenance. The mass of gas required for the initial inflation process can be calculated using equation 7.1.

$$m_{inf} = M_W \cdot \frac{P_{inf} \cdot v_{structure}}{R_A \cdot T} \tag{7.1}$$

where:

- $m_{inf}$ = Mass of gas required for initial inflation/ pressurization (Kg)
- $M_W$ = Molecular weight (Kg/mol)
- $P_{inf}$ = Inflation pressure (Pa)
- $v_{structure}$ = Volume of inflated structure ($m^3$)
- $R_A$ = Universal gas constant (8.3145 J/mol·K)
- $T$ = Temperature of gas (K)

As $m_{inf}$ is proportional to the molecular weight ($M_W$) of the gas it is evident that the lower the molecular weight of the gas, the lower the mass of gas required for the initial inflation process. This can clearly be seen in figure 7.2a where helium and hydrogen require significantly lower quantities of gas than their higher molecular weight counterparts. In the case of pressure maintenance, the mass of inflation gas required to make-up for leaks caused by micrometeoroid damage is proportional to the square root of the gas molecular weight. This can be seen in equation 7.2, where the influence of the gases specific heat ratio can also be noted.

$$m_{makeup} = \sqrt{M_W} \cdot P_m \cdot A_{structure} \cdot \sqrt{\frac{\gamma}{R_a \cdot T} \left(\frac{2}{\gamma+1}\right)^{\frac{\gamma+1}{2(\gamma-1)}}} \cdot \frac{G}{2} \cdot t^2_{maintenance} \tag{7.2}$$

where:

- $m_{makeup}$ = Mass of gas required for pressure maintenance (Kg)
- $P_m$ = Maintenance pressure (Pa)
- $A_{structure}$ = Structures cross sectional area (m$^3$)
- $\gamma$ = Gas specific heat ratio
- $T$ = Temperature of gas (K)
- $G$ = Growth rate due micrometeroid punctures (1/s)
- $t_{maintenance}$ = Duration of pressure maintenance (s)

This leads to the results presented in figure 7.2b, where the mass of gas required to compensate for the gas losses increases with time. Due to the mass requirements being proportional to the square root of the gas molecular weight this is a major issue for the higher molecular weight gases, particularly Xenon, yielding highly undesirable mass requirements relative to the lower molecular weight gases. However, as the tank volume is proportional to the number of moles required, and hence volume of stored gas, the lower the molecular weight of the gas the greater the volume requirements (Roe, 2000). This can clearly be seen in figure 7.2c, where xenon has far lower volume requirements than the low molecular weight gases helium and hydrogen despite having significantly higher mass requirements.

In addition to providing reduced volume requirements, higher molecular weight gases also provide a lower gas jet velocity. This is key to satisfying requirement REQ-ISI-04-04, which desires the gas velocity to be kept below 1.5 times the gas speed of sound. Thus to reduce gas jet velocity a gas with a minimal speed of sound is desirable. The gas speed of sound $a$ is given by equation 7.3.

$$a = \sqrt{\gamma \frac{Ra}{M_W} T} \tag{7.3}$$

As is the case for volume, the speed of sound is inversely proportional to the square root of the gas molecular weight. Thus it can generally be said that the higher the molecular weight of the gas the lower its speed of sound.

7

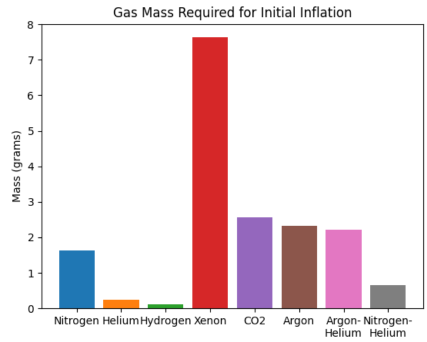


(a) Mass of Gas for Pressurization

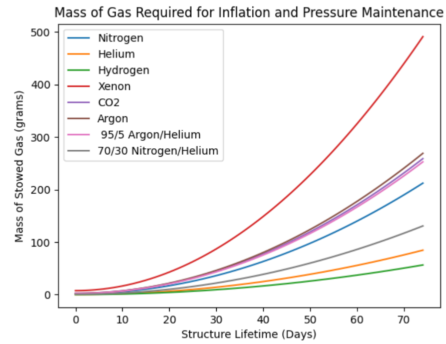


(b) Mass of Gas, $M_{gas} = M_{inf} + M_{makeup}$

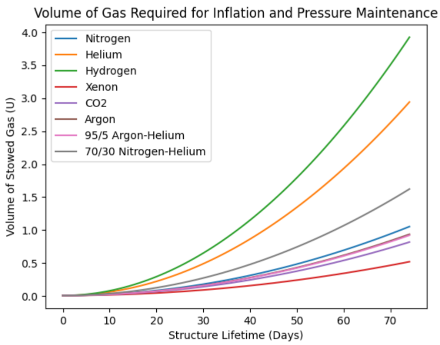


(c) Volume of Stowed Gas vs Structure Lifetime

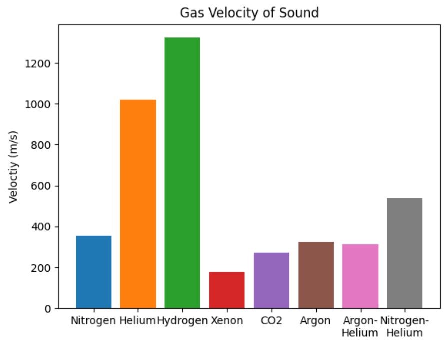


(d) Gas Velocity of Sound @ 300 K

Note: It is assumed all gases are stored in gaseous phase at 200 bar and 300K for ease of comparison. Further exploration of gas storage is done in section 8.4

Figure 7.2: Molecular Weight Impact on Inflation System Characteristics

## SPECIFIC HEAT RATIO

From this discussion regarding molecular weight it can be concluded that the the higher the molecular weight of the gas, the higher its mass requirements but the lower its volume and velocity requirements. However, this statement is not entirely true. As can be seen in equations 7.2 and 7.3, the specific heat ratio of a gas also plays a role in determining these parameters. In the case of makeup gas, as given in equation 7.2, the influence of a lower specific heat ratio can reduce the mass requirement. This is seen in the case of Carbon Dioxide which, from figure 7.2b, can be seen to have a reduced $M_{gas}$ requirement relative to the lighter Argon. Given that the volume is calculated based on these mass requirements the specific heat ratio shall also effect the volume requirements of the gas. This can be seen in the case of Argon and 95/5 Argon-Helium, where 95/5 Argon-Helium has a slightly lower volume requirement than Argon despite having a lower molecular weight. The impact of the specific heat ratio on Argon and 95/5 Argon-Helium is even more noticeable when examining velocity where it results in 95/5

Argon-Helium having a lower speed of sound, as seen in figure 7.2d.

### DISCUSSION

From this consideration of it is apparent that the very low molecular weight gases helium and hydrogen are highly unattractive for the purposes of inflating a pressure stabilized inflatable structure. As tank volume is proportional to gas volume, the required tank sizes necessary to stow these gases would cause significant issues when attempting to satisfy requirement REQ-ISI-01, while their high gas velocities are equally unsuitable. On the other hand, Xenon has the exact opposite characteristics, with attractive volume and velocity properties but major issues with the mass of gas required. As seen in figure 7.2, these issues increase with time and shall be exacerbated by further mass requirements for ullage and leakage (see section 8.4.6). As such, it was decided to eliminate Helium, Hydrogen and Xenon from the consideration for a suitable inflation gas. This leaves the following potential inflation gases, as summarized in table 7.7, with their properties calculated at 30 days.

| **Gas** | **$M_{inf}$ (grams)** | **Speed of sound (m/s)** | **$M_{gas}$ (grams)** | **Stowed Volume (U)** |
|---|---|---|---|---|
| Nitrogen-Helium | 0.65 | 539.66 | 22.03 | 0.273 |
| Nitrogen | 1.63 | 352.98 | 36.24 | 0.179 |
| Argon-Helium | 2.28 | 311.29 | 43.4 | 0.157 |
| Argon | 2.32 | 322.57 | 46.15 | 0.16 |
| Carbon Dioxide | 2.58 | 270.18 | 44.69 | 0.14 |

Table 7.7: Summary of gas properties @ 30 days

From table 7.7, it is apparent that while having the most attractive mass characteristics, 70/30 Nitrogen-Helium possesses relatively undesirable velocity and volume properties. The other gas mixture, 95/5 Argon-Helium, with its lower specific heat ratio, yields slightly more attractive velocity and volume characteristics than the heavier Argon, over which it already has an advantage in mass. However, these differences are slight and while it provides a more optimized solution relative to Argon, it was decided that due to the fact that more data is readily available on Argon, the 95/5 Argon-Helium shall not be further considered. As such, it was decided to eliminate both gas mixtures from the discussion. Before contemplating Nitrogen, Argon and Carbon Dioxide, the phase change properties of the three gases shall be presented so as to provide a more informed comparison. These are presented in table 7.8, with the data compiled from the NIST website[1].

From these tables, it can be seen that while Carbon Dioxide possesses the most attractive velocity and stowed volume properties of the three gases, its critical and triple points lie around the expected temperatures and pressures, well in excess of Nitrogen and Argon. This lack of stability at the expected temperature and pressure ranges is tenuous,

[1] https://webbook.nist.gov

7

| Gas | Phase Change Point | Temperature (K) | Pressure (bar) |
|---|---|---|---|
| Nitrogen | Critical Point | 126.2 | 34 |
| | Boiling Point | 77.4 | 1 |
| | Triple Point | 63.14 | 0.1252 |
| Argon | Critical Point | 150 | 48.9 |
| | Boiling Point | 87.5 | 1 |
| | Triple Point | 83.78 | 0.689 |
| Carbon Dioxide | Critical Point | 304 | 74 |
| | Triple Point | 216 | 5.185 |

Table 7.8: Inflation Gas Phase Change Data

and would complicate the design of the inflation system, necessitating careful control of the temperature and pressure. In addition, while Carbon Dioxide has been proposed for an inflatable space reflector (Friese et al., 1983) and is inert under most conditions, it can be toxic if exposed to moisture[2], and is thus generally not considered for cold gas propulsion applications (Anis, 2012). For these two reasons it shall not be further considered for this inflation application. This leaves only Nitrogen and Argon, with both possessing relatively similar properties, although Argon slightly outperforms Nitrogen with regards to velocity and volume requirements. However, upon the consideration of the far more extensive use of Nitrogen for inflatable space structures, it was decided that for this project, Nitrogen shall be selected as the most suitable inflation gas. This decision process is summarized in the graphical trade off table 7.9, where the mass and volume requirements are taken at 30 days. For more information on the color scheme see appendix D.

7

[2]https://ilmoproducts.com/industries-served/welding-cutting/gases-their-applications/carbon-dioxide

| Gas | PROP-G-01 | PROP-G-02 | PROP-G-03 | PROP-G-04 | PROP-G-05 | PROP-G-06 |
|---|---|---|---|---|---|---|
| Hydrogen | 0.651 U | 9.38 g | Excellent | Unreactive | 1323.68 m/s | Widely used |
| Helium | 0.489 U | 14.1 g | Excellent | Inert | 1019.4 m/s | Widely used |
| 70/30 Nitrogen-Helium | 0.273 U | 22.03 g | Acceptable | Unreactive | 539.66 m/s | Limited |
| Nitrogen | 0.179 U | 36.24 g | Acceptable | Unreactive | 352.98 m/s | Most popular |
| 95/5 Argon-Helium | 0.157 U | 43.4 g | Acceptable | Inert | 311.29 m/s | Limited |
| Argon | 0.16 U | 46.15 g | Acceptable | Inert | 322.57 m/s | Terrestrial Use |
| Carbon Dioxide | 0.14 U | 44.69 g | Undesirable | Can be toxic | 270.18 m/s | Terrestrial Use |
| Xenon | 0.091 U | 87.1 g | Acceptable | Inert | 177.93 m/s | Limited |

Table 7.9: Inflation Gas Graphical Grade Off Table

7

## 7.5. INFLATION SCHEME

A key factor in ensuring a reliable and controlled inflation process is the inflation scheme, which involves the sequencing of the inflation process so as to maximize control over the inflation rate. This inflation sequencing can enable the inflation system to compensate for the lack of deployment control provided by free deployment and ensure the structure inflates within an acceptable time-frame. Unfortunately, the literature available on inflation sequencing for inflatable space structures is very limited with Friese et al., 1983, Thunnissen et al., 1995 and Lichodziejewski et al., 2003 providing some of the only useful descriptions in the literature. The sequences described in these three sources are all quite similar and are in accordance with the general guidelines that should be followed for each of the inflatable structures shape transformation functions, as described in the literature review (Dunbar, 2021). Typically the only variation in inflation sequences is due to the stabilization method, with pressure stabilized structures having an additional pressure maintenance phase relative to rigidized structures who have an additional venting phase. For the inflation of the designed inflatable spherical structure, as is discussed in section 6.7.3, the inflation sequence shall contain both of these phases. This was done as the venting phase enables the design of a structure with a lower operating pressure as well as an inflation system that can also be utilized for rigidized applications. Therefore the general inflation sequence steps for this structure, which are encapsulated in requirements REQ-ISP-02 to REQ-ISP-06, are as follows:



1. Ascent Venting
    - As noted in the literature study (section 2.2.4) and structural design process (section 6.3) an important factor that must be considered in the design of a controllable inflation system is the impact of residual gases built up during the packaging process. The uncontrolled expansion of these gases during launch can be hugely detrimental to the successful implementation of the inflation sequence as it may lead to premature inflation of the structure, resulting in an unpredictable and unreliable deployment process, as was seen in the IAE experiment (Freeland et al., 1997). Due to the difficulty in completely negating residual gas build up during packaging, the conventional method of overcoming this issue is through ascent venting. During launch, the packaged structure should be vented to ambient pressure so as to allow any trapped gases to escape.
2. Inflation
    (a) Unfolding
    - The unfolding phase involves moving the structure from its packaged state to its open/deployed state in a smooth and controlled manner. Due to the use of free deployment, coupled with the delicate nature of the inflatable membrane prior to stiffening by internal pressure, precise control over the unfolding process is essential. If the inflation rate is too high, the structure will inflate too quickly, leading to high stresses and accelerations induced in the unfolding structure resulting in an unpredictable deployment situation and damage to the inflatable membrane.

It is therefore no surprise that this a vital stage in the inflation sequence, particularly for freely deployed structures like the one designed in this thesis project.

(b) Pressurization

- This phase entails pressurizing the inflatable structure to 15% of its yield stress so as to remove any wrinkles leftover from the packaging process and thus inflate the reflector to its desired deployed state. The motivation for the selection of this skin stress is discussed in section 6.7.3. The inflation rate is typically increased relative to the unfolding stage so as to ensure that the structure is inflated in a suitable inflation time (Griebel, 2011; Lichodziejewski et al., 2003). For additional control, it may be wise to reduce the inflation rate as it approaches design pressure so that the tension in the skin can build up more gradually (Griebel, 2011).

3. Venting

- As has been alluded to, for this system an inflation sequence was chosen that entails venting the structure to a lower predetermined pressure post inflation as is done by Friese et al., 1983 and Thunnissen et al., 1995 for inflating inflatable reflectors. As is discussed in section 6.7.3, this predetermined stress level is found at 2% of the membranes yield stress. This venting process should be carried out in a non-propulsive manner utilizing a zero thrust valve to vent the gas symmetrically (Lichodziejewski et al., 2003). This shall reduce the disturbances on the spacecraft and by extension the ADCS workload.
- This phase, while not typical for pressure stabilized structures, is included in this thesis project so as to satisfy the mission statement as it shall enable the design of an inflation system which is also suitable for rigidizable applications and will therefore be highly relevant for future BEOC inflatable applications. In addition, by reducing the internal pressure of the structure the amount of make-up gas required is reduced leading to a reduction in inflation system sizing and a longer mission duration.

4. Pressure Maintenance

- As the lunar inflatable reflector structure is a pressure stabilized structure, the inflation system must also be capable of providing pressure maintenance as the last phase of the inflation sequence. This pressure maintenance must be capable of replenishing the gas lost to micrometeoroid punctures and other sources of leakage as well as be capable of responding to pressure changes in the structure induced by thermal variations in the environment as the structure orbits the moon. Precise pressure maintenance is essential to ensuring the structures skin stress level stays within desirable limits.
- This phase is the most challenging in terms of meeting the stringent mass and volume requirements of the system and a trade off between sizing and mission duration must be carried out to account for this.

### 7.5.1. The Inflation Stage

As can be seen there are four distinct steps involved in the inflation sequence of the spherical inflatable reflector. Unsurprisingly, the most important step is the inflation process, which is further subdivided into unfolding and pressurization, as the inflation system is designed specifically with this step in mind. The primary driver of the inflation system's performance is the rate of inflation. As mentioned, if the inflation rate is too high during the unfolding phase, the structure will inflate too fast leading to an unpredictable deployment process as well as potentially damaging the inflating structure. On the other hand, if the inflation rate is too low during the pressurization phase, the structure will inflate too slowly, leaving it exposed to the on-orbit loads and environmental conditions for an extended period of time prior to reaching the skin stress necessary for suitable structural stability and surface accuracy. While no literature could be found exploring such effects it is likely that for pressure stabilized structure this could be detrimental to the operational performance of the reflector post inflation. For rigidized structures, particularly those that utilize rigidization processes which are time dependent such as UV rigidization, the impact of a slow pressurization could even be detrimental to the structural stability of the structure due to the potential for an uneven rigidization process. In the case of UV rigidization, this would take the form of an uneven curing of the UV resin prior to the structure reaching the desired skin stress.

Evidently, as seen in a variety of different inflation systems (Friese et al., 1983; Griebel, 2011; Lester et al., 2000; Malone and Williams, 1996), these two phases of the inflation stage require a variation in the provided inflation rate in order to ensure the structure is unfolded in a controlled fashion and pressurized in a suitable time frame. However, before exploring how this variation can be provided, a suitable inflation time must first be determined.

7

#### Inflation Time

In order to ensure that the structure is inflated in an appropriate time frame, minimum and maximum values for the inflation time of the structure must be determined. These inflation times will in turn dictate the rate of inflation of both phases of the inflation stage, as discussed in greater detail in the design of the control logic (see section 8.3.3), and by extension the mass flow rate through the inflation nozzle. Given that methods for establishing these times, such as testing and complex simulations, are beyond the scope of this thesis the only other option for gauging appropriate times is to examine the literature. However, given the limited literature available on inflation systems in general, the detail on suitable inflation times, never mind inflation rates, is very sparse.

| **Structure** | **Shape** | **Dimensions (m)** | **Total Inflation Time (s)** | **Reference** |
|---|---|---|---|---|
| MIRIAM | Sphere | $\phi = 4$ | 120 | Griebel, 2011 |
| 30 Inch Sphere | Sphere | $\phi = 0.76$ | 15 | Coffee et al., 1962 |
| 12 ft Sphere | Sphere | $\phi = 3.66$ | 238 | Coffee et al., 1962 |

| | | | | |
|---|---|---|---|---|
| NanoSat Device | Sphere | $\phi = 0.33$ | 4 | Nakasuka et al., 2009 |
| Solar Concentrator | Lenticular | $\phi = 4.17$, f = 2.05 | 110 | Lester et al., 2000 |

Table 7.10: Inflation Times for Spherical Inflatable Space Structures

The inflation times presented in table 7.10 were the only relevant values that could be found, with little information given regarding their selection. Given the variety in structural sizes, applications and times, this limited data makes estimating suitable inflation times based on relevant structures infeasible. As such, the only option for proceeding with the design of the inflation system is to make an initial estimate of the minimum and maximum inflation times for the 1.0 m diameter structure. Examining both the inflation times of the above spherical structures, as well as other inflatable space structures, in general it can be said that the inflation of an inflatable space structure seems to take anywhere from a few seconds for small simple structures to a few minutes for large complex structures. As such, a preliminary estimate regarding the minimum and maximum inflation times is given in table 7.11. This estimate shall inform the preliminary design of the system and while clearly not optimal shall nonetheless inform the exploration of the major design considerations. Thus, until further analysis is carried out these preliminary values shall be used as a guide for the inflation time, with the minimum and maximum times considered suitably conservative for a controlled inflation and pressurization.

| Parameter | Time (s) |
|---|---|
| Minimum Inflation Time | 10 |
| Maximum Inflation Time | 100 |

Table 7.11: Preliminary Estimate of Maximum and Minimum Inflation Times

7

### Types of Inflation Methods/Modes

There are two types of inflation methods/modes that can be utilized to facilitate the requirements of the desired inflation sequence. The two methods contain different characteristics and place different demands on the design of the inflation system. They can be differentiated by the length of inflation pulse that they utilize. One method utilizes numerous short pulses (milliseconds) to slowly inflate the structure while the other uses a small discrete number of long pulses (seconds). Given the popularity of using adapted propulsion systems as inflation systems, it is unsurprising that these two inflation modes correspond to the two main propulsion modes utilized in spacecraft propulsion; the pulsed mode of operation and the steady state mode of operation. Therefore, for this discussion the two inflation modes shall be referred to using these titles.

**The Pulsed Method**

The pulsed inflation method works just like a pulsed operation propulsion system. The method requires that the inflation system operate by opening the inflation control valve, typically a solenoid or piezoelectric valve, for a short time frame, allowing inflation gas to flow into the structure, before closing it again. This on/off cycle is repeated with a specified frequency until the desired inflation pressure is reached. The opening times and frequencies can be adjusted and tailored to the specific requirements of the inflation sequence. Like a pulsed operation propulsion system, which is typically utilized for precise RCS thruster maneuvers, this inflation method enables a highly precise and controllable inflation. In addition, utilizing these very small pulses of gas to slowly inflate the structure reduces the violent effects of gas expansion under vacuum conditions (Lester et al., 2000).

As far as the author could find, as of the time of writing there are only two distinct projects where the use of numerous short pulses is applied to inflate an inflatable space structure. Both of these projects explicitly state that this was done in order to provide an inflation system capable of controlled and precise deployment of the inflatable structure. While the use of short pulses are sometimes referred to in other works, such as by Thunnissen et al., 1995, and are likely used to inflate other inflatable structures, these are the only two projects where their use is explicitly mentioned. The first project entails the inflation of a Martian Inflatable Hypersonic Drag Balloon that was investigated by the University of the Federal Armed Forces of Germany (Griebel et al., 2004; Griebel, 2011. The other entails the design of a inflation control system specifically for an inflatable solar concentrator (Lester et al., 2000).



**The Steady State Method**

The steady state method utilizes long pulses of inflation gas so as to have a continuous gas flow into the inflatable structure. Unlike the pulsed method where the valve is opened and closed rapidly, this method simply involves holding open the inflation valve for long enough until either the inflation stage is finished or the structure is fully inflated at which point the valve is closed again. While it sounds simple and less complex, this continuous steady state method leads to a number of issues for the inflation of precision inflatable structures that require a multi stage inflation sequence as specified above. Firstly, the gas flow must be strictly controlled and regulated so as to ensure that it does not damage the inflatable structure. Secondly, in order to provide different inflation rates for unfolding and pressurization, the system must be able to adjust the gas flow rate.

From the literature, it appears that inflation systems utilizing the steady state method typically aim to adjust gas flow rates not through the use of complex proportional valves but by utilizing multiple different gas pathways. For example, for the design of the ITSAT inflatable solar array (Malone and Williams, 1996) the inflation system was designed with two gas flow pathways, a low rate path, for unfolding, and a high rate path, for pressurization. A diagram of this system can be seen in figure 7.3. This use of multiple pathways is also seen in Friese et al., 1983 for the inflation and pressure maintenance of the lenticular structure of an inflatable antenna. Indeed, for this system, the two separate pathways also utilize separate tanks, one for unfolding and pressure maintenance, and one for pressurization.

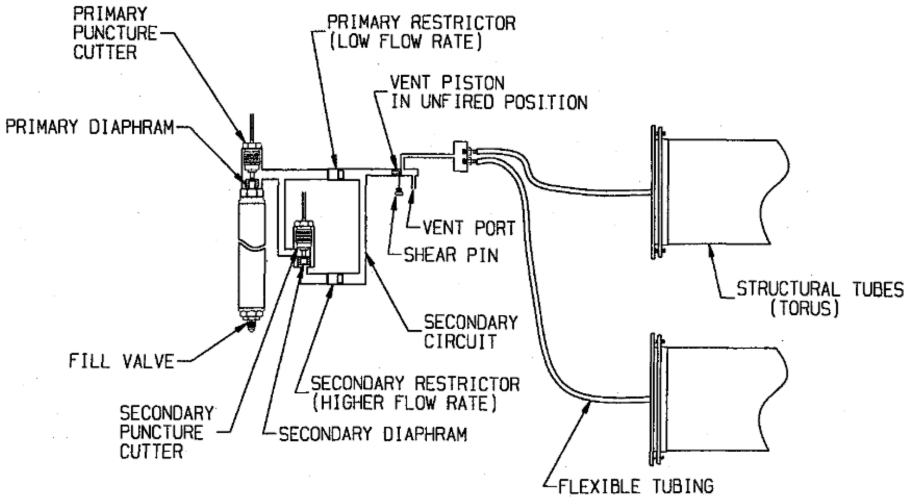


**Fig. 5 Inflation system schematic.**

Figure 7.3: ITSAT Steady State Method Inflation System (Malone and Williams, 1996)

Unfortunately, once again the literature on inflation systems that utilize the steady state method is limited. This is largely due to the ambiguity of the operational descriptions of many inflation systems. While there are a number of examples of steady state cold gas inflation systems being utilized for inflating structures without major concern for inflation sequencing, (Coffee et al., 1962; DiSebastian, 2001), the literature regarding their use for systems with stringent inflation sequencing is neither extensive nor clear. As of the time of writing, the author could only discern two such inflation systems, that used for the design of the ITSAT inflatable solar array as (Malone and Williams, 1996) and another used for the inflation of an inflatable antenna structure (Friese et al., 1983).

**Discussion**

Like the inflation scheme, the literature available on inflation methods is very limited. As has been alluded to in the descriptions above, of the inflation structures described in the literature the vast majority don't discuss their desired inflation mode, despite the clear importance it has for a controlled inflation system. However, despite the lack of literature, there are a few notable differences between the two methods that can be readily discussed.

The most notable difference between the two methods is the increased degree of controllability offered by the pulsed inflation method, as is evidenced by its popularity with precision RCS systems. For inflation systems utilizing this method, it enables a controllable inflation process that can be tailored for each stage of the inflation sequence by varying the pulse width and duty cycle. This contrasts with the steady state method where the control of inflation rates is more complex, requiring either a complex valve and throttling system or multiple gas pathways. As the use of a complex valve and throttling system was deemed undesirable due to the scope of this thesis, the steady state method would have to be implemented using multiple gas pathways. The increased degree of controllability of the pulsed method is also evidenced by its capacity to provide slower inflation rates. This is discussed by Nakasuka et al., 2009 who provides the only mention of a comparison between the two methods that could be found. The inflation system is equipped with a piezoelectric valve, with no mention of other additional flow control devices, and is designed for the inflation of a simple deorbit inflatable balloon. When the piezo-valve is kept open, in steady state mode, the balloon inflates rapidly (0.7s) due to the high inflation rate. However, when the piezo-valve is switched on/off, in pulsed mode, the balloon inflates almost an order of magnitude slower (4s), enabling a smoother and more controlled deployment. It can clearly be seen that pulse mode has the capability to significantly reduce inflation rates and therefore provide slower and more controlled inflation, even without the use of additional flow control devices.

| Requirement | Description | Preferred Method | Rationale |
|---|---|---|---|
| REQ-ISP-01 | Provides suitable inflation rates | Pulsed Method | Can provide suitable inflation rates that can be varied with relative ease |
| REQ-ISP-03 | Unfold structure in smooth and controlled fashion | Pulsed Method | Can provide slower more precise inflation rate |
| REQ-ISP-06 | Provide precise pressure maintenance | Pulsed Method | Can provide more precise pressure maintenance |
| REQ-ISI-01 | Low volume footprint | Pulsed Method | Requires less components as only a single gas pathway |
| REQ-ISI-02 | Minimal mass | Pulsed Method | Requires less components as only a single gas pathway |
| REQ-ISI-03 | Simple system | Pulsed Method | Requires less components and system interactions as only a single gas pathway |

Table 7.12: Evaluating Preferred Inflation Method with Respect to Requirements

The ability to provide small precise bursts of inflation is another key component of the inflation system controllability as it is highly desirable for precise pressure maintenance (Friese et al., 1983; Lester et al., 2000; Thunnissen et al., 1995). It enables the leak rates to be precisely compensated for throughout the mission, in a similar fashion to how precise RCS systems are often utilized to compensate for undesirable forces on spacecraft that require extreme stabilization and pointing precision. Without this capability steady state systems are not well suited for precise pressure maintenance capabilities.

7

Given all of these considerations, it is clear that in order to facilitate a controllable inflation system in accordance with the desired inflation scheme and inflation system requirements, the pulsed method is the preferable of the two. This conclusion is summarized in table 7.12, where a brief summary of the rationale behind this decision is provided. While it would be preferable to carry out a detailed analysis comparing the two methods, the clear advantages in inflation controllability possessed by the pulsed method made such an analysis unnecessary for this project. However, as this appears to be the first exploration of 'inflation modes/methods' for inflatable space structures a detailed investigation into the two methods may be worth exploring in the future.

## 7.6. CONCLUSION

This section established three key design variables ahead of the detailed inflation system design. Firstly, it was established that a cold gas regulated blowdown system provides the most attractive candidate for a micropropulsion based inflation system. Following this conclusion, nitrogen gas was found to be the most suitable inflation gas. Finally, the inflation sequence was specified and the pulsed mode of inflation highlighted as the most appropriate method for providing optimal inflation control.

# Bibliography


Anis, A. (2012). Cold gas propulsion system-an ideal choice for remote sensing small satellites. *Remote sensing-advanced techniques and platforms*, 447–462.

Chandra, A., Pat, T., Tonazzi, J. C. L., & Walker, C. K. (2021). Development and flight qualification of a small satellite x-band spherical membrane antenna. *2021 IEEE Aerospace Conference (50100)*, 1–8.

Coffee, C. W., Bressette, W. E., & Keating, G. M. (1962). *Design of the nasa lightweight inflatable satellites for the determination of atmospheric density at extreme altitudes*. National Aeronautics; Space Administration.

DiSebastian, J. D. (2001). *Rigex: Preliminary design of a rigidized inflatable get-away-special experiment* (tech. rep.). AIR FORCE INST OF TECH WRIGHT-PATTERSONAFB OH.

Dunbar, S. (2021). Literature review study - inflatable space structures, beyond earth orbit cubesat missions and micropropulsion inflation systems.

Freeland, R., Bilyeu, G., Veal, G., Steiner, M., & Carson, D. (1997). Large inflatable deployable antenna flight experiment results [Developing Business]. *Acta Astronautica*, *41*(4), 267–277. https://doi.org/https://doi.org/10.1016/S0094-5765(98)00057-5

Friese, G., Bilyeu, G., & Thomas, M. (1983). Initial'80s development of inflated antennas.

Gill, E. (2015). Generating , evaluating and selecting concepts. In *Ae4s12 space systems engineering*.

Griebel, H. S., Häusler, B., Rapp, H., & Mundt, C. (2004). Project archimedes-a novel approach to balloon deployment on mars. *55th International Astronautical Congress of the International Astronautical Federation, the International Academy of Astronautics, and the International Institute of Space Law*, QP–02.

Griebel, H. S. (2011). *Reaching high altitudes on mars with an inflatable hypersonic drag balloon*. Springer Science & Business Media.

Guidanean, K., & Veal, G. (2003). An inflatable rigidizable calibration optical sphere. *44 th AIAA/ASME/ASCE/AHS/ASC Structures, Structural Dynamics, and Materials Conference*.

Han, Z., Gong, L., Yan, S., Cao, W., Hng, H. H., Du, Z., & Yu, Y. (2021). A novel of spacecraft flexible compartment safe and stable inflatable expansion system with the environmental-friendly fuel. *Journal of Cleaner Production*, *279*, 123843.

Hinkley, D. (2008). A novel cold gas propulsion system for nanosatellites and picosatellites.

Lester, D., Wassom, S., Hancey, B., & Siefkas, P. (2000). Solar concentrator inflation control system. *41st Structures, Structural Dynamics, and Materials Conference and Exhibit*, 1571.

Lichodziejewski, D., Veal, G., Helms, R., Freeland, R., & Kruer, M. (2003). Inflatable rigidizable solar array for small satellites. *44th AIAA/ASME/ASCE/AHS/ASC Structures, Structural Dynamics, and Materials Conference*, 1898.

Malone, P. K., & Williams, G. T. (1996). Lightweight inflatable solar array. *Journal of Propulsion and Power, 12*(5), 866–872.

Nadja, K., & Karlheinz, K. (2004). Analytic hierarchy process ( AHP ). *European Journal Of Operational Research*.

Nakasuka, S., Senda, K., Watanabe, A., Yajima, T., & Sahara, H. (2009). Simple and small de-orbiting package for nano-satellites using an inflatable balloon. *Transactions of the Japan Society for Aeronautical and Space Sciences, Space Technology Japan*, *7*(ists26), Tf_31–Tf_36.

Roe, L. (2000). Inflation systems for near-term space missions. *41st Structures, Structural Dynamics, and Materials Conference and Exhibit*, 1570.

Roe, L. (2001). Inflation systems. In *Gossamer spacecraft: Membrane and inflatable structures technology for space applications* (pp. 407–416). American Institute of Aeronautics; Astronautics.

Shi, G., Chan, C. S., Li, W. J., Leung, K.-S., Zou, Y., & Jin, Y. (2009). Mobile human airbag system for fall protection using mems sensors and embedded svm classifier. *IEEE Sensors Journal*, *9*(5), 495–503.

Thunnissen, D. P., Webster, M. S., & Engelbrecht, C. S. (1995). Low-mass inflation systems for inflatable structures. *In Jet Propulsion Lab, California Inst. of Tech, Proceedings of the International Conference on Integrated Micro/Nanotechnology for Space Applications p(SEE N 96-36329 12-12), 1995*.

Underwood, C., Viquerat, A., Schenk, M., Taylor, B., Massimiani, C., Duke, R., Stewart, B., Fellowes, S., Bridges, C., Aglietti, G., et al. (2019). Inflatesail de-orbit flight demonstration results and follow-on drag-sail applications. *Acta Astronautica*, *162*, 344–358.

# 8

# INFLATION SYSTEM DESIGN

*The micropropulsion based inflation system is designed in this chapter. The first step in this process is the design of the inflator nozzle (section 8.2). Once the parameters for the nozzle have been established, the required inflation valve is discussed (section 8.3). Next, the design of the inflatant tank is investigated (section 8.4) followed by the design of the feed system (section 8.5). Finally, a suitable mass flow rate is selected (section 8.6). Once these steps are complete, the final design of the system is presented (section 8.7)*

## 8.1. Introduction

Following the concept generation process, the design of the cold gas micropropulsion based inflation system can begin. The aim of this chapter is to establish the design adjustments required in order to adapt such a micropropulsion system, that shall utilize nitrogen inflation gas and operate in the pulsed mode of inflation, in order to satisfy the desired inflation system requirements. This process shall entail tailoring each of the major micropropulsion system design features specifically for inflation applications. Once this has been complete, the performance of the system relative to the desired performance requirements shall be evaluated.

## 8.2. Nozzle Design

### 8.2.1. Introduction

The first major design feature that must be tailored for inflation applications is the nozzle. The first stage in this process is to establish via theoretical analysis the desired properties of the inflation system and more specifically the nozzle. This shall be done utilizing rocket propulsion theory and shall be done in two stages. First ideal rocket theory shall be used to gain a reasonable approximation of the performance of the inflation system via the design of an ideal nozzle. Once this is complete, the next stage of the analysis shall begin. This stage shall incorporate a more realistic approach to the nozzle's design by accounting for losses experienced by the system. The final output of this analysis shall be a cold gas micropropulsion based nozzle custom designed for inflation purposes.

### 8.2.2. Ideal Analysis

The ideal theoretical analysis shall be done utilizing ideal rocket theory which offers a reasonable approximation of the performance of actual micropropulsion systems (Zandbergen, 2018). The analysis shall begin with an initial preliminary investigation into the impact of the inflation systems design requirements on the design parameters of the nozzle. The outputs of this preliminary analysis are a set of refined requirements that shall drive the design of the nozzle which shall follow on from it. Important assumptions that are made during this analysis include the following:

8

- The inflation gas is homogeneous
- The inflation gas obeys the ideal gas law
- The heat capacity of the gas is constant
- The flow through the nozzle is one-dimensional, steady and isentropic.
- The flow through the nozzle has reached critical conditions in the throat

#### Considering Inflation System Requirements

The first step in the design of the nozzle for this system is to first assess the impact of the inflation system requirements on the system and thus further refine these requirements so that they can be utilized to properly inform the design of the nozzle. The most important requirements that must be considered for the design of the inflation system are derived from killer requirements REQ-ISP-01 and REQ-ISI-04:

- REQ-ISP-01: The inflation time shall take between 10 seconds and 100 seconds
  - Performance Parameter (s):
    - Mass flow rate
- REQ-ISI-04-01: The temperature of the inflation gas shall lie within the range of 160K to 430K.
  - Performance Parameter (s):
    - Chamber Temperature
    - Exit Temperature
- REQ-ISI-04-04: The inflation gas jet velocity shall be less than 1.5 times the Mach number
  - Performance Parameter (s):
    - Exit Velocity

The importance of these requirements to the design of the inflation system shall be discussed below.

**Inflation Rate**
As has been discussed in section 7.5, controlling the rate of inflation is essential to providing a reliable and controlled inflation process. This shall be done by operating the inflation system in pulsed mode, allowing the different stages of the inflation scheme to be fulfilled in the desired time frame. The first step in achieving inflation within the desired time frame (10-100 seconds) is the mass flow rate of inflation gas through the nozzle. It is desirable to have a low duty cycle pulsed inflation, so that rapid emptying of the tank is avoided, thus enabling the assumption of isothermal blowdown. In the discussion and analysis regarding pulsed inflation presented in section 8.3.3, it was established that in order to meet this time frame a steady state mass flow rate range of 0.1 to 0.9 g/s is required.



**Temperature**
Establishing thermal requirements for the inflation gas jet is not a straight forward process. This is in large part due to the dearth of information regarding the interaction between gas temperature and the inflation of inflatable structures. This thermal interaction during the inflation process is a complex one as it consists of the inflation gas jet interacting with both the inflatable membrane and the already present inflation gas, both of which are increasing/decreasing in temperature due to their interaction with the space thermal environment. Modelling this thermal interaction requires a detailed thermal analysis which is beyond the scope of this thesis. Thus, a number of simplifying assumptions regarding the thermal requirements of the inflation gas jet shall be made.

Firstly, the maximum acceptable temperature for the inflation gas shall be assumed to derive from the membrane materials (CP1) glass transition temperature (536 K). Assuming a 25% factor of safety this yields a maximum gas jet temperature of 430 K. On the other hand, establishing a minimum gas jet temperature is a bit more difficult. This is due to lack of information regarding the interaction between low temperature inflation gas and polyimide membranes. Therefore, a minimum acceptable gas temperature shall be assumed based off the phase change data of the inflation gas, Nitrogen. Evidently it is desirable for Nitrogen to stay in its gaseous state throughout the entire inflation process, with any condensation or deposition likely leading to detrimental consequences. Key Nitrogen phase change data from the NIST website is presented in table 7.8 from the section on the inflation gas selection discussion. As can be seen from this table, the temperature and pressure values of these points decrease proportionally, with the triple point occurring at a significantly lower temperature and pressure than the critical point. This relationship is apparent when examining figure 8.1.

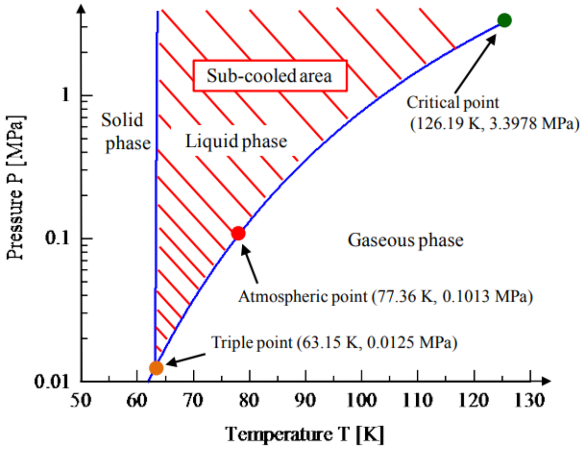


Figure 8.1: Nitrogen Phase Change Graph Nishimachi et al., 2012

8

Assuming that the exit pressure $P_e$ shall be lower than 34 bar, it can then be stated that if the temperature of the exit gas remains greater than 126.2 K then no condensation or deposition shall occur. As was the case for the maximum temperature an additional factor of safety of 25% shall be assumed. This yields a minimum exit gas temperature of about 160 K. This is clearly quite a conservative estimate, particularly as exit pressures well below 34 bars are anticipated. However, given the uncertainty surrounding the thermal interaction between the gas jet, the already present inflation gas, the structural membrane and the thermal space environment, such a conservative estimate was seen as an appropriate starting point until further research clarifies the subject.

**Velocity**

In a conventional propulsion system, maximizing the gas jet exit velocity is highly desirable as it improves the performance of the system. However, for an inflation system, the opposite is true where it is desired that the gas flow velocity be kept low enough so as to not damage the inflating inflatable membrane. Given that the minimum gas exit velocity is assumed to occur in the throat, where it equals the gas speed of sound $a_t$, it is desired that the inflation gas jet velocity be less than 1.5 times this velocity. As there does not appear to be any previous analysis on the impact of gas jet velocity on inflatable membranes this velocity requirement was seen as an appropriate starting point until further research clarifies the subject.

### ANALYSING THE IMPACT OF THESE REQUIREMENTS

Ideal rocket theory calculates the parameters according to a typical convergent-divergent nozzle. Using this theory, the exit velocity of a cold gas system can be written in terms of the chamber to nozzle exit temperature ratio using the following expression:

$$V_e = \sqrt{2\frac{\gamma}{\gamma-1} \cdot R \cdot T_c \cdot \left(1 - \frac{T_e}{T_c}\right)} \tag{8.1}$$

where:

- $V$ = Velocity (m/s)
- $\gamma$ = Gas specific heat ratio
- $R = \frac{R_A}{M}$ (J/kg · K)
- $T$ = Temperature (K)
- $c, e$ = Chamber, Exit

As the flow is assumed isentropic, Poisson' relations (expression 8.2) can be utilized to write equation 8.1 in terms of the chamber pressure to exit pressure ratio as follows:

$$\frac{T_e}{T_c} = \frac{P_e}{P_c}^{\left(\frac{\gamma-1}{\gamma}\right)} = \frac{\rho_e}{\rho_c}^{(\gamma-1)} \tag{8.2}$$

where:

- $P$ = Pessure (Pa)
- $\rho$ = Density (kg/m$^3$)

$$V_e = \sqrt{2\frac{\gamma}{\gamma-1} \cdot R \cdot T_c \cdot \left(1 - \frac{P_e}{P_c}\right)^{\left(\frac{\gamma-1}{\gamma}\right)}} \tag{8.3}$$

Using these two expressions the relationship between the gas jet velocity, the chamber and exit temperature as-well as the chamber and exit pressures can be investigated. Moreover, the velocity of the gas can be written in terms of the mass flow rate using the following expression:

$$\frac{m}{A} = \rho \cdot V \tag{8.4}$$

where:

- $m$ = Mass flow rate (kg/s)
- $A$ = Cross-sectional area (m$^2$)

Using this expression, equations 8.1 and 8.3 can be rewritten in terms of the mass flow rate:

$$\frac{m}{A_e} = \frac{P_c}{\sqrt{R \cdot T_c}} \sqrt{\frac{2}{\gamma+1}\left(\frac{T_e}{T_c}\right)^{\left(\frac{2}{\gamma-1}\right)}\left(1-\frac{T_e}{T_c}\right)} \tag{8.5}$$

$$\frac{m}{A_e} = \frac{P_c}{\sqrt{R \cdot T_c}} \sqrt{\frac{2}{\gamma+1}\left(\frac{P_e}{P_c}\right)^{\left(\frac{2}{\gamma}\right)}\left(1-\frac{P_e}{P_c}\right)^{\left(\frac{\gamma-1}{\gamma}\right)}} \tag{8.6}$$

Assuming that the flow becomes sonic in the nozzle throat, the critical conditions for the throat to chamber pressure, temperature, density and speed of sound ratios can be written as follows:

$$\frac{T_t}{T_c} = \frac{2}{\gamma+1} \tag{8.7}$$

$$\frac{P_t}{P_c} == \frac{T_t}{T_c}^{\left(\frac{\gamma}{\gamma-1}\right)} = \frac{2}{\gamma+1}^{\left(\frac{\gamma}{\gamma-1}\right)} \tag{8.8}$$

$$\frac{\rho_t}{\rho_c} = \frac{T_t}{T_c}^{\left(\frac{1}{\gamma-1}\right)} = \frac{2}{\gamma+1}^{\left(\frac{1}{\gamma-1}\right)} \tag{8.9}$$

$$\frac{a_t}{a_c} = \frac{T_t}{T_c}^{\left(\frac{1}{2}\right)} = \frac{2}{\gamma+1}^{\left(\frac{1}{2}\right)} \tag{8.10}$$

where:

- $a$ = Speed of sound (m/s)
  - $a = \sqrt{\gamma \cdot R \cdot T}$
- $t$ = throat

The equation for mass flow rate at the throat, where at sonic conditions $V_t = a_t$, is as follows:

$$m = \rho_t \cdot A_t \cdot V_t = \rho_t \cdot A_t \cdot a_t \tag{8.11}$$

Subbing the critical condition expressions into this equation yields the following equation for the critical mass flow rate in terms of throat area and chamber pressure:

$$m = \frac{\Gamma \cdot P_c \cdot A_t}{\sqrt{R \cdot T_c}} \tag{8.12}$$

where:

- $\Gamma$ = Vandenkerckhove constant $\left(\sqrt{\gamma}\left(\frac{2}{\gamma+1}\right)^{\frac{\gamma+1}{2(\gamma-1)}}\right)$

As the mass flow rate through the nozzle is constant, equation 8.12 can be subbed into equations 8.5 and 8.6, yielding the following expressions for the expansion ratio of the nozzle:

$$\frac{A_e}{A_t} = \frac{\Gamma}{\sqrt{\frac{2}{\gamma+1}\left(\frac{T_e}{T_c}\right)^{\left(\frac{2}{\gamma-1}\right)}\left(1-\frac{T_e}{T_c}\right)}} \tag{8.13}$$

$$\frac{A_e}{A_t} = \frac{\Gamma}{\sqrt{\frac{2}{\gamma+1}\left(\frac{P_e}{P_c}\right)^{\left(\frac{2}{\gamma}\right)}\left(1-\frac{P_e}{P_c}\right)^{\left(\frac{\gamma-1}{\gamma}\right)}}} \tag{8.14}$$

Using these equations relating the gas jet velocity, temperature ratios, pressure ratios and expansion ratio, the impact of the driving requirements relating to temperature, velocity and inflation rate can be assessed. Before doing this however, the exit velocity must be expressed in terms of the Mach number so as to adhere to requirement REQ-ISI-04-04. This can be done using the equation 8.15. The speed of sound at the nozzle throat $a_t$ can be calculated using equation 8.10.

$$M = \frac{V_e}{a_t} = \frac{V_e}{\sqrt{\gamma \cdot R \cdot T_t}} \tag{8.15}$$

Where:

- M = Mach Number

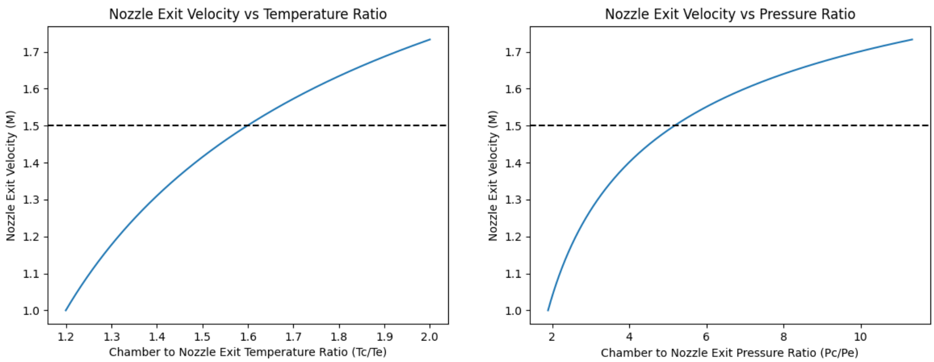


(a) Velocity vs Temperature Ratio

(b) Velocity vs Pressure Ratio

Figure 8.2: Graphing of Exit Velocity vs Temperature and Pressure Ratios

Figures 8.2 and 8.3 present the impact of the velocity requirement. The black dashed line indicates the maximum exit velocity requirement of 1.5 Mach. From the graphs presented, a number of clear conclusions can be made regarding the impact of this velocity constraint on the system design. Starting with the relationship with the temperature ratio, figure 8.2a, it can clearly be seen that in order to minimize the increase in gas jet velocity, the temperature ratio should be kept to a minimum. This relationship is also clear for the pressure drop across the nozzle, as can be seen 8.2b, and for the nozzle expansion ratio which, as can be seen 8.3a, must be limited to less than 1.3683. For simplicity this shall be rounded down to 1.36.

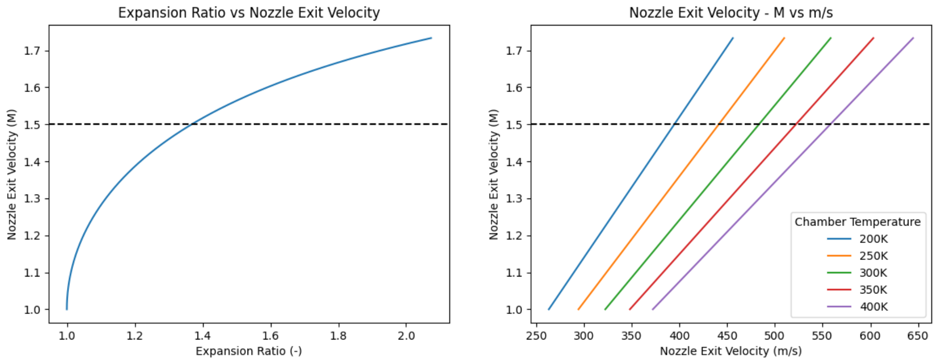


(a) Velocity vs Expansion Ratio

(b) Velocity in terms of M vs Velocity in terms of m/s

Figure 8.3: Graphing of Exit Velocity vs Expansion Ratio and in terms of M vs m/s

Finally, figure 8.3b presents the relationship between velocity in terms of the Mach number and m/s for a range of chamber temperatures. As can be clearly seen, lower chamber temperatures yield lower velocities (m/s) which is attractive given the desire to minimize the gas jet velocity.

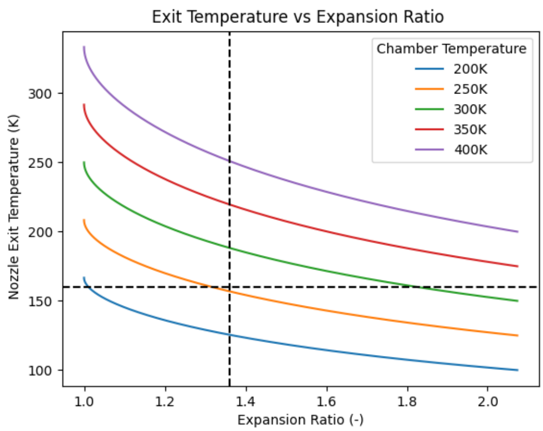


Figure 8.4: Exit Temperature vs Expansion Ratio

Figure 8.4 presents the impact of the temperature requirement on the expansion ratio of the nozzle. The vertical black dashed line indicates the maximum expansion ratio of 1.36 due to the velocity constraint while the horizontal black dashed line indicates the the minimum exit temperature requirement of 160 K. As can be seen, the velocity constraint is the driving requirement regarding a maximum expansion ratio for chamber temperatures above 250 K. However, for chamber temperatures below this value, the temperature constraint becomes the driving requirement. This is particularly evident for a chamber temperature of 200 K, which requires a severely restricted expansion ratio in under to ensure the exit temperature remains above 160 K. This graph also clearly indicates that in order to meet the critical conditions, the critical temperature ratio for nitrogen means that even at an expansion ratio of 1.0, i.e. the nozzle ends at the throat, the temperature of the gas jet still undergoes a drop relative to the chamber temperature. This value is thus the maximum gas jet exit temperature which decreases as the gases expand through the nozzle with increasing expansion ratio.

From figure 8.3b it is apparent that lower chamber temperatures yield a reduced gas exit velocity. However, as seen in figure 8.4, this comes at the expense of reduced gas exit temperatures. In this regard, of the chamber temperatures compared, 300 K provides the best balance of these requirements. Further optimization would yield an ideal chamber temperature but given that thermal control systems already aim to maintain satellite temperature around 300K such a chamber temperature is the obvious choice for this preliminary design. Maintaining chamber pressures above and below this value leads to additional undesirable system complexity. Higher temperatures would require a heating system and thus additional power, while lower temperatures would likely require additional insulation and other coolant features to ensure it remains colder than than the rest of the CubeSat.

**Results**

Unlike a nozzle design for a conventional propulsion system which typically starts the design process with a desired ΔV, thrust and Isp, the design process for the nozzle for this inflation system starts with the inflation system requirements, particularly the gas jet temperature and velocity requirements. In assessing the impact of these requirements on the design of the cold gas convergent-divergent nozzle, the following results were established.

- Mass Flow Rate:
  - The range of suitable mass flow rates for this design is 0.1 - 0.9 g/s.
- Chamber Temperature:
  - An optimal chamber temperature of 300K was selected to balance exit temperature and exit velocity requirements.
- Exit Temperature and Exit Velocity:
  - The maximum exit velocity of 1.5 time Mach is the driving design requirement as it determines the maximum acceptable expansion ratio. As seen in figure 8.4, at a chamber temperature of 300 K this yields a gas exit temperature above the minimum requirement of 160 K. Table 8.1 contains a list of

parameters calculated at the minimum expansion ratio of 1, in which case the nozzle ends at the throat and there is no divergent section, and at the maximum expansion ratio of 1.36 as dictated by the velocity requirement.

| **Parameter** | **Min. Expansion Ratio** | **Max. Expansion Ratio** |
|---|---|---|
| Expansion Ratio | 1 | 1.36 |
| Exit Velocity (Mach) | 1 | 1.495 |
| Exit Velocity (m/s) | 322.25 | 481.88 |
| Exit Temperature (K) | 250.038 | 188.28 |
| Temperature Ratio ($T_c/T_e$) | 1.2 | 1.59 |
| Pressure Ratio ($P_c/P_e$) | 1.89 | 5.11 |

Table 8.1: Calculated Values

- Throat Diameter and Chamber Pressure:
  - This preliminary analysis gives little detail regarding the throat dimensions or the chamber pressure. These parameters shall be discussed in greater detail in the real analysis section. See figure 8.9a for the relationship between throat diameter, chamber pressure and mass flow rate.

### PROPULSION PARAMETERS

As has been mentioned the driving design parameters for this inflation system derive from the desired inflation rate and properties of the gas jet. This is quite different to the design of a conventional cold gas nozzle, which focuses on maximizing performance relative to propulsion requirements such as Δ V, thrust and specific impulse. In order to try and adapt a micropropulsion system for inflation purposes it behooves the designer to establish the performance of such a system with relation to the main parameters used to described a propulsion system. This shall also be important for determining the impact that the inflation process has on the spacecraft and thus the ADCS requirements needed to compensate. These propulsion parameters are as follows:

8

- *Thrust*: The thrust generated by the inflation system can be described using equation 8.16. It should be noted that the ambient pressure $P_a$ reflects the pressure inside the inflatable structure. Initially, this value should be vacuum thanks to ascent venting. However, as the inflation process is completed this shall rise to the final desired pressure. However, this has a maximum value of about 276 Pa which is negligible compared to the exit pressure value which shall be on the order of magnitude of 100,000 Pa (bar). Thus, $P_a$ shall be assumed equal to 0.

$$F = m \cdot V_e + (P_e - P_a) \cdot A_e = m \cdot V_{eq} \tag{8.16}$$

  where:

  - $F$ = Thrust (N)
  - $V_{eq}$ = Equivalent velocity (m/s)

- *Specific Impulse (ISP):* The specific impulse can be calculated using 8.17. It is related to nozzle exit velocity, with a low ISP corresponding to a low velocity. Cold gas nitrogen systems have low Isp values compared to other propulsion systems.

$$ISP = \frac{V_{eq}}{g_o} \tag{8.17}$$

  where:

  – $g_o$ = Standard acceleration due to gravity on Earth (9.81 m/s$^2$)

- *Characteristic Velocity:* The characteristic velocity can be calculated using 8.18. Like Isp, the characteristic velocity is related to the nozzle exit velocity, reflecting the energy level of the inflatant. Unlike, Isp, it is independent of the nozzle pressure ratio. It can also be described in terms of the mass flow rate. For this nitrogen based system, $c^\star$ is 435.77 m/s.

$$c^\star = \frac{1}{\Gamma}\sqrt{R \cdot T_c} = \frac{P_c \cdot A_t}{m} \tag{8.18}$$

  where:

  – $c^\star$ = Characteristic velocity (m/s)

- *Thrust Coefficient:* The thrust coefficient can be calculated using 8.19. It determines the amplification of thrust due to the expansion of gas in the nozzle.

$$C_F = \frac{F}{P_c \cdot A_t} \tag{8.19}$$

  where:

  – $C_F$ = Thrust Coefficient

These parameters shall aid in the design of the system, as conventional propulsion system nozzles and thruster valves utilize these parameters to describe the components performance. In addition, each of these parameters shall be utilized to evaluate the real performance of the nozzle, through the use of correction factors. This shall be elaborated on in the following section.

8

### CONCLUSION

From this ideal analysis, a preliminary gauge of the nozzles design has been established. Importantly, the impact of the unique inflation system requirements, namely associated with inflation rate, gas temperature and gas velocity, has also been assessed leading to an understanding of how each of these parameters drive the design and performance of the nozzle. The impact of the temperature and velocity requirements in particular are highly unusual for conventional propulsion systems where maximizing exit velocity is key to achieving high performance. This gives a preliminary indication of the alternative design approach that must be followed for an inflation system adapted from such technology. Finally, an introduction to the propulsion parameters typically utilized in the design of a cold gas inflation system are also presented. The next stage in the design of the inflation nozzle is the performance of a more realistic analysis based on non-ideal assumptions.

### 8.2.3. REAL ANALYSIS

#### INTRODUCTION

As has been noted ideal Rocket Theory does not fully account for the real performance of the nozzle. While it does provide some preliminary guidelines for the design of the inflation system, it assumes that the flow through the nozzle is both one-dimensional and without friction and that the gas always acts as an ideal gas. Due to the limited validity of these assumptions, the ideal performance calculations do not necessarily fully reflect the real performance of the system. In order to correct the performance calculations to account for the discrepancy between real and ideal performance, correction factors may be introduced.

These corrections factors can be quite large for low thrust propulsion systems (<0.1N) and are largely due to viscous losses, although real gas effects and rarefaction effects may also contribute. However, as is noted in La Torre, 2011, for thrusters with a thrust >1mN, the effects of rarefaction can be neglected. Thus the losses experienced by this nozzle shall come from the following two sources:

- Real Gas Effects
- Flow Divergence
- Viscous Effects

The main correction factors stem from the the inflation performance requirements as well as the main propulsion performance parameters, as mentioned previously. They shall be investigated through a combination of theoretical calculations and experimental values from the literature. They are as follows:

- Thrust Correction Factor

$$\xi_F = \frac{F_{real}}{F_{ideal}} = C_d \xi_n \xi_c \tag{8.20}$$

- Nozzle Correction Factor

$$\xi_n = \frac{C_{F_{real}}}{C_{F\,ideal}} \tag{8.21}$$

- Heating Correction Factor

$$\xi_c = \frac{c^\star_{real}}{c^\star_{ideal}} \tag{8.22}$$

- Propellant Consumption Correction Factor

$$\xi_s = \frac{Isp_{real}}{Isp_{ideal}} \tag{8.23}$$

- Discharge Coefficient

$$C_d = \frac{m_{real}}{m_{ideal}} \tag{8.24}$$

- Velocity Correction Factor

$$\xi_V = \frac{V_{e_{real}}}{V_{e_{ideal}}} \tag{8.25}$$

- Temperature Correction Factor

$$\xi_T = \frac{T_{e_{real}}}{T_{e_{ideal}}} \tag{8.26}$$

Unsurprisingly, the most important factors for the design of the inflation system are the discharge coefficient, velocity correction factor and temperature correction factor.

### NOZZLE CONFIGURATION

The configuration of the nozzle directly impacts the losses accrued and thus has a major impact on the real performance of the nozzle.. By investigating how the different nozzle parameters impact its performance, an increased understanding of how the inflation nozzle shall look can be garnered. As has already been noted, the expansion ratio limited by the velocity constraints on the gas jet is entirely counter-intuitive for a conventional propulsion system while the idea of minimizing gas jet temperature is also quite unusual. In this section, a more detailed look at the nozzles configuration shall be examined to establish what other unusual design features a cold gas micropropulsion based inflation nozzle possesses.

**Nozzle Shape**

The ideal rocket theory utilized to calculate the ideal analysis assumes a convergent-divergent nozzle design. As can be seen lower gas jet velocity and highest gas jet temperature can be achieved in the case of a nozzle that reaches sonic conditions at the throat and has a limited diverging section. This may indicate the suitability of a solely convergent nozzle for such an application. However, despite this potential, cold gas thrusters generally utilize converging-diverging nozzle configurations. Seeing as the main research question attempts to ascertain the design adjustments required to adapt current cold gas micropropulsion technology for inflation purposes, it was thus decided to investigate the impact of the inflation requirements on the design of a converging-diverging nozzle. As such the use of a converging nozzle shall be left for future investigation.

There are two nozzle shapes that can be utilized for the converging-diverging configuration, conical and parabolic. However, for ease of manufacturing, simple conical nozzles are preferred for cold gas micropropulsion applications (La Torre, 2011; Özden et al., 2021). A schematic of a basic conical nozzle is shown in figure 8.5a below.

**Nozzle Dimensions**

The dimensions of a convergent-divergent nozzle can, unsurprisingly, be split into convergent and divergent parts. As can be seen in figure 8.5a above, the dominant features of a conical nozzle are the convergent half angle ($\beta$), the divergent half angle ($\alpha$) and of course the throat diameter. However, this schematic does not account for the sharpness of the edges which can impact the flow and nozzle performance. More detailed diagrams

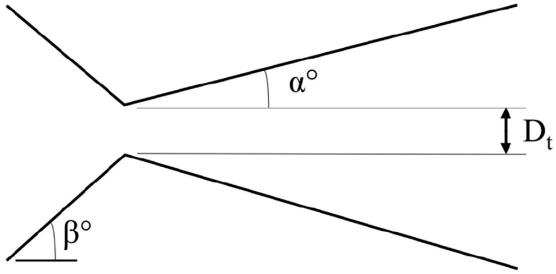


(a) Conical Convergent-Divergent Nozzle

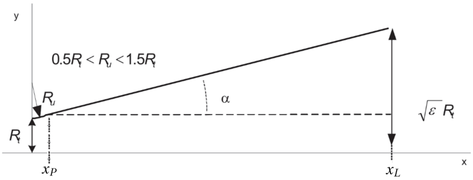


(b) Dimensions of divergent section

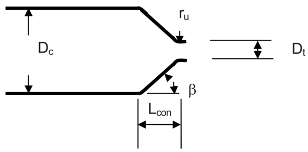


(c) Dimensions of Convergent section

Figure 8.5: Conical Nozzle (Zandbergen, 2018)

of the convergent and divergent sections can be seen in figures 8.5b and 8.5c. From these diagrams the leading dimensions of the nozzle can be listed as follows:

- Chamber Diameter ($D_c$)
  - According to Sutton and Biblarz, 2016 and Zandbergen, 2018, for monopropellant systems the cross sectional area of the chamber should be at least 3-4 times larger than that of the throat diameter in order to ensure contraction losses are minimized. Guidelines for cold gas systems are a little more vague as the nozzle is directly mounted onto the outlet of the control valve. Despite this Zandbergen, 2018 does also offer a conservative guideline for RCS cold gas thrusters that states chamber diameter should be at least 4 times throat diameter.
- Throat Radius ($R_t$)
  - The throat radius is key to the value of the Reynolds number. For throat Reynolds numbers over 100,000 the boundary layer is limited to the divergent section. However below this value, the boundary layer is also found within the throat.
- Throat Longitudinal Radius ($R_u$)
  - The Throat Longitudinal Radius dictates the sharpness of the nozzle throat, affecting both the length of the nozzle and boundary layer within the throat. It is generally given in relation to the throat radius, with values of 0.5Rt-1.5Rt most typical.

- Convergent Half Angle ($\beta$)
  - The convergent half angle typically varies from 30-60 degrees although for cold gas micropropulsion systems this can be as high as 90 degrees (Zandbergen, 2018). Its design is mostly aimed at reducing pressure losses due to flow contraction, with higher angles leading to increased pressure loss due to shorter convergent lengths ($L_{con}$) between the chamber and nozzle throat. It also contributes to the discharge coefficient as explored by Ahmad, 2001.
- Divergent Half Angle ($\alpha$)
  - The divergent angle plays a significant role in the performance of the system. It determines the flow divergence factor as shown in equation 8.31 and also plays a key role in the build of the boundary layer at the nozzle exit.
  - The angle selected generally lies between 12 and 18 degrees with the smaller the angle, the smaller the flow divergence factor. However, as the divergence angle also determines the length of the nozzle, the smaller the angle, the longer the nozzle. This in turn enables a greater distance along which the boundary layer can develop leading to increased viscous losses. Thus, when deciding on a divergence angle, nozzle designers must carry out a trade-off between the impact of boundary layer formation and divergence loss in order to establish the most suitable value for a nozzle with a specific expansion ratio.
- Divergent Length ($x_L$)
  - The divergent length reflects the length of the nozzle from the throat to the exit. As noted it is dependent on the value of the divergence angle but also the throat longitudinal radius. The boundary layer develops along the walls of the nozzle and thus, a longer nozzle yields a larger boundary layer. In order to determine the value of the divergent length for a conical nozzle, equation 8.27 can be used:

$$x_L = \frac{\left(\sqrt{\varepsilon} - 1\right) \cdot R_t + R_u \cdot \left(\frac{1}{cos(\alpha)} - 1\right)}{tan(\alpha)} \tag{8.27}$$

- Expansion Ratio ($\varepsilon$)
  - For this inflation system the expansion ratio plays an essential role in satisfying the desired gas exit temperature and velocity requirements. Moreover, as seen in equation 8.27, the expansion ratio contributes to the overall length of the nozzle and thus the viscous losses within it.

For this preliminary design, the choice of chamber diameter and convergent angle are less important for the real performance of the nozzle relative to the other dimensions (Louwerse, 2009). While they do play a role in the relationship of the thruster valve to the nozzle, and thus the real pulsing performance, as shall be discussed in section 8.3.3, a detailed analyses of the pulsing performance was beyond the scope of this project. Thus their impact on the performance of the nozzle shall not be further investigated.

8

### EFFECT OF NOZZLE DESIGN ON PERFORMANCE

In this section, the effect of the nozzles design on its performance shall be investigated. The main effects discussed are real gas effects, flow divergence and boundary layer formation. Their relation to the nozzles design parameters shall be explored.

#### Real Gas Effects

For the ideal performance of the nozzle, it is assumed that the inflation gas behaves as an ideal gas. However, in reality this is not necessarily true. Thus the selection of the chamber pressures can effect the performance of the system. One of the leading contributors to this is the compressibility of the gas at high pressures. This can be accounted for using the compressibility factor (Z) as is shown in equation below:

$$\frac{P}{\rho} = ZRT \tag{8.28}$$

It gives the ratio between the real and ideal density of the gas and thus affects the mass flow rate of the gas (Zandbergen, 2018). Thus, when determining the throat diameter for a given mass flow rate, the real diameter should be larger than the ideal calculation.

$$m_{real} = \left(Z_{plenum}\right)^{-0.5} \times m_{ideal} \tag{8.29}$$

In addition to compressibility, another effect of real gases is that unlike in IRT where specific heat is assumed constant, the specific heat of the gas varies with temperature and will thus vary depending on location in the nozzle. This additional correction yields the following equation:

$$m_{real} = \left(Z_{plenum}\right)^{-0.5} \cdot \frac{\Gamma(\gamma_t)}{\Gamma(\gamma_c)} \times m_{ideal} = \varphi \times m_{ideal} \tag{8.30}$$

The real gas effects can be summarized into one correction factor called the real gas correction factor ($\varphi$). Johnson, 1971 calculates this factor for nitrogen gas at a range of chamber temperatures and pressures as can be seen in figure 8.6. It can be seen from this figure that the correction factor decreases with decreasing chamber pressure and increasing chamber temperature.

#### Flow Divergence

For the ideal performance of the nozzle, it was assumed that the flow through the nozzle is one-dimensional. However, in reality this is not true and the assumption leads to an over estimation of the nozzles performance. In order to account for this, the flow divergence factor ($\lambda_n$) seen in equation 8.31 can be utilized.

$$\lambda_n = \left(\frac{1 + cos(\alpha)}{2}\right) \tag{8.31}$$

As mentioned previously, the divergence half angle is the design parameter that affects this correction factor and thus must be considered accordingly. The lower the angle, the lower the losses due to flow divergence. A graph of this is presented in figure 8.11a.

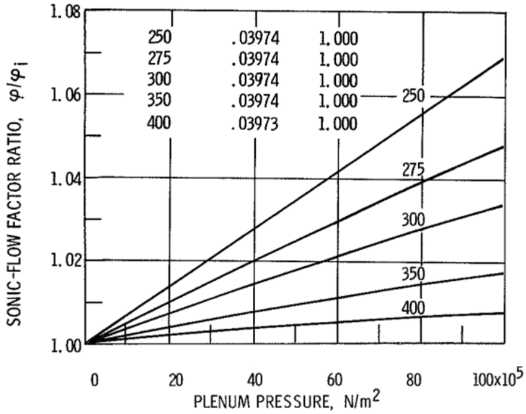


Figure 8.6: Real Gas Correction Factor for Nitrogen Gas (Johnson, 1971)

**Viscous Effects**

For the ideal performance, it is assumed that there is no friction within the nozzle. This statement of course has limited validity in reality, with friction losses impacting the performance of the nozzle through viscous effects. As the gas flows over the nozzles wall, friction with the walls surface causes the development of a boundary layer. The buildup of this boundary layer can reduce the performance of the nozzle. The magnitude of this impact is primarily governed by the Reynolds number $Re_t$, which for nozzles is calculated at the throat as seen in equation 8.32:

$$Re_t = \frac{\rho_t \cdot V_t \cdot D_t}{\mu_t} = \frac{4 \cdot m}{\pi \cdot \mu \cdot D} \tag{8.32}$$

where:

- $Re$ = Reynolds number
- D = Diameter (m)
- $\mu$ = Dynamic Viscosity (kg/m $\cdot s^{-1}$)

For throat Reynolds numbers over 100,000, the boundary layer is limited to the nozzle divergent section (Zandbergen, 2018). This mostly effects the nozzle quality factor. However, below 100,000 the effect of the boundary layer is also found in the nozzle throat where its presence reduces the available flow area, thereby effecting the discharge quality factor. The design of the nozzle, most notably its divergent half angle and longitudinal radius, impacts the buildup of this boundary layer and so should be carefully considered during the design process. In order to establish the impact of the boundary layer on the nozzles performance, the following properties of the boundary layer must be established:

- Boundary Layer Thickness

- Displacement Thickness
- Momentum Thickness
- Skin Friction Coefficient

There are numerous different approaches available for determining these values for the geometry of the nozzle, including the use of CFD. However, for this project it shall be assumed that the nozzle resembles a flat plat which is aligned parallel to a uniform stream (Zandbergen, 2018). This assumption allows a simple method for establishing the above parameters, although it must be noted that it is slightly inaccurate. The expressions for laminar and turbulent boundary layers according to this method are seen in figure 8.7. These expressions are based on the assumption that the boundary layer only starts developing in the nozzle divergent section, thus defining the nozzle throat as the leading edge of the flat plat, with its length measured along the nozzle wall.

| Property | Laminar | (a) Turbulent(†) | (b) Turbulent(‡) |
|---|---|---|---|
| Boundary layer thickness | $\frac{\delta}{x} = \frac{4.91}{\sqrt{\mathrm{Re}_x}}$ | $\frac{\delta}{x} \cong \frac{0.16}{(\mathrm{Re}_x)^{1/7}}$ | $\frac{\delta}{x} \cong \frac{0.38}{(\mathrm{Re}_x)^{1/5}}$ |
| Displacement thickness | $\frac{\delta^*}{x} = \frac{1.72}{\sqrt{\mathrm{Re}_x}}$ | $\frac{\delta^*}{x} \cong \frac{0.020}{(\mathrm{Re}_x)^{1/7}}$ | $\frac{\delta^*}{x} \cong \frac{0.048}{(\mathrm{Re}_x)^{1/5}}$ |
| Momentum thickness | $\frac{\theta}{x} = \frac{0.664}{\sqrt{\mathrm{Re}_x}}$ | $\frac{\theta}{x} \cong \frac{0.016}{(\mathrm{Re}_x)^{1/7}}$ | $\frac{\theta}{x} \cong \frac{0.037}{(\mathrm{Re}_x)^{1/5}}$ |
| Local skin friction coefficient | $C_{f,x} = \frac{0.664}{\sqrt{\mathrm{Re}_x}}$ | $C_{f,x} \cong \frac{0.027}{(\mathrm{Re}_x)^{1/7}}$ | $C_{f,x} \cong \frac{0.059}{(\mathrm{Re}_x)^{1/5}}$ |

* Laminar values are exact and are listed to three significant digits, but turbulent values are listed to only two significant digits due to the large uncertainty affiliated with all turbulent flow fields.

† Obtained from one-seventh-power law.

‡ Obtained from one-seventh-power law combined with empirical data for turbulent flow through smooth pipes.



Figure 8.7: Summary of expressions for laminar and turbulent boundary layers on a smooth flat plate aligned parallel to a uniform stream (Zandbergen, 2018)

The first step in determining the parameters of the boundary layer is to establish whether the boundary layer is fully laminar, fully turbulent or in transition. In his research into the gas flow in cold gas micro thruster nozzles, the highest Reynolds number encountered by La Torre, 2011 at a thrust of 1N was 130,000. At this value the Re difference between laminar and turbulent effects was less than 1.5%. Given this small difference, the author concludes that the flow through the nozzle remains laminar, “probably because turbulence has neither the time nor space to develop”. Given that the low expansion ratio of the inflation nozzle shall lead to a short nozzle length, as well as the fact that the thrust generated by the nozzle is $< 1$N for mass flow rates under 1.0 g/s and chamber pressures less than 10 bar (see equation 8.16), it shall be assumed for this study, that the flow through the nozzle is fully laminar. A complicating factor is these relations assume that there are constant conditions along the flat plate. This assumption is not valid for nozzles, where the conditions vary strongly. Thus, in order to account for this, the displacement thickness and momentum thickness values shall be determined at throat and nozzle exit conditions, with the actual value being considered the average of the two (Zandbergen, 2018). The calculation of these parameters shall be explored hereafter.

For determining the local Reynolds number along the flat plate, the length of the of the nozzle wall must be established. At the nozzle exit this is given as a function of the total nozzle length as seen in equation 8.33.

$$L_e = \frac{x_L}{cos(\alpha)} \tag{8.33}$$

where:

- $L_e$ = Length of nozzle wall (m). Corresponds to 'x' in figure 8.7.
- $x_L$ corresponds to divergent length of nozzle along x-axis as seen in figure 8.5b and equation 8.27.

The local Reynolds number for the values at the throat and exit can be calculated using equation 8.34. As the length at the nozzle throat cannot be taken as zero, it shall be assumed for the purposes of this calculations that $L_t$ can be taken as $0.1{\cdot}L_e$.

$$Re_L = \frac{\rho_e \cdot V_e \cdot L}{\mu_e} \tag{8.34}$$

Once this value has been established the laminar boundary layer expressions can be calculated, with the average momentum thickness and displacement thickness values being calculated. These two values can be utilized to calculate the momentum loss and reduction in nozzle expansion ratio respectively.

$$\theta_{avg} = \frac{\theta_e + \theta_t}{2} \tag{8.35}$$

$$\delta^{\star}_{avg} = \frac{\delta^{\star}_e + \delta^{\star}_t}{2} \tag{8.36}$$

where:

- $\theta$ = Momentum thickness (m)
- $\delta^{\star}$ = Displacement thickness (m) thickness
- avg = Average

The skin friction on the nozzle wall has an axial component that leads to the boundary layer effecting the thrust generated. This effect can be determined using the momentum thickness $\theta_{avg}$. Equation 8.37 can be used to calculate the loss in thrust due to momentum loss ($\Delta F_{momentum}$).

$$\Delta F_{momentum} = \left(\rho_e \cdot V_e \cdot 2\pi \cdot R_e \cdot \theta_{avg}\right) \cdot V_e \tag{8.37}$$

The presence of the boundary layer leads to a displacement of the core gas flow with a certain distance. This distance is given by the displacement thickness. For $Re_t > 100{,}000$, the effect of the displacement thickness is only considered for the exit diameter, as can be seen in figure 8.8. The effective exit diameter of the nozzle can thus be calculated using equation 8.38.

$$R_{e_{eff}} = R_e - \delta^{\star}_{avg} \tag{8.38}$$

$$A_{e_{eff}} = \pi \cdot (R_{e_{eff}})^2 \tag{8.39}$$

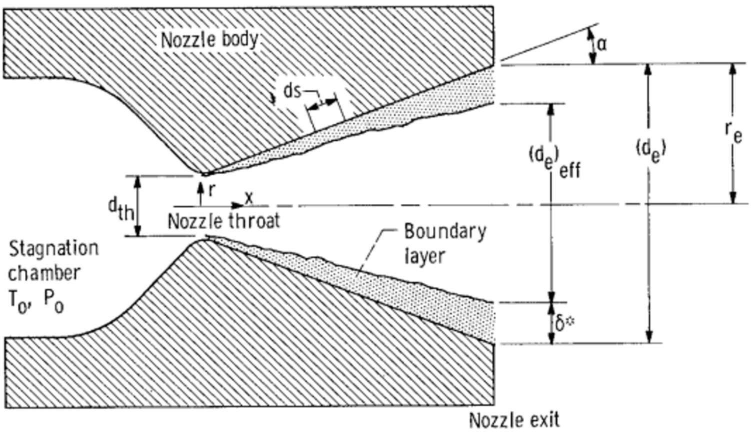


Figure 8.8: Effect of boundary layer on nozzle expansion ratio (Spisz et al., 1965)

At $Re_t < 100{,}000$ the displacement thickness within the nozzle throat increases and thus must be accounted for. This increase leads to a reduced throat area and hence the actual mass flow rate through the throat decreases. Instead of utilizing the flat plate method to calculate this displacement thickness, as it assumes the boundary layer only starts developing in the divergent region, this loss can be accounted for using by calculating the discharge coefficient $C_d$ using a relation developed by Tang and Fenn, 1978 for cold gas nozzles at low $Re_t$, as seen in equation 8.40. It should be noted that while the displacement thickness is no longer calculated using the flat plate method, the momentum loss still is. This may lead to some inaccuracies but shall be deemed sufficient for this preliminary analysis.

$$C_d = 1 - \left(\frac{\gamma+1}{2}\right)^{\frac{3}{4}} \cdot \left(\frac{-2.128}{\gamma+1} + 3.266\right) \cdot Re_{modified}^{-0.5} + 0.9428 \cdot \left(\frac{(\gamma-1)(\gamma+2)}{(\gamma+1)^{(}0.5)}\right) \cdot Re_{modified}^{-1} \tag{8.40}$$

where R is a modified throat Reynolds number given as:

$$Re_{modified} = Re_t \cdot \frac{R_u}{R_t}^{0.5} \tag{8.41}$$

At $Re_t < 100{,}000$, it can be assumed that the discharge coefficient is equal to the area contraction coefficient $C_A$ (Zandbergen, 2018).

$$C_d = C_A = \frac{A_{t_{eff}}}{A_t} \tag{8.42}$$

Using equation 8.42, the effective throat area can then be calculated from which the effective expansion ratio can be calculated using the following equation 8.43. For $Re_t >$ 100,000, $A_{t_{eff}}$ is assumed equal to $A_{t_{ideal}}$.

$$\varepsilon_{eff} = \frac{A_{e_{eff}}}{A_{t_{eff}}} \tag{8.43}$$

where:

- $\varepsilon$ = Expansion Ratio $\left(\frac{A_e}{A_t}\right)$

Utilising this value, the 'real' exit temperatures and pressures can be solved for using equations 8.13 and 8.14. Once these values have been established the 'real' exit velocity can also be established using equation 8.1. In addition, for $Re_t >$ 100,000 the 'real' mass flow rate can be calculated using equation 8.30, while for $Re_t <$ 100,000 it can be derived from the discharge coefficient calculated in equation 8.40. Finally, in order to calculate the correction factors the 'real' thrust generated by the nozzle must be calculated. This can be done using equation 8.44.

$$F_{real} = \left(\lambda_n \cdot m_{real} \cdot V_{e_{real}} + P_{e_{real}} \cdot A_{e_{eff}}\right) - \Delta F_{momentum} \tag{8.44}$$

### OPTIMIZING FOR NOZZLE PERFORMANCE

In order to finalize the design of the nozzle for this inflation system, the parameters that maximize the desired performance of the system must be determined. For this investigation, this shall be limited to the parameters that most affect the nozzle performance, the expansion ratio $\varepsilon$, the throat diameter $D_t$, throat longitudinal radius $R_u$ and divergent half angle $\alpha$.

8

**Throat Diameter**

From equation 8.32, it can be seen that the throat Reynolds number $Re_t$ is dependent on the throat diameter $D_t$. From the equation for the critical mass flow rate 8.12, $D_t$ is directly proportional to the mass flow rate through the throat and inversely proportional to the chamber pressure. These relationships are visualized in figure 8.9a. Thus, the throat Reynolds number is directly proportional to the mass flow rate and inversely proportional to the chamber pressure. This can clearly be seen in figure 8.9b, where the black dashed line signifies the threshold between the two boundary layer conditions, above and below a throat Reynolds number of 100,000. Therefore, the selection of the mass flow rate and chamber pressure values shall directly affect the throat diameter of the nozzle and by extension the boundary layer conditions of the flow through that nozzle. The importance of this distinction shall become clear in the following exploration of divergence angle and throat longitudinal radius.

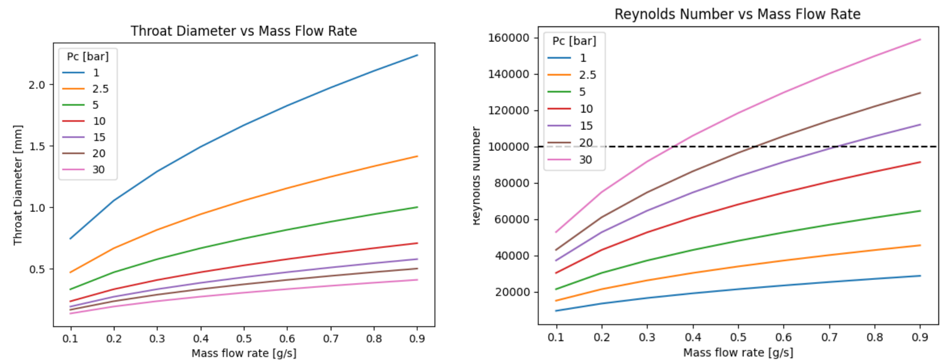


(a) Throat Diameter vs Mass Flow Rate and Chamber Pressure (b) Reynolds Number vs Mass Flow Rate and Chamber Pressure

Figure 8.9: Relationship between mass flow rate, chamber pressure and throat diameter

**Throat Longitudinal Radius**

The throat longitudinal radius $R_u$, also know as the throat curvature, dictates the sharpness of the nozzle throat. This shall impact the real performance of the nozzle in two major ways. Firstly, $R_u$ shall impact the length of the nozzle, as seen in equation 8.27, thereby impacting the development of the boundary layer within the throat and the resulting losses experienced. The contribution of $R_u$ to the total nozzle length, clearly visualised in figure 8.5b, is given in equation 8.45. Secondly, below $Re_t$ = 100,000, the sharpness of the throat shall effect the boundary layer development within the nozzle throat. This effects the discharge coefficient as noted in equation 8.40.

$$x_P = R_u \cdot sin(\alpha) \tag{8.45}$$



where:

- $x_P$ = Throat longitudinal length along x-axis (m)

The value for $R_u$ is typically chosen between 0.5Rt-1.5Rt. In order to select an appropriate value for the nozzle, the impact of $R_u$ on the desired nozzle performance is assessed, as seen in figure 8.10. This assessment is carried out for a nozzle with an expansion ratio of 1.36, with the results as follows.

- *Discharge Coefficient:* As noted, below $Re_t$ = 100,000 $R_u$ contributes to the discharge coefficient (equation 8.40). This contribution can clearly be seen in figure 8.10a, with increasing efficiency found at higher values of $R_u$. This is not surprising given the decreased sharpness of the nozzle throat at higher $R_u$ values. Above $Re_t$ = 100,000, its contribution to $C_d$ is no longer considered which can also be clearly seen.

- *Expansion Ratio Efficiency:* The contribution of $R_u$ to $C_d$ below $Re_t$ = 100,000 also leads to a variation in the Real vs Ideal expansion ratio $\varepsilon$ as can seen in figure 8.10b. Lower $C_d$ values means that the real mass flow rate through the nozzle is reduced due to the presence of the boundary layer at the throat, thus leading to a reduced effective throat area. In this assessment, for $R_u$ values < 1, this yield a real expansion ratio greater than the ideal, as can be seen in figure 8.10b. As the Reynolds number increases, the boundary layer at the nozzle exit increases thus reducing the real expansion ratio and in turn a reducing the efficiency until at $Re_t$ = 100,000 the boundary layer in the throat is no longer considered. This relationship is reversed for $R_u$ values > 1.

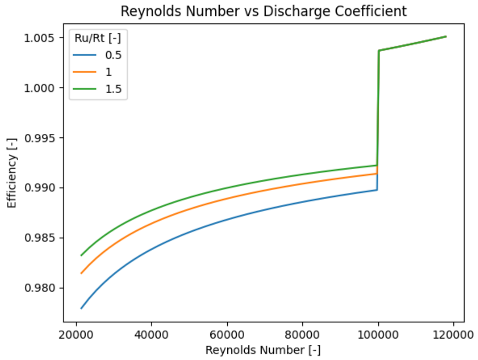


(a) Discharge Coefficient $C_d$ with $R_u$

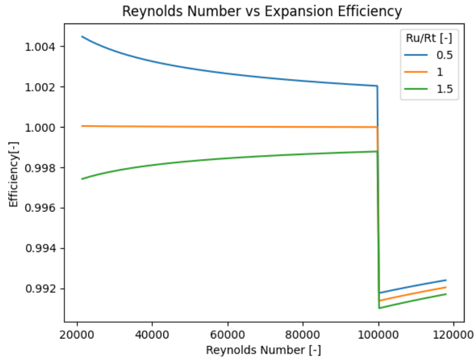


(b) Real vs Ideal Expansion Ratio $\varepsilon$ with $R_u$

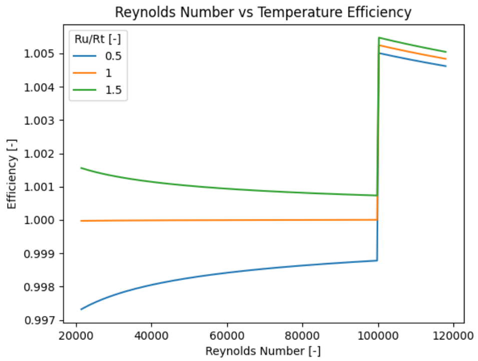


(c) Real vs Ideal Exit Velocity $T_e$ with $R_u$

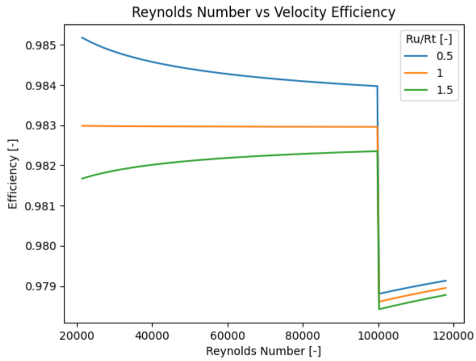


(d) Real vs Ideal Exit Velocity $V_e$ with $R_u$

Figure 8.10: Real vs Ideal Parameters across range of Reynolds numbers with different values for $R_u$ at static parameters: $\alpha = 15°$, $\varepsilon = 1.36$

- *Exit Temperature Efficiency:* From figure 8.4, it can be seen that the exit temperature is inversely proportional to the expansion ratio. As such it is no surprise that the relationship between $R_u$ and the temperature efficiency, presented in figure 8.10c, is the inverse of that for expansion efficiency. It can be clearly seen from this relationship that higher $R_u$ values are more attractive for the design of this inflation nozzle as they yield increased temperature efficiencies. This is highly desirable given the desire to maximize the gas exit temperature as noted in the thermal

8

constraints.

- *Exit Velocity Efficiency:* Unlike temperature, the exit velocity is proportional to the expansion ratio, as seen in figure 8.3a. Once again this relationship is mirrored in the relationship between $R_u$ and the velocity efficiency, as presented in figure 8.10d. Thus, with increasing $R_u$ values the velocity efficiency decreases. This is also attractive as it enables the reduction of the gas jet velocity as desired by the inflation system constraints.

From this investigation, it is apparent that maximizing the value of $R_u$ is attractive for optimizing the design of this inflation nozzle. It yields a more curved throat which minimizes the development of a boundary layer in the nozzles throat and maximizes the length of the nozzle. This leads to an increased discharge coefficient which in turn yields a higher temperature efficiency and lower velocity efficiency. This is attractive given the desire to maximize exit temperature and minimize exit velocity.

**Divergent Half Angle**

The selection of the divergence half angle $\alpha$ plays a significant role in maximizing the performance of the nozzle, through its influence on the flow divergence factor and the buildup of a boundary layer in the nozzle. In this investigation the contribution of $\alpha$ on these two influences shall be assessed, beginning with the flow divergence factor.

A graph of the variation in flow divergence factor with divergence half angle is presented in figure 8.11a. As can be seen the greater divergence half angle, the lower the flow divergence factor $\lambda_n$. This factors accounts for the non 1-dimensional flow in the nozzle and is multiplied by the non-pressure related terms in the thrust equation. With respect to its impact on the build up of the boundary layer at the nozzle exit, the length of the nozzle is largely dependent on the divergent half angle (see equation 8.27). This can be evidently seen in figure 8.11b where an increase in $\alpha$ leads to a decrease in nozzle length, resulting in a decrease in boundary layer thickness.

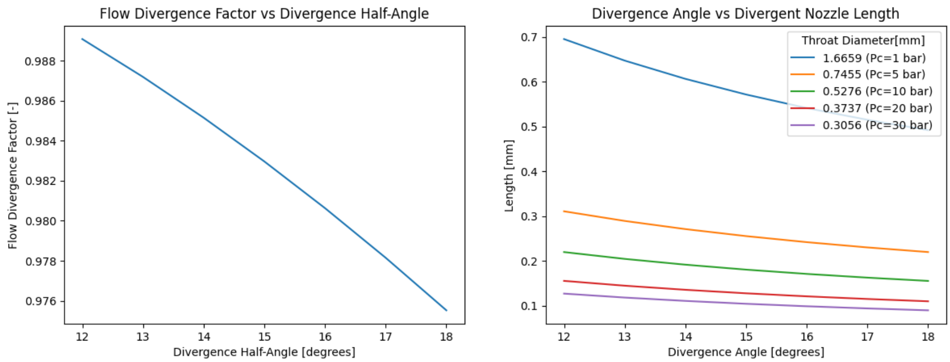


(a) Flow Divergence Factor with $\alpha$

(b) Length of Nozzle with $\alpha$

Figure 8.11: Flow Divergence Factor and Divergence Nozzle length with $\alpha$. Static Parameters: $Ru = 1R_t$, $\varepsilon = 1.36$, m = 0.5 g/s

As an increase in divergence half angle leads to a decrease in the flow divergence factor and an increase in efficiency, due to a decrease in the boundary layer thickness, it was deemed prudent to establish how each of these losses contribute to the real performance of the nozzle. This is done by establishing the losses incurred only due to $\lambda_n$ and then comparing them to losses that also considering viscous effects. This can be seen clearly in figures 8.12a and 8.12b. The first thing of note when examining these graphs is that the decline in efficiency with increasing $\alpha$ signals the dominance of $\lambda_n$ over the real performance of the nozzle. Thus smaller divergence angles shall yield a higher thrust and velocity efficiency. In addition, it can be clearly seen that the viscous losses yield a significant reduction in thrust efficiency at lower Reynolds numbers. A different situation arises for the velocity efficiency where it can be seen that at lower Reynolds numbers, the viscous losses contribution is almost negligible relative to $\lambda_n$. This is particularly apparent at larger $\alpha$ values where the boundary layer thickness is reduced.

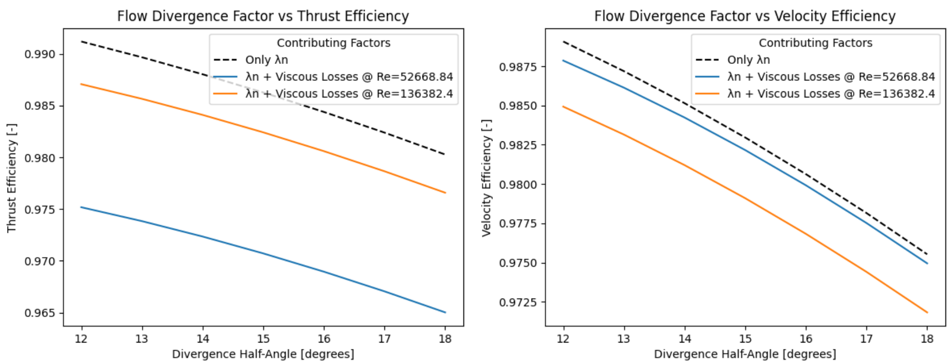


(a) Thrust Efficiency due to Flow Divergence Factor and Viscous Losses with $\alpha$

(b) Velocity Efficiency due to Flow Divergence Factor and Viscous Losses with $\alpha$

Figure 8.12: Contribution of Divergence Factor and Viscous Losses to Real Nozzle Performance with respect to $\alpha$. Static Parameters: $Ru = 1R_t$, $\varepsilon = 1.36$, m = 0.5 g/s

To further understand the relationship between $\alpha$ and the performance of the nozzle, the performance parameters for a range of $\alpha$ and $Re_t$ values shall be calculated as was done for $Ru$.

- *Discharge Coefficient:* As can be seen in figure 8.13a, the discharge coefficient is independent of $\alpha$ and rises gradually with $Re_t$ until it reaches the 100,000 threshhold and the presence of the boundary layer within the throat is no longer considered.

- *Expansion Ratio Efficiency:* From figure 8.13b it is apparent that $\alpha$ contributes to the expansion efficiency. Lower $\alpha$ angles lead to longer nozzle lengths which in turn lead to an increase in boundary layer thickness at the nozzle exit, thereby reducing the effective exit area relative to larger $\alpha$ values. This in turn means that at lower $\alpha$ angles, the expansion efficiency is reduced.

8

- *Exit Temperature Efficiency:* As was noted previously, the temperature efficiency is inversely proportional to the expansion efficiency. As such, lower expansion efficiencies yield higher temperature efficiencies. Thus, as seen in from 8.13c, lower $\alpha$ angles enable higher gas jet exit temperatures. Indeed, at both low and high Reynolds numbers, the values for $\alpha$ yield real $T_e$ values exceeding the ideal values. As mentioned during the investigation of $Ru$ this is highly desirable for meeting the thermal constraints imposed on the system.

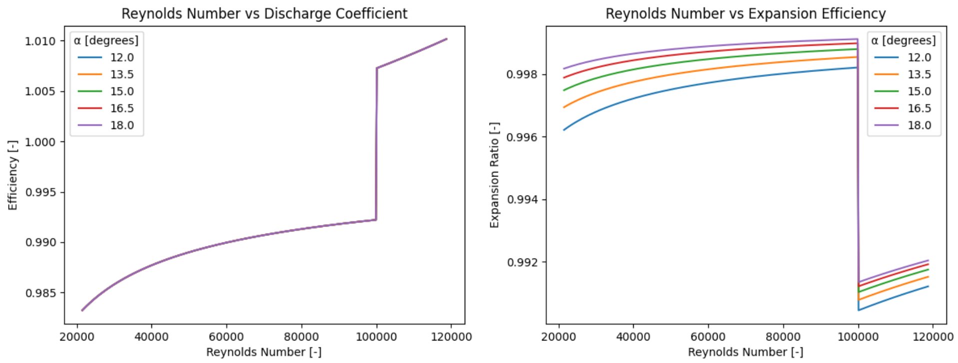


(a) Discharge Coefficient $C_d$ with $\alpha$

(b) Real vs Ideal Expansion Ratio $\varepsilon$ with $\alpha$

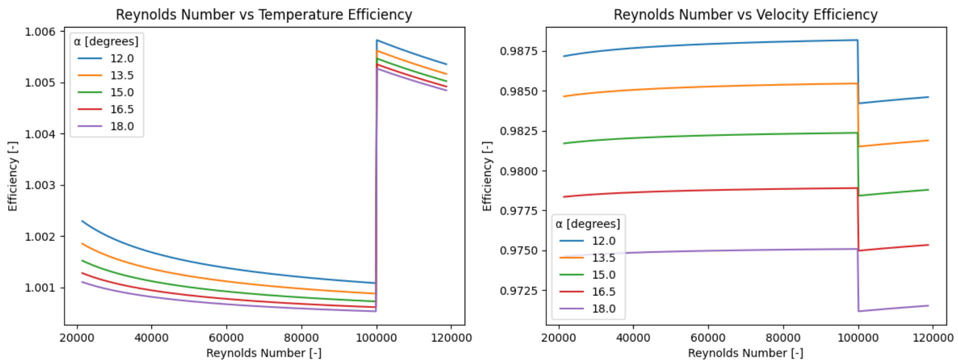


(c) Real vs Ideal Exit Temperature $T_e$ with $\alpha$

(d) Real vs Ideal Exit Velocity $V_e$ with $\alpha$

Figure 8.13: Real vs Ideal Parameters with different values for $\alpha$ at static parameters: $Ru = 1R_t$, $\varepsilon = 1.36$, m = 0.5 g/s

- *Exit Velocity Efficiency:* As noted for figure 8.12b, the velocity efficiency is dominated by $\lambda_n$, with viscous effects contributing little except at higher Reynolds numbers as seen in figure 8.13d. Thus, this means that higher $\alpha$ angles yield lower exit velocity efficiencies. As minimizing the gas jet velocity is another key driving inflation requirement, a lower exit velocity efficiency is highly desirable.

As can be seen from figures 8.13c and 8.13d, the driving requirements of this nozzle design, a maximized exit temperature and minimized exit velocity, demand opposing $\alpha$ angle requirements. Low $\alpha$ angles yield high temperature efficiencies but also high velocity efficiencies with the relationship reversing with higher $\alpha$ angles. Therefore, in order to satisfy both requirements and thus optimize the performance of the nozzle, a middle $\alpha$ angle of 15 $^\circ$ was deemed the most appropriate choice.

**Expansion Ratio**

As has been apparent from the discussion regarding $R_u$ and $\alpha$, the expansion ratio, which dictates the exit area of the nozzle and as a result the nozzle length, plays an integral role in the real performance of the nozzle. Given its role in the development of the boundary layer, and by extension the discharge coefficient, it was deemed prudent to further investigate the minimum and maximum expansion ratio values determined in the ideal analysis (1-1.36). As such low expansion ratios are highly unusual for cold gas convergent-divergent nozzles, this investigation shall consider potential fabrication constraints on achieving these expansion ratios and the consequences on the real performance of the nozzle.

- *Maximum Expansion Ratio:* Given the low expansion ratio range, as dictated by the velocity requirements, the difference in the throat diameter and the exit diameter is on the order of $\mu$m, as seen in figure 8.14a. In addition, due to the throat diameter deriving from chamber pressure and mass flow rate, this difference shall vary according to these parameters. Given the low nozzle length (figure 8.11b), it was deemed prudent to establish a minimum acceptable difference in throat and exit diameter in order to ensure that appropriate parameters are selected.

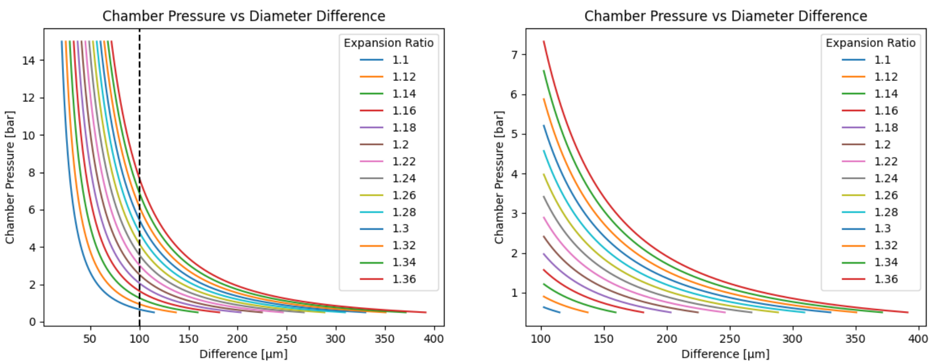


(a) Difference in throat across expansion range

(b) Max $P_c$ given minimum $\varepsilon$ at difference of 100 $\mu$m m = 1 g/s

Figure 8.14: Difference in throat and exit diameters with $P_c$ and $\varepsilon$ at m = 0.5 g/s

From different papers exploring the development of cold gas micro-thrusters such as La Torre, 2011 , Özden, 2019 and Louwerse, 2009, it is apparent that using micro-propulsion fabrication methods, throat diameters of 50-500 $\mu$m (0.05 - 0.5 mm) are readily achievable. However, none of these papers explore expansion ratios as low as the maximum ideal expansion ratio of 1.36. Given this requirement is unique among micropropulsion systems, it is therefore unsurprising that the difference in throat and exit diameter is also neither explored nor referred to. Without doing a detailed exploration and/or testing of the different fabrication techniques for micro nozzles, it is difficult to determine a minimal acceptable diameter difference. It was thus decided to base this decision off a reference cold gas micro nozzle fabricated by Jung and Huh, 2008 which provides the most similar dimensions of any micro nozzle found in the literature to those required for the inflation nozzle. It has a throat diameter of 0.298 mm and expansion ratio of 2, yielding a difference of 118 $\mu$m between the nozzle throat and exit diameters. As a consequence it was decided to assume a minimum diameter difference of 100 $\mu$m for the preliminary design of the inflation nozzle. The vertical black dashed line in figure 8.14a represents this requirement. It can clearly be seen from figure 8.14b, that this results in a maximum acceptable chamber pressure $P_c$, given $P_c$ is inversely proportional to throat diameter, for a given expansion ratio. The lower the expansion ratio, the lower the maximum acceptable chamber pressure. Or said inversely, there is a maximum acceptable expansion ratio given a certain chamber pressure. This is very clear demonstrated in figure 8.15, which demonstrates that at higher mass flow rates, the maximum acceptable chamber pressure is higher due to the throat diameter being proportional to mass flow rate, see figure 8.9a.

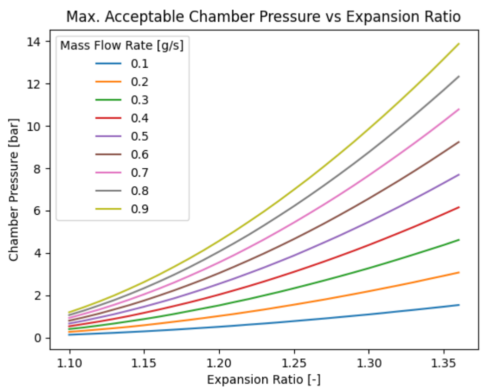


Figure 8.15: Max $P_c$ across mass flow rate range

- *Minimum Expansion Ratio:* As this expansion ratio range yields low nozzle lengths, the throat curvature $R_u$ shall contribute a significant % of this length. The higher the value of $R_u$ the higher its contribution (see equation 8.45). This in turn places a constraint on $R_u$ as its contribution must clearly remain less than the total length of the nozzle. As such a maximum contribution of 60 % is arbitrarily selected. At lower expansion ratios, this restriction on length limits the range of $R_u$ values, as seen in figure 8.16a. Indeed it was found that for expansion ratios below 1.084, $R_u$ values equal to or greater than $0.5R_t$ are not feasible. Thus, the minimum expansion ratio $\varepsilon$ must be greater than 1.084. For simplicity, the minimum acceptable expansion ratio is updated to 1.1.

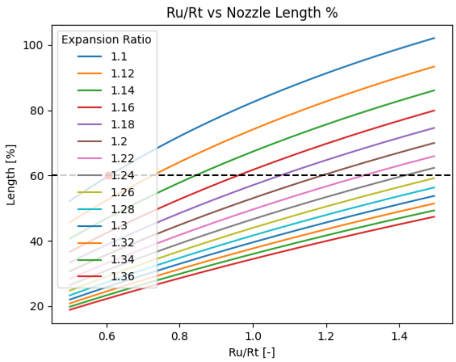


(a) Acceptable $R_u$ range given length limit

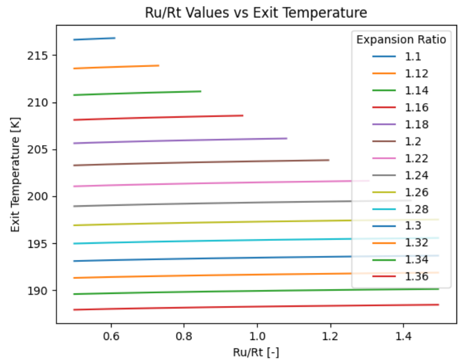


(b) Real $T_e$ given $R_u$ range and $\varepsilon$

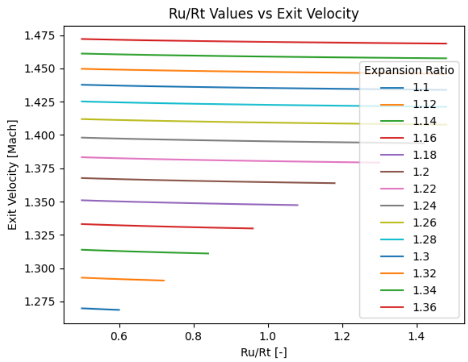


(c) Real $V_e$ given $R_u$ range and $\varepsilon$

Figure 8.16: Real Parameters given $\varepsilon$

As discussed previously, higher $R_u$ values are desirable for maximizing temperature efficiency and minimizing velocity efficiency. However, as is clear from figure 8.16a, due to the fabrication constraint the maximum value for $R_u$ is dependent on the value of $\varepsilon$. This makes its selection straightforward, with the selection of the most suitable the expansion ratio $\varepsilon$ now being the main design consideration. Thus, as seen in figures 8.16b and 8.16c, the real exit temperature and velocity values are calculated for $\varepsilon$ with the maximum $R_u$ values as dictated by the length constraint seen in figure 8.16a. It can be noted that despite the higher efficiencies available at increasing $R_u$, expansion ratios with a maximum $R_u$ value of $1.5R_t$, $\varepsilon$ = 1.26 and above, still yield exit temperature and velocity values significantly less desirable than lower expansion ratios. This indicates that while higher throat curvature is desirable for increasing efficiency, its impact in the selection of the most suitable nozzle design is relatively limited compared to the expansion ratio.

**Discussion**

From this investigation into the optimization of the nozzles performance a number of statements can be made.

- With respect to the throat diameter, its size, and the resulting $Re_t$ value stem from the mass flow rate and chamber pressure. Both of these parameters shall depend on further design decisions and so shall not be discussed here.
- With respect to the throat curvature it was found that maximizing the value of $R_u$ was seen as the most appropriate for optimizing nozzle performance as it enables a higher discharge coefficient and temperature efficiency as well as lower velocity efficiency.
- With respect to the divergence half angle, it was found that in order to maximize the temperature efficiency, a low $\alpha$ angle should be used. However, in order to minimize velocity efficiency a high $\alpha$ angle should be used. Thus, an $\alpha$ angle of $15°$ was chosen as a compromise.
- With respect to the expansion ratio, it was found that considering a fabrication constraint on the minimum difference in the nozzle throat and exit diameters of 100 $\mu$m the maximum expansion ratio is dependent on the chosen chamber pressure and mass flow rate parameters selected. In addition, considering an additional fabrication constraint on the contribution of $R_u$ to the total nozzle length, a minimum acceptable expansion ratio was found at 1.1. This also limits the selection of an appropriate $R_u$ value.

The results of this exploration won't become clear until the chamber pressure and mass flow rate values are specified. This shall be done with the selection of the most appropriate mass flow rate value following the full design of the system (section 8.6). However, figure 8.17 demonstrates the impact of these considerations on the design of the nozzle utilizing values determined at different mass flow rates in section 8.6. As can be seen, higher mass flow rates have a major impact on the throat diameter of the nozzle while the minimum 100 $\mu$m fabrication constraint on the diameters is evident. With respect to the fabrication constraint on the throat curvature, the effect of different expansion ratios on its selection is clearly demonstrated. Most notable of all, however, is the low nozzle lengths relative to the throat diameter which is as a result of the minimization of the expansion ratio in order to satisfy the velocity requirements.

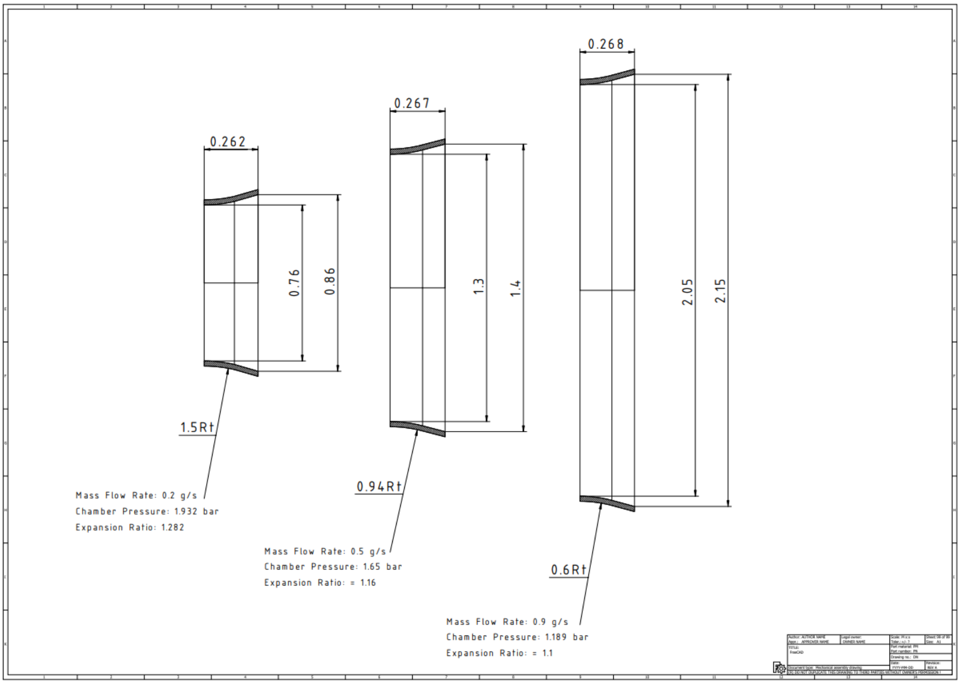


Figure 8.17: Variation in Nozzle Design with mass flow rate (see table 8.19)

### 8.2.4. CONCLUSION

This section explored the design of a micropropulion based inflation nozzle. The design of such a nozzle is clearly unique relative to conventional propulsion systems due to the unusual requirements dictated by the inflation system requirements, particularly those related to gas exit temperature and gas exit velocity. In order to maximize the temperature and minimize the velocity, the expansion ratio must be kept to a minimum. This low expansion ratio is the leading driver behind the performance of the system and the other leading nozzle parameters, such as the divergence half angle and throat curvature $R_u$, are considered with respect to it. In optimizing these properties it was desired to maximize the temperature efficiency and minimize the velocity efficiency. Such an approach is counter intuitive for conventional propulsion system design and once again highlights the unique considerations that must be made when adapting cold gas micropropulsion technology for inflation purposes. As the nozzle design parameters and performance characteristics are dependent on the selection of chamber pressure and mass flow rate, they shall not be elaborated on here. Instead they are detailed in section 8.6, where a discussion into the selection of these two variables, informed by the design of the inflation system, is carried out.

## 8.3. INFLATION VALVE

### 8.3.1. INTRODUCTION

In order to facilitate the desired pulsed inflation mode as discussed in section 7.5.1, an inflation control valve is required. As is the case for cold gas RCS systems, this control valve, referred to as the thruster control valve for propulsion applications, is at the heart of the inflation system as it is used for controlling the inflation process. These valves, which are normally closed, are opened to allow gas flow into the nozzle thereby generating thrust, or for this application providing inflation. This opening and closing of the valve enables the on/off actuation required for pulsed mode operation. The pulse width and duty cycle of the pulse mode is controlled by the response characteristics of the valve. A diagram of a cold gas thruster with the nozzle mounted directly onto the thruster control valve is shown in figure 8.18.

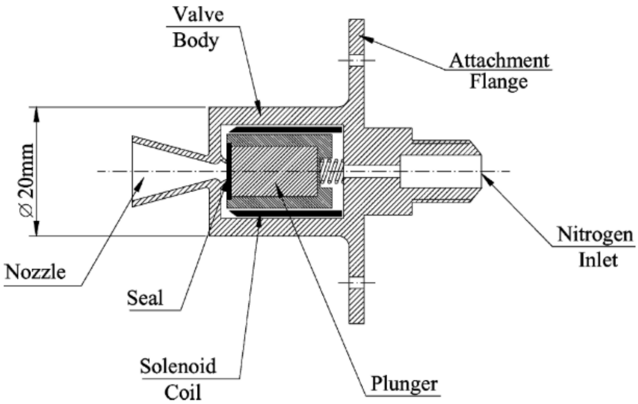


Figure 8.18: Schematic of a cold gas thruster (Adler et al., 2005)

In this section, a preliminary discussion regarding the selection of an appropriate inflation valve as well as its desired operational performance shall be explored. However a detailed exploration of the influence of the inflation valve design on the performance of the system is not carried out due to time constraints. For example, the influence of rise time and thrust decay are neglected. Instead it shall be assumed that the nozzle reaches steady state performance conditions instantaneously when the valve opens and goes to zero instantaneously when the valve closes. This is of course not fully representative of the real situation but does provide sufficient information to demonstrate the potential that a micropropulsion based inflation system has for providing controllable inflation. In keeping with this simplified approach, a complex control logic is not developed regarding the pulsed performance and instead a simple logic based on PWM is used to demonstrate how control logic's typically used for RCS systems can also be implemented for inflating precise inflatable structures.

### 8.3.2. VALVE SELECTION

In keeping with the desire to utilize cold gas micropropulsion technology, it is desired that a thruster valve currently being utilized in such systems be selected for this inflation system.

#### VALVE TYPES

According to Oh and Ahn, 2006, there are four common actuation principles utilized for mechanically active cold gas micro-valves. They are:

- Magnetic
- Electric
- Piezoelectric
- Thermal

In addition, there are two options for manufacturing thruster valves either utilizing MEMs technology, as is discussed by Louwerse, 2009 and Mueller et al., 2001, or conventional fabrication technology. MEMS devices are attractive for their low power and mass requirements as well as their rapid response times although issues with pressure handling and leak rate are still being investigated. While these devices are typically utilized for low thrust applications (<=10mN), many are still at the research stage. For thrust applications (10mN - 10N) the most commonly utilized thruster valve type is the conventional miniature solenoid valve (Bzibziak, 2000; Zandbergen, 2013). These valves are utilized in the majority of available COTS cold gas thruster control valves. As such a miniature solenoid valve shall be utilized for the inflation valve of the inflation system. A schematic of such a valve is visualised in figure 8.19.

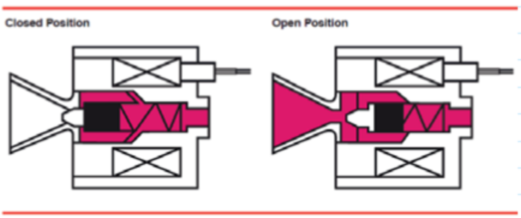


Figure 8.19: Schematic of a solenoid thruster valve (Zandbergen, 2018)

#### SOLENOID THRUSTER VALVE

It is desired that a COTS thruster valve can be utilized for this inflation system, thereby demonstrating the suitability of current cold gas micropropulsion technology for this application. Thus, as is done for other feed system components (see section 8.5.3), an exploration of current cold gas COTS thruster valves shall be carried out.

With respect to commercially available miniature solenoid valves, some of which are suitable for propulsion applications, there are a range of companies that provide them.

These include companies such as The Lee Company [1], Clippard [2], Parker Hannifin [3] and more. However, for this project, the investigation shall be limited to COTS cold gas thruster valves utilized in RCS and/or micropropulsion applications. From a search for such valves, the cold gas thruster assemblies (thruster valve + nozzle) presented in table 8.2 were found, each of which are compatible with nitrogen gas. As many of these commercial valves are designed to be compatible with different nozzles, it is feasible to consider that the custom designed inflation nozzle could be mounted onto one of these COTS cold gas thruster valves. It also must be noted that for the Moog microthrusters, the mass flow rate is calculated from thrust and specific impulse values using IRT. While this flow rate is not necessarily indicative of the range of mass flow rates that the valve is capable of handling and nor does is it indicate the actual flow rate through the valve, it does give us the mass flow rate at the throat which can be utilized in the nozzle design. From the COTS valves a number of statements regarding the selection of the most appropriate thruster valve can be made.

Firstly, bar the bulky VACCO 48003040 all thrusters have mass requirements less than 70 grams. This small mass requirement translates to a similarly small volume requirement, with the MOOG 058E142A and MOOG 058-118 clearly possessing the most attractive volumetric properties. Of the microthrusters presented, three are suitable for operation at the desired mass flow rate range of 0.1-0.9 g/s. These are the MOOG 058E142A, MOOG 058E151 and Nammo SVT01. However, given the low MEOP of the Nammo SVT01 valve, it shall not be considered as a viable option. Of the remaining two valves, it can clearly be seen that the MOOG 058E142A provides significantly more attractive mass and volume requirements, although it does have a shorter cycle life and higher power requirements than the MOOG 058E151. While the power requirements are not explored in detail in this thesis, the power requirements of both valves are well within the power budget provided by REQ-BEOC-03 although the lower requirements of the MOOG 058E151 are clearly attractive. The shorter cycle life of the MOOG 058E142A, while well within the expected requirements of the initial inflation process, could become an issue with an extended pressure maintenance lifespan. This would place additional constraints on the control logic required for pressure maintenance, limiting the acceptable frequency and pulse widths. However as the control logic required for pressure maintenance is not explored in this thesis, and given the relatively limited maintenance lifespan (see section 8.6), it shall be assumed that the cycle life provided by the MOOG 058E142A is sufficient. As such, given the desire to minimize the mass and volume requirements of the inflatable system, as given by key requirements REQ-BEOC-01 and REQ-BEOC-02, the COTS MOOG 058E142A solenoid thruster valve shall be utilized for the for dimensioning and designing of this inflation system.

[1] https://www.theleeco.com/products/solenoid-valves/

[2] https://www.clippard.com/products/electronic-valve-mme-3

[3] https://ph.parker.com/gb/en/solenoid-valves

[4] https://www.moog.com/content/dam/moog/literature/Space_Defense/spaceliterature/propulsion/moog-coldgasthrusters-datasheet.pdf

[5] https://www.nammo.com/wp-content/uploads/2021/03/2021-Nammo-Cheltenham-Spacecraft-Cold-Gas-Thruster-Valve.pdf

[6] https://www.vacco.com/images/uploads/pdfs/cold_gas_thrusters.pdf

[7] https://marotta.com/products/flow-controls/satellite-propulsion-controls/cold-gas-microthruster/

8

Table 8.2: COTS Cold Gas Microthrusters

| **Parameter** | **MOOG 058E146** | **MOOG 058E142A** | **MOOG 058E151** | **MOOG 058-118** | **Nammo SVT01** | **VACCO 48003040** | **Marotta CGMT** |
|---|---|---|---|---|---|---|---|
| Dimensions (mm) | $\phi$14 x 57 | $\phi$14 x 20.3 | $\phi$19.1 x 41 | $\phi$6.6 x 25.4 | $\phi$16 x 52 | $\phi$32 x 66 | - |
| Mass (grams) | 40 | 16 | 70 | 23 | 60 | 376 | $< 60$ |
| Nom Thrust (N) | 0.04 | 0.12 | 0.12 | 3.6 | 0.1 | 8.9 | 0.1 |
| Isp (s) | 60 | 57 | 65 | 57 | 72 | - | - |
| Nom. Pressure (bar) | 1.5 | 6.89 | 6.89 | - | - | - | - |
| MEOP (bar) | 10 | 20.7 | 27.6 | 15.7 | 1-2.5 | 16 | 6.89-154.5 |
| Mass Flow rate (g/s) (GN2) | 0.07 | 0.21 | 0.18 | 6.43 | 0.14 | 12.1 | - |
| Cycle Life | $5\times10^5$ - $2\times10^6$ | $2\times10^4$ | $1\times10^6$ | $> 1 \times 10^4$ | $1.5\times10^6$ | $1.5\times10^5$ | |
| Min. Pulse Width (ms) | 5 | 8 | 8 | 8 | 10 | 11 | 10 |
| Power - Open (W) | 10 | <35 | 10.5 | 30 | - | 20 | 7 |
| Power - holding (W) | 1 | - | 1.5 | - | - | - | - |
| Reference | Webpage [4] | Webpage [4] | Webpage [4] | Webpage [4] | Webpage [5] | Webpage [6] | Webpage [7] |

### 8.3.3. PULSING PERFORMANCE

In order to determine the width and frequency of the pulses required to fulfil the requirements of both the unfolding and pressurization stages, an inflation control logic for the operation of the inflation valve must be utilized. As has been noted, pulsed operation is utilized by RCS thrusters for precise maneuvers. It is therefore unsurprising that these thrusters also utilize a control logic with the most popular control strategies including bang-bang, Pulse-Width Modulation (PWM) and Pulse-Width Pulse-Frequency (PWPF) modulation (Chen et al., 2014; Kindracki et al., 2017; Morrow, 2012; Silik and Yaman, 2019). These methods can be utilized for the development of an inflation control logic as is clearly demonstrated by Griebel, 2011 and Lester et al., 2000 who use the PWM and PWPF methods respectively.

#### CONTROL LOGIC TYPES

Utilizing these methods there are two options for the design of the control logic available to designers.

- Simple:
  - The first option involves establishing these parameters pre-flight via assumptions, simulations and experimental measurements carried out in a lab. This option is simple, reliable and requires no additional components for operation. However, it does have its drawbacks. As the system has a pre-determined set of commands, it is unable to adapt to variations in on-orbit conditions such as variations in tank pressure, gas temperature or unforeseen issues such as delayed deployment or inaccurate estimates of residual gas (Griebel, 2011). This becomes particularly pressing for pressure maintenance, where inaccurate estimates of gas leakage would leave the inflation system incapable of accounting for the difference between the actual internal pressure of the structure and the nominal internal pressure.

8

- Complex:
  - The second option involves the development of a more sophisticated control logic which utilizes a closed loop system that calculates the required parameters in real time using information provided by sensors. This option offers a far more precise, controllable and adaptable inflation system that is also capable of providing accurate pressure maintenance to account for gas leakages. In addition, it enables the inflation system to accurately account for variations in thermal environment during both the inflation process and operation. However, this improved precision and controllability requires a complex control logic and reliable sensor information.

The additional complexity of the more complex approach was deemed undesirable by Griebel, 2011 who decided that the simple method was good enough for the inflation of the Martian Inflatable Hypersonic Drag Balloon. However, given both the surface accuracies required of inflatable reflectors as well as the need for precise pressure maintenance, Lester et al., 2000 deems the greater degree of control and precision essential to the development of the solar concentrator inflation control system. Therefore, it would be desirable to develop a complex control logic for this inflation system. However, given the constraints of this thesis project this was deemed untenable and shall be left for exploration in future work. Thus a simple method inspired by Griebel, 2011 shall be utilized to demonstrate the feasibility of using control logic's typically utilized for RCS systems for inflation purposes and determine the desired pulse width and frequency that shall enable the inflation requirements of this project to be fulfilled.

### SIMPLE LOGIC DESIGN

The first step in this process is to determine the desired functionality of the control logic. For this preliminary design, the focus of this simple method shall solely be on the initial inflation of the structure, with pressure maintenance left for future work. From killer requirement REQ-ISP-01, it is desired that this initial inflation process take between 10 and 100 seconds. In addition, from the description of the inflation sequence (section 7.5) this inflation process can be split into two distinct phases; unfolding and pressurization. In order to further quantify the desired performance parameters, the inflation sequence detailed by Griebel, 2011 for a comparable spherical structure is utilized as inspiration. This inflation sequence is seen below.

1. Unfolding Phase:
   - Pressure: Complete when 5% of final pressure/mass is reached/expelled.
   - Time: Complete in 8-10% of total inflation time.
2. Fast Pressurization Phase:
   - Pressure: Complete when 95% of final pressure/mass is reached/expelled.
   - Time: Complete in 55-60% of total inflation time.
3. Gradual Pressurization Phase:
   - Pressure: Complete when 100% of final pressure/mass is reached/expelled.
   - Time: Complete in 30-35% of total inflation time.

Using these parameters, the pulse widths and frequencies required to satisfy the inflation system requirements can be determined. In addition, as discussed previously, a number of simplifying assumptions are made. These are as follows:

- No time delay from command signal to valve opening
- Rise time and decay time are neglected. Steady state conditions reached instantaneously.

These assumptions reduce the complexity of this preliminary exploration of the pulsed operation of the inflation system. In future work, these assumptions should be accounted for. See papers cited above for more detail.

### INFLATION RATE

A python script is written for to determine the desired valve operating parameters that stem from these inflation phase parameters. Three different pulse widths are calculated for each of the three phases. Based on the PWM method, the frequency is kept constant and the pulse widths are varied until the desired parameters are achieved. The minimum pulse width is solely dependent on the thruster valve response time and is found by a single open/close cycle. From table 8.2 the MOOG 058E142A has the minimum pulse width of 8 ms. In addition, a minimum frequency of 1 Hz is assumed. Figure 8.20a highlights the relationship between inflation time and frequency at a mass flow rate of 0.5 g/s. The different slopes represent the three phases of inflation and described by the parameters above. Unsurprisingly, the higher the frequency the lower the inflation time. As shown in figure 8.20b, this is also true for mass flow rate.

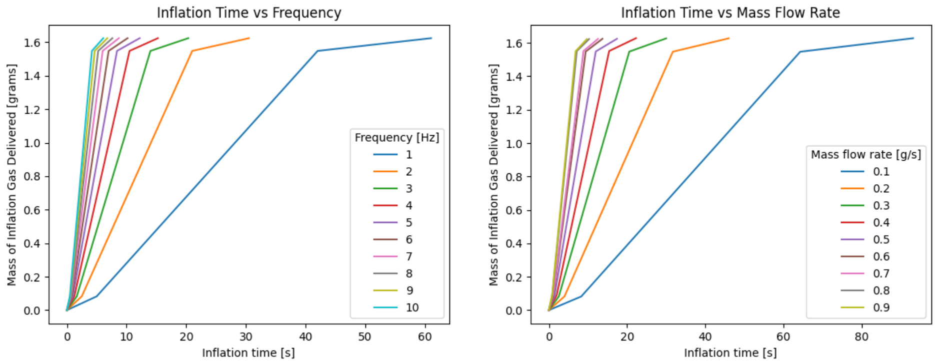


(a) Inflation Time vs Frequency at Mass flow rate = 0.5 g/s (b) Inflation Time vs Mass flow rate at Frequency = 3.5 Hz

Figure 8.20: Graphing of Inflation Phase vs Time

8

The pulsed performance at different mass flow rates within the desired range yields a variation in the required pulse widths and duty cycles. The equation for duty cycle is given in equation 8.46. The variation in pulse widths required to satisfy the time and pressure requirements for each phase can be seen for a variety of mass flow rates in table 8.3. The smallest pulse width is set at the minimum pulse width of 8ms and as can be seen is utilized for the gradual pressurization phase, with the pulse widths for the other two phases changes in accordance with flow rate.

Table 8.3: Pulse Widths at Various Mass Flow Rates

| **Mass Flow Rate (g/s)** | **PW1 (ms)** | **PW2 (ms)** | **PW3 (ms)** |
|---|---|---|---|
| 0.1 | 28.75 | 74.75 | 8 |
| 0.5 | 32.53 | 73.75 | 8 |
| 0.9 | 35.25 | 77.0 | 8 |

These different mass flow rates lead to different inflation times and different duty cycles. Evaluating the impact on these variables at different frequencies yields the results contained in table 8.4.

$$\text{Duty Cycle} = \frac{\text{Pulse Width}}{\text{Period}} \tag{8.46}$$

Where:

- Period = 1/frequency

Table 8.4: Duty Cycles at various Frequencies and Mass Flow Rates

| Frequency (Hz) | DC1 (%) | DC2 (%) | DC3 (%) | Inflation Time (s) |
|---|---|---|---|---|
| *m = 0.1 g/s* | - | - | - | - |
| 1 | 2.825 | 7.475 | 0.8 | 327 |
| 2.5 | 7.06 | 18.6875 | 2 | 130.8 |
| 3.5 | 9.8875 | 26.1625 | 2.8 | 93.43 |
| 5 | 14.125 | 37.375 | 4 | 65.4 |
| 10 | 28.25 | 74.75 | 8 | 32.7 |
| *m = 0.5 g/s* | - | - | - | - |
| 1 | 3.3 | 7.925 | 0.8 | 62 |
| 2.5 | 8.25 | 19.8125 | 2 | 24.8 |
| 3.5 | 11.375 | 25.8125 | 2.8 | 19.14 |
| 5 | 16.5 | 39.625 | 4 | 12.4 |
| 10 | 33 | 79.25 | 8 | 6.2 |
| *m = 0.9 g/s* | - | - | - | - |
| 1 | 3.55 | 7.7 | 0.8 | 35 |
| 2.5 | 8.8125 | 19.25 | 2 | 14 |
| 3.5 | 12.3375 | 26.95 | 2.8 | 10.0 |
| 5 | 17.625 | 38.5 | 4 | 7.0 |
| 10 | 35.25 | 77.0 | 8 | 3.5 |

DC = Duty Cycle



As can be seen in table 8.4, lower mass flow rates yield longer inflation times. In fact for an ideal mass flow rate of 0.1 g/s, at frequencies less than 3.5 Hz the inflation time lies outside the desired range of 10 - 100 seconds. In order to reduce this inflation time, the frequency must be increased, which in turn leads to an increase in duty cycle. However, in order to assume that the tank pressure in the tank drops in an isothermal fashion, lower duty cycles are desirable (Zandbergen, 2018). Thus a maximum duty cycle must be specified. In addition, although it is assumed that there is no time delay, which leads to saturation points (Rekleitis et al., n.d.), it seems prudent to also specify a minimum duty cycle. Once again Griebel, 2011 is referred to for estimating these values, with a desired duty cycle range of approximately 2.5-26% being assumed for this simple control logic. As can be seen from the table, this range is satisfied at around 3.5 Hz for each of the flow rates, with DC2 and DC3 being the two defining duty cycles. Clearly, these values don't exactly meet the desired duty cycle requirement with the value for DC2 being slightly greater than desired. However, for this simple control logic it shall be deemed sufficient and so a frequency of 3.5 Hz shall be assumed.

#### SELECTING THE OPTIMAL MASS FLOW RATE

As the desired inflation time of 10-100 seconds is selected somewhat arbitrarily, as discussed in section 7.5.1, it is not entirely clear which mass flow rate offers the best/most optimal solution. Establishing the most suitable inflation time would require using testing or complex simulations of the inflation process and control logic. However, both of these solutions are beyond the scope of this thesis project. Instead the results presented in figure 8.20 and table 8.4 shall be utilized to as the basis for selecting the most appropriate mass flow rate.

From examining table 8.4 it can be seen that low mass flow rates require higher operational frequencies, and thus higher duty cycles, to meet inflation times that higher mass flow rates can achieve at lower frequencies and lower duty cycles. For example, at 0.1 g/s, an operational frequency of 5 Hz is required to facilitate an inflation time of 65.4 s while at 0.5 g/s this can be achieved at 1 Hz and thus lower duty cycles. This capacity for lower duty cycles is attractive as it reduces the requirements placed on the inflation valve and allows for greater flexibility with regards the pulse width and inflation time. This greater flexibility inherently enables the inflation system to provide a greater degree of control over the inflation process. However, it be must noted that this flexibility is subject to the maximum and minimum duty cycle requirements that are an important consideration for the real performance of the inflation nozzle. While this doesn't provide any significant advantage for the simplified approach taken in this thesis, for the more complex control logic desired for a real inflation process the potential for increased controllability with higher flow rates would be very beneficial. Thus, while the development of a complex control logic is left for future work, it is postulated that higher mass flow rates (within an acceptable duty cycle range) offer greater potential for controllability than lower mass flow rates.



### 8.3.4. CONCLUSION

This section provides a preliminary investigation into the suitability of utilizing a cold gas micropropulsion thruster valve for inflation purposes. While the scope of the investigation is kept quite simple, it is apparent that operating the inflation system in a pulsed mode of operation utilizing a rapid response solenoid thruster valve enables a controllable inflation rate, which can be varied to achieve precise control of the inflation process. This is demonstrated here by solving for the pulse performance parameters of frequency, pulse width and duty cycle using a simplified PWM approach. This approach demonstrates that the inflation system can provide a smooth and controlled unfolding phase, as dictated by key requirement REQ-ISP-03, followed by a rapid pressurization stage so as to inflate the structure within the desired inflation time, as dictated by killer requirement REQ-ISP-01, while also providing a slower and more controlled pressurization stage so as to provide a gradual approach to the final operating skin stress of the structure, thus satisfying key requirement REQ-ISP-04. Moreover, this pulsed mode approach provides the flexibility to provide precise pressure maintenance as dictated by key requirement REQ-ISP-06. All of this functionality can be provided by a miniature COTS solenoid thruster valve.

## 8.4. INFLATANT TANK

### 8.4.1. INTRODUCTION

The inflatant storage system allows for the storage of the inflation gas until its use for inflation. The storage system has a major impact on the performance and features of the inflation system, as can be clearly seen in the inflation system concept generation process (Chapter 8). In this section, the design of a tank for this cold gas micropropulsion based inflation system shall be discussed.

### 8.4.2. STORAGE SYSTEM TYPES

Cold gas micropropulsion systems can generally be categorized into three subcategories; pressurized gas, heated gas and liquefied gas, as shown in figure 8.21.

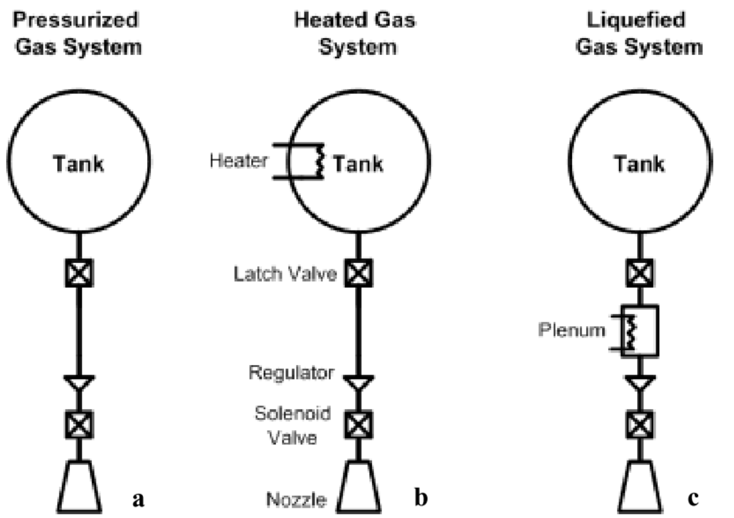


**Figure 3. Three possible variations of cold gas propulsion systems. (a) Pressurized Gas System, (b) Heated Gas System, (c) Liquefied Gas Svstem.**



Figure 8.21: Cold Gas Storage System Types (Lev et al., 2014)

#### PRESSURIZED GAS

Pressurized gas systems are the simplest and most common form of cold gas system. They store the inflatant in the form of pressurized gas within the propellant tank. As was outlined in section 7.4, the molecular weight of the inflation gas has a significant bearing on the size of the tank required for a pressurized gas system. Lower molecular weights mean lower mass requirements but larger volume requirements. This leaves the designer with two options when using low molecular weight gases, store the gas at low pressure and have high storage volume and low tank mass, or store the gas at high pressure and have low storage volume but high tank mass.

- Low Pressure Storage

  - Storing the inflation gas at low pressure (<10 bar) is typically preferred for cold gas micropropulsion system. Lower tank pressures yield a lower risk of failure, reduced leakage, lower mass requirements and a less complex feed system with no need for pressure regulation. However, this does come at a cost. Storing the inflation gas at low pressure means that the mass of inflation gas that can be stored within the limited volume specifications of a CubeSat inflation system is severely limited. This becomes even more of an issue for systems requiring make-up gas, severely limiting the lifespan of the inflatable structure.

- High Pressure Storage

  - In order to reduce volume constraints it is highly desirable to store the inflation gas at higher pressures. Indeed this is the more common approach for nitrogen cold gas propulsion systems with numerous small satellite RCS and main propulsion systems having storage pressures of 100-200 bar (Anis, 2012; Cardin and Acosta, 2000; Harris, 2003; Zaberchik et al., 2019). Indeed, the RCS system for the sloshsat FLEVO small satellite stores nitrogen at pressures in excess of 470 bar (Adler et al., 2005). The cold gas inflation systems that have previously been utilized for inflating inflatable space structures also utilize storage pressures of 100-200 bar (Coffee et al., 1962b; Freeland and Bilyeu, 1993; Griebel, 2011; Rasse et al., 2014; Wright et al., 2012). Interestingly, a number of systems utilize mini gas cartridges typically used in terrestrial applications such as hospitality and medicine. Nakasuka et al., 2009 utilize an N2 cartridge typically used for beer server with an initial storage pressure of 198 bar, while Chandra et al., 2021 (CATSAT) utilizes 4 x 18ml Argon/Helium Cartridges developed by a company called picocyl [8] . The storage pressure of these cartridges isn't clear although a minimum pressure of 50 bars is likely. Examining nitrogen mini cartridges commercially available in Europe, NTG [9] supply a cartridge that can supply 18.5 grams of nitrogen stored at 138 bar.
  - However, storing the inflation gas at these pressures leads to a number of issues. Firstly there is increased system mass and complexity due to the need for pressure regulation, while leakage also becomes more of an issue at higher operating pressures. In addition, such high pressure tanks on CubeSats may be at odds with launch and safety constraints as dictated by the launch vehicle provider. This desire to maintain low tank pressures during launch gives rise to the next storage option.

### Heated Gas

Unlike compressed gas, the heated gas storage system stores the inflatant in a partially liquid phase enabling a more compact stowage of the inflatant. Once the system is in space and prior to operation, the entire propellant tank is heated above the inflatants

[8] https://www.picocyl.com/

[9] http://www.ntg-europe.de/pdf/standardspecifications_en.pdf

critical temperature enabling the full vaporization of the inflatant. Once this is complete, the system operates in the same way as a pressurized gas system. This system is inherently more complex than a compressed gas system. For example, the release of propellant from the tank can lead to a decrease in temperature and pressure which can in turn lead to re-liquidation of the propellant. Heating and temperature control are thus essential. These reasons contributed to the drawback of CO2 as an inflation gas (section 7.4).

Given the critical temperature and pressure values of nitrogen gas are 126K and 34 bar respectively, the additional complexity required to maintain the nitrogen inflation gas below this temperature (i.e. at cryogenic temperatures) is highly undesirable for this application. The storage of cryogenic inflation gases may be desirable for large spacecraft inflation systems as noted by Roe, 2000 and would enable a greatly reduced volume requirement. However, as pointed out by Griebel, 2011 "no inflation system has ever existed that stored inflation gas in this way".

### LIQUEFIED GAS SYSTEM

Like the heated gas system, this system stores the inflatant as a liquid. However, unlike heated gas the evaporation of the inflatant is not caused by heat but rather by utilizing expansion chambers. Such a system can be seen in figure 8.22. When the high pressure liquid enters the expansion chamber, the drop in pressure as it expands enables vaporization. Such a system was utilized for the MEPSI cold gas inflation system that was used to inflate the AeroCube 3 structure (Hinkley, 2008). As discussed for the heated gas system, the storage of nitrogen as a liquid is not considered feasible. Despite this, the use of expansion chambers is an interesting method of reducing gas pressures before reaching the thruster which can also be utilized for compressed gas systems as noted by Hinkley, 2008 "This same technology can be used for holding gas or fluid for inflating structures in space".

8

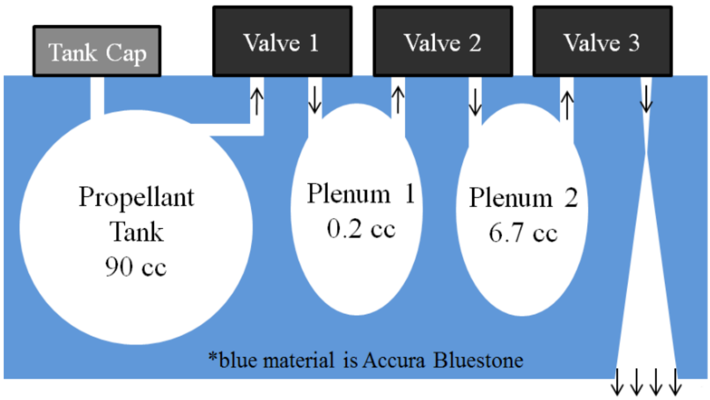


Figure 8.22: Use of expansion chambers in a liquefied gas system (Arestie et al., 2012)

Indeed, Griebel, 2011 utilizes the method in the design of an inflation system for the Mars Drag Balloon. The main advantage of the inflation system designed using this method is its mechanical simplicity. However, as noted in Lev et al., 2014 the use of this method is still relatively new and has primarily been utilized in small 3D printed cold gas micropropulsion systems where low propellant tank pressures make additive manufacturing suitable. (Arestie et al., 2012; Hinkley, 2008 ).

### 8.4.3. TANK DESIGN

Given the additional complexity required to store nitrogen as a liquid, such as the need for cryogenic temperatures and propellant management devices (PMD's), it is apparent that the nitrogen gas required for inflation should be stored as a compressed gas. Thus a pressurized gas storage system shall be utilized for this inflation system. From this point on the design of an appropriate propellant tank shall be discussed. The tank shall follow the same design process used for the design of nitrogen pressurant tanks. It thus contains no additional pressurant gas or propellant management devices and empties in a blowdown fashion, as discussed in section 8.

#### TANK SHAPE

The storage tank takes the form of a thin-walled container. The two most common tank shapes are spherical and cylindrical. The spherical tank is popular as it is the optimum shape for minimizing mass. The cylindrical tank on the other hand tends to offer better use of the available volume in the CubeSat. Indeed, when volume constraints are a priority conformal tanks offer the best solution. These tanks are volumetrically efficient as they can be specifically designed in a shape that maximizes the use of the available volume. Although uncommon in large spacecraft they are seen as a legitimate option for small satellite propulsion systems (Collicott et al., 2019).

- Spherical:
  - The spherical tank is a popular shape as it is seen as the optimum shape for minimizing mass and maximizing propellant volume capacity. However, the spherical shape makes it more difficult to integrate into the CubeSat as it makes an inefficient use of the available volume.
- Cylindrical:
  - The cylindrical tank offers a proven and popular solution which provides a high propellant volume capacity. It makes better use of the available volume than the spherical tank and is a popular shape among cold gas micropropulsion systems as well as inflation systems (Chandra et al., 2021; Coffee et al., 1962a; Freeland and Bilyeu, 1993; Nakasuka et al., 2009; Wright et al., 2012). In addition, high pressure nitrogen cartridges found in terrestrial applications are primarily cylindrical in shape.
- Conformal:
  - The conformal tank provides the best solution for maximizing volumetric efficiency within the CubeSat. Indeed it is for this reason that a cuboid shaped conformal tank is proposed for the LUMIO main propulsion system propellant tank and RCS tank (Nett, 2021). However, while such a tank provides the

best integration into the satellite, the complexity of a custom shaped tank with respect to design and testing is perceived as a disadvantage. For example, in the case of a cuboid shaped tank, issues with mass, stress concentrations and leakages arise that must be accounted for. These issues shall only be exacerbated by higher storage pressures.

Given volume is a primary concern for this inflation system, as dictated by key requirement REQ-BEOC-01, the volumetrically inefficient spherical tank is clearly undesirable. On the other hand the volumetrically efficient conformal tank promises the best use of the available spacecraft volume. However, given the additional design constraints and issues that must be addressed it was decided that a simpler and proven tank shape is more suitable. It is for this reason, that the popular cylindrical tank shall be utilized for the design of the inflatant storage tank. This also yields the possibility of utilizing high pressure nitrogen cartridges found in terrestrial applications, which are primarily cylindrical in shape. Further optimization of the inflation system may see the use of a conformal tank.

### 8.4.4. TANK MATERIAL

For cold gas propulsion systems there are a number of materials that are commonly used in propellant storage tanks. These can generally be grouped into two categories; metallic tanks and composite over-wrapped tanks. Historically metallic tanks have been the most popular form of propellant storage tank, particularly metals that provide high yield and specific strengths. Materials such as Aluminum and Titanium alloys provide lightweight, high strength and durable characteristics that have seen them used extensively.

Table 8.5: Key Material Properties

| **Material** | **Density** | **Yield Strength** | **Specific Strength** | **Young's Modulus** | **Fracture Toughness** | **CTE** |
|---|---|---|---|---|---|---|
| Units | $kg/m^3$ | $N/mm^3$ | N-m/kg | GPa | $Pa.m^{0.5}$ | strain/$°C$ |
| Aluminium 7075 T6 | 2,770 - 2,830 | 359 - 530 | 1.28E5 - 1.89E5 | 69-76 | 2.66E7 - 2.68E7 | 2.29E-5 - 2.41E-5 |
| AISI 302 Steel, Annealed | 7,810 - 8,010 | 205 - 310 | 2.59E4 - 3.92E4 | 189 - 197 | 6E7 - 7.2E7 | 1.6E-5 - 2.0E-5 |
| Ti-6Al-4V, STA | 4,410-4,450 | 827 - 1,140 | 1.87E5-2.41E5 | 110 - 117 | 8.2E7 - 1E8 | 8.7E-6 - 9.1E-6 |
| Epoxy/S-glass fiber | 1,840-1,970 | 1,700-1,760 | 8.73E5-9.42E5 | 47.6-47.8 | 7.76E7-9.49E7 | 1.73E-6 - 3.67E-6 |

[9] https://www.matweb.com/

Composite overwrapped tanks have become increasingly popular in recent years (Harris, 2003; McLaughlan et al., 2011; Tam and Griffin, 2002; Thunnissen et al., 1995). They are a combination of composite fibers wrapped over a fluid retention barrier that serves as an internal liner, which are typically a thin ductile metal such as aluminum. The composite fibers are typically produced from carbon, Kevlar or glass. These tanks offer a significant weight advantage at approximately one half of their metallic counterparts (McLaughlan et al., 2011). In addition, they are typically custom designed for the desired application to maximize the desired tank properties. However, this in turn means they are more costly to manufacture and require a more complex design process. In addition, they have additional failure modes relative to metallic tanks.

For these reasons it was decided for this preliminary design of the inflation system, a popular metallic material would be utilized. As is proposed by Nett, 2021 for the design of the LUMIO propulsion system, the popular titanium space alloy Ti-6Al-4V STA is chosen as the tank material. In addition to its extensive flight heritage, this material offers an extensive range of attractive properties relative to other popular metals, as can be seen in the table above. With further optimization it would be highly advantageous to explore the design of a composite overwrapped propellant tank in future work.

### 8.4.5. Tank Sizing

#### Inflatant Tank Capacity

In order to design an inflatant tank for this inflation system, the available tank volume capacity must be established. Unlike in a conventional propulsion system, where the sizing for the tank is based off the required propellant mass and maximum allowable tank pressure, for this investigation the sizing of the tank shall be derived off historical/statistical data first, followed by the derivation of the inflatant mass and tank pressure. This was done for two reasons.

1. Firstly, it enables the designer to assess the impact of gas losses due to micrometeroid punctures on the mass requirements of the inflation system. As the maintenance life is dependent on the quantity of gas that can be carried, this in turn demonstrates the feasible operational lifespan of the pressure stabilized structure given the volume and pressure constraints of the BEOC mission.

2. From this investigation the operational tank pressures required to facilitate both the inflation and pressure maintenance of the structure over this lifespan can be established. This is important as it shall have a significant impact on the design of the feed system (see section 8.5)

An initial investigation was carried out by gathering data from similarly sized micropropulsion systems. Due to the limited data available on similarly sized cold gas micropropulsion systems, other chemical propellant micropropulsion systems are also utilized for this process. The systems gathered are graphed in figure G.1. It contains a graph of the tank capacity versus the propulsion system size for these reference Cubesat systems. Given a maximum inflation system volume of 1U, as dictated by REQ-ISI-01, an initial estimate for the inflatant tank capacity of about 0.4U was gauged from this graph. As seen in figure 8.23, using a cylindrical tank configuration such a tank size leaves very little space for the remaining components of the inflation system. Given the bulky nature of some of the COTS inflation system components, as discussed in section 8.5, this is highly undesirable.

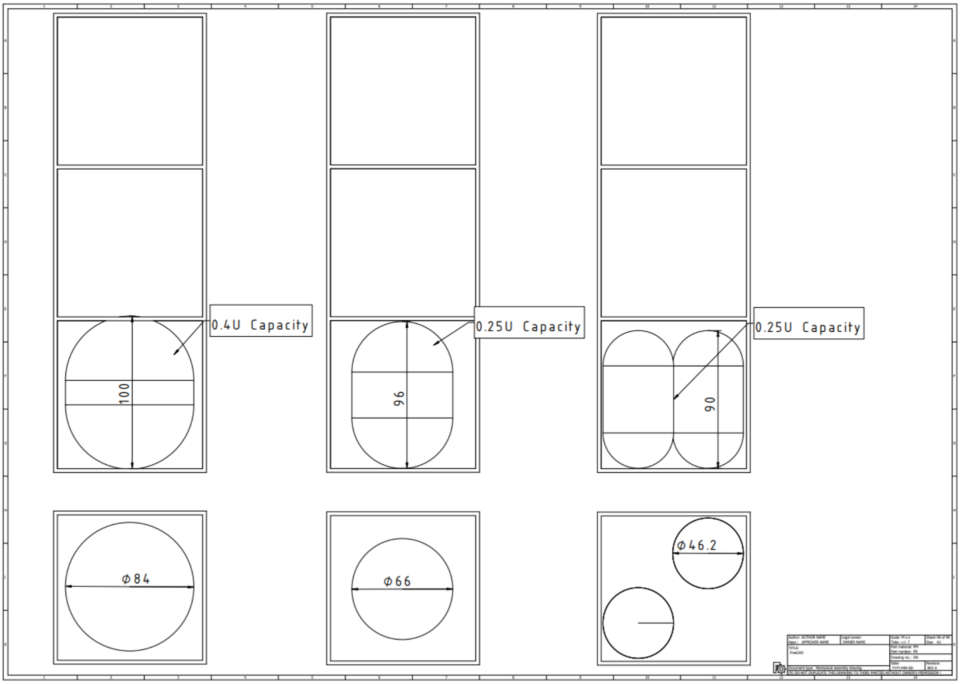


Figure 8.23: 3D Graphic of 0.4U vs 0.25U Inflatant Tanks within 3U Volume

8

In addition, due to the uncertainty regarding the size of the ejection mechanism, reducing the radius of the tank and increasing its length shall not be considered for this preliminary design. Thus, as a conformal tank configuration shall not be explored in this thesis, a lower inflatant volume capacity should be considered. Of the systems explored in the initial investigation, it can be seen that the LUMIO RCS system proposed by Nett, 2021, with a system size of 1U, has a smaller tank capacity then indicated by the trend line. This system has a tank capacity of 0.267U, which is 1.5 times smaller than the 0.4U tank, and given it is sized specifically for LUMIO may present a more appropriate initial estimate for this preliminary design. Rounding for simplicity, a tank with a capacity of 0.25U can be seen in figure 8.23, where the increased volume available for other inflation components is apparent. Furthermore, it can also be seen that utilizing multiple smaller tanks, as is done for Catsat (Chandra et al., 2021), can further increase the volumetric efficiency of the system. Seeing as the system must be able to house a pressure regulator and multiple latch valves, as discussed in section 8.5, this would be beneficial. However, this shall be left further exploration and a single tank shall be utilized.

The major knock on effect of a smaller tank capacity is its impact on the required storage pressure. While the LUMIO mission dictates a maximum storage pressure of 50 bar (Cervone et al., 2021), thesis supervisor Dr Angelo Cervone, who is involved with the LUMIO mission, pointed out that it may be feasible to relax this constraint to a maximum storage pressure of 200-250 bar. This is due to the LUMIO maximum storage effectively being selected based on similar CubeSat missions, with a higher pressure feasible as long as it does not compromise the structure or its operation. Thus, the reduction in tank volume can certainly be accounted for with an increase in pressure, as shall be discussed in the following pages.

### TANK SIZE

In order to calculate the mass and external volume of the inflatant tank, the wall thickness must be found. The inflatant tank consists of a cylindrical section and two domed caps. For simplicity, it shall be assumed that these caps are hemi-spherical in shape. The internal volume of the inflatant tank can thus be calculated using equation 8.47, while the total external volume can be calculated using equation 8.48.

$$v_{tank_{internal}} = \frac{4}{3} \cdot \pi \cdot r_{tank}^3 + \pi \cdot r_{tank}^2 \cdot l_{cylinder} \tag{8.47}$$

$$v_{tank_{External}} = \frac{4}{3} \cdot \pi \cdot (r_{tank} + t_{sphcap})^3 + \pi \cdot (r_{tank} + t_{cyl})^2 \cdot l_{cylinder} \tag{8.48}$$

$$l_{tank} = l_{cylinder} + 2 \cdot (r_{tank} + t_{capsph}) \tag{8.49}$$

where:

- $v$ = Volume (U = mm$^3$/1E6)
- $r$ = Radius (mm)
- $l$ = Length (mm)
- $cyl$ = Cylinder
- $sphcap$ = Spherical cap

As a radius for the tank has been determined, see figure 8.23, these thickness values, $t_{cyl}$ (cylindrical section) and $t_{sphcap}$ (spherical caps), can be calculated. As is determined by Nett, 2021, the ultimate stress is more appropriate for dimensioning this than the yield stress. Using the equations established by Nett, 2021 as well as the relevent safety factors, the wall thickness values can thus be calculated as follows:

$$t_{cyl} = \frac{P_{tank} \cdot r_{tank}}{\sigma_u} \times j_{bu} \cdot j_u \tag{8.50}$$

$$t_{sphcap} = \frac{P_{tank} \cdot r_{tank}}{2 \cdot \sigma_u} \times j_{bu} \cdot j_u \tag{8.51}$$

where:

- $t$ = thickness (m)

8

- $\sigma_u$ = Ultimate Stress (1100 MPa)
- $j_{bu}$ = Burst Safety Factor = 2.5
- $j_u$ = Ultimate Load Factor = 1.25

Evidently, the thickness is dependent on the tank storage pressure which shall now be discussed.

### 8.4.6. STORAGE PRESSURE

As has been discussed at the start of this chapter, there are two design options for pressurized gas systems based on the storage pressure; low pressure storage (<10bar) or high pressure storage (>10bar). In order to select the appropriate storage pressure, the mass of inflatant gas that can be stored at different pressures must be quantified. This can be done using the following equation:

$$M = \frac{Z \cdot v \cdot P}{R \cdot T} \tag{8.52}$$

where:

- $M$ = Gas mass (Kg, convert to grams)

The total mass of inflation gas required shall consist of the gas required for the initial inflation, the make up gas required for pressure maintenance, the gas required to maintain the final tank pressure above that of the regulator inlet and then the gas required to account for leakages. This is demonstrated in equation 8.53.

$$M_{gas} = M_{inflation} + M_{makeup} + M_{Ullage} + M_{Leakage} \tag{8.53}$$

8

A description of each of these contributing factors is as follows:

- $M_{inflation}$
  - $M_{inflation}$ is the mass of gas required to inflate the structure to its desired skin stress level. This is found to be 1.63 grams.
- $M_{makeup}$
  - The mass of gas carried onboard for pressure maintenance of the structure is given by $M_{makeup}$. It's value is determined by the hole growth rate of the inflatable structure stemming from the local micrometeroid flux, as discussed in section 6.6. The mass of makeup gas required to sustain the desired pressure levels increases exponentially with time. This mass can be calculated for this structure as a function of time using equation 7.2. As has been alluded to $M_{makeup}$ is the deciding factor in determining the operational lifespan of the pressure stabilized structure.
- $M_{Ullage}$

- $M_{Ullage}$ is dependent on the residual pressure requirements of the tank, i.e. the final tank pressure, which is dependent on the minimum regulator inlet pressure as discussed in section 8.5.4.

- $M_{Leakage}$
  - The mass of gas required for leakage, $M_{Leakage}$, must also be considered. This is TBD but for this preliminary design a conservative margin of 25% shall be assumed to account for gas leakages in the system.

Using this equation, it can be found that for the minimum mass flow rate of 0.1 g/s, the relatively low molecular weight of nitrogen gas requires that a storage pressure of 21 bar is required just for initial inflation. This clearly exceeds the threshold for low pressure storage. Thus high pressure gas storage is a necessity. Figure 8.24a, shows the total mass of gas required for a range of pressure maintenance time-frames against the storage pressures (equation 8.54) necessary to meet the volume constraint of 0.25U.

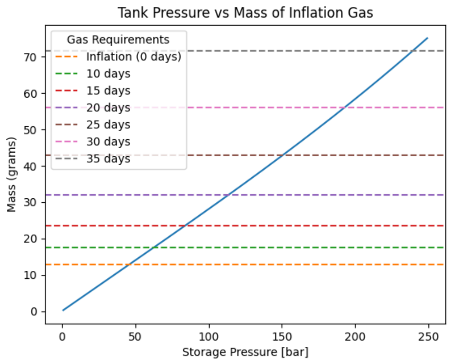


(a) Total Mass of Inflation Gas vs Tank Storage Pressure.

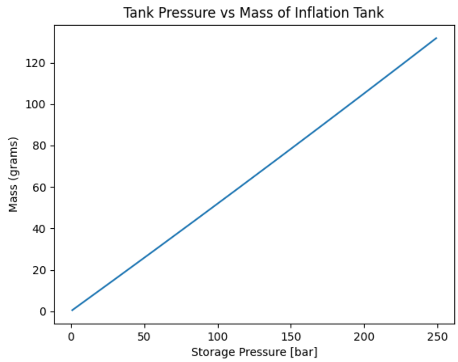


(b) Tank Mass vs Storage Pressure

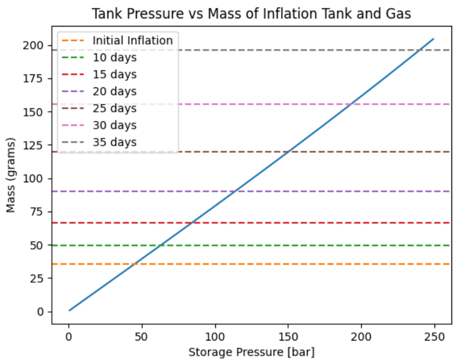


(c) Tank and Inflation Gas Mass vs Storage Pressure.

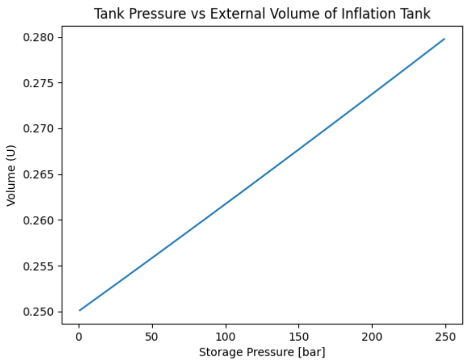


(d) External Volume of Inflatant Tank with Storage Pressure

Figure 8.24: Size of Tank with Storage Pressure. Static Parameters: m = 0.5 g/s, $M_{Ullage}$ = 8.63 grams (see section 8.6)

$$P_{tank} = \frac{M_{gas} \cdot R \cdot T}{V_{tank}} \tag{8.54}$$

As can be seen in figure 8.24a, the gas required for initial inflation at 0.5 g/s, clearly marked by the dashed orange line, is 45 bar, just under the 50 bar LUMIO maximum storage pressure requirement. Across the mass flow rate range this pressure varies from 21 bar at 0.1 g/s to 69 bar at 0.9 g/s due to the increasing ullage gas requirements (see section 8.6). This indicates that for an inflatant tank capacity of 0.25U, the LUMIO maximum storage pressure of 50 bar is either not capable of providing sufficient storage for the inflation gas or can only provide limited pressure maintenance. Thus, as has been noted previously, for this thesis this LUMIO pressure requirement shall be relaxed, enabling maximum storage pressures of 200-250 bar. However, as can be seen in figure 8.24a, even at these higher storage pressures, the system can only carry enough makeup gas for about 35 days of pressure maintenance. This is well below the 393 days desired by requirement REQ-BEOC-04-02. Indeed, the 3.92 Kg's of inflatant gas that would be necessary to meet such a mission duration exceeds the total mass budget for the inflatable system (REQ-BEOC-02). This clearly demonstrates the limitations of pressure stabilized inflatable optical reflectors and further emphasises the need for advancements in rigidization technology as noted in section 6. Without such advancements, long duration CubeSat inflatable reflectors cannot become a realistic option for BEOC missions.

Given that a long term mission is out of the question, a reduced mission lifetime must be considered. Based on the MEOP of the upstream high pressure latch valve MV602L (see section 8.5.3), the maximum tank pressure shall be taken as 200 bar. This limits the mission duration under the current design parameters to about a month. It should also be noted that while not accounted for in this thesis, thermal variations in the operating environment shall also require makeup gas, thus further constraining this mission lifetime. However, it is conceivable that with further design iterations it may be possible to extend this lifespan. This could be done by either increasing the tank capacity or reducing the mass of make up gas. A list of possible ways that this could be done is given below.

- The tank capacity could possibly be increased if:
  - A conformal tank is utilized.
  - Multiple smaller tanks are utilized.
  - The inflation system components can be stored in a volumetrically efficient manner.
  - The designed ejection mechanism has minimal volume requirements, thus reducing the volume constraints on the tank.
  - The mass of ullage gas $M_{Ullage}$ is minimized.
  - The mass of gas required for leakage $M_{Leakage}$ is minimized.
- The quantity of make up gas $M_{makeup}$ required could possibly be reduced if:
  - Further detailed analysis of the lunar micrometeroid environment yields a lower growth rate.

- A smaller diameter structure is utilized.
- A lower stabilization pressure is utilized.

However, irrespective of these possible solutions it is apparent that the lifespan of a pressure stabilized BEOC reflector shall invariably be limited. This is presents a clear issue for long duration BEOC missions and indicates that utilizing a pressure stabilized structure for such a purpose is likely unfeasible, particularly given the current uncertainty regarding the micrometeroid environments across the solar system. Therefore, without further advancements in rigidization technology, inflatable reflectors shall likely be limited to short duration missions. This does not satisfy the desire to facilitate long term BEOC reflector applications but it does open the door for alternative mission parameters where shorter operational parameters such as month long missions are desirable.

### 8.4.7. CONCLUSION

In this section, the design of the storage tank for the inflation system has been explored. With respect to how the inflation gas shall be stored, given the additional complexity required to store nitrogen gas as a liquid, the most appropriate way to store the inflation gas is as a compressed gas. Given the molecular weight of nitrogen this requires a high pressure storage tank. A cylindrical tank was chosen as it provides a simple and proven tank shape. However, it may be desirable to increase the volumetric efficiency of the tank, either by utilizing a custom conformal tank or by splitting the cylindrical tank into a number of smaller tanks. Each of these approaches has benefits and drawbacks which should be explored with further optimization of the inflation system. With regards to optimization, it would be desirable to explore the design of a compressed overwrapped tank. However, for this preliminary design the popular titanium space alloy Ti-6Al-4V STA was deemed the most appropriate.

Table 8.6: Tank Parameters

| **Component** | **Value** |
|---|---|
| Internal Volume (U) | 0.25 |
| $R_{tank}$ (mm) | 33.02 |
| $L_{cylinder}$ (mm) | 28.96 |
| $t_{cyl}$ (mm) | 1.76 |
| $t_{sphcap}$ (mm) | 0.88 |
| $L_{tank}$ (mm) | 96.76 mm |
| Initial Tank Pressure (bar) | 200 |
| Tank Mass (dry) (grams) | 103.18 |
| Wet Mass (grams) | 58.42 |
| Total Tank mass (grams) | 161.6 |

With regards to sizing of the tank, while an initial investigation indicated that a 1U inflation system may be able to contain a tank with a capacity of 0.4U, the use of a cylindrical tank configuration meant facilitating the volume requirements of the remaining inflation components was infeasible. As such, a reduced tank size of 0.25U is considered.

This leads to an increase in the required storage pressure. However, regardless of the stored pressure it is apparent that it is unfeasible to provide a mission lifetime of 393 days, as this would require a wet mass greater than the total mass budget of the inflatable system. A storage pressure of 200 bar was thus chosen, facilitating a month long mission lifetime. The tank parameters are summarized in table 8.6. While a variety of possible solutions have been proposed to increase this lifetime, the the limitations of pressure stabilized inflatable optical reflectors are evident. Without further advancements in rigidization technology these structures cannot provide a competitive option for long duration BOEC missions.

# 8.5. FEED SYSTEM

## 8.5.1. INTRODUCTION

The feed system of the cold gas inflation system ensures the transport of the nitrogen inflation gas from the inflatant tank to the inflation valve and nozzle. It consists of a number of different components that enable the transportation of the gas with the desired flow and pressure rate. These components usually include a pipe system to deliver the propellant and valves to control the supply. These components together are known as the feed system. The design of the feed system for this inflation system shall be discussed in this section.

## 8.5.2. FEED SYSTEM TYPES

As has been discussed in section 8, the inflation system shall be based on a cold gas regulated blow down system. There are a number of different variations on the feed system that can be utilized to implement such a design. This discussion shall be limited to the two main system types, one based on the use of a mechanical pressure regulator and one based on the use of expansion chambers. Although these feed systems shall be discussed as discrete types, it should be noted that feed systems that utilize both pressure regulators and expansion chambers/plenums are possible. However, this combination is primarily associated with liquid propellant systems.

### MECHANICAL PRESSURE REGULATOR

The conventional method for providing a regulated blow down system is through the use of a mechanical pressure regulator. A basic schematic of such a system is seen in figure 8.25 below.

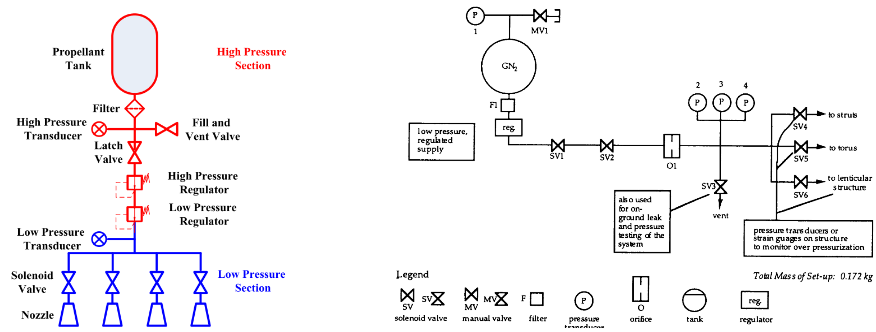


(a) Cold Gas Regulated Propulsion System Schematic (Zaberchik et al., 2019)

(b) Cold Gas Regulated Inflation System Schematic (Thunnissen et al., 1995)

Figure 8.25: Mechanical Pressure Regulated Systems

As has been discussed in the concept generation section, the use of a mechanical pressure regulator for pressure control is widely found across cold gas propulsion systems as it gives two significant advantages over a straight blowdown system. Firstly, it enables the propellant to be stored at far higher pressures than the operational chamber pressure, allowing a greater quantity of propellant to be stored. Secondly, unlike blow down systems where the chamber pressure drops with the tank pressure, the chamber pressure in a regulated system remains constant as long as the tank pressure remains above the regulator pressure. This is advantageous as it allows the thruster (the control valve and nozzle) to operate at a constant mass flow rate, thus generating a constant thrust level for propulsion systems or, in the case of inflation, a constant inflation rate. Unsurprisingly this is highly attractive from a performance standpoint and as is mentioned in section 8 enables a greater degree of inflation control. This method is commonly found among inflation systems that utilize converted cold gas propulsion technology such as IAE, where the storage pressure of 210 bar is reduced down to 4.14 bar (Freeland and Bilyeu, 1993). Lester et al., 2000, Thunnissen et al., 1995 and Wright et al., 2012 also utilize this method to provide controlled cold gas inflation systems.

### EXPANSION CHAMBER

As was mentioned in section 8.4.2, liquefied cold gas systems usually utilize a number of expansion chambers, wherein the liquefied propellant vaporizes. This process can be utilized as an alternative option to a mechanical pressure regulator, with the desired inflatant pressure obtained by optimizing the volume and number of the expansion chambers.

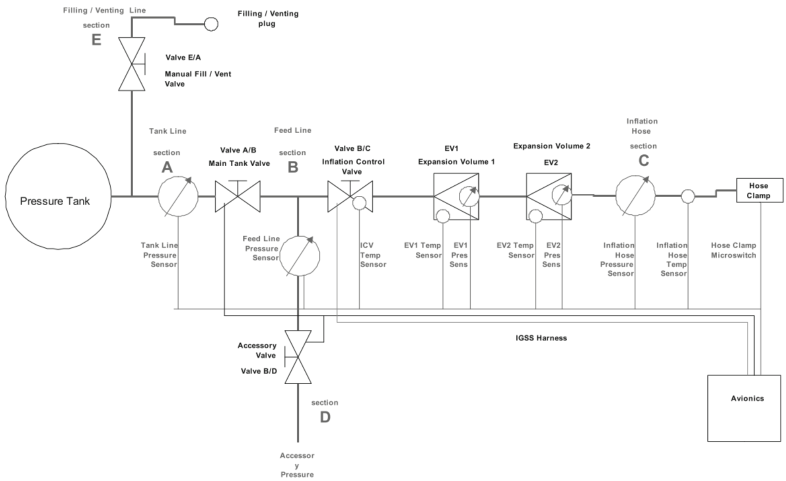


Figure 8.26: Expansion Chamber based Inflation System (Griebel, 2011)

These systems are less commonly utilized for compressed gas systems but can be used to reduce the pressure of the gas as it expands within the expansion chamber. They operate by feeding the propellant into the expansion chambers until a certain gas pressure is reached, at which point the propellant inlet valve is closed. Once this is done, the outlet valve is opened allowing the propellant at the reduced pressure to flow into either another expansion chamber for further pressure reduction or to the inflation control valve. As the inflatant in the chamber is depleted, the pressure shall drop accordingly. When the pressure reaches a certain value, the inlet valve is opened again refilling the chamber. In this fashion a controllable system can be developed and utilized to provide inflation and pressure maintenance to an inflatable space structure. Assuming no pressure regulator is used further downstream of the expansion volumes, this leads to non-constant flow rate similar to a straight blow down system.

Unfortunately, the literature on these systems, particularly for compressed gas applications is quite limited although as is discussed in section 8, the use of a chamber/plenum does provide the basis for the design of the high performing CGG refill design candidate. Given the non-constant flow rate this system does not possess the same inflation control characteristics that gives the regulated blow down candidate its edge in the inflation system design candidate trade off process. However, it is conceivable that the impact of such an issue can be reduced by introducing the inflation control valve before the expansion chambers, as is done in the system proposed for the inflation system of the Mars Inflatable Hypersonic Drag Balloon (Griebel, 2011). The designers of this inflatable spherical structure developed a unique compressed gas inflation system that utilizes a series of expansion chambers as seen in figure 8.26. Unfortunately, the available literature on the design of this system is limited and as such, its performance and design are not as well understood as that of a mechanical regulated system.

### FEED SYSTEM SELECTION

In order to assess the suitability of these systems with respect to the system requirements, a graphical trade off table is utilized. This can be seen in table 8.7. For more information on the color scheme see appendix D.

| **Feed System** | **Concept Maturity** | **Inflation Control** | **Complexity** | **Mass** | **Volume** |
|---|---|---|---|---|---|
| Pressure Regulator | Extensive | Excellent. Constant flow rate | Complexity associated with regulator | Bulky regulator + additional associated components | Bulky regulator + additional associated components |
| Expansion Chamber | Limited | Cyclical non-constant flow rate | Complexity associated with chamber(s) | Chamber(s) + additional associated components | Chamber(s) + additional associated components |

Table 8.7: Feed System Graphical Trade Off

It is apparent from this discussion, that of these two types of feed system, the pressure regulator system is preferable to that of the expansion chamber system. Not only does it reflect the desirable inflation control properties indicative of the regulated blow down concept initially discussed in section 8, its far greater concept maturity as an inflation system sees it as the significantly more attractive feed system type. Moreover, given the perceived similar mass, volume and complexity requirements a system that utilizes both a pressure regulator and an expansion chamber provides no advantage to the inflation system required for this project. However, the use of a chamber in conjunction with a pressure regulator may prove beneficial for structures that have more than one inflatable chamber. This can be seen in the design of the inflation system for a hypersonic inflatable aerodynamic decelerator (HIAD) as explored by Wright et al., 2012. In summary, the use of a mechanical pressure regulator provides the most appropriate feed system for the design of this inflation system.

### 8.5.3. FEED SYSTEM LAYOUT

The layout of the pressure regulated feed system shall be described in this section. A schematic of the desired layout shall be presented along with an investigation into the relevant components.

#### SCHEMATIC

The schematic presented in figure 8.27 follows a typical design for a cold gas propulsion system that utilizes a mechanical pressure regulator. A fill/drain valve is included although it is feasible that if a compressed nitrogen cylinder is used this may be unnecessary.

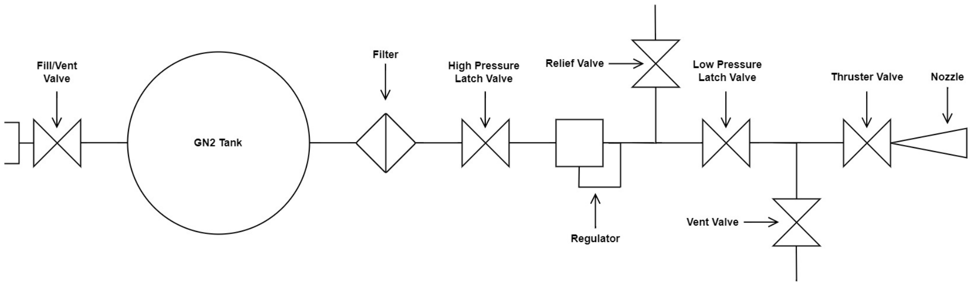


Figure 8.27: Feed System Layout Schematic

From the tank, the gas shall flow through a filter which is vital for filtering out impurities or particulates in the flow ensuring that neither the feed system nor the inflatable structure is damaged as desired by killer requirement REQ-ISI-04. Following the filter a normally closed high pressure isolation latch valve is included to isolate the tank from the rest of the system during non-operational periods. When in the open position, the gas flows through the isolation valve to the mechanical pressure regulator, which reduces the pressure level coming from the tank and maintains a desired constant pressure level downstream of it. After the regulator, a pressure relief valve is included for safety and redundancy reasons. Downstream is a normally open low pressure isolation latch valve. This is vital for enabling vent requirements REQ-ISP-02 (ascent venting) and REQ-ISP-05 as it isolates the rest of the inflation system from the thruster and the vent valve. The normally closed vent valve is included after this isolation valve. Finally, this is followed by the normally closed thruster valve and nozzle. This thruster valve is operated in pulse mode to provide controlled inflation to the structure.

During launch, both isolation valves are closed. The high pressure valve isolates the tank from the rest of the system while the low pressure valve isolates the system from the vent valve and nozzle. The normally closed vent valve is energized to open the valve while the thruster valve is also energized. In this fashion, ascent venting of the packaged inflatable structure can be implemented satisfying REQ-ISP-02. A similar process is utilized for venting the structure down to predetermined pressure post pressurization, satisfying REQ-ISP-05, while it can also be utilized in the case of over-pressurization of the structure. It should be noted that no sensors are included in the schematic, although they shall be required to monitor the upstream and downstream pressures and temperatures of the pressure regulator, the flow rate entering the inflatable structure as well as the pressure levels in the structure itself. The information provided by theses sensors shall be utilized by the complex control logic to implement the desired inflation scheme as described in section 8.3.

### COMPONENTS

From the schematic above based on a typical cold gas feed system, the following list of components are required for the preliminary design of this inflation system.

- Inflatant Tank
- Feed Lines
  - High Pressure
  - Low Pressure
  - Fittings/Joints
- Filter
- Valves
  - Fill/Vent Valve
  - Isolation-Latch Valves
    - High Pressure
    - Low Pressure
  - Regulator Valve
  - Relief Valve
  - Start/Stop Thruster (Inflation) Valve
- Nozzle
- TBD
  - Sensors
  - Non-propulsive venting nozzle

Ideally, it would be desired that all of these components are COTS so as to reduce the cost and time for development of such an inflation system. In addition, this would indicate the need for minimal design adjustments to current micropropulsion technology in order to facilitate the design of a feed system for inflation applications. Unsurprisingly, this is highly desirable. Thus, the design of the feed system shall investigate the use of COTS components and their suitability for the desired inflation system characteristics. For this investigation, an exploration of a selection of the main components shall be carried out. With the tank and inflation valve are dealt with in their own respective sections of this thesis, section 8.4 and section 8.3, these main components shall include the feed lines, fill/vent valve, filter, latch valves and the regulator. The selection of the sensors and a non-propulsive venting nozzle are TBD and shall be left for future work. It should be noted that as most components provide flow details in various different volumetric standards, all are converted to standard liter per minute (SLPM) for ease of comparison. The desired mass flow rate range (0.1 - 0.9 g/s) for Nitrogen gas expressed in SLPM is about 5-45 SLPM.

**Feed Lines**

It is assumed that the same diameter tubing is utilized through the system. Given the flow rates a tubing diameter of 4 mm was deemed suitable with the gas velocity through the tubing remaining well below the maximum flow velocity as given by equation 8.55 (Zandbergen, 2018):

$$V = 175 \cdot (1/\rho)^{0.43} \tag{8.55}$$

For the high pressure stage upstream of the regulator stainless steel tubing shall be utilized. Swagelok provides a range of stainless steel tubing. The SS-T6M-S-1,0M-6ME with an outer pipe diameter of 6mm and wall thickness of 1mm, provides working pressures up to 420 bar and a weight factor of 0.125 kg/m [10]. For the low pressure stage flexible tubing can be utilized. This enables more flexibility in routing the tube up to through the ejection mechanism to the inflatable structure. PFA tubing was chosen for this application. As Swaglok does not appear to provide weight factors for PFA tubing, the 3/16" PFA tubing provided by Parker [11] shall be utilized. It has an internal diameter of 1/8" (3.175mm), a working pressure of 22 bar and a weight of 0.021 kg/m. A summary of these piping characteristics is contained in figure G.1.

| **Type** | **Internal Diameter [mm]** | **MEOP [bar]** | **Weight Factor [kg/m]** |
|---|---|---|---|
| High Pressure Tubing | 4 | 420 | 0.125 |
| Low Pressure Tubing | 3.175 | 22 | 0.021 |

Table 8.8: Feed Lines

[10]https://www.swagelok.com/downloads/webcatalogs/en/ms-01-181.pdf
[11]http://www.texloc.com/tube_HP_pfa_table.html

**Fill/Vent Valve**

For the filling and venting of the inflatant tank, a Fill/Vent Valve (FVV) can be utilized. Table 8.9 provides a list COTS FVV's.

| **Parameter** | **Omnidea FVV** | **Nammo FVV** | **VACCO FVV** |
|---|---|---|---|
| Dimensions (mm) | 76 x $\phi$25$^\star$ | 78.5 x $\phi$22$^\star$ | 107.5 x $\phi$30$^\star$ |
| Mass (grams) | 91 | 50 | 113 |
| Operating Pressure (bar) | 350 | 328 | 275 |
| Leak rate internal (scc/s (GHe)) | <1 x $10^{-5}$ | «1 x $10^{-4}$ | <1 x $10^{-6}$ |
| Leak rate external (scc/s (GHe)) | <1 x $10^{-6}$ | <1 x $10^{-6}$ | <1 x $10^{-6}$ |
| Port diameter | 6.35mm | 6.35mm | 6.35mm |
| Filter Mesh Size ($\mu$m) | 2 | - | - |
| Reference | Webpage [12] | Webpage [13] | Webpage[14] |

$^\star$ = Dimensions given relate to attachments as such estimate of bodies diameter are made

Table 8.9: COTS Fill/Vent Valves

This component is not as integral to the performance of the system although maximizing its mass and volume requirements is important. From the 3D models presented in figure H.2, it is apparent that the VACCO FVV in particular is excessively large and while smaller the similarly sized Omnidea and Nammo options are still relatively bulky. However, it must be noted that the actual body dimensions for each of the valves are unclear and so estimates are made based on the provided drawings. It should also be noted that in figure H.2, the interfaces/ end connections of the Nammo FVV are considered not integral to its performance and are thus reduced in length. Despite this, it is apparent that all components are undesirably bulky. Clearly a smaller more compact FVV would be more desirable and unless a more suitable COTS can be found it is likely that there is a need for a custom sized component or the use of a custom built nitrogen cartridge could be explored. However, for this preliminary design the Nammo FVV shall be used for sizing due to it having the lowest mass and, based off the estimate, the most compact.

8

**Filter**

As has been mentioned, the filter is required to remove any impurities or particulates from the gas flow. Table 8.10 contains COTS high-pressure inline filters that were found. The first step in exploring the suitability of these COTS filter is to evaluate their size relative the volume constraints of the system. This is done by examining the 3D models presented in figure H.1 presented in the appendices. It is apparent that the Omnidea (due to both its size and shape), VACCO F1D10636-01 and VACCO F1D10286-02 filters are all clearly unsuitable for this system. Thus, the VACCO F1D10588-01 is the only one of the COTS filters presented that is a feasible option. This is further emphasized by the fact that is the only filter suited for the desired flow rates, although as discussed in section

[12] http://www.omnidea-rtg.de/site/images/stories/Downloads/Omnidea-RTG_Catalogue_Feb2016.pdf
[13] https://www.nammo.com/product/fdv-fvv/
[14] https://www.vacco.com/images/uploads/pdfs/V1E10648-01Rev.pdf

8.5.4, it experiences large undesirable pressure losses with increasing flow rates. However, as it is the only feasible COTS option it shall be used for the design and preliminary sizing of the inflation system.

| **Parameter** | **Omnidea Filter** | **VACCO F1D10636-01** | **VACCO F1D10588-01** | **VACCO F1D10286-02** |
|---|---|---|---|---|
| Dimensions (mm) | 50 x 30 x 30 | 88 x $\phi$28.5 OD | 42 x $\phi$14 OD | 53 x $\phi$28.5 OD |
| Mass (grams) | 76 | 250 | 24 | 113 |
| MEOP (bar) | 350 | 330 | 300 | 290 |
| ΔP vs Flow rate | 1 bar @ 5417.5 SLPM | 1.3 bar @ 6462.4 SLPM | 0.05 bar @ 5.798 SLPM | 0.02 bar @ 0.36 SLPM |
| Flow Coefficient | 0.704 | 0.76 | 0.0051 | 0.025 |
| Leak rate (scc/s (GHe)) | 0 | <1 x $10^{-6}$ | <1 x $10^{-6}$ | - |
| Filter Mesh Size ($\mu$m) | 2 | 10 | 40 | 2 |
| Port diameter (mm) | 6.35 | 6.35 | 6.35 | 6.35 |
| Reference | Webpage [12] | Webpage[15] | Webpage[15] | Webpage[15] |

Table 8.10: COTS Filter

**High Pressure Latch Valve**

The high pressure latch valve is required to isolate the tank from the rest of the system during non-operational periods. It is normally closed. For this isolation valve it is desired to use a solenoid latch valve so that the power requirements when in the open position can be reduced. High pressure COTS isolation latch valves that were found are contained in the following table 8.11.

Relative to the filter COTS components, the presented high pressure latch valves, except for the VACCO V8E10580-01, in table 8.11 provide flow rates in the desired flow rate range. As shown in section 8.5.4, they are particularly well suited for flow rates that tend towards 0.1 g/s. With respect to the size of the components, figure H.3 clearly indicates that the VACCO V8E10580-01's large size is unsuitable for the given volume constraints. Although the size of the two MOOG valves is unclear, the high mass of the MOOG 51E207 indicates it is likely similar in size to the VACCO V8E10580-01's while an estimate regarding the MOOG 051-212B, based on a similar sized MOOG cold gas thruster valve (The

[15]https://www.vacco.com/images/uploads/pdfs/VACCO_Filtration_Catalog101117FINALwithbookmarks.pdf
[16]https://www.moog.com/content/dam/moog/literature/Space_Defense/spaceliterature/propulsion/moog-electric-propulsion-isolation-valve-datasheet.pdf
[17]https://www.vacco.com/images/uploads/pdfs/latch_valves_high_pressure.pdf
[18]https://marotta.com/wp-content/uploads/2020/09/MV602L.pdf

| Parameter | MOOG 051-212B | MOOG 51E207 | VACCO V8E10580-01 | Marotta MV602L* |
|---|---|---|---|---|
| Dimensions (mm) | - | - | 79 x$\phi$34 OD | 24 x$\phi$8.5 OD |
| Mass (grams) | 170 | <230 | 160 | 100 |
| MEOP (bar) | 186 | 310 | 208 | 200 |
| $\Delta$P vs Flow rate | 1 bar at 20 SLPM (69 bar) | <0.69 bar at 42.1 SLPM (124 bar) | 0.5 bar at 141.5 SLPM (208 bar) (GHe) | 12.3 bar at 47.57 SLPM (100 bar) |
| Flow Coefficient | 0.00589 | 0.01108 | 0.0121 | ESEOD 0.014" $C_d = 0.6$ |
| Leak rate internal (scc/s (GHe)) | <8 x $10^{-4}$ | <1 x $10^{-4}$ (GN2) | <8 x $10^{-4}$ (GN2) | <1 x $10^{-4}$ |
| Leak rate external (scc/s (GHe)) | <1 x $10^{-6}$ | <1 x $10^{-6}$ | <1 x $10^{-6}$ | <1 x $10^{-6}$ |
| Response time (ms) | <50 | <50 | 15 | 30 |
| Cycle Life | > 18,000 | > 600 | > 20,000 | - |
| Port diameter | 3.175mm | - | 6.35mm | 6.35mm |
| Filter Mesh Size ($\mu$m) | 5 | - | 40 | - |
| Reference | Webpage[16] | (Bzibziak, 2000) | Webpage [17] | Webpage [18] |

* = The interfaces/ end connections are not considered integral to its performance and are thus not accounted for in the dimensions provided.

Table 8.11: COTS HP Isolation Valves

8

MOOG 58E163A [19]), does indicate it may provide a more attractive size than the VACCO V8E10580-01. Despite this promise, it is evident that the Marotta MV602L provides not only the most attractive size but also the the most attractive mass properties of the COTS valves presented. One drawback of note, as discussed in section 8.5.4, is that both it and the MOOG 051-212B experience a significant increase in losses with increasing flow rate relative to the VACCO V8E10580-01 and MOOG 51E207. While undesirable, the Marotta MV602L is still clearly the best suited of the COTS HP Latch valves. However, it should be acknowledged that an optimal solution would provide reduced pressure losses, likely necessitating a custom built component.

**Low Pressure Latch Valve**

The low pressure latch valve is required to isolate the venting system from the rest of the

[19]https://www.moog.com/content/dam/moog/literature/Space_Defense/spaceliterature/propulsion/moog-coldgasthrusters-datasheet.pdf

system during venting periods. It is normally open. For this isolation valve it is desired to use a solenoid latch valve so that the power requirements when in the open position can be reduced. Low pressure COTS isolation latch valves that were found are contained in the following table 8.12.

| **Parameter** | **V1E10728-01** | **Nammo LP** | **Marotta SPV187*** |
|---|---|---|---|
| Dimensions (mm) | 79 x$\phi$34 OD | 21 x$\phi$16 OD | 20 x$\phi$17 OD |
| Mass (grams) | 168 | 35 | 45 |
| MEOP (bar) | 28.5 | 20 | 10 (Nominal) |
| ΔP vs Flow rate | 0.2 bar at 8.05 SLPM | <0.05mbar at 0.054 SLPM | 0.12 bar at 23.76 SLPM |
| Flow Coefficient | 0.047 | 0.009 | ESEOD 0.067" $C_d = 0.6$ |
| Leak rate internal (scc/s (GHe)) | <3 x $10^{-4}$ | <1 x $10^{-4}$ | <1 x $10^{-4}$ |
| Leak rate external (scc/s (GHe)) | <1 x $10^{-6}$ | <1 x $10^{-6}$ | <1 x $10^{-6}$ |
| Response time (ms) | 15 | - | 100 |
| Cycle Life | 1,000 | - | - |
| Port diameter | 6.35mm | 6.35mm | 3.175mm |
| Filter Mesh Size ($\mu$m) | 40 | 25 | - |
| Reference | Webpage [20] | Webpage[21] | Webpage[22] |

* = The interfaces/ end connections are not considered integral to its performance and are thus not accounted for in the dimensions provided.

Table 8.12: COTS Low Pressure Valve

Despite attractive volume and mass properties, the low flow rate Nammo LP is unsuitable for the desired inflation flow rates due to the pressure losses it experiences as noted in section 8.5.4. However, it may be suitable for the venting process where the reduction in pressure is less critical and can take a number of hours. Further research into this process is required, but is not explored here due to the limited timeframe of the project. Thus, while not considered for the low pressure latch valve, it shall be utilized for the preliminary sizing of the venting valve.

With respect to the low pressure latch valve, of the two remaining valves, the Marotta SPV187 provides significantly more attractive mass and volume properties (see figure H.4) as well as pressure loss characteristics (section 8.5.4). It is apparent that is the most

[20]https://www.vacco.com/images/uploads/pdfs/latch_valves_low_pressure.pdf
[21]https://www.nammo.com/product/low-pressure-inline-fcv/
[22]https://marotta.com/wp-content/uploads/2020/09/SPV187.pdf

suitable of the three COTS LP valves presented here and shall be used for the preliminary design of the system. In addition, it is the only one of the components discussed so far that may not require a custom component to provide optimal performance.

**Regulator Valve**

Regulator valves are inherently bulky components and shall contribute significantly to the overall volume and mass of the inflation system. Table 8.13 provides details on the available COTS regulators found.

| **Parameter** | **Cobham B47630-1** | **Nammo Cold Gas PR** | **VACCO 66250 PR** | **US Para Plate 9014 Series** |
|---|---|---|---|---|
| Dimensions (mm) | 88 x 95 x 52 | 12 x $\phi$60 OD | 110 x $\phi$50 OD | 44 x $\phi$25 OD |
| Mass (grams) | 450 | 250 | 363 | 100 |
| Inlet Pressure (bar) | 330-40 | 250 | 250-24 | 205 |
| Regulated Pressure (bar) | 20-22 | 6 | 14.6 | 0-13.8 |
| Max Flow rate (SLPM (GN2)) | 3225 | 4.75 | 260-1160 | 190* |
| Leak rate internal (scc/s (GHe)) | <2.8 x $10^{-2}$ | <1 x $10^{-4}$ (GN2) | <0.3 (GN2) | - |
| Leak rate external (scc/s (GHe)) | <1 x $10^{-3}$ | <1 x $10^{-6}$ (GN2) | - | - |
| Cycle Life | 1 x $10^{6}$ | 1 year Mission Life | - | - |
| Port diameter (mm) | 9.525 | 6.35 | 6.35 | 6.35 |
| Integrated Filtration | Yes | - | Yes | Yes |
| Relief Valve | Yes | - | Yes | No |
| Stages | 1 | 1 | 1 | 2 |
| Reference | Webpage [23] | Webpage [24] | Webpage [25] | Webpage [26] |

* = Based off flow rate/pressure level graph

Table 8.13: COTS Mechanical Pressure Regulators

Of the presented COTS regulators it can be clearly seen from the 3D models presented in figure H.5 that the Cobham B47630-1 and VACCO 6250 are unsuitable for the volume constraints of the inflation system. The Nammo, while less massive than the other two, is also quite bulky with the US Para Plate 9014 Series presenting the only regulator with attractive mass and volume properties. In addition, the Nammo's max flow rate lies about 0.1 g/s, and is unsuitable for higher mass flow rates. As such it is ill suited for this system, with the US Para Plate 9014 Series offering a more suitable flow rate range. However, unlike the other regulators, in order to ensure that this regulator provides a constant outlet pressure it is likely that it must be utilized in a two stage configuration as is done for the similar cold gas system, Adelis-SAMSON (Zaberchik et al., 2019). An image of this configuration is provided in figure 8.28.

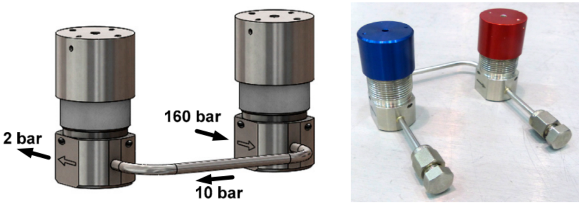


Figure 8.28: Adelis-SAMSON Two Stage Pressure Regulation System (Zaberchik et al., 2019)

Unfortunately, few details are available on the Adelis-SAMSON regulator system which was custom built and so its flow characteristics are unknown. However, from the details provided it is apparent that the individual regulators are similar in size and mass (110 grams) to the US Para Plate 9014 Series regulator and are required to regulate a tank pressure of 160 bar. As the operation of the regulator shall not be investigated in detail it shall be assumed that the US Para Plate 9014 Series regulator two stage system shall provide the same pressure regulation properties as that used for the Adelis-SAMSON, i.e. the first regulator shall reduce the system pressure down to at most 10 bar and the second regulator shall reduce the pressure down again to at most 2 bar, as seen in figure 8.28. Despite requiring a two stage system, the total mass (200 grams) is still the lowest of the regulators evaluated and given its shape also provides the greatest volumetric efficiency. Thus US Para Plate 9014 Series regulator shall be utilized for the preliminary sizing of this system in a two stage configuration. However, seeing as it does not contain an integrated relief valve, a COTS relief valve from The Lee company, such as the 250 PRI [27], shall be utilized for the sizing of the system with its performance being neglected for this present thesis discussion. For a custom regulator it may be desirable to have an integrated relief valve.



[23] https://www.cobhammissionsystems.com/space-propulsion-systems/hypersonic-reaction-control-regulator/hypersonic-reaction-control-regulator/docview/

[24] https://www.nammo.com/wp-content/uploads/2021/03/2021-Nammo-Ireland-Mechanical-Pressure-Regulator.pdf

[25] https://www.vacco.com/images/uploads/pdfs/regulators.pdf

[26] https://circoraerospace.com/pdf/Pressure-Regulators-Mini)-9014-Series.pdf

[27] https://www.theleeco.com/product/250-pri/

**Summary**

A summary of the components required for this inflation system design is contained in table 8.14.

| **Component** | **Selected COTS Option** |
|---|---|
| Fill/Vent Valve | Nammo FVV |
| Inflatant Tank | NA |
| **High Pressure Section** | - |
| Stainless Steel Tubing | Swagelok |
| Filter | VACCO F1D10588-01 |
| HP Latch Valve | Marotta MV602L |
| *Regulator* | US Para Plate 9014 Series x2 |
| *Relief Valve* | Lee Company 250 PRI |
| **Low Pressure Section** | - |
| PFA Tubing | Parker |
| LP Latch Valve | Marotta SPV187 |
| Vent Valve | Nammo LP |
| Inflation Valve | MOOG 058E142A |
| Nozzle | NA |

Table 8.14: Component Summary



### 8.5.4. PRESSURE LOSS

One of the most critical considerations for the feed system is its pressure distribution. The pressure variations from the tank, through the feed system and into the thruster determine the inflatant flow rate. As has been discussed, the major pressure variation in this system shall be induced by the pressure regulator which will reduce the high pressure gas coming from the tank to a pressure more suitable for the nozzle. However, as the inflation gas flows through the feed system, friction losses lead to a further drop in pressure. These must be accounted for in the design of the system.

#### PRESSURE LOSS DUE TO FRICTION

To calculate the pressure loss due to friction, the Darcy-Weisbach relation, equation 8.56, is used.

$$\Delta P = f \frac{L}{D} \frac{1}{2} \rho V^2 \tag{8.56}$$

where:

- $\Delta P$ = Pressure loss (Pa)

- $f$ = Friction factor
- $L$ = Characteristic length (m)
- $D$ = Pipe diameter (m)
- $\rho$ = Flow density (m/s)
- $V$ = Flow velocity (m/s)

This equation is primarily used for calculating the pressure loss in the piping. The friction factor f, is dependent on the Reynolds number of the flow and the pipe smoothness. The Reynolds number is calculated using the pipes hydraulic diameter as seen in equation 8.57.

$$Re_D = \frac{\rho \cdot V \cdot D}{\mu} \tag{8.57}$$

A moody chart or empirical relations can be utilized to calculate the friction factor according to the Reynolds number value, which indicates laminar, transitional or turbulent flow. For this project, the following empirical relations shall be utilized (Zandbergen, 2018).

- For fully development incompressible laminar flow ($Re_D < 2320$)

$$f = \frac{64}{Re_D} \tag{8.58}$$

- For fully development incompressible turbulent flow
  - $2320 < Re_D < 2 \times 10^4$

$$f = 0.316 \cdot \left(\frac{1}{Re_D}\right)^{0.25} \tag{8.59}$$

  - $2 \times 10^4 < Re_D < 10^6$

$$f = 0.184 \cdot \left(\frac{1}{Re_D}\right)^{0.2} \tag{8.60}$$

- For non-smooth pipes at high Reynolds number, the friction coefficient is independent of $Re_D$ and can be found using the following equation:

$$f = 8 \cdot \left(2.457 \cdot \log\left(3.707 \cdot \frac{1}{e/D}\right)\right)^{-2} \tag{8.61}$$

where:

- e = Surface roughness (mm)

8

### PRESSURE LOSS DUE TO AREA CHANGE

In the case of the gas flowing from a pipe with diameter of one size to a pipe with a diameter of another, or in the upstream case to/from the tubing to/from the major components, there is a pressure loss associated with the change in area. This pressure loss is defined in terms of the resistance coefficient $\zeta$. This resistance coefficient is calculated under two different conditions:

- Sudden Contraction:

$$\zeta_c = 0.5 \cdot \left(1 - \frac{A_{small}}{A_{large}}\right)^{\frac{3}{4}} \tag{8.62}$$

- Sudden Expansion:

$$\zeta_e = \left(1 - \frac{A_{small}}{A_{large}}\right)^2 \tag{8.63}$$

Once $\zeta$ is found, the pressure loss due to the area change can be calculated using equation 8.64:

$$\Delta P = \frac{1}{2} \cdot \zeta \cdot \rho \cdot \left(V_{small}^2 - V_{large}^2\right) \tag{8.64}$$

### PRESSURE LOSS DUE TO FLOW COEFFICIENT

For calculating the pressure loss in components such as valves, filter etc, it is best to use values provided by the manufacturer. However, this is not necessarily a straight forward process. If data is provided it is typically given for one particular fluid/gas. Utilizing such values would therefore not be appropriate for gauging the pressure loss for nitrogen. Therefore, in order to find the pressure loss across the valves presented above the gas flow coefficient $C_v$ must be calculated. A guide to calculating this value for gas and fluids is presented in this document provided by Swagelok [28].

- For calculating the $C_v$ for gas flow:

$$C_v = \frac{Q_g}{N_2 \cdot P_1 \left(1 - \frac{2\Delta P}{3P_1}\right) \cdot \sqrt{\frac{\Delta P}{P_1 \cdot G_g \cdot T_1}}} \tag{8.65}$$

- For calculating the $C_v$ for liquid flow:

$$C_v = \frac{Q_l}{N_1 \sqrt{\frac{\Delta P}{G_f}}} \tag{8.66}$$

where:

- $C_v$ = Gas flow coefficient
- $Q_g$ = Gas flow rate (SLPM)

[28] https://www.swagelok.com/downloads/webcatalogs/EN/MS-06-84.PDF

- $Q_l$ = liquid flow rate (LPM)
- $P_1$ = Inlet pressure (bar)
- $\Delta P$ = Pressure drop (bar)
- $T_1$ = Upstream temperature (K)
- $G_g$ = Gas specific gravity
- $G_f$ = Liquid specific gravity
- $N_1$ = Liquid numerical constant (14.42)
- $N_2$ = Gas numerical constant (6950)

Using these equations, $C_v$ can be calculated for feed system components given the inlet pressure, temperature, pressure loss and flow rate of the gas. Once this has been done, the pressure loss across the components can then be calculated for a range of inlet pressures and flow rates. This is done for all of the COTS components presented previously except the two Marotta components who's data is provided in terms of the Equivalent Square Edge Orifice Diameter (ESEOD), which is given by d in the equation 8.67, and the discharge coefficient $C_d$. For these components the following equation for orifice flow is utilized [29].

$$Q = C_d \cdot \frac{\pi}{4} \cdot d^2 \sqrt{\frac{2 \cdot \Delta P}{\rho \cdot \left(1 - \left(\frac{d}{D}\right)^4\right)}} \tag{8.67}$$

where:

- $Q$ = Flow rate ($m^3/s$)
- $C_d$ = Discharge Coefficient
- $d$ = ESEOD (m)
- $\Delta P$ = Pressure drop (Pa)

### PRESSURE LOSS ACROSS MAJOR COMPONENTS

One of the leading factors in gauging the suitability of a COTS component is to establish its pressure loss characteristics at the desired pressure levels and flow rate range. This plays a crucial role in establishing the suitability of cold gas micropropulsion technology for CubeSat inflation applications. In this section the pressure loss across the upstream and downstream components shall be investigated, with the associated graphs only plotting the sub critical pressure drop across the valves, as reaching a critical pressure drop ($\Delta P > 1/2 P_{input}$) is clearly undesirable. These results informed the decision making process carried out above regarding the main COTS components.

[29] https://www.engineeringtoolbox.com/orifice-nozzle-venturi-d_590.html

For components upstream of the pressure regulator, the system pressure shall decrease as the tank empties. This in turn means that the pressure loss across the upstream components shall vary over time. This relationship between pressure loss and tank pressure shall be investigated for the upstream components. The components downstream of the pressure regulator, on the other hand, do not experience a change in pressure with a constant downstream pressure ensured by the regulator. Thus, the pressure loss across the downstream components shall be investigated with respect to different regulated pressures. The upstream and downstream components can be seen in the feed system layout presented in figure 8.27.

**Filter**

Figure 8.29 presents graphs of the pressure drop against the tank pressure for each of the COTS filters presented in table 8.10. It can clearly be seen from this table that the Omnidea and VACCO F1D10636-01 filters are designed for flow rates far in excess of the desired range and as such their pressure loss characteristics shall not be explored.

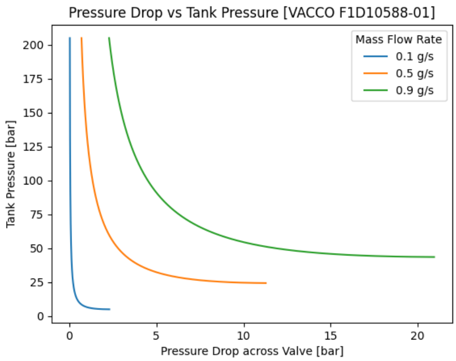


(a) VACCO F1D10588-01

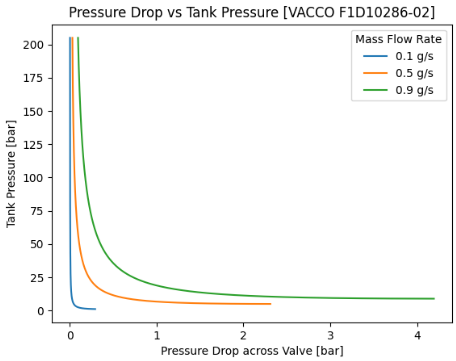


(b) VACCO F1D10286-02

Figure 8.29: Graphing of Pressure Loss Across COTS Filters

Of the remaining two valves it can be seen from figure 8.29, that the VACCO F1D10286-02 provides the more attractive pressure loss characteristics thanks to its higher flow coefficient value. However, as discussed in section 8.5.3,its bulky nature makes it an unfeasible option. The VACCO F1D10588-01, on the other hand, has attractive mass and volume properties and is well suited to the lower end of the flow rate range, as seen in figure 8.29a. However, it does experience a substantial increase in pressure losses with increasing flow rate.

**High Pressure Latch Valves**

The pressure losses across the COTS high pressure latch valves presented in table 8.11 are graphed in figure 8.30. It can be clearly seen that all of the valves experience significantly lower pressure losses as the flow rate tends towards 0.1 g/s. This is particularly true for the Moog 051-212B and Marotta MV602L, both of whom exhibit similar pressure losses and experience significant increases in losses with higher mass flow rates.

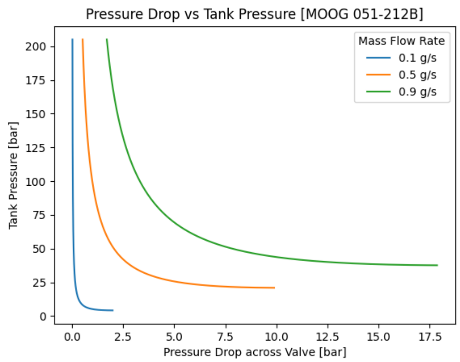


(a) Moog 051-212B

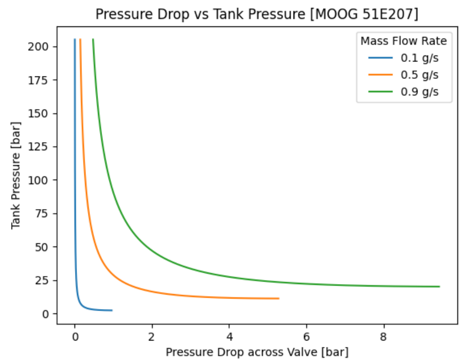


(b) Moog 51E207

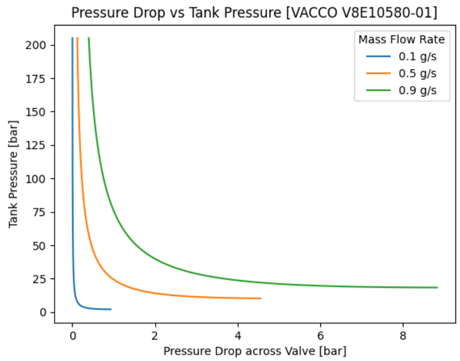


(c) VACCO V8E10580-01

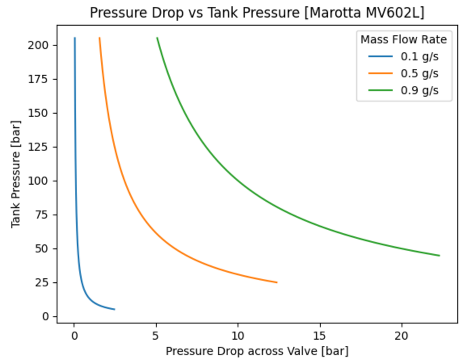


(d) Marotta MV602L



Figure 8.30: Graphing of Pressure Loss Across COTS HP Valves

The VACCO V8E10580-01 and MOOG 51E207 on the other hand, experience lower pressure losses as well as a less significant increase with higher mass flow rates. The fact that these two are better equipped to handle higher flow rates relative to the MOOG 051-212B is unsurprising due to their higher flow coefficient values.

**Low Pressure Latch Valves**

The pressure loss across the low pressure latch valve depends on the chosen regulated pressure. Figure 8.31 presents the pressure loss across the VACCO V1E10728 and Marotta SPV187 valves at a range of downstream regulated pressures. It is apparent that the higher the regulated pressure, the lower the pressure loss. The low flow rate Nammo valve is not presented as results clearly indicated its flow coefficient value is unsuitable for the desired mass flow rate range.

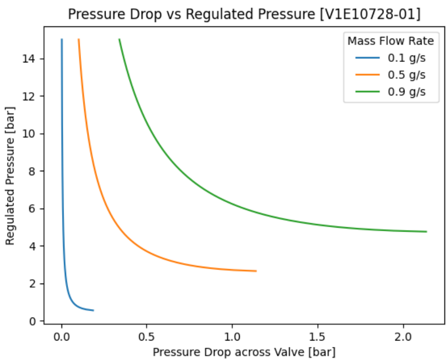


(a) VACCO V1E10728-01

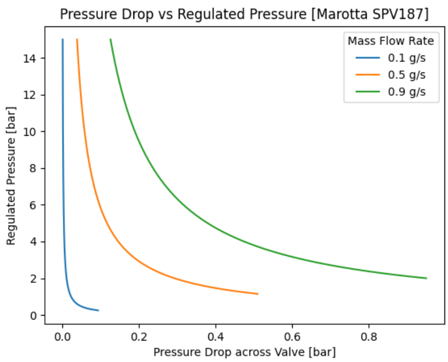


(b) Marotta SPV187

Figure 8.31: Graphing of Pressure Loss Across COTS LP Valves

Of the two valves presented it is apparent that the Marotta SPV187 experiences pressure losses about half those of the VACCO V1E10728-01, resulting in chamber pressures closer to the regulated pressure.

### PRESSURE LOSS ACROSS SYSTEM

In conjunction with the other components discussed for this feed system, the most appropriate COTS components can be utilized to gain an estimate of the upstream and downstream pressure losses utilizing the equations given at the start of this pressure loss section. This shall enable an appropriate estimation of the system performance as the pressure loss through the system dictates the quantity of usable inflation gas within the inflatant tank as well as the operational chamber pressure of the nozzle and by extension the nozzles expansion ratio. It is thus an important consideration in gauging the impact of the feed system layout on the performance of the inflation system.

8

#### Geometry Estimation

In order to make a preliminary estimate of the mass and volume requirements of the feed system, in addition to the pressure drop across it, the systems geometry must be established. For this preliminary design an estimate of the systems geometry shall be made based off a rough 3D model of how the major system components may be placed within the systems volume constraints. This model can be seen in figure 8.32. From this 3D model an estimate of the piping and associated components such as 90 degree bends and T-Junctions can be estimated. It is envisioned that the upstream section shall consist of two 20mm long straight sections and three 90 bends to guide the gas from the tank through the filter and latch valve and onto the regulator system. The regulator system is assumed to be a whole unit so additional piping shall not be considered. Meanwhile, downstream of the regulator it is envisioned that the flexible tubing will consist of four 90 degree bends and three straight sections as well as two T-Junctions that are assumed to have the same diameter as the tubing. Unlike their upstream counterparts, the tubing sections that consist of a 90 degree bend(s) and a straight section are one uniform piece of flexible tubing. The 90 degree bends are included here to demonstrate the minimum acceptable bend radius for the flexible tubing[11]. These components shall be required to guide the gas from the regulator through the latch valve and up to the inflation valve and nozzle from where the structure is inflated. A synopsis of this estimated geometry can be found in table 8.15.

| Component | Length (mm)/ Equivalent Length | Flow Coefficient (Cv) | Inner Diameter (mm) | e/D |
|---|---|---|---|---|
| **High Pressure Section** | | | | |
| Straight | 20 | - | 4 | $3.75\times10^{-4}$ |
| 90 Bend | 20D | - | 4 | $3.75\times10^{-4}$ |
| Filter | 42 | 0.0051 | 6.35 | - |
| 90 Bend | 20D | - | 4 | $3.75\times10^{-4}$ |
| Latch Valve | 24 | ESEOD 0.014" $C_d = 0.6$ | 6.35 | - |
| 90 Bend | 20D | - | 4 | $3.75\times10^{-4}$ |
| Straight | 20 | - | 4 | $3.75\times10^{-4}$ |
| *Regulator* | - | - | 6.35 | - |
| **Low Pressure Section** | | | | |
| Relief Valve | 18D | - | 6.35 | $2.36\times10^{-4}$ |
| T-Junction | 20D | - | 3.175 | $4.72\times10^{-4}$ |
| Straight (flex) | 50 | - | 3.175 | 0 |
| 90 Bend (flex) | 19.05 | - | 3.175 | 0 |
| Latch Valve | 20 | ESEOD 0.067" $C_d = 0.6$ | 3.175 | - |
| 90 Bend | 19.05 | - | 3.175 | 0 |
| Straight | 100 | - | 3.175 | 0 |
| 90 Bend | 19.05 | - | 3.175 | 0 |
| Straight | 50 | - | 3.175 | 0 |
| 90 Bend | 19.05 | - | 3.175 | 0 |
| T-Junction | 20D | - | 3.175 | $4.72\times10^{-4}$ |
| Inflation Valve | 300D | - | 6.35 | $2.36\times10^{-4}$ |

Table 8.15: Geometry Estimation

In order to calculate the pressure loss through components where insufficient information is given an estimate can be made using the darcy weisbach equation (equation 8.56). This shall be done for the piping components as well as for the relief valve and inflation valve. In order to utilize the darcy weisbach equation for the components where the length is unknown, it is taken to be equal to its characteristic length, which is usually expressed in pipe diameters. Table 8.15 provides estimates of these $L_{eq}/D$ values (Zandbergen, 2018). For all these components, except the flexible tubing, a surface roughness estimate for stainless steel tubing is taken to be 0.0015 mm. For the flexible tubing the surface roughness is assumed equal to 0. Both of these values are taken from Zandbergen, 2018.

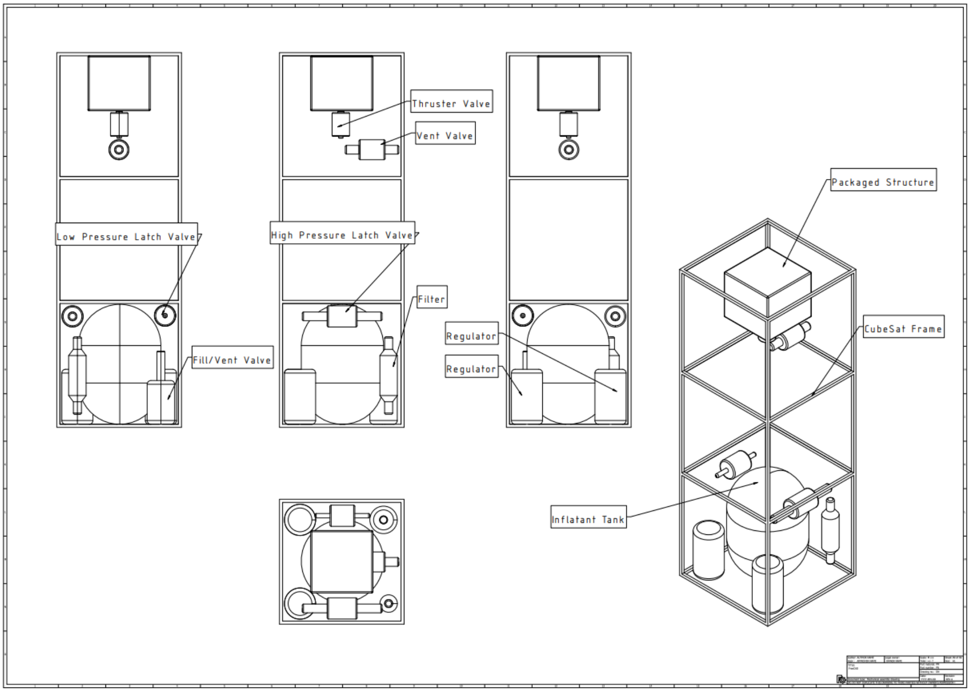


Figure 8.32: Basic 3D Model of System. Tubing not included.



**Upstream Pressure Loss**

A graph of the pressure drop against tank pressure is shown in figure 8.33a. As the inflation gas leaves the tank, the pressure inside the tank decreases. Comparing the pressure drop values to those presented for the latch valve and filter components in figures 8.30d and8.29a, it is apparent that both the VACCO F1D10588-01 filter and Marotta MV602L are far better suited for the reduced flow rates values now being examined. In addition, it also clear that they both the dominate the upstream pressure loss. This can be seen in table 8.25 which provides a breakdown of the losses of each contributing component.

As noted, as the pressure in the tank decreases, it tends towards the regulator inlet pressure. In order to avoid choked flow, the tank pressure must remain above the minimum inlet pressure of the regulator. Therefore the final tank pressure is given by the equation 8.68.

$$P_{\text{tank}_{final}} = P_{\text{regulator inlet}_{min}} + P_{\text{Losses}_{Upstream}} \tag{8.68}$$

The final tank pressure against the regulator inlet pressure is graphed in figure 8.33b. As mentioned, lower mass flow rates are more suitable for the COTS components being uti-

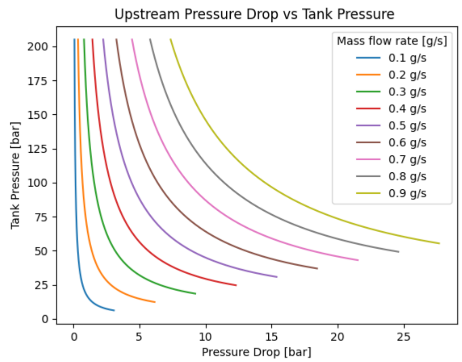


(a) Upstream Pressure Drop at multiple mass flow rates

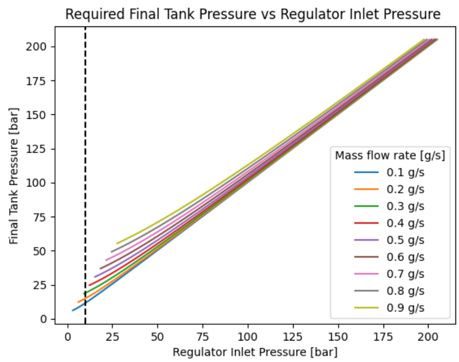


(b) Upstream Tank Pressure vs Regulator Inlet

Note: Black dashed line = Minimum Regulator Inlet Pressure

Figure 8.33: Graphing of Upstream Pressure Loss across mass flow rate range

lized and thus enable lower operational pressures due to their reduced losses. This can be clearly seen in figures 8.33a and 8.33b where the reduced losses enable lower final tank pressures and by extension a lower ullage gas requirement. It should be noted however, that due to the minimum regulator inlet pressure of 10 bar, the advantage of mass flow rates of $\leq 0.3$ g/s is somewhat negated, as seen in figure 8.33b. Establishing this upstream relationship is an important consideration when determining the most suitable mass flow rate for the inflation of the structure, as well as the desired performance parameter of the pressure regulator.

**Downstream Pressure Loss**

8

A graph of the pressure drop against regulated pressure is shown in figure 8.34a. The isolation valve is the main contributor to the pressure loss in the downstream condition as can be seen in table 8.26. As noted the COTS Marotta SPV187 isolation valve is well suited for the desired flow rate and pressure range and as such the downstream pressure losses are closer to the optimum than their upstream counterparts.

$$P_{\text{chamber}} = P_{\text{regulator outlet}} - P_{\text{Losses}_{downstream}} \tag{8.69}$$

As the regulator is upstream of the nozzle chamber, the chamber pressure can be determined as a function of the regulator outlet pressure and the pressure losses as seen in equation 8.69. This relationship is graphed in figures 8.34a and 8.34b. Meanwhile figure 8.34c graphs the maximum acceptable chamber pressure for a given expansion ratio for each of the mass flow rates, according to the fabrication constraints as discussed in section 8.2.

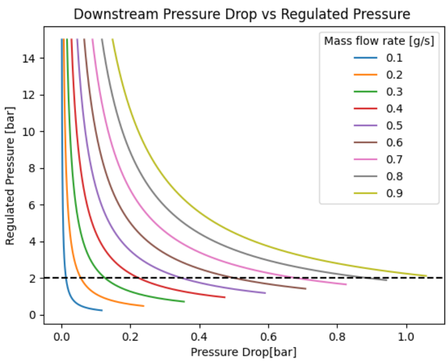


(a) Downstream Pressure Drop vs Regulated Pressure

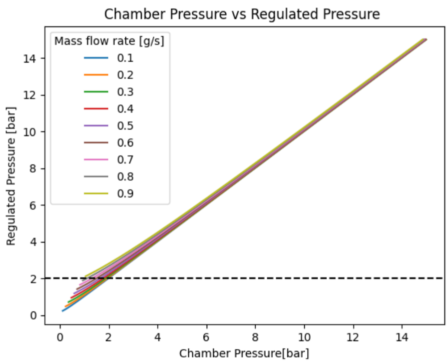


(b) Chamber Pressure vs Regulated Pressure

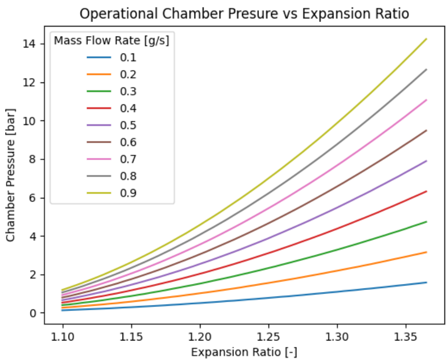


(c) Max. Operational Chamber Pressure vs Expansion Ratio

Note: Black dashed line = Minimum Regulator Outlet Pressure

Figure 8.34: Graphing of Downstream Pressure Loss across mass flow rate range

As can be seen from table 8.16, due to the minimum regulator outlet pressure of 2 bar, mass flow rates ≤ 0.8 g/s yield minimum chamber pressures greater than that required to achieve the minimum expansion ratio of 1.1. This is an important result to establish as it indicates that at these mass flow rates the pressure losses experienced in the feed system shall impede the selection of the most optimal nozzle expansion ratio ($\varepsilon = 1.1$). Table 8.26 provides a breakdown of the downstream losses of each contributing component.

| **Mass Flow Rate (g/s)** | **Min. Regulated Pressure (bar)** | **Min. Chamber Pressure (bar)** | **Max. Chamber Pressure (bar) @ $\varepsilon$ = 1.1** |
|---|---|---|---|
| 0.1 | 2 | 1.986 | 0.132 |
| 0.2 | 2 | 1.948 | 0.265 |
| 0.3 | 2 | 1.878 | 0.397 |
| 0.4 | 2 | 1.781 | 0.53 |

| | | | |
|---|---|---|---|
| 0.5 | 2 | 1.656 | 0.662 |
| 0.6 | 2 | 1.504 | 0.794 |
| 0.7 | 2 | 1.325 | 0.926 |
| 0.8 | 2 | 1.119 | 1.059 |
| 0.9 | 2.12 | 1.071 | 1.192 |

Table 8.16: Minimum Chamber Pressures

**Summary**
This section explored the relationship between the estimated geometry of the system and the pressure loss across it. It indicated the suitability of the upstream COTS components for lower flow rates as well as showing the relationship between the final tank pressure and the minimum regulator inlet pressure. It was apparent from this exploration that lower mass flow rates induce lower pressure losses across the system and as such require lower ullage gas mass requirements enabling larger quantities of usable gas to be stored within the inflatant tank. The exploration of the downstream pressure loss indicated the same relationship between lower mass flow rates and pressure loss. In addition, it also showed the relationship between the regulator outlet pressure and the nozzle chamber pressure. This investigation showed that at mass flow rates less than or equal to 0.8 g/s the pressure losses experienced downstream of the regulator actually impede the selection of the minimum optimal expansion ratio. Finally, it must be considered that while not entirely accurate, these pressure loss calculations do give a good working value for the preliminary design of the inflation system

### 8.5.5. CONCLUSION

This section provides the last major stage of the design process for the inflation system. From investigating two different possible feed system types, it becomes apparent that in order to satisfy the desired inflation requirements the use of mechanical pressure regulator offers a more suitable feed system than utilizing expansion/refill chambers. Thus a pressure regulated feed system is designed and its layout is formulated. This layout, which does not account for additional sensors that are required, incorporates an additional aspect not seen in conventional cold gas feed systems, the venting subsection. This section is isolated from the rest of the feed system during venting operations allowing the structure to be vented as needed. While not explored in detail here, this design feature is important for the relevance of this inflation system design to rigidizable inflatable structures. This is important as the limitations of pressure stabilized structures makes the development of long duration BEOC inflatable reflectors unfeasible at present, as noted in section 8.4, and thus advancements in rigidization technology are required. With the incorporation of this venting section, this feed system shall be suitable for inflating and venting such structures.

As is done for the inflation valve, a range of COTS options are evaluated for the major feed system components. They are evaluated primarily according to their mass, volume and pressure loss characteristics. This investigation helped to inform the selection of the most appropriate COTS components and whether a custom component is desirable or needed. As was the case for the inflation valve it was found that current COTS components have the potential to be utilized in the design of a BEOC inflation system, thus successfully addressing the desire to utilize current micropropulsion technology as stated in the projects mission statement. For the upstream section components, the VACCO F1D10588-01 filter and Marotta MV602L high pressure latch valve were found to be the most promising, although both yield large increases in losses with increasing mass flow rate. Custom built components may provide more suitable pressure characteristics, thereby reducing ullage gas requirements and increasing maintenance life. In addition, none of the COTS Fill/Vent valves evaluated provided particularly attractive options due to their relative bulk. As such, a custom component may also be required. Downstream the Marotta SPV187 is clearly a suitable COTS component for the low pressure latch valve.

Addressing the pressure loss across the system, it is apparent that operating the system at lower mass flow rates shall enable a greater quantity of usable inflatant to be stored onboard due to the reduction in the required final tank pressure. However, it was also found that operating at lower mass flow rates (≤0.8 g/s) impeded the selection of the minimum nozzle expansion ratio. This arises from the consideration of a 2 bar minimum regulator outlet pressure stemming from a similar cold gas system (Zaberchik et al., 2019).

## 8.6. Mass Flow Rate

The final step in this design process of the inflation system is to tie the design considerations made regarding the inflatant tank and pressure losses upstream with those made regarding the nozzle, inflation valve and pressure losses downstream. This can be done through the selection of an optimal mass flow rate. A critical factor in the design considerations of all the main components of the inflation system, the optimal mass flow rate shall be identified by evaluating its on the upstream and downstream conditions of the system.

8

### 8.6.1. Upstream

The upstream considerations regarding the mass flow rate consist of its impact on the regulator inlet pressure, the final tank pressure and the mission lifetime. As noted in section 8.5, as the tank empties, the higher the mass flow rate the higher the pressure losses experienced upstream. From figure 8.33, it is apparent that this means higher mass flow rates reach the critical pressure limit at higher pressures, thus requiring higher final tank pressures and by extension higher minimum regulator inlet pressures. This can be clearly seen in table 8.17, where the consequence of the higher final tank pressures is apparent in the higher quantity of ullage gas required. As alluded to in section 8.4, this reduces the quantity of usable inflatant gas that can be stored within the inflatant tank thus lessening the duration for which pressure maintenance can be maintained. This results in a difference in maintenance life between 0.1 g/s and 0.9 g/s of 5.5 days, varying from 27.5 to 33 days. As a result of these relatively short lifespans, which are a consequence of the drawbacks of using pressure stabilized structures, the importance of the maintenance life is somewhat diminished with the longer mission duration's of lower mass flow rates being desirable but not hugely impactful to the overall design of the system.

Table 8.17: Upstream Conditions

| Mass Flow Rate (g/s) | Min. Regulator Inlet Pressure (bar) | Final Tank Pressure (bar) | Ullage Gas Mass (grams) | Maintenance Life (days) |
|---|---|---|---|---|
| 0.1 | 10.0 | 11.55 | 3.24 | 33 |
| 0.2 | 10.0 | 14.93 | 4.18 | 32.5 |
| 0.3 | 10.0 | 18.96 | 5.31 | 32 |
| 0.4 | 12.5 | 24.75 | 6.92 | 31.5 |
| 0.5 | 15.5 | 30.85 | 8.63 | 30.5 |
| 0.6 | 18.5 | 36.95 | 10.33 | 30 |
| 0.7 | 22 | 43.36 | 12.12 | 29 |
| 0.8 | 25 | 49.46 | 13.82 | 28.5 |
| 0.9 | 28 | 55.56 | 15.53 | 27.5 |

### 8.6.2. DOWNSTREAM

The downstream consideration regarding the mass flow rate consist of its impact on the regulator outlet pressure, chamber pressure and expansion ratio, as well as the nozzle performance and the inflation rate. These considerations shall be tackled sequentially in this discussion.

#### CHAMBER PRESSURE

As noted in section 8.5, the regulator shall provide a minimum outlet pressure of 2 bar. This causes a problem for mass flow rates ≤ 0.8 g/s. From figure 8.34c, it can be seen that at lower mass flow rates, the maximum acceptable chamber pressure required for minimizing expansion ratio is lower. As a result, at a minimum regulator outlet pressure of 2 bar, the lower pressure losses experienced at mass flow rates less than ≤ 0.8 g/s yield chamber pressures higher than these maximum acceptable values. This hinders the selection of a minimum expansion ratio, as was clearly noted in table 8.16.

| Mass Flow Rate (g/s) | Chamber Pressure (bar) | Regulated Pressure (bar) | Min. Expansion Ratio |
|---|---|---|---|
| 0.1 | 1.986 | 2.0 | > 1.36 |
| 0.2 | 1.943 | 2.0 | 1.282 |
| 0.3 | 1.873 | 2.0 | 1.223 |
| 0.4 | 1.775 | 2.0 | 1.186 |
| 0.5 | 1.650 | 2.0 | 1.160 |
| 0.6 | 1.498 | 2.0 | 1.141 |
| 0.7 | 1.318 | 2.0 | 1.120 |
| 0.8 | 1.111 | 2.0 | 1.102 |
| 0.9 | 1.189 | 2.207 | 1.1 |

8

Table 8.18: Chamber Pressures and Expansion Ratio

Table 8.18 gives the minimum achievable expansion ratios for the mass flow rate range. It can clearly be seen that for mass flow rates ≤ 0.8 g/s, the lower the mass flow rate, the higher the minimum achievable expansion ratio. This results in a major difference in expansion ratio between 0.8 g/s, which is close to optimal, and 0.1 g/s, which exceeds the maximum of 1.36 and is thus discounted. In addition, for mass flow rates greater than 0.8 g/s a regulator outlet pressure greater than 2 bar is required to satisfy the minimum expansion ratio requirements.

### NOZZLE PERFORMANCE

Table 8.19 details the performance and configuration of the inflation system thruster. This is done for the mass flow rate range of 0.2 g/s to 0.9 g/s using the equations and relations discussed in section 8.2. These results shall be discussed with regards to the most important parameters associated with the selection of the most desirable mass flow rate. These are most notably the three key inflation requirements; real mass flow rate $m_{real}$, real gas exit temperature $T_{e_{real}}$ and real gas exit velocity $V_{e_{real}}$. Given the low chamber pressures and mass flow rates, the throat Reynolds number $Re_t$ is well below the 100,000 threshold. Thus the development of a boundary layer within the throat shall contribute to the real performance of the system.

- Real Mass Flow Rate
  - The contribution of the boundary layer build up in the throat can best be demonstrated in its impact on $m_{real}$ in the form of the discharge coefficient $C_d$. As seen in equation 8.40, $C_d$ is dependent $Re_t$ and throat curvature $R_u$, with higher $Re_t$ and $R_u$ both contributing to an increase in $C_d$ (see figure 8.10a). However, from table 8.19 it can be seen that across the mass flow rate range $C_d$ stays about the same. This is because while $Re_t$ increases with increasing mass flow rate, $R_u$ decreases due to the corresponding decrease in expansion ratio $\varepsilon$. This decrease arises from the fabrication constraint imposed on $R_u$.
- Real Exit Temperature
  - The impact of the decrease in expansion ratio $\varepsilon$ with increasing mass flow rate can also be appreciated by examining $T_{e_{real}}$. From 0.2 g/s to 0.7 g/s, $T_{e_{real}}$ increases from 195.439 K to 213.607 K due to the decrease in $\varepsilon$. While all of these temperatures are well above the minimum $T_{e_{real}}$ requirement of 160 K (REQ-ISI-04-01), higher values are attractive due to the desire to maximize $T_{e_{real}}$. For mass flow rates ≥ 0.8 g/s, $T_{e_{real}}$ lies at around 216K, due to the relatively constant $\varepsilon$. As was discussed in section 8.2.3, this relationship highlights the impact of the expansion ratio $\varepsilon$ on the exit temperature $T_{e_{real}}$, with the decrease in efficiency $\xi_T$ with a decreasing $R_u$ having a limited impact on results.

8

- Real Exit Velocity
  - This variation in parameters with mass flow rate and expansion ratio is also true for $V_{e_{real}}$. It decreases from 458.247.785 m/s (Mach 1.422) to 416.536 (Mach 1.293) from 0.2 g/s to 0.7 g/s and for mass flow $\geq$ 0.8 g/s $V_{e_{real}}$ lies at around 410 m/s (Mach 1.272). While all mass flow rates satisfy the the $V_{e_{real}}$ requirement (REQ-ISI-04-04), which desires the gas velocity be less than 483.38 m/s (Mach 1.5), lower values are attractive due to the desire to minimize $V_{e_{real}}$. Once again, the efficiency $\xi_V$ which increases with decreasing $R_u$ has a limited impact on results.

These results indicate that, given the design adjustments discussed during the design of the inflation nozzle (section 8.2), mass flow rates from 0.2 g/s to 0.9 g/s all satisfy the desired driving velocity and thermal requirements of the nozzle design. Moreover, given the discussion regarding chamber pressure, higher mass flow rates enable the nozzle to be designed with lower expansion ratios. This derives from the fabrication constraint of 100 $\mu$m imposed on the difference in throat and exit diameters. This in turn means that in order to maximize the temperature and minimize the velocity of the exit gas jet, selecting a higher mass flow rate is desirable. Meanwhile with regards to the mass flow rate requirement, the fabrication constraint imposed on the throat curvature leads to a constant discharge coefficient across the mass flow rate range and thus no difference in efficiency. On the other hand, its impact on the velocity and thermal requirements is quite limited. The results of all these considerations on the design of the nozzle can be seen in figure 8.17.

Table 8.19: Nozzle Performance Parameters across refined mass flow rate range

| **Parameter** | **0.2 (g/s)** | **0.3 (g/s)** | **0.4 (g/s)** | **0.5 g/s** | **0.6 g/s** | **0.7 g/s** | **0.8 g/s** | **0.9 g/s** |
|---|---|---|---|---|---|---|---|---|
| $P_c$ (bar) | 1.932 | 1.873 | 1.775 | 1.65 | 1.498 | 1.318 | 1.111 | 1.189 |
| E ($\varepsilon$) | 1.282 | 1.223 | 1.186 | 1.16 | 1.141 | 1.12 | 1.102 | 1.1 |
| $D_t$ (mm) | 0.758 | 0.943 | 1.118 | 1.297 | 1.491 | 1.717 | 2.0 | 2.049 |
| $D_e$ (mm) | 0.858 | 1.043 | 1.218 | 1.397 | 1.592 | 1.817 | 2.1 | 2.149 |
| $L_{nozzle}$ (mm) | 0.262 | 0.267 | 0.267 | 0.267 | 0.272 | 0.268 | 0.265 | 0.268 |
| $Re_t$ | 18904 | 22797 | 25624 | 27621 | 28828 | 29206 | 28664 | 31452 |
| $R_u$ ($R_t$) | 1.5 | 1.3 | 1.1 | 0.94 | 0.84 | 0.72 | 0.6 | 0.6 |
| $E_{real}$ | 1.28 | 1.224 | 1.189 | 1.165 | 1.147 | 1.128 | 1.112 | 1.109 |
| $m_{real}$ (g/s) | 0.196 | 0.295 | 0.393 | 0.492 | 0.59 | 0.688 | 0.785 | 0.884 |
| $T_{e_{real}}$ (K) | 195.439 | 201.263 | 205.312 | 208.388 | 210.8 | 213.607 | 216.115 | 216.5 |
| $V_{e_{real}}$ (m/s) | 458.247 | 445.301 | 436.075 | 428.934 | 423.25 | 416.536 | 410.446 | 409.504 |
| $V_{e_{real}}$ (Mach) | 1.422 | 1.382 | 1.353 | 1.331 | 1.313 | 1.293 | 1.274 | 1.271 |
| $F_{real}$ (N) | 0.114 | 0.169 | 0.225 | 0.28 | 0.334 | 0.388 | 0.442 | 0.497 |
| $Isp_{real}$ (s) | 59.035 | 58.543 | 58.207 | 57.954 | 57.757 | 57.531 | 57.333 | 57.309 |
| $c^{\star}_{real}$ (s) | 435.777 | 435.777 | 435.777 | 435.777 | 435.777 | 435.777 | 435.777 | 435.777 |
| $C_{F_{real}}$ (s) | 1.329 | 1.318 | 1.31 | 1.305 | 1.3 | 1.295 | 1.291 | 1.29 |
| $C_d$ | 0.982 | 0.983 | 0.983 | 0.983 | 0.983 | 0.983 | 0.982 | 0.983 |
| $\xi_T$ | 1.001 | 0.999 | 0.998 | 0.997 | 0.996 | 0.995 | 0.993 | 0.993 |
| $\xi_V$ | 0.982 | 0.984 | 0.985 | 0.987 | 0.988 | 0.99 | 0.992 | 0.992 |
| $\xi_F$ | 0.963 | 0.966 | 0.967 | 0.968 | 0.969 | 0.969 | 0.969 | 0.97 |
| $\xi_{Isp}$ | 0.98 | 0.982 | 0.984 | 0.985 | 0.985 | 0.986 | 0.987 | 0.987 |
| $\xi_n$ | 0.98 | 0.982 | 0.984 | 0.985 | 0.985 | 0.986 | 0.987 | 0.987 |
| $\xi_c$ | 1 | 1 | 1 | 1 | 1 | 1 | 1 | 1 |

8

### INFLATION PERFORMANCE

Section 8.3 deals with establishing the controllability of the inflation system through the pulsed operation of the inflation valve. A simple control logic is utilized to demonstrate this controllability by enabling the inflation system to provide three distinct inflation phases. These different phases have varying inflation rates due to their utilization of different pulse widths at an operational frequency of 3.5 Hz. While the pulse widths and duty cycles vary slightly with increasing mass flow rate, the main variation is the inflation time. The different inflation times for the refined mass flow rate range, at the $m_{real}$ value are shown in table 8.20.

Table 8.20: Inflation Times for mass flow rate range

| **Real Mass Flow Rate (g/s)** | **Unfolding time (s)** | **Fast Pressurization time (s)** | **Gradual Pressurization time (s)** | **Total time (s)** |
|---|---|---|---|---|
| 0.196 | 4.0 | 27.43 | 14.57 | 46.0 |
| 0.295 | 2.57 | 18.29 | 9.71 | 30.57 |
| 0.393 | 2.0 | 14.0 | 7.43 | 23.43 |
| 0.492 | 1.71 | 11.43 | 6.0 | 19.14 |
| 0.59 | 1.14 | 8.29 | 4.57 | 14.0 |
| 0.688 | 1.14 | 8.0 | 4.29 | 13.43 |
| 0.785 | 0.86 | 6.29 | 3.43 | 10.57 |
| 0.884 | 0.86 | 6.0 | 3.14 | 10.0 |

As can be seen all mass flow rates can deliver inflation times within the desired inflation range of 10-100 seconds as given by killer requirement REQ-ISP-01 while it also evident that with increasing mass flow rate, both the inflation time and the difference in inflation times decreases. As noted in section 8.3.3 it is difficult to discern which of these mass flow rate values is most suitable based solely on these inflation times. This is primarily due to the fact that the desired inflation time range, as dictated by REQ-ISP-01, is based on a preliminary estimation that, due to the limited literature, cannot be validated until further testing and/or complex simulations of the inflation process are carried out. However, it was decided that in order to maximize the reliability and controllability of the inflation process, a number of considerations should be considered.

8

- Firstly, while a minimal inflation time of 10 s was selected, it is deemed prudent to choose a relatively slow inflation time in order to ensure that the structure deploys in a smooth and controlled fashion. As such, the slower inflation rates offered by lower mass flow rates are attractive.

- Secondly, while the simple logic utilized demonstrates the potential of utilizing RCS pulse logic to provide a controllable inflation process, it derives from an inflation sequence designed by Griebel, 2011 and as can be seen from the relatively fast unfolding times is perhaps not ideally tailored to meet REQ-ISP-03, which desires a smooth unfolding process. These times are not a consequence of the designed system but rather of this control logic, which as can be seen provides more suitable times for gradual pressurization. This should be addressed in future work where the development of a more suitable 'complex' logic should be designed.

- Finally, as discussed in section 8.3.3, higher mass flow rates have the potential to offer the control logic designer increased flexibility in duty cycle and frequency options while still maintaining the capacity to inflate the structure within a reasonable time frame. As such they offer the potential for increased controllability. However, this controllability is subject to the maximum and minimum duty cycle requirements that are an essential consideration for the real performance of the inflation nozzle. Importantly, the current logic's duty cycle requirements limit this potential.

Having clarified these consideration, it is apparent that based off of the pulse logic utilized for the demonstration of the controllability of this inflation system, lower mass flow rates provide a more attractive inflation performance.

### 8.6.3. SELECTION

As noted, mass flow rates from 0.2 g/s to 0.9 g/s all satisfy the desired inflation system requirements. However, in order to finalize the preliminary design of this inflation system, the most appropriate flow rate should be selected. From the discussion above regarding the impact of the mass flow rate on the key design considerations, both upstream and downstream, the following conclusions can be made.

- Higher mass flow rates enable the design of nozzle with lower expansion ratios, which in turn allows the system to generate lower gas jet exit velocities and higher gas jet exit temperatures.
- Lower mass flow rates enable slower inflation times and as such a greater controllability of the inflation process.
- Lower mass flow rates enable a greater quantity of usable propellant to be stored in the tank thanks to their lower ullage gas mass requirements. This in turn allows pressure maintenance to be sustained for longer thereby increasing the mission length.

These statements are clearly represented in table 8.21. It can be seen that the exit temperature and exit velocity values increase and decrease respectively with increasing mass flow rate. The most attractive values are found at 0.8 g/s and 0.9 g/s. Due to both mass flow rates being capable of facilitating the minimum expansion ratio of 1.1, the temperature and velocity characteristics are effectively the same, lying around 216 K and 410 m/s respectively. These values are 21 K greater and 42 m/s lower than those found at 0.2 g/s. However, while higher mass flow rates provide more attractive exit temperature and exit velocity values, they provide faster inflation times and shorter maintenance lives. Taking 0.8 g/s and 0.9 g/s again it can be seen that they both yield effectively the same inflation time, which is about 36 s faster than that of 0.2 g/s. In addition, they also yield a reduction in maintenance life of about 5 days relative to 0.2 g/s.

| Mass Flow Rate (g/s) | Inflation Time (s) | Exit Temperature (K) | Exit Velocity (m/s) | Maintenance Life (days) |
|---|---|---|---|---|
| 0.2 | 46.0 | 195.439 | 458.247 | 32.5 |
| 0.3 | 30.57 | 201.263 | 445.301 | 32 |
| 0.4 | 23.43 | 205.312 | 436.075 | 31.5 |
| 0.5 | 19.14 | 208.388 | 428.934 | 30.5 |
| 0.6 | 14.0 | 210.8 | 423.25 | 30 |
| 0.7 | 13.43 | 213.697 | 416.536 | 29 |
| 0.8 | 10.57 | 216.115 | 410.446 | 28.5 |
| 0.9 | 10.0 | 216.5 | 409.504 | 27.5 |

Table 8.21: Properties across mass flow rate range

Until more detailed analysis and research detailing the interaction of the inflation gas jet and the inflating membrane becomes available finding an optimal mass flow rate based on these considerations isn't feasible. Until this is done prioritizing between killer requirement REQ-ISP-01, regarding the inflation time, and killer requirement REQ-ISI-04, regarding the inflation gas jet temperature and velocity, cannot be done in a satisfactory manner. As such, it was decided the best approach for this preliminary design is to compromise. This decision shall enable a suitably conservative mass flow rate selection given the current knowledge ascertained by the author in the development of this thesis work. Thus a mass flow rate of 0.5 g/s shall be selected, half way between 0.2 g/s and 0.8 g/s.

While this selection is evidently not optimal, the limitations of this thesis means that it deemed a suitable starting point for the preliminary design of a cold gas micropropulsion based inflation system. Future work exploring an optimal mass flow rate should explore the development of a complex control logic as well as test/simulate the complex deployment/inflation process and the interaction between the gas jet and the inflating structure. This would enable a more comprehensive and refined understanding of the inflation environment and in turn the constraints that it places on the design of the inflation system.

## 8.7. CONCLUSION

In conclusion, the inflation system designed in this thesis successfully addresses the mission statement of this thesis project to "design a micropropulsion based inflation system that provides a suitable and controllable inflation process for inflatable reflectors utilized in beyond Earth orbit CubeSat missions". This is emphasized by the inflation system design successfully addressing all of the inflation system requirements outlined in section 4.4. The design process undertaken in the pursuit of this aim indicated the suitability of adapting such cold gas micropropulsion system technology for such applications with minimal design adjustments required. While a relatively unique approach is required to facilitate the design of the nozzle, the general design of the system is very similar to that of a typical cold gas RCS micropropulsion system. This is hugely exciting for the inflatable space industry as it provides a clear indication of the potential of these systems for providing compact and precise inflation systems for beyond Earth orbit Cubesat inflatable structures.

### 8.7.1. SUMMARY OF SYSTEM PERFORMANCE

With the finalized selection of the mass flow rate the key system performance parameters can be summarized. This is done in using a series of tables, describing the nozzle performance, the inflation performance, the tank parameters, the pressure drop characteristics and the inflation system mass budget. The volume budget of the system is addressed in the summary graphic, figure 8.35, and can clearly be seen to comfortably fit within within the 1U volume requirement (REQ-ISI-01). The only major system budget not addressed is that of the power budget. This is left for future work.

#### SUMMARY OF NOZZLE PERFORMANCE

| Parameter | Value |
|---|---|
| E ($\varepsilon$) | 1.16 |
| $D_t$ (mm) | 1.297 |
| $D_e$ (mm) | 1.397 |
| $R_u$ ($R_t$) | 0.94 |
| $\alpha$ (°) | 15 |
| $L_{nozzle}$ (mm) | 0.267 |
| *Nozzle Performance* | - |
| $m_{real}$ (g/s) | 0.492 |
| $P_c$ (bar) | 1.65 |
| $T_{e_{real}}$ (K) | 208.388 |
| $V_{e_{real}}$ (m/s) | 428.934 |
| $V_{e_{real}}$ (Mach) | 1.331 |
| $F_{real}$ (N) | 0.28 |

Table 8.22: Nozzle Performance Parameters

Examining the nozzle performance from table 8.22, it can clearly be noted that temperature and velocity requirements, REQ-ISI-04-01 and REQ-ISI-04-04, both of which are sub requirement of the killer requirement REQ-ISI-04, are satisfied. The gas exit temperature is comfortably above the minimum temperature of 160K while the gas exit velocity is comfortably below the maximum velocity of mach 1.5. Due to the lack of literature evaluating the interaction between the inflatable membrane and a cold gas jet, these values were chosen as a conservative estimate and until they are investigated further, achieving them with a simple cold gas system utilizing convergent-divergent nozzle shall require such an unusual configuration. Should it turn out these requirements can be relaxed, a more conventional convergent-divergent nozzle configuration may be feasible although it also may be worthwhile investigating either the use of some sort of inhibitor between the nozzle and the inflating structure to slow/warm the gas as it enters the structure or to focus on the design of an alternative nozzle configuration, such as a convergent nozzle. The impact of the thrust generated is not considered but would place additional requirements on the ADCS system.

### SUMMARY OF INFLATION PERFORMANCE

| Parameter | Value |
|---|---|
| $f$ (Hz) | 3.5 |
| *Pulse Widths* | - |
| $PW_{unfolding}$ (ms) | 32.5 |
| $PW_{Pressurization_{fast}}$ (ms) | 73.75 |
| $PW_{Pressurization_{slow}}$ (ms) | 8.0 |
| *Duty Cycles* | - |
| $DC_{unfolding}$ % | 11.375 |
| $DC_{Pressurization_{fast}}$ % | 25.8125 |
| $DC_{Pressurization_{slow}}$ % | 2.8 |
| *Inflation Times* | - |
| $t_{unfolding}$ (s) | 1.71429 |
| $t_{Pressurization_{fast}}$ (s) | 11.42857 |
| $t_{Pressurization_{slow}}$ (s) | 6.0 |
| $t_{inflation}$ (s) | 19.14286 |

Table 8.23: Inflation Performance Parameters

The inflation performance is given in table 8.23. This table clearly demonstrates the successful design of a cold gas inflation system that can provide a controllable inflation process, courtesy of the pulsed inflation method, within the desired time frame, satisfying killer requirement REQ-ISP-01. The use of this method shall also enable precise pressure maintenance, thereby succesfully satisfying key requirement REQ-ISP-06. One point of note however, is the degree to which key requirement REQ-ISP-03 is satisfied. This requirement dictates that the structure slowly unfold in a smooth and controlled fashion. As can be seen from the table, an unfolding time of 1.7 s is yielded based on the inflation sequence discussed in section 8.3.3. While it is suspected that such an unfolding time is too fast, without testing and simulation it is impossible to validate. As noted this issue arises not from the capabilities of the inflation system or the pulsed method, but rather from the selection of the parameters for the inflation sequence, as clearly seen by the times for fast and gradual pressurization. As such, while the inflation sequence utilized in this thesis is useful for demonstrating the capacity of the designed inflation system for controllable inflation, it may not necessarily provide suitable unfolding times. Future work should explore the development of a more suitable complex logic, with specific focus on the use of sensory feedback. The parameters for such work would have to be informed by the use of complex simulations and testing. This would also enable validation of the estimated suitable inflation times.

### SUMMARY OF TANK PARAMETERS

| **Component** | **Value** |
|---|---|
| Initial Tank Pressure (bar) | 200 |
| Final Tank Pressure (bar) | 30.85 |
| Inflatant Tank Capacity (U) | 0.25 |
| $R_{tank}$ (mm) | 33.02 |
| $L_{tank}$ (mm) | 96.76 |
| Inflatant Tank Mass (grams) | 103.18 |
| *Inflation Gas* | - |
| Initial Inflation (grams) | 1.63 |
| Ullage Gas (grams) | 8.63 |
| Makeup Gas (grams) | 36.48 |
| Leakage Gas (grams) | 11.68 |
| Total Inflation Gas (grams) | 58.42 |
| Mission Lifetime (days) | 30.5 |

Table 8.24: Tank Parameters

The quantity of gas that the system can carry is limited. This limitation arises from the requirement to carry additional unusable gas to compensate for leakages and to maintain the tank pressure above that of the minimum regulator inlet pressure. As can be seen this unusable gas contributes almost 35% of the total inflation gas which is clearly undesirable. As is noted in table 8.24 this means that only sufficient makeup gas can be carried to provide pressure maintenance for to 30.5 days, well below the 393 days desired in requirement REQ-BEOC-04-02. This issue with limited pressure maintenance clearly indicates the limitations of pressure stabilized inflatable optical reflectors and emphasises the need for further advancements in rigidization technology for these structures. Something for which, as has been noted, this inflation system is very much suited for.

### UPSTREAM PRESSURE BUDGET

A more straight forward approach to reducing the makeup gas requirements is to utilize components that yield lower pressure losses with the upstream COTS components contributing large pressure losses due to being ill-suited to the desired flow rates. This can be seen in the upstream pressure budget presented in table 8.25.

| **Component** | **ΔP (Pa)** |
|---|---|
| *Upstream* | - |
| Initial Tank Pressure | 200 (bar) |
| Final Tank Pressure | 30.85 (bar) |
| *Losses @ 30.85 bar* | - |
| Straight | 1.74 |
| 90 Bend | 6.97 |
| Expansion Loss | 6.82 |
| Filter | 537,457.68 |
| Contraction Loss | 6.42 |
| 90 Bend | 6.97 |
| Expansion Loss | 10.88 |
| Latch Valve | 996,190.85 |
| Contraction Loss | 6.42 |
| 90 Bend | 6.97 |
| Straight | 1.74 |
| Expansion Loss | 6.82 |
| Total ΔP | 15.38 (bar) |
| Min. Regulator Inlet | 15.51 (bar) |

Table 8.25: Upstream Pressure Losses at Tank pressure of @ 0.5 g/s

### DOWNSTREAM PRESSURE BUDGET

Table 8.26 contains the downstream pressure budget which operates at a constant regulated pressure of 2.3 bar. As can be seen the major contributors to the pressure loss downstream are the latch valve, the inflation valve and of course the flexible tubing that is accounted for in the straight and 90 bend sections.



| **Component** | **ΔP (Pa)** |
|---|---|
| Regulator Outlet Pressure | 2.0 (bar) |
| Relief Valve | 110.91 |
| Contraction Loss | 327.89 |
| T-Junction | 286.04 |
| Straight (50mm) | 419.17 |
| 90 Bend | 159.7 |
| Latch Valve | 29331.14 |
| 90 Bend | 159.7 |
| Straight (100mm) | 838.34 |
| 90 Bend | 159.7 |
| Straight (50mm) | 419.17 |
| 90 Bend | 159.7 |
| T-Junction | 286.04 |
| Expansion Loss | 457.71 |

| | |
|---|---|
| Inflation Valve | 1848.52 |
| Total $\Delta$P | 0.35 (bar) |
| Chamber Pressure | 1.65 (bar) |

Table 8.26: Downstream Pressure Losses at regulated pressure of 2.0 bar @ 0.5 g/s

### MASS BUDGET

Finally, table 8.27 provides the overall mass budget for the inflation system. As can be seen utilizing COTS components the mass budget for this preliminary design comes in comfortably under the 1kg requirement dictated by REQ-ISI-02. Meeting this mass requirement is essential for ensuring that the inflatable system as a whole can compare competitively with other more conventional spacecraft deployable structures. It is hoped that further iterations of this design, and further utilization of micropropulsion technology for the different components could further reduce this mass requirement, and also maximize the mass of inflation gas that can be carried.

Table 8.27: Mass Budget

| **Component** | **Mass (grams)** | **%** |
|---|---|---|
| Inflatant Tank (dry) | 103.18 | 13.70 |
| Nitrogen Gas | 58.42 | 7.76 |
| Fill Vent/Valve | 50 | 6.64 |
| Filter | 24 | 3.19 |
| HP Latch Valve | 100 | 13.28 |
| LP Latch Valve | 45 | 5.98 |
| Regulator | 200 | 26.56 |
| Relief Valve | 4.5 | 0.60 |
| Vent Valve | 35 | 4.65 |
| Thruster Assembly | 16 | 2.13 |
| Piping | 60.8 | 8.08 |
| Pressure Transducers | 56[30] | 7.44 |
| **Total** | **752.9** | **100** |

[30] Estimate based off the Adelis-SAMSON Cold Gas System (Zaberchik et al., 2019)

### SUMMARY GRAPHIC

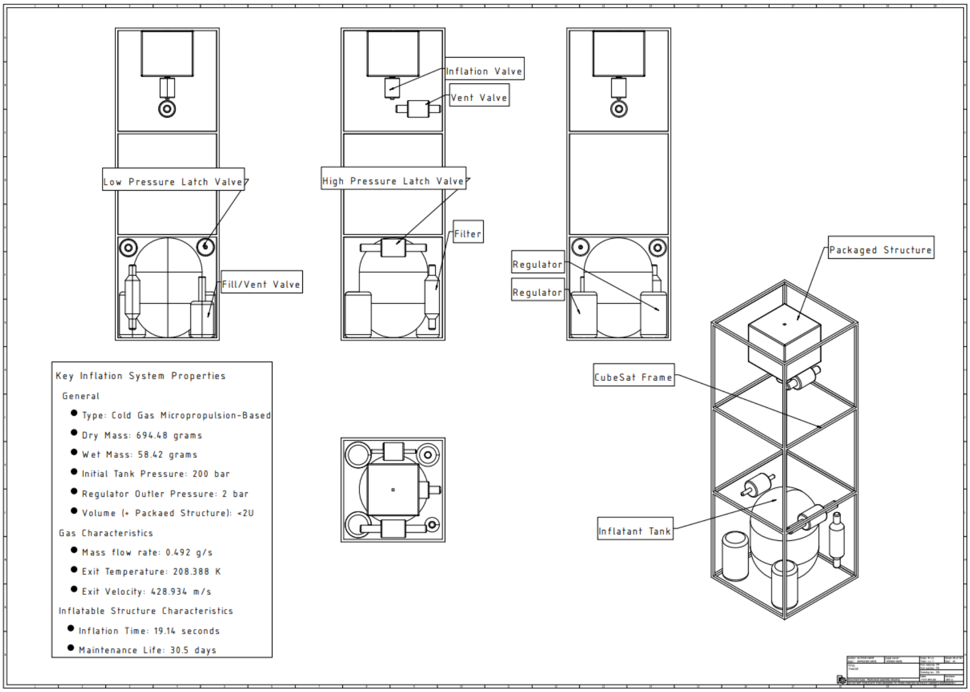


Figure 8.35: Inflation System Summary Graphic

As can be seen from figure 8.35, the inflation system and packaged inflatable reflector both fit comfortably within the 3U volume requirement set by key requirement REQ-BEOC-01. Indeed there is over 1.5 U available for both the ejection mechanism and any additional system components required, although it is hoped that such components shall be compact in order to facilitate a minimal volume requirement. This clearly demonstrates the exciting potential for inflatable structure for facilitating large deployable structures within relatively compact CubeSat volumes. Indeed, with further advancements in rigidization technology, removing the need for makeup gas, the size of both the inflatant tank and the inflation system as a whole could be further reduced providing an even more compact system.

# Bibliography

Adler, S., Warshavsky, A., & Peretz, A. (2005). Low-cost cold-gas reaction control system for the sloshsat flevo small satellite. *Journal of spacecraft and rockets*, *42*(2), 345–351.

Ahmad, R. A. (2001). Discharge coefficients and heat transfer for axisymmetric supersonic nozzles. *Heat transfer engineering*, *22*(6), 40–61.

Anis, A. (2012). Cold gas propulsion system-an ideal choice for remote sensing small satellites. *Remote sensing-advanced techniques and platforms*, 447–462.

Arestie, S., Lightsey, E. G., & Hudson, B. (2012). Development of a modular, cold gas propulsion system for small satellite applications. *Journal of Small Satellites*, *1*(2), 63–74.

Bzibziak, R. (2000). Update of cold gas propulsion at moog. *36th AIAA/ASME/SAE/ASEE Joint Propulsion Conference and Exhibit*, 3718.

Cardin, J., & Acosta, J. (2000). Design and test of an economical cold gas propulsion system.

Cervone, A., Speretta, S., Menicucci, A., Bertels, E., Topputo, F., Merisio, G., et al. (2021). Selection of the propulsion system for the lumio mission: An intricate trade-off between cost, reliability and performance. *72nd International Astronautical Congress (IAC 2021)*, 1–9.

Chandra, A., Pat, T., Tonazzi, J. C. L., & Walker, C. K. (2021). Development and flight qualification of a small satellite x-band spherical membrane antenna. *2021 IEEE Aerospace Conference (50100)*, 1–8.

Chen, H.-S., Rizal, Y., & Ho, M.-T. (2014). Cold gas attitude control systems. *2014 CACS International Automatic Control Conference (CACS 2014)*, 167–172.

Coffee, C. W., Bressette, W. E., & Keating, G. M. (1962a). *Design of the nasa lightweight inflatable satellites for the determination of atmospheric density at extreme altitudes*. National Aeronautics; Space Administration.

Coffee, C. W., Bressette, W. E., & Keating, G. M. (1962b). *Design of the NASA Lightweight Inflatable Satellites for the determination of atmospheric density at extreme altitudes* (tech. rep.). NASA Langley Research Center. Washington.

Collicott, S. H., Beckman, E. A., & Srikanth, P. (2019). Conformal tanks: Small-sat propellant management technology. *AIAA Propulsion and Energy 2019 Forum*, 3874.

Freeland, R., & Bilyeu, G. (1993). In-step inflatable antenna experiment. *Acta Astronautica*, *30*, 29–40.

Griebel, H. S. (2011). *Reaching high altitudes on mars with an inflatable hypersonic drag balloon*. Springer Science & Business Media.

Harris, J. (2003). Ultralight propellant tank for nasa space technology 5. *39th AIAA/ASME/SAE/ASEE Joint Propulsion Conference and Exhibit*, 4608.

Hinkley, D. (2008). A novel cold gas propulsion system for nanosatellites and picosatellites.

Johnson, R. C. (1971). *Real gas effects in flow metering* (tech. rep.).

Jung, S.-C., & Huh, H.-I. (2008). Characteristic study of micro-nozzle performance and thermal transpiration based self pumping in vacuum conditions. *Proceedings of the Korean Society of Propulsion Engineers Conference*, 866–870.

Kindracki, J., Tur, K., Paszkiewicz, P., Mężyk, Ł., Boruc, Ł., & Wolański, P. (2017). Experimental research on low-cost cold gas propulsion for a space robot platform. *Aerospace science and technology*, *62*, 148–157.

La Torre, F. (2011). Gas flow in miniaturized nozzles for micro-thrusters.

Lester, D., Wassom, S., Hancey, B., & Siefkas, P. (2000). Solar concentrator inflation control system. *41st Structures, Structural Dynamics, and Materials Conference and Exhibit*, 1571.

Lev, D. R., Herscovitz, J., & Zuckerman, Z. (2014). Cold gas propulsion system conceptual design for the samson nanosatellite. *50th AIAA/ASME/SAE/ASEE Joint Propulsion Conference*, 3759.

Louwerse, M. C. (2009). Cold gas micro propulsion. *University of Twente*, 176.

McLaughlan, P. B., Forth, S. C., & Grimes-Ledesma, L. R. (2011). *Composite overwrapped pressure vessels, a primer* (tech. rep.).

Morrow, J. M. (2012). *Design and analysis of lunar lander control system architectures* (Doctoral dissertation). Massachusetts Institute of Technology.

Mueller, J., Marrese, C., Polk, J., Yang, E., Green, A., White, V., Bame, D., Chakraborty, I., Vargo, S., & Reinicke, R. (2001). An overview of mems-based micropropulsion development at jpl.

Nakasuka, S., Senda, K., Watanabe, A., Yajima, T., & Sahara, H. (2009). Simple and small de-orbiting package for nano-satellites using an inflatable balloon. *Transactions of the Japan Society for Aeronautical and Space Sciences, Space Technology Japan*, *7*(ists26), Tf_31–Tf_36.

Nett, F. (2021). On the design of a propulsion system for the lunar meteoroid impact observer (lumio).

Nishimachi, S., Hayakawa, N., Kojima, H., Hanai, M., & Okubo, H. (2012). Pressure and temperature dependence of breakdown characteristics of sub-cooled liquid nitrogen. *2012 Annual Report Conference on Electrical Insulation and Dielectric Phenomena*, 440–443.

Oh, K. W., & Ahn, C. H. (2006). A review of microvalves. *Journal of micromechanics and microengineering*, *16*(5), R13.

Özden, A. (2019). *Performance characteristics of a cold gas thruster with real gas effects* (Master's thesis). Middle East Technical University.

Özden, A., BARAN, Ö. U., Aksel, M. H., & Ak, M. A. (2021). Su2 real gas models'performance predictions on a cold gas thruster. *Isı Bilimi ve Tekniği Dergisi*, *41*(1), 77–88.

Rasse, B., Damilano, P., & Dupuy, C. (2014). Satellite inflatable deorbiting equipment for leo spacecrafts. *Journal of Space Safety Engineering*, *1*(2), 75–83.

Rekleitis, G., Tortopidis, I., Paraskevas, I., Psarros, D., Kaliakatsos, I., Roditis, I., & Papadopoulos, E. (n.d.). The ntua simulators for space robots on orbit.

Roe, L. (2000). Inflation systems for near-term space missions. *41st Structures, Structural Dynamics, and Materials Conference and Exhibit*, 1570.

Silik, Y., & Yaman, U. (2019). Single axis attitude controller design using pulse width modulated thruster. *2019 20th International Conference on Research and Education in Mechatronics (REM)*, 1–6.

Spisz, E. W., Brinich, P. F., & Jack, J. R. (1965). *Thrust coefficients of low-thrust nozzles* (tech. rep.). NATIONAL AERONAUTICS and SPACE ADMINISTRATION CLEVELAND OH LEWIS RESEARCH CENTER.

Sutton, G. P., & Biblarz, O. (2016). *Rocket propulsion elements*. John Wiley & Sons.

Tam, W., & Griffin, P. (2002). Design and manufacture of a composite overwrapped pressurant tank assembly. *38th AIAA/ASME/SAE/ASEE Joint Propulsion Conference & Exhibit*, 4349.

Tang, S., & Fenn, J. (1978). Experimental determination of the discharge coefficients for critical flow through an axisymmetric nozzle. *AIAA Journal*, *16*(1), 41–46.

Thunnissen, D. P., Webster, M. S., & Engelbrecht, C. S. (1995). Low-mass inflation systems for inflatable structures. *In Jet Propulsion Lab, California Inst. of Tech, Proceedings of the International Conference on Integrated Micro/Nanotechnology for Space Applications p(SEE N 96-36329 12-12), 1995*.

Wright, H., Cutright, A., Corliss, J., Bruce, W., Trombetta, D., Mazaheri, A., Coleman, M., Olds, A., & Hancock, S. (2012). Heart flight test overview. *9th International Planetary Probe Workshop, Toulouse, France*.

Zaberchik, M., Lev, D. R., Edlerman, E., & Kaidar, A. (2019). Fabrication and testing of the cold gas propulsion system flight unit for the adelis-samson nano-satellites. *Aerospace*, *6*(8), 91.

Zandbergen, B. (2013). Micropropulsion systems for cubesats. *CubeSat Technology and Applications*, 1–36.

Zandbergen, B. (2018). Thermal Rocket Propulsion Course AE4S01. (August).

# 9

# CONCLUSIONS AND RECOMMENDATIONS

*This chapter concludes the thesis work, providing an overview of the results as well as recommendations for future work. The first step in this process is to answer the research questions (section 9.1). After this the compliance of the work with respect to the requirements generated is evaluated (section 9.2). Finally, recommendations pertaining to the design of BEOC inflatable reflectors and CubeSat inflation systems are proposed (section 9.3).*

## 9.1. Research Questions

The research questions are addressed in order with their answers informing the main research question.

### 9.1.1. What are the design characteristics of the BEOC Inflatable Reflector?

In order to maximize the relevance of the inflation system designed in this thesis project, it was decided to explore the design of a spherical inflatable reflector. Such a reflector can be utilized to satisfy the major BEOC applications through its use as either an antenna, concentrator or hybrid system. However, instead of tailoring the design of the reflector to any one specific application, a generic spherical inflatable structure is designed thereby informing the design of an inflation system that can be utilized for all spherical inflatable applications. The focus of the design is on addressing the desire to highlight the competitiveness of such structures relative to conventional reflectors and to inform the design and performance requirements of the inflation system.

The key design characteristics that must be addressed in order to meet these aims are identified in the literature study and include the geometry, shape transformation functions, materials, fabrication methods, environmental conditions and mechanical properties of the structure. Each of these characteristics are explored within the constrained scope of the requirements. As such, the diameter of the structure is based off the desire to provide a deployed area the same size as the high performing CubeSat KaTENna parabolic mesh reflector. Following this the investigation into the shape transformation functions of packaging, deployment and stabilization informs the design requirements of the inflation system. While a detailed exploration of each function is not carried out, the following design decisions were made. Firstly, the residual gas build up during packaging necessitates that the inflation system provide ascent venting. Secondly, the use of the free deployment method requires that the inflation process provides sufficient control to unfold and pressurize the structure in a controlled manner. Finally, the limitations of current rigidization technology means that pressure stabilization is the only suitable stabilization method, in turn necessitating that the inflation system be capable of providing pressure maintenance.

9

This investigation also informs the selection of the material for the structure with the CP-1 polymer film being identified as the most suitable following a trade off analysis. A brief exploration of the fabrication methods for a spherical inflatable structure is then discussed, but their implications on the preliminary design of this reflector is not assessed. However, the impact of the on-orbit environmental conditions are evaluated. A micrometeroid flux model is utilized to estimate the rate of hole growth in the structure due to micrometeroid punctures, thereby informing the makeup gas requirements of the inflation system. Following this, a simplified analytical method is used to assess the thermal characteristics of the structure, informing the expected temperatures during the inflation process. Finally, the mechanical properties of the structure are evaluated. Unsurprisingly, as a pressure stabilized structure, the internal pressure loading, as the most dominant structure load, is a key mechanical property. This pressure loading is determined based on the following pressurization approach. Firstly the structure is pressurized to 15% of its Yield strength to remove any wrinkling. Following this it is then vented down to 2% of its Yield strength so as to minimize the makeup gas requirements of the inflation system. The next step is the selection of the most suitable membrane thickness.

Having completed these steps and assessed the design characterstics of the BEOC inflatable reflector, this investigation established both the attractive properties of the spherical inflatable structure relative to conventional CubeSat reflectors and the informed the generation of the requirements for a suitable inflation system.

### 9.1.2. WHAT ARE THE DESIGN CHARACTERISTICS OF THE INFLATION SYSTEM?

In order to ensure that a suitable micropropulsion-based inflation system is designed there are a number of key design characteristics that must be addressed.

The first step in this process was to identify the most suitable design concept out of those identified in the literature study. A trade off analysis utilizing the AHP method provided a quantitative comparison of each of the micropropulsion based design candidates according to the criteria of concept maturity, inflation control, volume footprint, mass and complexity. The cold gas regulated blow down design candidate is selected as the most suitable candidate thanks to its to its high degree of inflation control and concept maturity. Following this, nitrogen gas is identified as the most suitable inflation gas. Its identification stems from an attractive blend of desirable gas properties that are derived from key inflation requirements. Having established both the system and gas types, the next key design characteristic is the inflation scheme. This inflation scheme encompasses the key functional and performance requirements of the inflation system. As such it consists of ascent venting, inflation, venting and pressure maintenance. With a focus on the inflation stage, a multi-phase inflation sequence is identified in order ensure a reliable and controllable inflation process. As this sequence requires that the inflation system be capable of varying the inflation rate, the pulsed mode of inflation, which is commonly used for precision RCS system, is selected as the best method for facilitating this sequencing, offering a high degree of inflation control.

With the system type, inflation gas and inflation scheme all specified, the key design characteristics related to the detailed design of the inflation system shall now be explored. These include the inflation nozzle, the inflation control valve, the inflatant tank and the inflatant feed system. The aim of the detailed design process was to establish the design adjustments required to adapt these components of the micropropulsion system for inflation purposes. In this vain, it was found that in order to adapt a conventional cold gas micro nozzle for inflation purposes a unique design approach is required. This counter-intuitive approach is driven by the desire to maximize the gas jet temperature and minimize the gas jet velocity. The result of this process yielded a design approach that aims to minimize the nozzle expansion ratio and maximize its throat curvature. As such the designed nozzle has an unusually low expansion ratio, enabling it to generate gas temperatures in excess of 190 K and velocities less than 460 m/s.

Other than the unique design approach required for adjusting the nozzle for inflation purposes, the general design of the rest of the system is very similar to that of a typical cold gas micropropulsion system. This can be seen in the use of COTS components for the design of the feed system and the use of RCS control logic for the pulsed operation

9

of the inflation control valve. However, additional components are required to facilitate the desired ascent venting function while the design approach for the inflatant tank is slightly different. This is done so as to enable the designer to assess the impact of the gas losses incurred by micrometeroid punctures on the mass requirements of the inflation system over time.

The design approach followed in the design of this inflation system, is to the authors knowledge, the first detailed exploration of a micropropulsion based inflation system specifically tailored for providing precise inflation control within the constraints of a CubeSat platform. The design characteristics explored in this pursuit clearly address the mission statement of the project by successfully establishing that a controllable inflation system can be developed through the adaption of cold gas micropropulsion technology. This is hugely promising for the inflatable space industry and provides a clear indication that such systems can play a key role in the enabling the development of further advancements in inflatable space structure technology.

### 9.1.3. What is the theoretical performance of the inflation system?

This question is asked in order to determine if the design of the inflation system meets the desired key inflation performance characteristics. This is succinctly addressed in section 8.7 where the capacity of the inflation system to deliver the key functionalities, as set out by the inflation scheme, as well as desirable gas characteristics is established. It is noted that further research is required with respect to the interaction between the inflation gas jet and the inflating membrane in order to further refine the desired requirement. Despite this, the theoretical results presented provide a clear indication that the design approach followed in the design of this micropropulsion based inflation system can enable the precise and controllable inflation of an inflatable reflector, within the constraints of a BEOC platform.

### 9.1.4. Main Research Question

The answers given to the sub-research questions above can be utilized to answer the main research question which is formulated as follows:



- *What are the design adjustments required in order to adapt current micropropulsion technology so that it can be utilized in the development of a controllable inflation system for beyond Earth orbit CubeSat inflatable reflectors?*

It is apparent that, apart from the inflator nozzle, there are limited adjustment required to adapt current cold gas micropropulsion technology so that it can be utilized in the design of a compact and controllable inflation system. As such, it has been established that the need for a suitable and controllable inflation system in order to enable and enhance the development of BEOC missions can be addressed through the use of micropropulsion-based inflation systems. This successfully fulfils the mission statement of the project.

## 9.2. REQUIREMENTS

The compliance of the designed inflatable system, consisting of both the inflatable structure and the inflation system, with respect to the requirements set out in section 4 is evaluated in this section. The compliance is graded according to the following colors:

| Cell Color | Compliance |
|---|---|
| Green | Compliant |
| Cyan | Partly Compliant |
| Yellow | TBD |
| Red | Not Compliant |

Table 9.1: Compliant Grades

### 9.2.1. BEOC MISSION INTERFACE REQUIREMENTS

| ID | Compliance |
|---|---|
| REQ-BEOC-01 | Designed components within requirements |
| REQ-BEOC-02 | Designed components within requirements |
| REQ-BEOC-03 | TBD |
| REQ-BEOC-04 | Not Compliant |
| REQ-BEOC-04-01 | Compliant |
| REQ-BEOC-04-02 | Not Compliant |

Table 9.2: BEOC Requirements

While the inflatable reflector and inflation system satisfy their mass and volume requirements, as the ejection mechanism and any additional components are not explored, key requirements REQ-BEOC-01 and REQ-BEOC-02 can only be marked as partly compliant. REQ-BEOC-03 which relates to system power is not investigated, in part because the application of the inflatable structure is not explored. Thus it is marked at TBD. While REQ-BEOC-04-01 is deemed as compliant, with cold gas systems suitable for a period of storage, it should be noted that the impact of leakage is not assessed. This should be explored. As pressure stabilization has been established as the only currently suitable stabilization technology, REQ-BEOC-04-02 and thus REQ-BEOC-04 as a whole are not compliant. Instead of being suitable for a 393 day mission, pressure maintenance can only be maintained for 30.5 days given the system constraints. As a key requirement, this is a major issue that must be addressed if inflatable structures are to become a feasible option for BEOC missions with advancements in rigidization technology, such as UV, required.

### 9.2.2. BEOC INFLATABLE REFLECTOR REQUIREMENTS

| ID | Compliance |
|---|---|
| REQ-IRP-01 | Compliant |

| | |
|---|---|
| REQ-IRP-02 | TBD |
| REQ-IRI-01 | Compliant |
| REQ-IRI-02 | Compliant |
| REQ-IRI-03 | Compliant |
| REQ-IRI-04 | Compliant |
| REQ-IRI-04 | Compliant |

Table 9.3: Inflatable Reflector Requirements

The design of the inflatable reflector is compliant with majority of the requirements specified. However, as the application of the structure is not explored, further work is required on REQ-IRP-02 and key requirement REQ-IRP-03 which relate to surface accuracy. While fulfilling these requirements, enables the successful demonstration of the micropropulsion-based inflation system, significantly more detailed work is required to design a feasible inflatable reflector structure.

### 9.2.3. MICROPROPULSION BASED INFLATION SYSTEM REQUIREMENTS

| ID | Compliance |
|---|---|
| REQ-ISP-01 | Compliant |
| REQ-ISP-02 | Not explored in detail |
| REQ-ISP-03 | Compliant |
| REQ-ISP-04 | Compliant |
| REQ-ISP-05 | Compliant |
| REQ-ISP-06 | Compliant |
| REQ-ISI-01 | Compliant |
| REQ-ISI-02 | Compliant |
| REQ-ISI-03 | TBD |
| REQ-ISI-04 | Compliant |
| REQ-ISI-04-01 | Compliant |
| REQ-ISI-04-02 | Compliant |
| REQ-ISI-04-03 | Compliant |
| REQ-ISI-04-04 | Compliant |

Table 9.4: Inflation System Requirements

The micropropulsion based inflation system designed in this thesis project successfully addresses the majority of the requirements, including the two killer requirements REQ-ISP-01 and REQ-ISP-04. REQ-ISP-02 which details ascent venting is not explored in detail in this design process, although it is partly elaborated on. Further research is required. As is the case for REQ-BEOC-03, REQ-ISI-03 relating to the inflation systems power requirements are not explored. As most of the onboard power shall be available during the initial inflation process, this is not seen as a significant hurdle.

## 9.3. Recommendations and Future Work

This sections details the recommendations that have arisen during the project. Considering that the thesis explores the design of both an inflatable structure and an inflation system, many topics were investigated. However, as is the case with any research undertaken, there are various aspects of both systems that could be improved with further exploration. As such, future work into both inflatable structures and inflation systems should consider the following recommendations.

### 9.3.1. Inflatable Space Structures

#### Application

The inflatable reflector designed in this thesis is primarily designed in order to demonstrate the competitiveness of such a structure relative to conventional CubeSat reflector structures and to facilitate the generation of functional and performance requirements for the inflation system. As such, the design of the structure is in itself quite limited. To start with, future work should explore the application of a spherical reflector to one of the promising BEOC applications, be that telecommunications, power or propulsion. This would require exploring the desired optical properties of the structure which could be done utilizing ray tracing models, FEA analysis and ground testing.

#### Shape Transformation Functions

The investigation into the shape transformation functions of the inflatable structure are quite limited in this thesis. The development of these functions for CubeSat inflatable reflectors is still in its infancy and further research into any of the functions would be hugely beneficial. In the case of packaging, packaging methods for parabolic and spherical reflector structures are still relatively unexplored and it is recommended that further work explore such methods paying particular attention to their impact on both the deployment dynamics and the structural properties of the structure. With regards to deployment, the design and development of a suitable ejection mechanism is required. Given the uncertainty regarding its mass and volume, this is a major aspect of the inflatable system that must be investigated before verifying the competitiveness of inflatable reflectors for BEOC applications. Finally, pressure stabilization is clearly ill suited for long duration BEOC missions. As such future work exploring advancements in rigidization techniques is recommended.

9

#### Fabrication

The design of the structure assumes that it is an ideal spherical shell constructed from a homogeneous material. This is clearly not realistic and any future work should assess the impact of fabrication methods on the properties of the structure as well as its performance for BEOC reflector applications. In addition, research into suitable fabrication methods is still in its infancy, with research into suitable methods recommended.

#### Environmental Orbital Conditions

The analysis of the micrometeroid and the thermal environments in this thesis is quite limited and further detailed work on both aspects is recommended. With respect to the micrometeroid environment, it is recommended that future work aim to utilize more accurate lunar flux models in order to more precisely gauge the rate of hole growth in lunar orbit. Moreover, there remains uncertainty surrounding the damage incurred by micrometeoroid punctures, with the approximations used in this thesis yielding somewhat surprising results, with thinner walls yielding lower rates of hole growth. It is recommended that this phenomenon be further investigated. With regards to the thermal analysis, the analytical method used does not accurately represent the real thermal characteristics of the inflatable reflector. As such it is recommended that a comprehensive thermal analysis utilizing FEA and ray tracing models be carried out.

#### Mechanical Properties

A detailed analysis of the properties of the deployed structures is also recommended. In this thesis, the structure is approximated as a uniform thin shell structure with the investigation into the mechanical properties of the structure is carried out using this approximation. This investigation focuses solely on static deforming loads, with the dynamic loads incurred due to inputs such as spacecraft dynamic loads not considered. In addition, it is recommended that further work into suitable skins stress levels, and by extension the internal pressure, be investigated.

### 9.3.2. Inflation System

#### Inflation System Type

While the cold gas regulated blowdown candidate was selected and designed in this thesis work, the CGG refill candidate, which makes use of the attractive mass and volume characteristics of CGG technology, is an exciting candidate that is worthy of further exploration. Moreover, the list of design candidates eliminated due to their exploration being beyond the scope of the thesis may also be worthy of investigation.

#### Inflation Scheme

The venting and pressure maintenance phases of the inflation scheme are not investigated in this thesis project with the primary focus being on the inflation phase. It is recommended that future work consider the performance of these phases. With respect to the inflation phase, it is investigated by developing a simplified control logic which is utilized to demonstrate the feasibility of such a system for inflation purposes. However, its actual inflation performance is not optimal and it is recommended that a more suitable 'complex' control logic be developed.



#### Nozzle

The nozzle is the main system component requiring adjustment for inflation purposes. The driving requirements behind the design of the nozzle derive from constraints placed on the inflation rate as well as the temperature and velocity of the gas jet. However, these requirements are based on preliminary estimates due to the lack of literature available on the interaction between the gas jet and the inflating membrane. It is recommended that future work explore this interaction so as to further refine these requirements. With respect to the actual design process, it is recommended that the real analysis of the nozzle be further refined by accounting for the real pulsing performance of the inflation control valve. Moreover, the fabrication constraints considered should also be investigated further as they are imposed due to the uniquely low expansion ratio of the nozzle. Due to this unique design process, it may be worthwhile exploring alternative options, such as utilizing a converging nozzle, or indeed multiple different nozzles. This may help to facilitate different gas jet requirements and reduce the unusual fabrication requirements the converging-diverging nozzle demands. Finally, this thesis does not explore the interface between the nozzle and the inflatable structure, nor how it would be mounted with respect to the ejection mechanism. This also requires further exploration.

#### Other Components

The general design of the rest of the system is quite similar to a conventional cold gas propulsion system. However, there are further refinements to the design that are recommended. Firstly, it is recommended that further optimization of the inflatant tank be carried out so as to maximize the mass of inflatant that can be carried. This may entail exploring the design of a custom conformal tank, or exploring a compressed overwrapped tank material. In addition, analysis of the gas leakage is required. Further optimization is also recommended for the feed system, where the potential use of expansion chambers/plenums may be worthy of investigation. Moreover, the layout and constituent components of the system should also be further refined. Suitable sensors should be selected and the performance of the venting section evaluated. Finally, while the COTS components utilized demonstrate the suitability of micropropulsion technology for inflation applications, it is recommended that future work investigate the design of suitable custom built components so as to further optimize the system. This is particularly true for the pressure regulator whose performance is assumed based of a reference system.

# A

# Inflatable Reflector Design Concepts

A

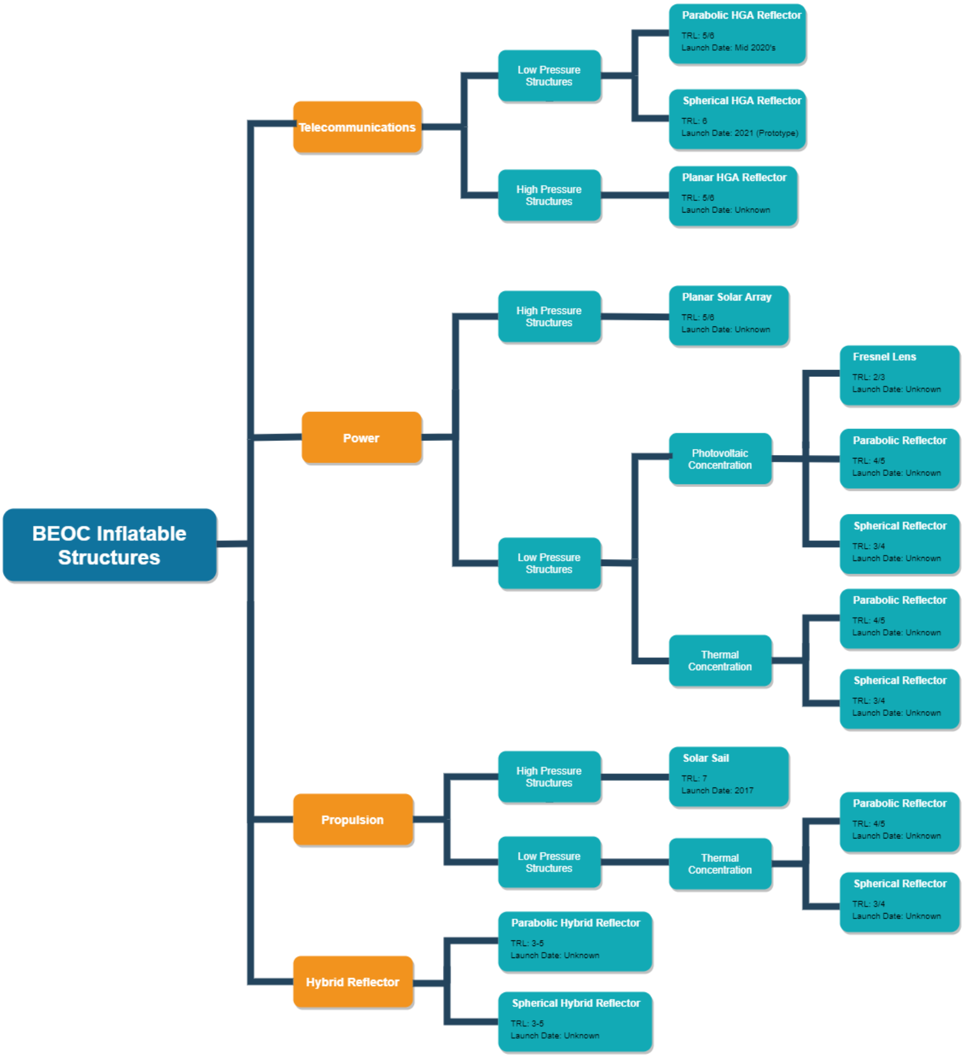


Figure A.1: Design options for the application of an inflatable structure as solutions to the technological challenges facing BEOC missionss

# B

# Inflation System Design Concepts

B

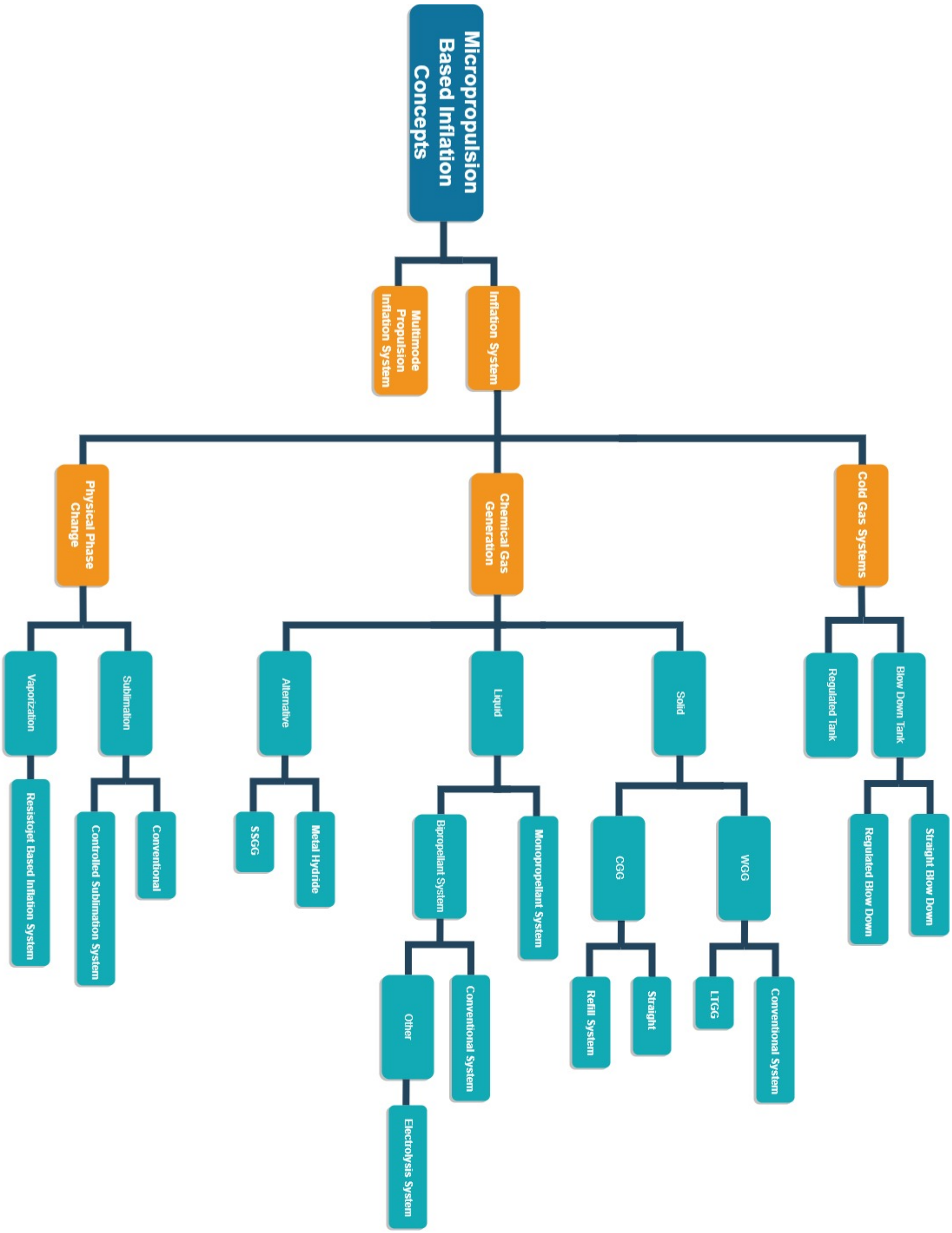


Figure B.1: Design Option Tree of Wide Range of Inflation System Concepts

# C

# Reference Deployable CubeSat Systems

## C.1. Reference Table

| System | Reference |
|---|---|
| CatSat | (Chandra et al., 2021) |
| Babuscia | (Babuscia et al., 2020) |
| Gregorian | (Fenn et al., 2021) |
| OS4 | (Staehle et al., 2020) |
| AeroCube3 | (Hinkle et al., 2008) |
| NanoSat Device | (Nakasuka et al., 2009) |
| 30 Inch Sphere | (Coffee et al., 1962) |
| 12 ft Sphere | (Coffee et al., 1962) |
| ECHO 1 | (Clemmons, 1964) |
| KaTENna | Tendeg [1] |
| KaPDA | Tendeg [1] |
| M-ARGO | (Walker et al., 2017) |
| MarCo | (Chahat et al., 2020) |

Table C.1: Reference BEOC Reflector Structures

## C.2. Parameters Table

[1]https://www.tendeg.com/products

Table C.2: Reference Deployable CubeSat Systems

| Name | Mission Parameter | Configuration | CubeSat Size (U) | Inflatable Mass (kg) | Deployed CSA ($m^2$) | Reflector Area Density ($kg/m^2$) | RPE ($m^2/U$) | System Volume/CubeSat Size (%) |
|---|---|---|---|---|---|---|---|---|
| *Inflatable* | *Reflector* | | | | | | | |
| CatSat | LEO/GEO | Spherical | 6 | 0.0139∗ | 0.196 | 0.071 | TBC | 25 |
| Babuscia | LEO | Spherical | 3 | 0.17∗ | 0.785 | 0.216 | 3.272 | 20 |
| Gregorian | BEOC | Parabolic⋆ | 12 | 1.77 | 4.524 | 0.391 | 3.6192 | TBD |
| OS4 | Neptune | Parabolic⋆ | 12 | 7.22 | 19.635 | 0.368 | TBC | TBC |
| *Inflatable* | *De-Orbit* | | | | | | | |
| AeroCube 3 | LEO | Spherical | 1 | 0.04∗ | 0.28 | 0.141 | 1.81 | 15.5 |
| NanoSat Device⋆⋆ | LEO | Spherical | 3 | 0.135 | 0.42 | 0.323 | TBC | 13.3 |
| *Inflatable* | 1960's NASA Balloons | | | | | | | |
| 30 Inch Sphere⋆⋆ | LEO | Spherical | NA | 0.137 | 0.456 | 0.3 | 3.93 | NA |
| 12 ft Sphere⋆⋆ | LEO | Spherical | NA | 4.2 | 10.521 | 0.4 | 1.51 | NA |
| ECHO I⋆⋆ | LEO | Spherical | NA | 51.5 | 182.415 | 0.282 | 1.643 | NA |
| *Non-Inflatable* | *Reflector* | | | | | | | |
| KaTENna | GEO/BEOC | Parabolic Mesh | 12 | 2.5 | 0.785 | 3.183 | 0.262 | 25 |
| KaPDA | GEO/BEOC | Parabolic Mesh | 6 | 1.4 | 0.196 | 7.13 | 0.123 | 26.67 |
| M-ARGO | BEOC(0.8AU) | Planar | 12 | 1 | 0.173 | 5.787 | 0.3 | NA† |
| MarCo | BEOC(1.5AU) | Planar | 6 | 1 | 0.197 | 5.085 | 0.237 | NA† |

∗ = Calculated using available data
⋆= Parabolic structure are composed of reflector and torus structures
⋆⋆ = Structure constructed from laminate material
† = Stowed externally on side of CubeSat
Gregorian = Data only for the primary reflector
System Volume = Refers to the total inflatable system volume including inflation system and ejection/deployment mechanism
TBC = To be confirmed (Value couldn't be attained)

C

# D

# GRAPHICAL TRADE OFF

The graphical trade off tables is used in the analysis and selection of various different design characteristics in this thesis. The advantage of such a trade off method is that it is fast, easy to handle and stresses the unacceptable design candidates (Gill, 2015). Four colors are used to define the different degrees to which the design candidate performs relative to the desired requirement. These are demonstrated in table D.1.

| **Cell Color** | **Compliance** |
|---|---|
| Green | Excellent/ Exceeds Requirements |
| Cyan | Good/ Meets Requirements |
| Orange | Limited/ Undesirable |
| Red | Unacceptable |

Table D.1: Compliant Grades

# E

# INFLATABLE STRUCTURE DESIGN

## E.1. MATERIAL THICKNESS

| Structure | Material | Thickness ($\mu m$) | Reference |
|---|---|---|---|
| Inflatable CubeSat Antenna (Babuscia Reflector) | Half-Aluminized/ Transparent Mylar | 50.6/25.4 | (Babuscia et al., 2020) |
| Gregorian inflatable reflector | Half-Aluminized/ Transparent Melinex | 25.4 | (Fenn et al., 2019) |
| AeroCube 3 | Aluminized Mylar | 25.4 | (Fuller et al., 2010) |
| ECHO I | Aluminized Mylar | 12.7 | (Clemmons, 1964) |
| TST | TBD | 12.7 | (Walket et al., 2017) |
| Lunar Flashlight | Aluminized CP1 | 3 | (Johnson et al., 2015) |
| NeaScout | Aluminized CP1 | 2.5 | (Johnson et al., 2015) |

Table E.1: Membrane thickness value from reference structures

## E.2. KEY ASSUMPTIONS

A number of significant key assumptions are made in the design of this structure. This was done so as to facilitate the design of a structure that can inform the requirements of the inflation system within the time constraints of the thesis. They are as follows:

### APPLICATION OF REFLECTOR

- The key design features of a spherical inflatable reflector remain consistant across the applications of telecommunications, power and propulsion.

- The optical properties of the structure are less important than the key design considerations explored in this thesis for dictating the inflation system requirements.

### GEOMETRY OF REFLECTOR

- An inflatable reflector cross sectional area of 0.785 $m^2$ can be utilized to demonstrate the attractive characteristics of such structures relative to high performing mesh reflectors such as the KaTENna antenna.

E

### SHAPE TRANSFORMATION FUNCTIONS

The shape transformation functions are not investigated in detail, with only the sufficient detail required to inform inflation system design parameters explored

- *Packaging*

  - A PE value of 40% is assumed to be feasible based on similar reference systems
  - The residual gas build up can be completely negated through the use of ascent venting.

- *Deployment*

  - The free deployment method is selected based on its use for similar reference systems. The use of free deployment necessitates additional inflation control.
  - An ejection mechanism can be designed that satisfies REQ-BEOC-01, REQ-BEOC-02 and REQ-BEOC-03.

- *Stabilization*

  - Based off current rigidization technology, pressure stabilization is the only method currently suitable for inflatable reflector applications.

### MATERIAL

- Due to a lack of available information, the optical properties of Kapton HN and Upilex-S are assumed based on statements made in relevant literature.

- While the performance of a VDA reflective coating is not explored, based off the information provided it is assumed suitable for this application.

### Fabrication

- Instead of investigating the effects of potential fabrication issues on the structural or thermal properties of the structure, it is assumed that the structure is an ideal spherical shell constructed from a homogeneous material.

### Environmental Conditions

- *Orbit*

  – It is assumed that the structure will operate in a 500 km-altitude circular orbit about the moon (Cipriano et al., 2018).

- *Micrometeroids*

  – An estimation of the flux and the rate of hold growth is calculated using a simple verifiable method presented by Thomas and Friese, 1980. The lunar flux is calculated using a simplified Earth flux model. It is assumed this can be corrected for by utilizing a correction factor of 0.7 (Badyukov, 2020). In addition, it is assumed that the distribution and flux of the micrometeroids is uniform over time.

  – An approximate method developed by Chodimella et al., 2006 is used to gauge the damage caused by micrometeroids. This method makes a number of assumptions including that all micrometeroids are spherical in shape. As a consequence the impact crater is assumed to be circular.

- *Thermal*

  – It is assumed that the thermal characteristics of the structure can be calculated using a simplified thermal analysis that approximates the structure as a uniform opaque spherical reflector coated in VDA. The validity of this assumption is limited due to the structure consisting of both a transparent canopy and a reflective interior coating.

  – As such, the thermal requirements are assumed based off relevant inflatable structures and not their impact on the properties of the structure. This requires further work with FEA.

  – Thermal variations due to varying orbital parameters are also not considered although the shadow conditions are calculated. In addition, it is assumed that such variations do not impact pressure maintenance of the structure. In reality, this is not true.

  – In addition, thermal analysis regarding variations in the relationship between the skin stress and the internal pressure are not investigated. Thus, as it is assumed that inflation occurs at a constant temperature, an approximation of the desired skin stress at 343K is made.

### MECHANICAL PROPERTIES

- The structure is approximated as a uniform thin shell structure. In addition, it is considered a single body system with no analysis relating to the coupled system of it and the CubeSat explored. The mass, volume and structural loads of the structure are calculated according to these conditions.
- Due to limited information regarding the variation of the mechanical properties of CP-1 with thermal variations, the desired skin stress values are calculated based off the yield strength at 300K.
- The dynamic loads incurred during the deployment process or due to inputs such as spacecraft dynamics are not considered and are left for future work.

# F

# AHP Comparison Matrices

The comparison matrices for the design candidates with respect to the different selection criteria are contained in this section. They are key to utilizing the AHP trade off method.

| Concept Maturity | CGB Straight | CGB Regulated | CG Regulated | LTGG | CGG Straight | CGG Refill |
|---|---|---|---|---|---|---|
| **CGB Straight** | 1.00 | 0.67 | 3.00 | 5.50 | 3.50 | 2.50 |
| **CGB Regulated** | 1.50 | 1.00 | 3.50 | 6.00 | 4.00 | 3.00 |
| **CG Regulated** | 0.33 | 0.29 | 1.00 | 3.00 | 2.00 | 0.50 |
| **LTGG** | 0.18 | 0.17 | 0.33 | 1.00 | 0.50 | 0.25 |
| **CGG Straight** | 0.29 | 0.25 | 0.50 | 2.00 | 1.00 | 0.33 |
| **CGG Refill** | 0.40 | 0.33 | 2.00 | 4.00 | 3.00 | 1.00 |

CGB = Cold Gas Blowdown
LTGG = Low Temperature Gas Generator
CGG = Cool Gas Generator
CG = Cold Gas

Table F.1: Concept Maturity Comparison Matrix

| Inflation Control | CGB Straight | CGB Regulated | CG Regulated | LTGG | CGG Straight | CGG Refill |
|---|---|---|---|---|---|---|
| **CGB Straight** | 1.00 | 0.33 | 0.33 | 3.00 | 4.00 | 0.50 |
| **CGB Regulated** | 3.00 | 1.00 | 1.00 | 6.00 | 7.00 | 2.00 |
| **CG Regulated** | 3.00 | 1.00 | 1.00 | 6.00 | 7.00 | 2.00 |
| **LTGG** | 0.33 | 0.17 | 0.17 | 1.00 | 1.50 | 0.25 |
| **CGG Straight** | 0.25 | 0.14 | 0.14 | 0.67 | 1.00 | 0.20 |
| **CGG Refill** | 2.00 | 0.50 | 0.50 | 4.00 | 5.00 | 1.00 |

CGB = Cold Gas Blowdown
LTGG = Low Temperature Gas Generator
CGG = Cool Gas Generator
CG = Cold Gas

Table F.2: Inflation Control Comparison Matrix

F

| Volume Footprint | CGB Straight | CGB Regulated | CG Regulated | LTGG | CGG Straight | CGG Refill |
|---|---|---|---|---|---|---|
| **CGB Straight** | 1.00 | 1.50 | 1.50 | 0.29 | 0.29 | 0.50 |
| **CGB Regulated** | 0.67 | 1.00 | 1.00 | 0.25 | 0.25 | 0.33 |
| **CG Regulated** | 0.67 | 1.00 | 1.00 | 0.25 | 0.25 | 0.33 |
| **LTGG** | 3.50 | 4.00 | 4.00 | 1.00 | 0.67 | 2.00 |
| **CGG Straight** | 3.50 | 4.00 | 4.00 | 1.50 | 1.00 | 2.00 |
| **CGG Refill** | 2.00 | 3.00 | 3.00 | 0.50 | 0.50 | 1.00 |

CGB = Cold Gas Blowdown
LTGG = Low Temperature Gas Generator
CGG = Cool Gas Generator
CG = Cold Gas

Table F.3: Volume Footprint Comparison Matrix

| Mass | CGB Straight | CGB Regulated | CG Regulated | LTGG | CGG Straight | CGG Refill |
|---|---|---|---|---|---|---|
| CGB Straight | 1.00 | 2.00 | 2.00 | 0.33 | 0.33 | 0.67 |
| CGB Regulated | 0.50 | 1.00 | 1.00 | 0.25 | 0.25 | 0.40 |
| CG Regulated | 0.50 | 1.00 | 1.00 | 0.25 | 0.25 | 0.40 |
| LTGG | 3.00 | 4.00 | 4.00 | 1.00 | 0.67 | 2.00 |
| CGG Straight | 3.00 | 4.00 | 4.00 | 1.50 | 1.00 | 2.00 |
| CGG Refill | 1.50 | 2.50 | 2.50 | 0.50 | 0.50 | 1.00 |

CGB = Cold Gas Blowdown
LTGG = Low Temperature Gas Generator
CGG = Cool Gas Generator
CG = Cold Gas

Table F.4: Mass Comparison Matrix



| Complexity | CGB Straight | CGB Regulated | CG Regulated | LTGG | CGG Straight | CGG Refill |
|---|---|---|---|---|---|---|
| CGB Straight | 1.00 | 2.00 | 3.00 | 0.40 | 0.33 | 0.50 |
| CGB Regulated | 0.50 | 1.00 | 2.50 | 0.33 | 0.29 | 0.40 |
| CG Regulated | 0.33 | 0.40 | 1.00 | 0.25 | 0.22 | 0.29 |
| LTGG | 2.50 | 3.00 | 4.00 | 1.00 | 0.67 | 2.00 |
| CGG Straight | 3.00 | 3.50 | 4.50 | 1.50 | 1.00 | 2.50 |
| CGG Refill | 2.00 | 2.50 | 3.50 | 0.50 | 0.40 | 1.00 |

CGB = Cold Gas Blowdown
LTGG = Low Temperature Gas Generator
CGG = Cool Gas Generator
CG = Cold Gas

Table F.5: Complexity Comparison Matrix

# G

# Initial Tank Sizing

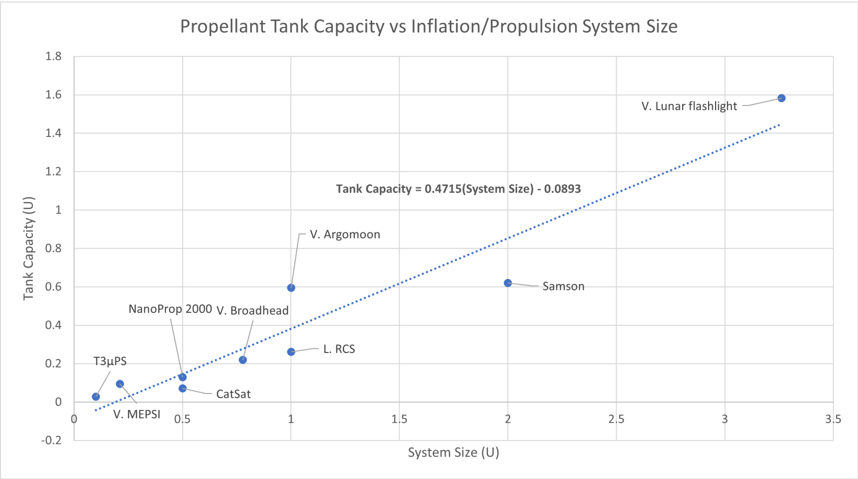


Figure G.1: Determining Inflatant Tank Capacity from reference systems

[2]https://gomspace.com/UserFiles/Subsystems/flyer/Flyer_NanoProp_20000.pdf
[3]https://cubesat-propulsion.com/wp-content/uploads/2015/10/Mepsi-micro-propulsion-system.pdf
[4]https://www.cubesat-propulsion.com/wp-content/uploads/2018/09/VACCO-Micro-Propulsion-Systems-Summary-web2-Sept2018.pdf

| System | Reference |
|---|---|
| T3$\mu$Ps | (Migliaccio et al., 2010) |
| Samson | (Lev et al., 2014) |
| CatSat | (Chandra et al., 2021) |
| LUMIO RCS (Proposed) | (Nett, 2021) |
| NanoProp 2000 | Gomspace [1] |
| VACCO MEPSI | VACCO [2] |
| VACCO Broadhead | VACCO [3] |
| VACCO ArgoMoon | VACCO [4] |
| VACCO Lunar Flashlight | VACCO [4] |

Table G.1: Reference Micropropulsion Systems

# H

# Feed System Components

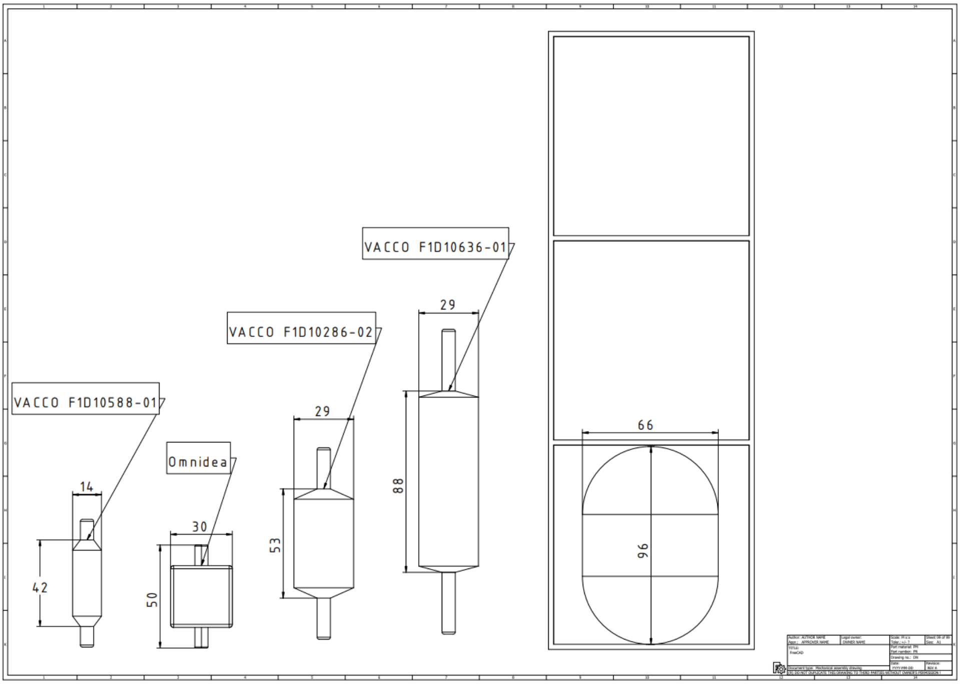


Figure H.1: 3D Graphic of COTS Filters.

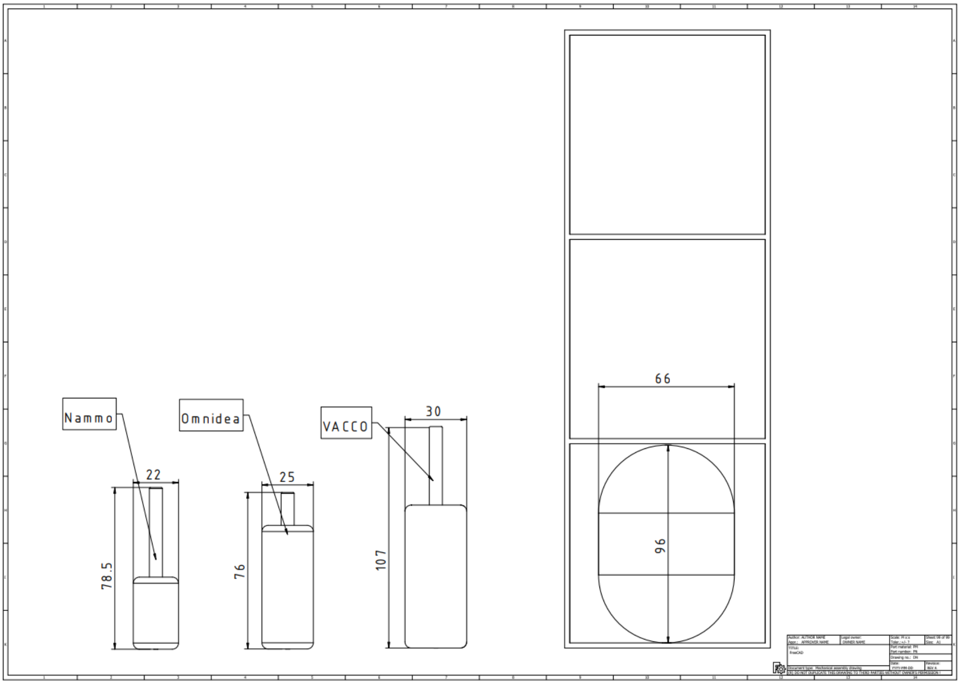


Figure H.2: 3D Graphic of COTS Fill/Vent Valve.

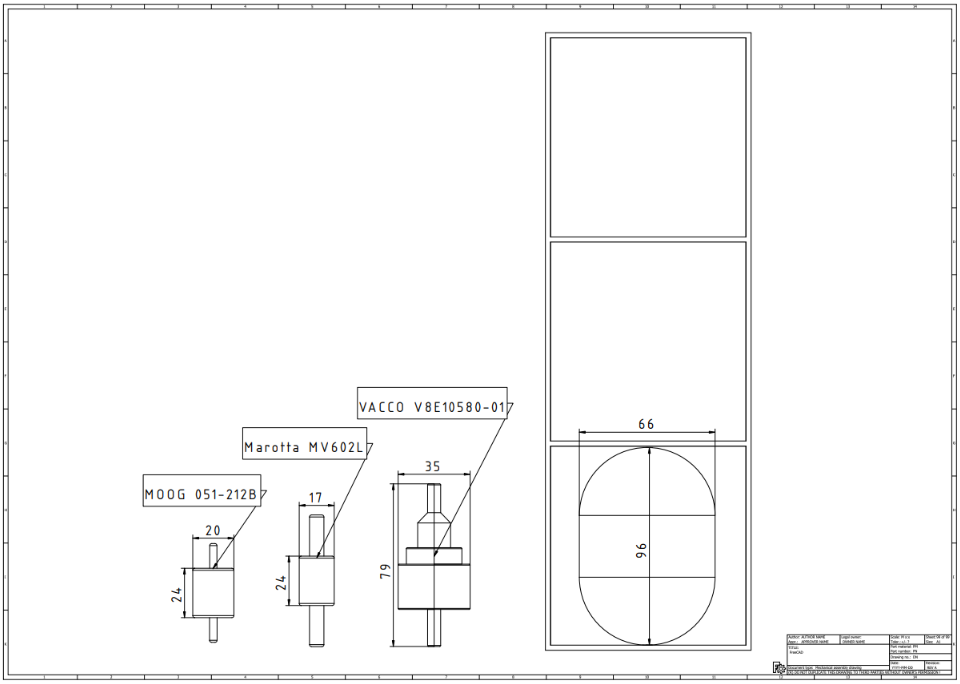


Figure H.3: 3D Graphic of COTS High Pressure Latch Valve

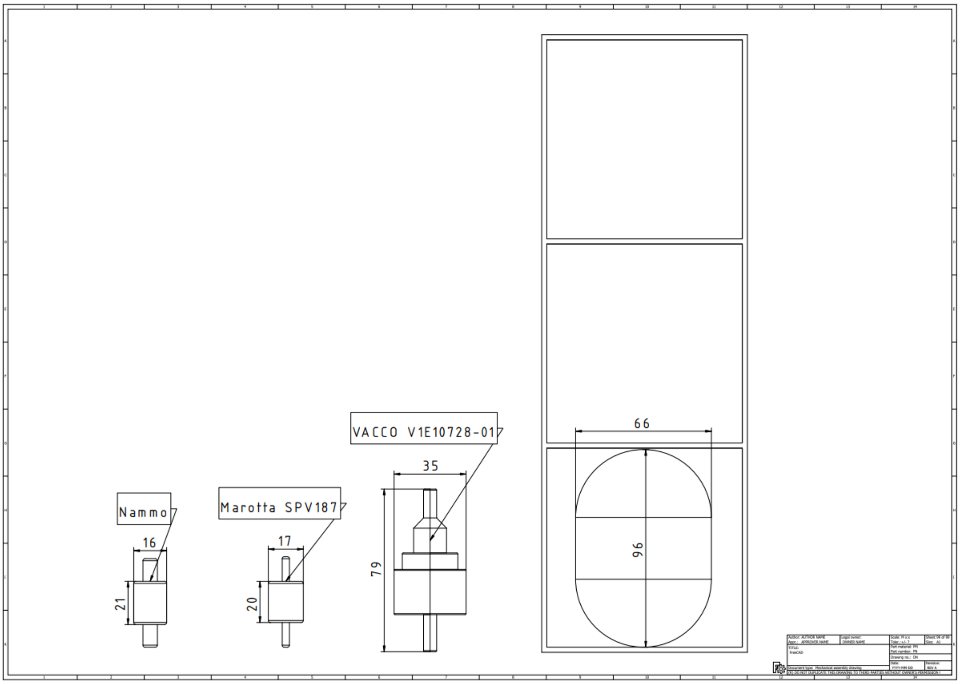


Figure H.4: 3D Graphic of COTS Low Pressure Latch Valve

H

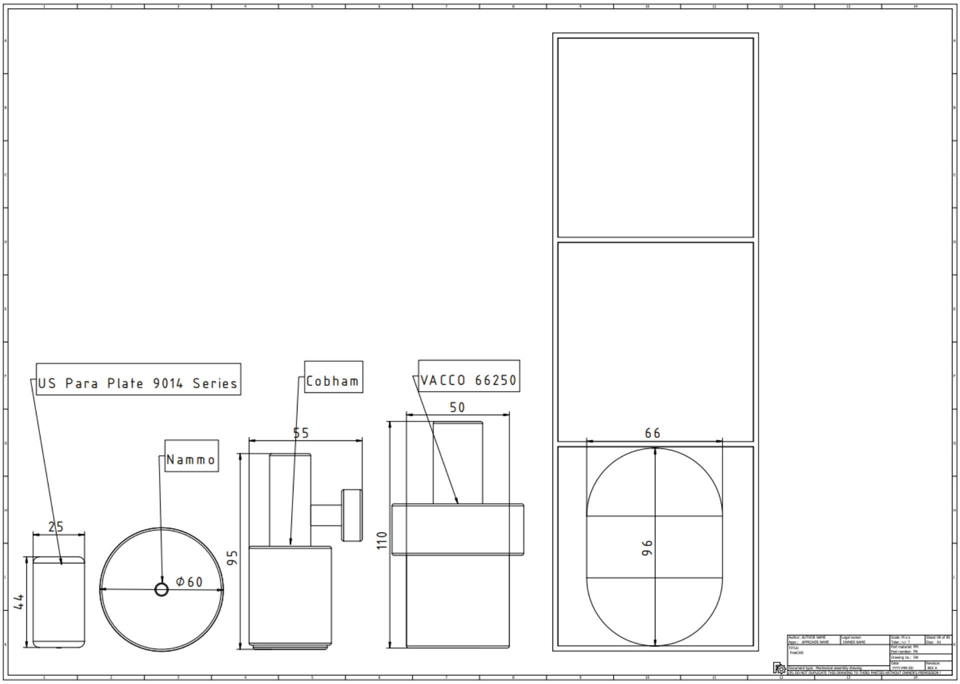


Figure H.5: 3D Graphic of COTS Pressure Regulators